



This work is protected by copyright and other intellectual property rights and duplication or sale of all or part is not permitted, except that material may be duplicated by you for research, private study, criticism/review or educational purposes. Electronic or print copies are for your own personal, non-commercial use and shall not be passed to any other individual. No quotation may be published without proper acknowledgement. For any other use, or to quote extensively from the work, permission must be obtained from the copyright holder/s.



Keele University

# Investigating the chondrogenic phenotype in clinically relevant cells: the effect of *hTERT* expression

**Tina Patricia Dale**

Ph.D. Thesis

Cell and Tissue Engineering

July 2016

Faculty of Medicine and Health Sciences

Research Institute for Science and Technology in Medicine

# Abstract

---

Damaged or diseased mature articular cartilage cannot undergo effective tissue repair and due to its avascular, hypocellular nature defects become widespread and painful. No 'gold standard' treatment exists for this indication and the ultimate recourse is prosthetic joint replacement. Cartilage is therefore an ideal target for regenerative medicine therapies aiming to recapitulate native cartilage.

Despite over fifty years of research and encouraging outcomes, re-creation of the hyaline tissue has yet to be consistently achieved, possibly as a result of the application of a sub-optimal cell type. Chondrocytes and bone marrow mesenchymal stem cells (MSCs) have been used clinically, with future prospects for other alternative MSC sources and human embryonic stem cell (hESC)-derived cells. Further *in vitro* study of cellular chondrogenic capacity is desirable but hampered by cell changes and senescence. This work examines the hypothesis that the re-introduction of the catalytic sub-unit human telomerase reverse transcriptase (*hTERT*) can extend the proliferative cell capacity of cells whilst concomitantly bypassing changes associated with cell aging and senescence. The utility of umbilical cord blood (UCB) as a possible alternative source of more naive MSCs was also investigated.

Human bone marrow MSCs, chondrocytes, and hESC-derived cells were transduced with *hTERT* and their resulting chondrogenic capacity, assessed principally by extracellular matrix (ECM) production and gene expression, examined and compared to that of the three non-transduced, parental cell sources.

UCB was not found to be a viable alternative MSC source due to a very low cell number and colony recovery; however, foetal bovine serum (FBS) batch and atmospheric oxygen tension were

identified as key to influencing recovery outcomes. Of the three parental cell types examined for chondrogenic potential MSCs and chondrocytes produced similar amounts of sGAG but chondrocytes produced a more homogeneous ECM with persistent chondrogenesis, whereas MSCs became hypertrophic. hESC derived cells had a more muted chondrogenic response with similarities to both chondrocytes and MSCs. *TERT* extended the proliferative capacity of all three cell types, two extensively but was also associated with changes in cell phenotype and a reduction, although not complete ablation, in the subsequent chondrogenic capacity.

Taken together the results demonstrate that with current differentiation techniques primary articular chondrocytes provide the most optimal result, supporting their continued use for clinical therapies, and this capacity may not be preserved by the application of *hTERT* transduction strategies.

**Keywords:** articular cartilage, chondrogenesis, cell therapy, regenerative medicine, extracellular matrix, telomerase, *hTERT*, senescence, immortal, chondrocyte, mesenchymal, embryonic, stem cell, hypertrophy, umbilical cord blood.

# Contents

---

Abstract	I
Contents	III
Figures	VIII
Tables	XI
Schemes	XI
Supplementary figures	XII
Abbreviations	XIII
Publications and presentations	XVI
Acknowledgements	XVIII
1 Introduction	1
1.1 The human skeleton	2
1.2 Synovial joints	2
1.3 Articular cartilage	4
1.3.1 Embryonic articular cartilage development	4
1.3.2 Postnatal articular cartilage	7
1.3.3 Mature articular cartilage	8
1.4 The extracellular matrix	11
1.4.1 Collagen	11
1.4.2 Articular cartilage proteoglycans and glycosaminoglycans	13
1.4.3 Small leucine-rich repeat proteoglycans	14
1.4.4 Glycosaminoglycans	15
1.5 Cartilage ageing, damage and degeneration	16
1.5.1 Ageing	16
1.5.2 Damage and degeneration	17
1.6 The role of regenerative medicine	20
1.6.1 Autologous chondrocyte implantation	21
1.7 Cells with prospects for use in cell therapies	25
1.7.1 Autologous chondrocytes	25
1.7.2 Stem cells	26
1.7.2.1 Mesenchymal stem cells	27
1.7.2.2 Umbilical cord blood stem cells	34
1.7.2.3 Embryonic stem cells and their derivatives	36
1.7.2.4 Induced pluripotent stem cells	37
1.8 Cell Senescence	38
1.8.1 Replicative senescence	39
1.8.2 Telomerase enzyme	41

1.9	Hypoxic culture	42
1.10	Summary and hypotheses	44
2	Materials and methods	46
2.1	Materials	47
2.2	General cell culture techniques	50
2.2.1	Enzymatic sub-culture with trypsin	50
2.2.2	Haemocytometer cell counting	50
2.2.3	Cryopreservation of cells	51
2.2.4	Cell counting using the Millipore Scepter cell counter	51
2.3	Isolation and culture of cells	52
2.3.1	Isolation and culture of bone marrow mesenchymal stem cells from bone marrow aspirate	52
2.3.2	Isolation and culture of bone marrow mesenchymal stem cells from bone marrow mononuclear cell preparations	53
2.3.3	Culture of human chondrocytes	53
2.3.4	Culture of embryonic stem cell derived progenitor cells	54
2.3.5	Culture of human embryonic stem cell line H1	54
2.3.5.1	Conditioning of media on mouse embryonic fibroblasts	54
2.3.5.2	Matrigel coating of tissue culture flasks	55
2.4	Umbilical cord blood collection	55
2.5	Density separation of cord blood	56
2.6	MACS cell separation	59
2.6.1	Labelling cells with beads	59
2.6.2	Separating cells	59
2.7	Retroviral transduction of cells with <i>hTERT</i>	60
2.8	Longitudinal proliferation study	63
2.9	Senescence associated $\beta$ -Galactosidase staining	64
2.10	Tri-lineage differentiation	65
2.10.1	Chondrogenic differentiation	65
2.10.2	Osteogenic differentiation	65
2.10.3	Adipogenic differentiation	65
2.11	Histological staining of differentiated monolayers	66
2.11.1	Alcian blue monolayer staining	66
2.11.2	Alizarin red S monolayer staining	66
2.11.3	Oil Red O monolayer staining	66
2.12	Flow cytometry	67
2.13	Preparation of monolayer samples for DMMB and PicoGreen analysis	67
2.13.1	Preparation of cell monolayers	67
2.13.2	Preparation of media	68
2.14	DMMB sulphated GAG quantification	69

2.15	PicoGreen double stranded DNA assay -----	69
2.16	Cell pellet creation-----	69
2.17	Pellet size -----	70
2.18	Micro computed tomography -----	71
2.18.1	Sample scanning -----	71
2.18.2	Sample processing-----	72
2.19	Cell lysis and homogenisation -----	73
2.19.1	Lysis of monolayers and trypsinised cells -----	73
2.19.2	Lysis of cell pellets -----	73
2.20	RNA extraction -----	74
2.21	Reverse transcription – polymerase chain reaction-----	74
2.21.1	Primer Sequences -----	75
2.22	Agarose gel electrophoresis-----	76
2.23	Quantitative reverse transcription-polymerase chain reaction -----	77
2.23.1	qRT-PCR primer sequences -----	79
2.23.2	qRT-PCR data analysis -----	80
2.23.2.1	Hierarchical clustering -----	81
2.24	Pellet and tissue histology and immunohistochemistry-----	81
2.24.1	Porcine tissue control samples -----	81
2.24.2	Embryonic chick femur control samples-----	82
2.24.3	Paraffin embedding -----	82
2.24.4	3-Aminopropyltriethoxysilane coating of slides -----	82
2.24.5	Paraffin embedded sample sectioning-----	82
2.24.6	Section de-paraffinisation -----	83
2.24.7	Haematoxylin and eosin staining-----	83
2.24.8	Toluidine blue staining -----	83
2.24.9	Picosirius red staining-----	83
2.25	Immunohistochemistry-----	84
2.25.1	Heat induced epitope retrieval -----	84
2.25.2	Enzymatic antigen retrieval -----	84
2.25.3	Primary antibody staining-----	84
2.25.4	Secondary antibody staining -----	85
2.25.5	Staining with the diaminobenzidine substrate. -----	85
3	Pilot study to determine the viability of human umbilical cord blood as a source of MSCs ---	87
3.1	Introduction -----	88
3.2	Aim -----	89
3.3	Methods-----	90
3.3.1	Statistical analysis -----	91
3.4	Results -----	93

3.4.1	UCB1-3 -----	95
3.4.2	UCB4-6 -----	99
3.4.3	UCB7-9 -----	99
3.4.4	UCB10-12 CD45 depletion using MACS technology-----	102
3.4.5	The influence of FBS batch on MSC recovery from MNC preparations-----	104
3.4.5.1	Colony recovery -----	104
3.4.5.2	Cell morphology following recovery -----	107
3.4.5.3	Cell recovery -----	107
3.5	Discussion-----	111
3.6	Conclusion -----	119
4	Characterisation of cells following transduction with hTERT -----	122
4.1	Introduction -----	123
4.2	Aims -----	125
4.3	Methods-----	125
4.3.1	Statistical analysis -----	126
4.4	Results -----	128
4.4.1	Ectopic <i>hTERT</i> expression in transduced cells -----	128
4.4.2	Cell proliferative capacity-----	130
4.4.3	Cell morphology-----	133
4.4.4	SA $\beta$ Gal activity -----	139
4.4.5	Tri-lineage differentiation capacity -----	142
4.4.6	Flow cytometry analysis-----	145
4.4.6.1	Cell size and complexity -----	145
4.4.6.2	Cell immunophenotype-----	149
4.5	Discussion-----	154
4.6	Conclusion -----	159
5	Chondrogenesis of cells in monolayer culture -----	161
5.1	Introduction -----	162
5.2	Aims -----	164
5.3	Methods-----	164
5.3.1	Statistical analysis -----	165
5.4	Results -----	166
5.4.1	Monolayer associated sGAG -----	166
5.4.2	Media associated sGAG -----	170
5.4.3	Total sGAG changes -----	172
5.4.4	DNA quantification -----	175
5.4.5	Monolayer sGAG normalised to DNA -----	178
5.4.6	Media sGAG normalised to monolayer DNA-----	180
5.4.7	Total normalised sGAG -----	182

5.4.8	Empty vector cell cultures -----	183
5.5	Discussion-----	186
5.6	Conclusion -----	188
6	Chondrogenesis of cells in pellet culture -----	189
6.1	Introduction -----	190
6.2	Aim -----	191
6.3	Methods-----	191
6.3.1	Statistical significance -----	192
6.4	Results -----	194
6.4.1	Pellet formation and size determination -----	194
6.4.1.1	Pellet density-----	202
6.4.2	sGAG production in pellets -----	204
6.4.3	sGAG content of pellet media -----	207
6.4.4	Total sGAG changes -----	208
6.4.5	DNA content of cell pellets -----	210
6.4.6	Pellet sGAG normalised to DNA -----	214
6.4.7	Media sGAG normalised to pellet DNA -----	216
6.4.8	Total normalised sGAG -----	217
6.4.9	Gene expression -----	218
6.4.10	Pellet histology -----	233
6.4.10.1	Haematoxylin and eosin staining -----	233
6.4.10.2	Picrosirius red staining -----	237
6.4.10.3	Toluidine blue staining -----	242
6.4.11	Pellet immunohistochemistry-----	245
6.4.11.1	Tissue controls -----	245
6.5	Discussion-----	251
6.6	Conclusions-----	257
7	Summative discussion, conclusions and further work -----	259
7.1	Summative discussion -----	260
7.2	Conclusions-----	267
7.3	Future perspectives -----	268
8	References -----	270
9	Appendices-----	302
9.1	Appendix A – Ethical approval documents, Keele Independent Peer Review -----	303
9.2	Appendix A – Ethical approval documents, REC committee review-----	304
9.3	Appendix A – Ethical approval documents, NHS R&D department approval -----	308
9.4	Appendix B – Supplementary figures -----	310
9.4.1	FBS batch testing results -----	310
9.4.2	The influence of BMA13 pellet size on sGAG deposition -----	311

9.5	Appendix C - Certificates of Analysis for FBS batches	312
9.5.1	FBS1 (Lonza)	312
9.5.2	FBS2 (Biosera)	313

## Figures

---

FIGURE 1-1.	SYNOVIAL JOINT ANATOMY.	3
FIGURE 1-2.	THE MAJOR STEPS IN SYNOVIAL JOINT FORMATION.	6
FIGURE 1-3.	LIGHT MICROGRAPHS OF ARTICULAR CARTILAGE.	7
FIGURE 1-4.	CLASSIFICATION OF ARTICULAR CARTILAGE INTO ZONES.	9
FIGURE 1-5.	ELECTRON MICROGRAPHS SHOWING THE ECM COMPARTMENTS OF ARTICULAR CARTILAGE.	11
FIGURE 1-6.	ATOMIC FORCE MICROSCOPY (AFM) HEIGHT IMAGES OF FOETAL EPIPHYSEAL AGGREGAN.	13
FIGURE 1-7.	PATHOLOGY OF OSTEOARTHRITIS.	18
FIGURE 1-8.	CATABOLIC AND ANABOLIC FACTORS THAT REGULATE CHONDROCYTE FUNCTION.	19
FIGURE 1-9.	THE STEPS INVOLVED IN THE ACI PROCEDURE.	22
FIGURE 2-1.	HAND HELD CELL SCEPTER COUNTER.	52
FIGURE 2-2.	CORD AND PLACENTAL BLOOD COLLECTION.	58
FIGURE 2-3.	DENSITY GRADIENT SEPARATION OF BLOOD.	59
FIGURE 2-4.	THE PHOENIX-A SYSTEM FOR RETROVIRAL VECTOR PRODUCTION.	61
FIGURE 2-5.	SUMMARY OF THE PROTOCOL FOR PHOENIX-A TRANSDUCTION OF TARGET CELLS.	63
FIGURE 2-6.	SCANCO MEDICAL $\mu$ CT 40 SCANNER.	71
FIGURE 2-7.	ANALYSIS OF $\mu$ CT SCANNED SAMPLES.	72
FIGURE 2-8.	ETHIDIUM BROMIDE GEL ELECTROPHORESIS.	77
FIGURE 2-9.	QRT-PCR THERMAL CYCLE PROGRAMME.	79
FIGURE 3-1.	BOX AND WHISKER PLOT OF UCB SAMPLES.	94
FIGURE 3-2.	UCB1 RECOVERED CELL MORPHOLOGIES.	96
FIGURE 3-3.	CELLS FROM UCB2 AND UCB3.	98
FIGURE 3-4.	CELLS RECOVERED FROM UCB7 AND UCB8.	100
FIGURE 3-5.	IMMUNOPHENOTYPING OF CELLS FROM UCB8.	101
FIGURE 3-6.	UCB12 SAMPLE FOLLOWING MACS SEPARATION.	102
FIGURE 3-7.	CD45 EXPRESSION OF CD45 MACS SEPARATED CELLS.	103
FIGURE 3-8.	CELL MORPHOLOGY FOLLOWING CD45 MACS SEPARATION.	103
FIGURE 3-9.	CFU-F RECOVERY OF MSCS FROM MNCS.	105
FIGURE 3-10.	CFU-F FORMATION.	106
FIGURE 3-11.	CFU-F CELL MORPHOLOGY.	108
FIGURE 3-12.	CELL RECOVERY IN FBS1 AND FBS2 IN 2% OR 21% O <sub>2</sub> .	109
FIGURE 3-13.	CELL SIZE FOLLOWING RECOVERY FROM MNCS.	110

FIGURE 4-1. RT-PCR DETERMINATION OF <i>HTERT</i> EXPRESSION. -----	129
FIGURE 4-2. RT-PCR DETERMINATION OF <i>HTERT</i> EXPRESSION STABILITY. -----	129
FIGURE 4-3. CELL GROWTH CURVES -----	132
FIGURE 4-4. GROWTH CURVE OF BMA13 IN THE PRESENCE AND ABSENCE OF BFGF. -----	133
FIGURE 4-5. OK3 AND OK3H CELL MORPHOLOGY. -----	135
FIGURE 4-6. BMA13, BMA13H AND BMA13EV CELL MORPHOLOGY. -----	137
FIGURE 4-7. CONFLUENT BMA13, BMA13H AND BMA13EV. -----	137
FIGURE 4-8. 1C6, 1C6H AND 1C6EV CELL MORPHOLOGY. -----	139
FIGURE 4-9. SABGAL STAINING OF CELLS. -----	139
FIGURE 4-10. SABGAL STAINING. -----	141
FIGURE 4-11. QUANTIFICATION OF CELLS WITH SABGAL ACTIVITY. -----	142
FIGURE 4-12. TRI-LINEAGE DIFFERENTIATION OF PARENTAL AND TRANSDUCED CELLS. -----	144
FIGURE 4-13. SPONTANEOUS PELLET FORMATION IN MONOLAYER CHONDROGENIC CULTURES. -----	145
FIGURE 4-14. FLOW CYTOMETRY RESULTS. -----	147
FIGURE 4-15. RELATIVE CELL SIZE. -----	148
FIGURE 4-16. RELATIVE CELL COMPLEXITY. -----	148
FIGURE 4-17. IMMUNOPHENOTYPE OF OK3 AND OK3H. -----	150
FIGURE 4-18. IMMUNOPHENOTYPE OF BMA13 AND BMA13H. -----	151
FIGURE 4-19. IMMUNOPHENOTYPE OF 1C6 AND 1C6H. -----	152
FIGURE 4-20. QUANTIFICATION OF IMMUNOPHENOTYPE MARKERS. -----	153
FIGURE 4-21. POSSIBLE ROUTE TO CELL IMMORTALISATION. -----	157
FIGURE 5-1. CURRENT CLINICAL TRIALS. -----	162
FIGURE 5-2. MONOLAYER ASSOCIATED SGAG. -----	168
FIGURE 5-3. FOLD CHANGE IN MONOLAYER ASSOCIATED SGAG. -----	169
FIGURE 5-4. MEDIA ASSOCIATED SGAG. -----	171
FIGURE 5-5. TOTAL SGAG AT DAY 20. -----	173
FIGURE 5-6. TOTAL SGAG. -----	174
FIGURE 5-7. MONOLAYER DNA CONTENT. -----	176
FIGURE 5-8. FOLD CHANGE IN DNA CONTENT. -----	177
FIGURE 5-9. MONOLAYER ASSOCIATED SGAG NORMALISED TO DNA CONTENT. -----	179
FIGURE 5-10. MEDIA SGAG NORMALISED TO DNA. -----	181
FIGURE 5-11. TOTAL NORMALISED SGAG AT DAY 20. -----	182
FIGURE 5-12. TOTAL NORMALISED MEAN FOLD CHANGE. -----	183
FIGURE 5-13. MONOLAYER AND MEDIA ASSOCIATED ABSOLUTE AND NORMALISED SGAG FROM EMPTY VECTOR CELLS. -----	184
FIGURE 5-14. EMPTY VECTOR MONOLAYER DNA CONTENT. -----	185
FIGURE 6-1. CELL PELLET FORMATION. -----	194
FIGURE 6-2. CELL PELLET IMAGES. -----	195

FIGURE 6-3. CALCULATED PELLET VOLUME. -----	197
FIGURE 6-4. $\mu$ CT DETERMINED PELLET IMAGES. -----	199
FIGURE 6-5. $\mu$ CT DETERMINED PELLET VOLUME. -----	200
FIGURE 6-6. PELLET SIZE AT DAY 20. -----	201
FIGURE 6-7. $\mu$ CT DETERMINED DENSITY ANALYSIS. -----	203
FIGURE 6-8. RELATIVE PELLET DENSITY AT DAY 20. -----	204
FIGURE 6-9. 1C6H $\mu$ CT DENSITY ANALYSIS. -----	204
FIGURE 6-10. SGAG CONTENT OF CELL PELLETS. -----	206
FIGURE 6-11. FOLD CHANGE IN PELLET ASSOCIATED SGAG. -----	207
FIGURE 6-12. SGAG IN SPENT CULTURE MEDIA AT DAY 20. -----	208
FIGURE 6-13. TOTAL SGAG IN PELLETS AND SPENT CULTURE MEDIA AT DAY 20. -----	209
FIGURE 6-14. TOTAL SGAG. -----	210
FIGURE 6-15. CELL PELLET DNA CONTENT. -----	212
FIGURE 6-16. FOLD CHANGE IN PELLET DNA CONTENT. -----	213
FIGURE 6-17. CELLULAR MATERIAL ON MICROCENTRIFUGE TUBES. -----	213
FIGURE 6-18. PELLET ASSOCIATED SGAG NORMALISED TO DNA CONTENT. -----	215
FIGURE 6-19. FOLD CHANGE IN NORMALISED PELLET ASSOCIATED SGAG. -----	216
FIGURE 6-20. MEDIA SGAG NORMALISED TO PELLET DNA. -----	217
FIGURE 6-21. TOTAL NORMALISED SGAG AT DAY 20. -----	218
FIGURE 6-22. HEATMAPS OF RELATIVE GENE EXPRESSION. -----	221
FIGURE 6-23. HEATMAPS OF RELATIVE GENE EXPRESSION. -----	222
FIGURE 6-24. COMPLETE GENE EXPRESSION HIERARCHICAL CLUSTERING DENDROGRAMS AND HEATMAP. -----	223
FIGURE 6-25. BOX AND WHISKER PLOTS OF RELATIVE GENE EXPRESSION IN OK3 CELL PELLETS. -----	226
FIGURE 6-26. BOX AND WHISKER PLOTS OF RELATIVE GENE EXPRESSION IN OK3H CELL PELLETS. -----	227
FIGURE 6-27. BOX AND WHISKER PLOTS OF RELATIVE GENE EXPRESSION IN BMA13 CELL PELLETS. -----	228
FIGURE 6-28. BOX AND WHISKER PLOTS OF RELATIVE GENE EXPRESSION IN BMA13H CELL PELLETS. -----	229
FIGURE 6-29. BOX AND WHISKER PLOTS OF RELATIVE GENE EXPRESSION IN 1C6 CELL PELLETS. -----	230
FIGURE 6-30. BOX AND WHISKER PLOTS OF RELATIVE GENE EXPRESSION IN 1C6H CELL PELLETS. -----	231
FIGURE 6-31. GENES UPREGULATED IN BOTH MM AND PCHM. -----	232
FIGURE 6-32. H AND E STAINING OF PORCINE ARTICULAR CARTILAGE. -----	233
FIGURE 6-33. H AND E STAINING OF PELLETS AT DAY 1. -----	234
FIGURE 6-34. H AND E STAINING. -----	235
FIGURE 6-35. H AND E STAINING OF PELLETS AT DAY 20. -----	236
FIGURE 6-36. PICROSIRIUS RED STAINING OF PORCINE CARTILAGE AND TENDON. -----	237
FIGURE 6-37. PICROSIRIUS RED COLLAGEN STAINING AT DAY 1. -----	239
FIGURE 6-38. PICROSIRIUS RED COLLAGEN STAINING AT DAY 20. -----	240
FIGURE 6-39. PICROSIRIUS RED CROSS-POLARISED LIGHT COLLAGEN STAINING AT DAY 20. -----	241

FIGURE 6-40. TOLUIDINE BLUE STAINING OF PORCINE CARTILAGE AND E11 CHICK FEMUR. ....	242
FIGURE 6-41. TOLUIDINE BLUE SGAG STAINING AT DAY 1. ....	243
FIGURE 6-42. TOLUIDINE BLUE SGAG STAINING AT DAY 20. ....	244
FIGURE 6-43. POSITIVE CONTROL ANTIBODY STAINING. ....	245
FIGURE 6-44. COLLAGEN I DAY 20 IMMUNOPEROXIDASE STAINING. ....	246
FIGURE 6-45. COLLAGEN II DAY 20 IMMUNOPEROXIDASE STAINING. ....	247
FIGURE 6-46. COLLAGEN VI DAY 20 IMMUNOPEROXIDASE STAINING. ....	248
FIGURE 6-47. COLLAGEN X DAY 20 IMMUNOPEROXIDASE STAINING. ....	249
FIGURE 6-48. AGGREGAN DAY 20 IMMUNOPEROXIDASE STAINING. ....	250

## Tables

---

TABLE 1-1. JOINT CLASSIFICATION. ....	2
TABLE 1-2. TYPES OF COLLAGEN AND THEIR ROLE WITHIN ARTICULAR HYALINE CARTILAGE. ....	12
TABLE 1-3. BIOMATERIALS INTENDED FOR USE AS CELL CARRIERS FOR CELL IMPLANTATION FOR CARTILAGE REPAIR. ....	24
TABLE 1-4. MESENCHYMAL AND TISSUE STEM CELL COMMITTEE OF THE INTERNATIONAL SOCIETY FOR CELLULAR THERAPY RECOMMENDED MSC MARKERS. ....	29
TABLE 1-5. EXPRESSION OF A RANGE OF MARKERS IN HMSCS. ....	30
TABLE 2-1. LIST OF MATERIALS, CATALOGUE NUMBERS AND SUPPLIERS. ....	47
TABLE 2-2. RT-PCR PRIMER SEQUENCES. ....	76
TABLE 2-3. QRT-PCR PRIMER SEQUENCES. ....	80
TABLE 3-1. SUMMARY OF THE UCB PLATING CONDITIONS. ....	90
TABLE 3-2. DETAILS OF THE 12 UCB SAMPLES OBTAINED. ....	94
TABLE 3-3. HUMAN MONOCYTE SUB-TYPES. ....	113
TABLE 6-1. DENDROGRAM CLUSTERING CORRELATION COEFFICIENTS. ....	224
TABLE 7-1. KEY ADVANTAGES AND DISADVANTAGES ASSOCIATED WITH CELL TYPES WITH POTENTIAL CELL THERAPY APPLICATIONS. ....	261

## Schemes

---

SCHEME 1. SUMMARY OF THE METHODOLOGY ADOPTED IN CHAPTER 3. ....	92
SCHEME 2. SUMMARY OF THE METHODOLOGY ADOPTED IN CHAPTER 4. ....	127
SCHEME 3. SUMMARY OF THE METHODOLOGY ADOPTED IN CHAPTER 5. ....	165
SCHEME 4. SUMMARY OF THE METHODOLOGY ADOPTED IN CHAPTER 6. ....	193

## Supplementary figures

---

SUPPLEMENTARY FIGURE 1. FBS BATCH TEST RESULTS. -----	310
SUPPLEMENTARY FIGURE 2. SPATIAL PATTERNING OF CHONDROGENESIS INDEPENDENT OF CELL PELLET SIZE. -----	311

# Abbreviations

---

1C6	Human H1 hESC-derived MSC-like clonally-derived cells
1C6EV	Empty vector transduced human H1 hESC-derived MSC-like clonally-derived cells
1C6H	<i>hTERT</i> transduced human H1 hESC-derived MSC-like clonally-derived cells
2D	Two dimensional
3D	Three dimensional
ACAN	Aggrecan core protein
ACI	Autologous chondrocyte implantation
ACT	Autologous chondrocyte transplantation
ACTB	$\beta$ -Actin
ADP	Adenosine diphosphate
AER	Apical ectodermal ridge
aFGF	Acidic fibroblast growth factor
AFM	Atomic force microscopy
ALCAM	Activated lymphocyte cell adhesion molecule
BCAM	Basal cell adhesion molecule
bFGF	Basic fibroblast growth factor
BMA	Bone marrow aspirate
BMA13	MSCs derived from bone marrow aspirate 13 (13 <sup>th</sup> BMA processed in our lab group)
BMA13EV	Empty vector transduced MSCs from bone marrow aspirate 13
BMA13H	<i>hTERT</i> transduced MSCs from bone marrow aspirate 13
BMAC	Bone marrow aspirate concentrate
BMP	Bone morphogenetic proteins
BMSC	Bone marrow stromal cell
BSA	Bovine serum albumin
CD	Cluster of differentiation
CDK4	Cyclin-dependent kinase 4
CFU-F	Colony forming unit-fibroblast
COL10A1	Collagen alpha-1(X) chain
COL1A2	Collagen alpha-2(I) chain
COL2A1	Collagen alpha-1(II) chain
COL3A1	Collagen alpha-1(III) chain
COL6A3	Collagen alpha-3(VI) chain
COMP	Cartilage oligomeric matrix protein
dH <sub>2</sub> O	Distilled water
DMEM	Dulbecco's Modified Eagle Medium
DMSO	Dimethyl sulphoxide
ECM	Extracellular matrix
EDTA	Ethylenediaminetetraacetic acid
ESC(s)	Embryonic stem cell(s)

EV	Empty vector
FBS	Foetal bovine serum
FGF(s)	Fibroblast growth factor(s)
FS	Forward scatter
GAG	Glycosaminoglycan
Gal	Galactose
GAPDH	Glyceraldehyde 3-phosphate dehydrogenase
GDF5	Growth and differentiation factor 5
GGF	Glial growth factor
GlcA	Glucuronic acid
GM-CSF	Granulocyte-macrophage colony-stimulating factor
GMO	Genetically modified organism
GvHD	Graft versus host disease
HEK	Human embryonic kidney
hESC(s)	Human embryonic stem cell(s)
HIF	Hypoxia inducible factor
HLA	Human leukocyte antigen
hMSC(s)	Human mesenchymal stem cell(s)
HRE(s)	Hypoxia response element(s)
HRP	Horseradish peroxidase
HSC(s)	Haematopoietic stem cell(s)
hTERT	Human telomerase reverse transcriptase
ICAM1/3	Intercellular adhesion molecule 1/3
Ig	Immunoglobulin
IGF1	Insulin like growth factor 1
KO-DMEM	Knockout Dulbecco's Modified Eagle Medium
KO-SR	Knockout Serum Replacement
LAMP	Lysosomal associated membrane protein
LFA	Lymphocyte function-associated antigen
L-Glut	L-glutamine
LNGFR	Low affinity nerve growth factor receptor
MACS	Magnetic activated cell sorting
MEF(s)	Mouse embryonic fibroblast(s)
MeICAM	Melanoma-cell adhesion molecule
MHC	Major histocompatibility complex
MM	Maintenance media
MMULV	Moloney murine leukaemia virus
MNC(s)	Mononuclear cell(s)
MSC(s)	Mesenchymal stem cell(s)
GalNAc	N-acetylgalactosamine
GlcNAc	N-acetylglucosamine
NCAM1	Neural cell adhesion molecule 1
NEAA	Non-essential amino acids
NICE	National Institute for Health and Care Excellence

OATS	Osteochondral Autograft Transplant System
OCT4	Octamer binding protein 4
OK3	Primary knee articular cartilage chondrocytes (commercially sourced)
OK3EV	Empty vector transduced primary knee articular cartilage chondrocytes
OK3H	<i>hTERT</i> transduced primary knee articular cartilage chondrocytes
PBS	Phosphate buffered saline
PChM	Pro-chondrogenic media
PCR	Polymerase chain reaction
PDGFR	Platelet-derived growth factor receptor
PECAM1	Platelet endothelial adhesion molecule1
PFA	Paraformaldehyde
Phoenix-A	Phoenix-amphotropic
PSA	Penicillin, streptomycin, amphotericin B
(q)RT-PCR	(Quantitative) reverse transcription-polymerase chain reaction
ROS	Reactive oxygen species
SA $\beta$ Gal	Senescence-associated $\beta$ galactosidase
SASP	Senescence-associated secretory phenotype
sGAG	Sulphated glycosaminoglycan
SLRP	Small leucine rich proteoglycans
SMA	Smooth muscle actin
SOX5	SRY (sex determining region Y)-box 5 /transcription factor SOX5
SOX6	SRY (sex determining region Y)-box 6 /transcription factor SOX6
SOX9/SOX9	SRY (sex determining region Y)-box 9/transcription factor SOX9
SS	Side scatter
SSEA	Stage-specific embryonic antigen
SV40-Tag	Simian vacuolating virus 40-large T antigen
TAE	Tris acetate EDTA
TE	Tris EDTA
TEP1	Telomerase associated protein 1
TERT	Telomerase reverse transcriptase
TGF- $\beta$	Transforming growth factor $\beta$
TRAP	Tartrate resistant acid phosphatase
UC	Umbilical cord
UCB	Umbilical cord blood
VCAM	Vascular cell adhesion molecule
VEGF	Vascular endothelial growth factor

# Publications and presentations

---

## Associated publication

Work detailed in Chapters 4 and 5 has been published in:

Dale, T. P., de Castro, A., Kuiper, N. J., Parkinson, E. K. & Forsyth, N. R. *Immortalisation with hTERT Impacts on Sulphated Glycosaminoglycan Secretion and Immunophenotype in a Variable and Cell Specific Manner*. PLoS ONE 10, e0133745 (2015).

## Other publications

Webb WR, Dale TP, Lomas AJ, Zeng G, Wimpenny I, El Haj AJ, Forsyth NR, Chen GQ. *The application of poly(3-hydroxybutyrate-co-3-hydroxyhexanoate) scaffolds for tendon repair in the rat model*. Biomaterials. **34(28)**, 6683-94 (2013).

Kay AG, Dale TP, Akram KM, Mohan P, Hampson K, Maffulli N, Spiteri MA, El Haj AJ, Forsyth NR. *BMP2 repression and optimized culture conditions promote human bone marrow-derived mesenchymal stem cell isolation*. Regen. Med. **10**, 109–125 (2015).

Kumar, Deepak; Dale, Tina; Yang, Ying; Forsyth, Nicholas. *Self-renewal of human embryonic stem cells on defined synthetic electrospun nanofibers*. Biomed Mater. **10(6)**:065017 (2015)

## Under review

Rahul Agrawal, Tina P. Dale, Mohammed A. Al-Zubaidi, Nicholas R. Forsyth, Ritu Kulshreshtha. *Pluripotent and multipotent stem cells display distinct hypoxic miRNA expression profiles*. PLOS One

## Oral presentations

### TCES (Tissue and Cell Engineering Society) 2015 – Oral presentation

TP Dale, A DeCastro, EK Parkinson, NJ Kuiper, NR Forsyth. *Cell line creation using hTERT immortalisation impacts on sulphated glycosaminoglycan secretion and chondrogenic potential*. Eur Cell Mater. 2015; vol 29, supplement 3, page 19.

### **MSCA (Mercia Stem Cell Alliance) 2014 – Teaser talk**

TP Dale, A DeCastro, EK Parkinson, NJ Kuiper, NR Forsyth. *Immortalisation with hTERT Impacts on Sulphated Glycosaminoglycan Secretion and Immunophenotype in a Variable and Cell Specific Manner.*

### **Poster presentations**

#### **MSCA 2014**

TP Dale, A DeCastro, EK Parkinson, NJ Kuiper, NR Forsyth. *Immortalisation with hTERT Impacts on Sulphated Glycosaminoglycan Secretion and Immunophenotype in a Variable and Cell Specific Manner.*

#### **TERMIS (Tissue Engineering and Regenerative Medicine International Society) EU Genoa 2014**

TP Dale, A DeCastro, EK Parkinson, NJ Kuiper, NR Forsyth. *Immortalisation with hTERT Impacts on Sulphated Glycosaminoglycan Secretion and Immunophenotype in a Variable and Cell Specific Manner.*

#### **BIRAX (Britain Israel Research and Academic Exchange Partnership) 2014**

TP Dale, A DeCastro, EK Parkinson, NJ Kuiper, NR Forsyth. *Immortalisation with hTERT Impacts on Sulphated Glycosaminoglycan Secretion and Immunophenotype in a Variable and Cell Specific Manner.*

#### **MSCA 2013**

TP Dale, A DeCastro, EK Parkinson, NJ Kuiper, NR Forsyth. *Telomerase transduction influences cell proliferation and sulphated glycosaminoglycan production and retention in a cell specific manner*

#### **TERMIS EU Istanbul 2013**

TP Dale, NJ Kuiper, NR Forsyth. *Quantification of Sulphated Glycosaminoglycan Production During Chondrogenesis by Human Primary Chondrocytes and Stem Cells.*

#### **BIRAX 2011**

Tina P Dale, Alasdair Kay, Khondoker Akram and Nicholas R Forsyth. *Evaluating Hypoxic Systems for Mesenchymal Stem Cell Recovery.*

# Acknowledgements

---

I would like to sincerely thank my supervisor Nick Forsyth for having confidence in me and my work, for allowing me the freedom to work independently but being supportive when I needed it and I'm especially grateful for his optimism in the face of my tendency for pessimism. I would also like to thank my co-supervisor Nikki Kuiper and my advisor Catriona Kelly for their supportive comments.

The umbilical cord blood work was possible firstly due to the study participants, who kindly agreed to donate their cord blood to the project and due to the contributions of the University Hospital of North Midlands, particularly the obstetrics and gynaecology Consultant Ms Fidelma O'Mahony and the obstetrics theatre staff, but also the Research and Development Office who ensured that we met the requirements for ethical approval for the project.

I would like to acknowledge the kind contributions of Prof. Ken Parkinson and Alice de Castro along with the Blizzard Institute at QMUL/Barts and The London for providing facilities and their support for the transduction of my cells.

The work described in this Thesis was principally funded by the EPSRC as part of the Loughborough, Keele and Nottingham Universities' Centre for Doctoral training in Regenerative Medicine and the umbilical cord blood work further supported via a North Staffordshire Medical Institute grant.

I'd like to thank Hari and Mike for providing some control tissue for histology. But mostly for them, and pretty much everyone else at the Guy Hilton, past and present, thank you for making it a great place to come to work every day, even when things aren't going so well. It's like having a great big, dysfunctional family and there's always a shoulder to cry on.

Finally, thank you Ryan for all the support, encouragement and nagging it took to help get me to this point.



Keele University

---

# **Chapter 1**

---

## ***Introduction***

## 1.1 The human skeleton

The human body is supported by the skeletal system that acts as a series of levers which, along with the muscles and essential connective tendons and ligaments, enable movement. Typically consisting of 270 bones at birth and reducing to 206 at skeletal maturity as a result of the fusion of bones the skeleton can be subdivided into the vertebral column, ribcage and skull forming the axial skeleton and the pelvis, and bones of the shoulders and limbs forming the appendicular component of the skeleton<sup>1</sup>. Where bones come into contact with each other joints or articulations are formed and these can be classified broadly into three types according to the resulting anatomy and physiology as shown in Table 1-1. The joints permitting movement are the synovial or diarthroidal joints.

**Table 1-1. Joint classification.** Joints can be classified by both structural characteristics or by the degree of movement associated with the joint type; as indicated these usually overlap. (From information in Graaf *et al*, 2001<sup>2</sup>.)

Joint classification - structural	General features	Joint classification – by degree of movement	Examples
<b>Fibrous</b>	Immovable – connected by fibrous connective tissue	Synarthroses	Cranial sutures
<b>Cartilaginous</b>	Slightly movable – connected by fibrocartilage	Amphiarthroses	Pubic symphysis, intervertebral disks
<b>Synovial</b>	Movable – complex joint structure determines extent of movement	Diarthroses	Many including: shoulder, hip, knee, elbow, ankle

## 1.2 Synovial joints

Synovial (diarthroidal) joints are those that allow relatively free movement around the joint, with the extent of the movement being dictated by the specific joint anatomy. In general, the bones

forming synovial joints (Figure 1-1A) are separated by a synovial fluid filled cavity and are completely encapsulated by a fibrous synovial capsule and the synovial membrane. Type B fibroblastic synoviocytes within the synovial membrane secrete hyaluronan and proteoglycan 4 (lubricin/superficial zone protein) into the synovial fluid, around 1 mL of which typically fills the joint space in the knee<sup>3</sup>. The ends of the bones forming synovial joints are covered in a thin layer of articular cartilage which is essential to protect the bone surfaces. The joints may be further stabilised by the presence of supporting ligaments and muscles (Figure 1-1B).

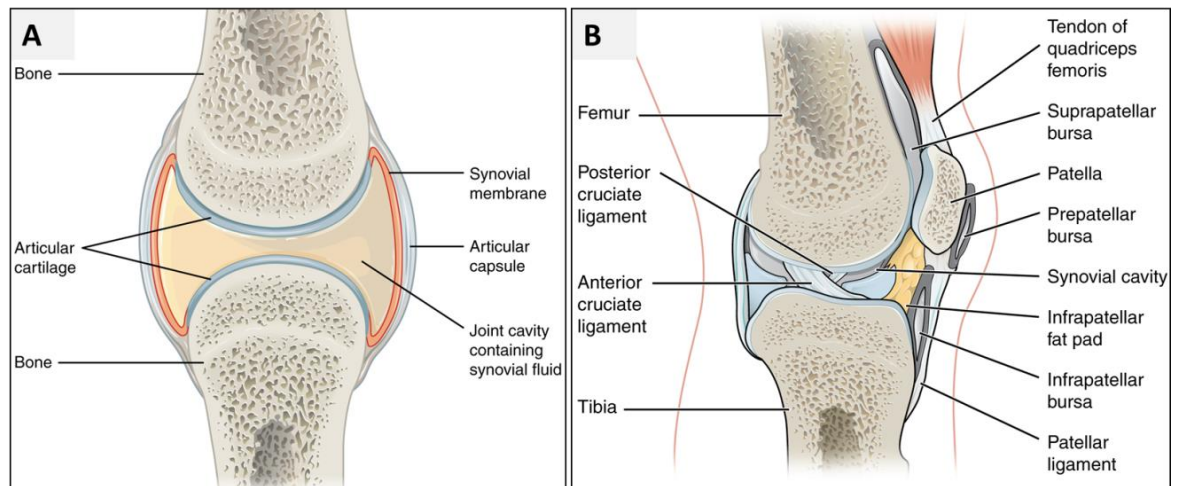


**Figure 1-1. Synovial joint anatomy.** (A) Typical features of a simplified synovial joint (knee). (B) Supporting anatomical structures that may be necessary for joint stability. (Images adapted from OpenStax Anatomy and Physiology<sup>4</sup>.)

Licensed by Rice University under a Creative Commons Attribution License (by 4.0).

The articular, hyaline cartilage that overlays the bones provides both an extremely low friction gliding surface to allow free movement and acts to protect and cushion the bone, preventing damage from the high forces generated within joints<sup>5</sup>. It also protects the subchondral bone from fluid influx and fluid flow that can cause osteolysis and bone cysts<sup>6</sup>. The high degree of anisotropic structural organisation and specific ECM composition found within the thin (1-4 mm) layer of

hyaline cartilage confers the necessary biomechanical properties to ensure normal function for many years.

### **1.3 Articular cartilage**

#### **1.3.1 Embryonic articular cartilage development**

During embryonic development a cartilaginous precursor of the appendicular component of the human skeleton is produced. The majority of this template goes on to be replaced by mineralised bone tissue via the process of endochondral ossification<sup>7</sup>. The cartilaginous tissue template develops from early undifferentiated mesenchymal tissue originating from the mesodermal germ layer of the embryo. Knowledge of the events of limb patterning during embryogenesis are incomplete<sup>8</sup>; however, it appears that initially proliferation of undifferentiated cells is driven by the mitogenic influence of fibroblast growth factors (FGFs) secreted from the embryonic limb bud apical ectodermal ridge (AER), this proliferation continues; possibly as a result of reducing the proximity of the more distal cells to the AER the FGF mitotic influence is gradually reduced. As the morphogenetic gradients from several signalling centres influencing the cells change, cells begin the process of chondrogenic differentiation. Broadly, this proceeds via condensation of the tissue where mesenchymal cells become very closely associated, expressing a variety of cell adhesion molecules including N-Cadherin, neural-cell adhesion molecule 1 (NCAM1), thrombospondin-4, versican and tenascin-C<sup>9</sup>. Condensation is followed by cell differentiation and the onset of the synthesis of a cartilaginous ECM<sup>10</sup>.

The molecular mechanisms driving the process of chondrogenesis and importantly the prevention of terminal differentiation and endochondral ossification are not yet fully characterised; nevertheless, some important signalling molecules including transforming growth factor beta (TGF- $\beta$ ), transcription factor SOX9, Wnt9a, Noggin and growth and differentiation factor 5 (GDF5) have been identified<sup>11</sup>. SOX9 is a key transcription factor expressed throughout chondrogenesis, directly controlling levels of cartilage ECM protein gene expression and negatively regulating

endochondral ossification promoting a long-term hyaline cartilage phenotype. The *SOX9* gene is expressed in all chondrogenic cells but is down-regulated in hypertrophic chondrocytes<sup>12</sup>. *SOX9* acts both directly and in combination with the transcription factors *SOX5* and *SOX6* to promote the chondrogenic phenotype, including direct upregulation of type II collagen and aggrecan<sup>13</sup>.

The early pre-cartilaginous mesenchymal blastema that forms the presumptive bone is continuous, with no defined joint positions; the joint positions become defined when an 'interzone' develops at the prospective joint location (Figure 1-2). Mesenchymal cells in the interzone area form a thin layer of very closely associated cells distinguishable from the remaining blastema. It is believed that the interzone area then becomes a signalling centre controlling the subsequent joint development. Following interzone specification joint development continues with inhibition of cartilage promoting bone morphogenetic proteins (BMPs) by antagonists like *Noggin* and *Chordin*. The loss of this BMP inhibition is known to cause abnormal syntosis whereby the joint(s) fails to form and the bone remains completely fused<sup>14</sup>. The converse also appears to be the case with *Noggin* overexpression negatively impacting the process of osteogenesis<sup>15</sup>. Following the interzone development the cartilage anlagen separates or 'cavitates' to create the joint space<sup>16</sup>. Although the signals specifying the interzone have yet to be fully elucidated, the next stage of cavitation appears to be as a result of changes in the cluster of differentiation (CD)44 receptor expression and hyaluronan glycosaminoglycan (GAG) production and distribution in response to mechanical stimuli at the joint position<sup>17</sup>.

It is likely that the articular cartilage develops from the cells located immediately adjacent to the interzone region<sup>16</sup>. A study of the gene expression of cells within the interzone region in a mouse model has demonstrated a variation in the expression of the cartilage matrix protein *matrilin-1*<sup>18</sup>. The study confirmed that articular chondrocytes, known to lack the expression of *matrilin-1*<sup>19</sup>, don't express *matrilin-1* at any stage of joint development in contrast to other chondrogenic cells destined to become other joint tissues<sup>18</sup>. As an exception to this, within osteoarthritic tissues *matrilin-1* is expressed by articular chondrocytes prior to histological evidence of tissue

degeneration<sup>20</sup>. Studies such as these provide strong evidence that articular cartilage chondrocytes are distinct from chondrocytes that form cartilage destined for endochondral ossification and that these cells are specified at an extremely early stage of the joint formation process<sup>18</sup>.

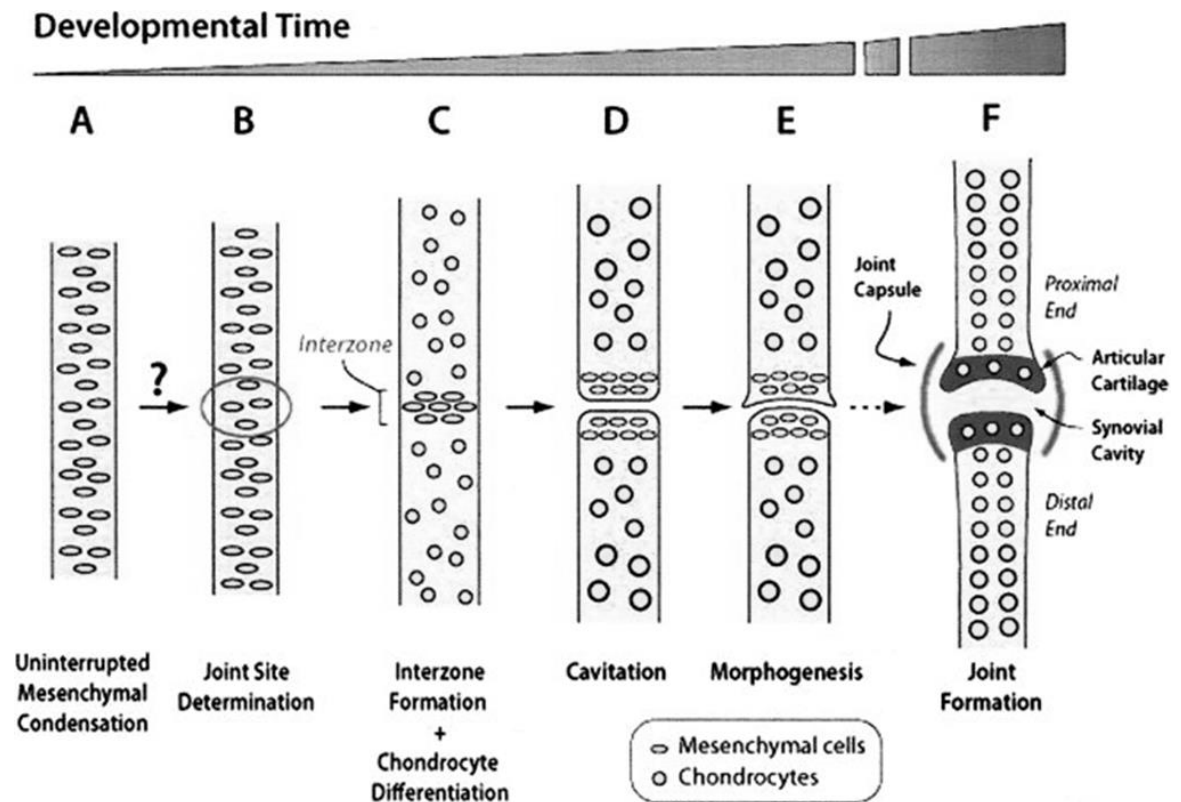


**Figure 1-2. The major steps in synovial joint formation.** A: Mesenchymal pre-chondrogenic condensations appearing in the early limb autopod exhibit no overt signs of joint formation and are thus interrupted. B: Unknown patterning mechanisms determine the exact location for joint initiation. C: The interzone forming at each prescribed joint site represents the first overt morphological sign of joint formation and is characterised by further gathering and condensation of cells. Mesenchymal cells constituting the bulk of the condensations differentiate into chondrocytes and establish the cartilaginous skeleton. D: The cavitation process begins and will eventually lead to a physical separation of the adjacent skeletal anlagen and formation of the synovial cavity. E: Morphogenetic processes begin to mould the opposing sides of the joint into reciprocal shapes and interlocking structures. F: Eventually, all the distinct components of a mature joint form and include articular cartilage, capsule and a full-fledged synovial cavity. Note that the above phases of joint development are continuous and are presented here as distinct events only for descriptive purposes.

Reprinted from Pacifici *et al*, 2005<sup>21</sup> with permission from John Wiley and Sons Inc.

### 1.3.2 Postnatal articular cartilage

Following birth mammalian articular cartilage continues to act as a growth plate region for the epiphyseal bone contributing to its growth in all directions. At this stage of development the cartilage is thicker and much more isotropic in its organisation than it will later become. Structural changes in the articular cartilage of rabbits' cartilage have been observed to occur mainly in the first 3 months following birth (Figure 1-3) which represents puberty/sexual maturity in these animals<sup>22</sup>.

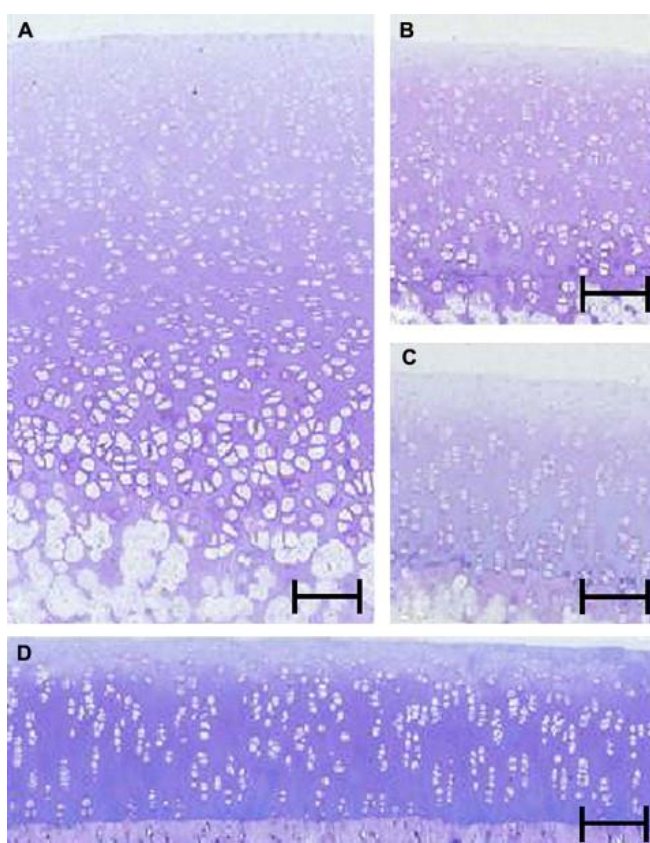


**Figure 1-3. Light micrographs of articular cartilage.** Tissue derived from the medial femoral condyle of New Zealand white rabbits 1 month (A), 2 months (B), 3 months (C) and 8 months (D) after birth. The images illustrate the transition from an isotropic cellular organization 1 month after birth (A) to a highly anisotropic one by the third postnatal month (C). At this latter stage, the architecture resembles that in the adult animal (D). The change in structural organization is accompanied by a decrease in the overall height of the articular cartilage layer. One-micrometre-thick sections stained with toluidine blue. Scale bars: A = 220  $\mu\text{m}$ ; B, C, D = 110  $\mu\text{m}$

Reprinted from Hunziker et al, 2007<sup>22</sup> with permission from Elsevier

These changes leading to the maturation of the cartilage appear to be as a result of the resorption of the cartilage and replacement with bone tissue by endochondral ossification whilst new articular cartilage is deposited in an appositional manner at the articular surface by a body of stem cells and transit amplifying cells residing and proliferating in the superficial and transitional zones<sup>22,23</sup>.

### **1.3.3 Mature articular cartilage**

At skeletal maturity human articular cartilage has a very low cellularity with a relatively small number of chondrocytes (<5% wet weight or approximately 1.65% of the total tissue volume<sup>24</sup>) embedded within a dense, highly hydrated ECM. Tissue cellularity decreases with both depth from the articular surface, and age, continuing to change during adolescence. Cells, particularly in the deeper tissue layers, can frequently be found in pairs, clusters or columns rather than in isolation<sup>25</sup> and in the mature tissue are post-mitotic<sup>13</sup>. The tissue is avascular, alymphatic and aneural throughout and relies upon diffusion gradients with the synovial fluid and subchondral bone for nutrient and waste exchange, a process that is assisted by tissue fluid flow induced by pressure changes within the joint. The poor nutrient and oxygen supply confer a lower metabolic activity to the cells and the paucity of cells ensures that the rate of tissue turnover is extremely low with the collagen II in the ECM having a half-life of 117 years in comparison with the collagen found in skin which has a half-life of 15 years when determined by the rate of accumulation of advanced glycation end products<sup>26</sup>.

The ECM consists primarily of collagen fibres embedded in a proteoglycan rich ground substance at a ratio estimated to be between 10:2 to 10:3 by mass (1:2 to 1:3 considering only hydroxyproline content)<sup>27</sup> and is highly hydrated varying from 65-80% with progression from the surface<sup>28</sup>. Through the tissue depth zones with varying composition and structural organisation can be noted within cartilage (Figure 1-4). With the progression from the articulating surface to

the sub-chondral bone they can be categorised as: i. superficial or tangential zone, ii. middle zone, iii. deep zone, iv. calcified zone.

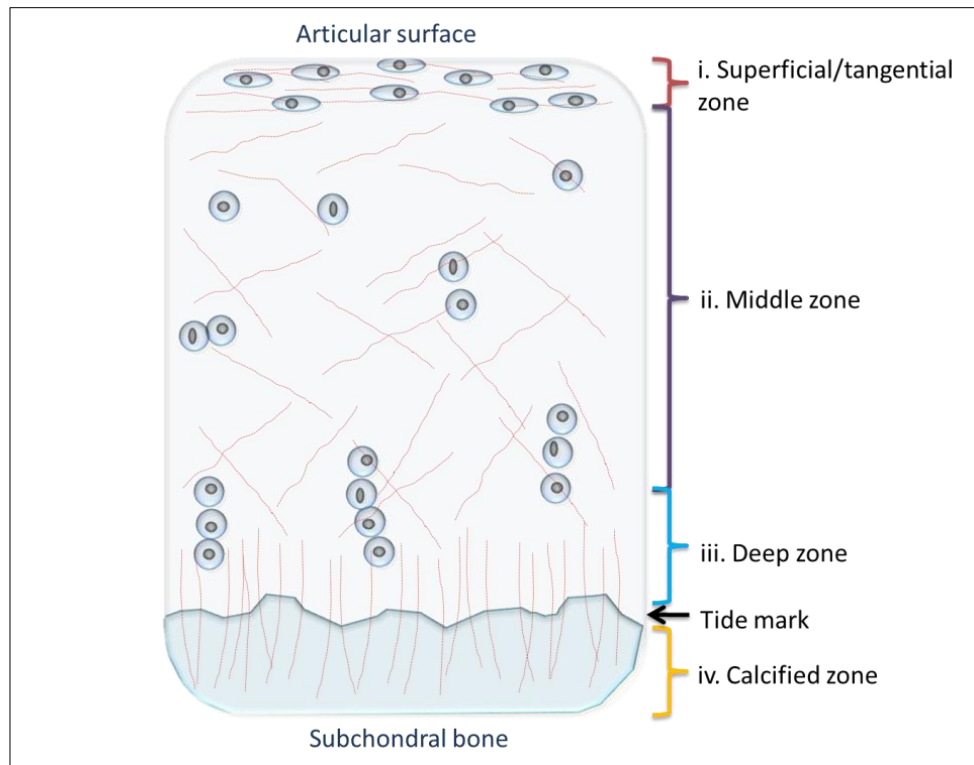


**Figure 1-4. Classification of articular cartilage into zones.** Cartilage is typically divided into four zones, from the surface: superficial zone, middle zone, deep zone and calcified zone separated from the cartilage by the tide mark.

The superficial zone accounts for 10% of the total cartilage depth and effectively resists shear and tensile stresses. Within this layer thin collagen fibres are numerous and aligned parallel to the surface, chondrocytes are present in relatively high numbers and are flattened and found as single cells; compared to the deeper zones the proteoglycan concentration is relatively low<sup>29</sup>. The middle zone accounts for a further 40-60% of the cartilage thickness, collagen fibres are thicker and are aligned obliquely rather than horizontally with fewer chondrocytes adopting a more rounded morphology, they are also more commonly found in clusters rather than in isolation<sup>24</sup>. The middle zone is suited to resisting compressive forces. The deep zone, making up the

remaining 30% of the cartilage, also resists compressive forces; here the largest collagen fibres are found arranged perpendicularly to the articulating surface, as are columns of chondrocytes. These fibres act to anchor the cartilage to the bone as they continue through the deep zone into the calcified zone. The calcified zone is bordered by a 'tide mark' marking the onset of tissue that has progressed further through the process of endochondral ossification and has become mineralised sub-chondral bone tissue.

There are further distinctions apparent within the matrix dependent upon the proximity to the embedded chondrocytes; immediately surrounding cells is the pericellular matrix with both cell(s) and the immediate pericellular matrix together forming the chondron<sup>30</sup> (Figure 1-5), surrounding the chondron is the territorial matrix with the remaining ECM being classified as interterritorial matrix. The pericellular matrix components in direct contact with the chondrocytes influence their behaviour and chondrocytes enzymatically isolated from the surrounding pericellular matrix have been found to behave differently *in vitro* than intact chondrons that retain the pericellular matrix<sup>30</sup>. Cellular turnover of the matrix is believed to occur only in the immediate vicinity of the chondrocytes (within 8µm) of the cell membrane, in young tissue this means that much of the matrix is within this zone of potential remodelling, whereas in older, more hypocellular tissue this zone excludes a significant proportion of the matrix<sup>25</sup>.

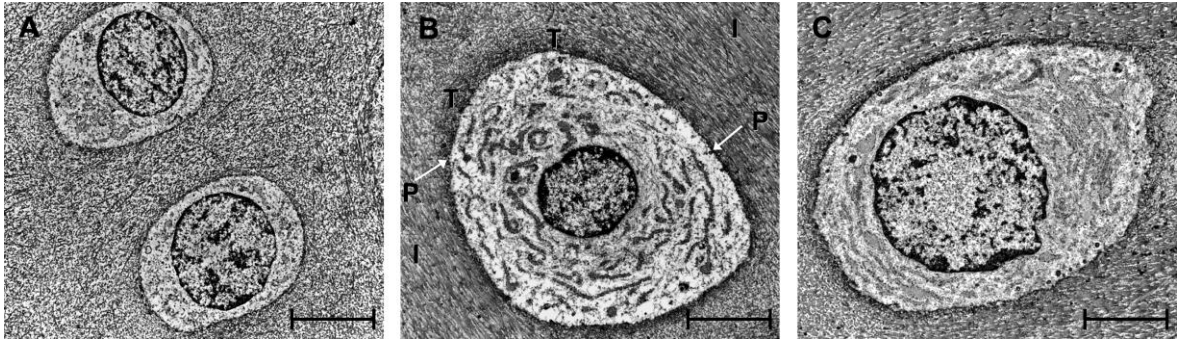


**Figure 1-5. Electron micrographs showing the ECM compartments of articular cartilage.** Electron micrographs of chondrocytes within the radial zone of articular cartilage tissue derived from the medial femoral condyle of New Zealand white rabbits 1 month (A), 3 months (B) and 8 months (C) after birth. In 1-month-old rabbits (A), the collagen fibrils are distributed randomly (isotropically) and homogeneously throughout the entire extracellular space. No distinct compartmentalisation of the matrix is apparent. In 3- (B) and 8-month-old rabbits (C), the extracellular space is organized into distinct pericellular (P), territorial (T) and interterritorial (I) compartments. The narrow pericellular matrix compartment is highly electron-dense owing to the abundance of RHT-precipitated proteoglycans. Within the territorial compartment, the collagen fibrils are arranged in a typically basket-like fashion around the cells. Within the interterritorium, which constitutes the bulk of the extracellular space, the collagen fibrils are oriented parallel to each other and in a predominantly longitudinal direction. Scale bars: A = 10  $\mu\text{m}$ ; B, C = 5  $\mu\text{m}$ .

Reprinted from Hunziker et al, 2007<sup>22</sup> with permission from Elsevier

## 1.4 The extracellular matrix

### 1.4.1 Collagen

A key component of ECM throughout the body the collagens represent a family of proteins that typically assemble in a hierarchical manner allowing the formation of supra-molecular structures including fibrils/fibres and sheets. At the simplest level collagen consists of a triple helical structure of amino acid chains, referred to as  $\alpha$  chains, forming the procollagen molecule<sup>31</sup>. Different combinations of identical or differing  $\alpha$  chains constitute the different collagen types and this, along with interaction of the procollagen with other ECM constituents including other collagens, controls the higher level protein structure following procollagen processing<sup>32</sup>.

Hyaline cartilage ECM contains abundant collagen (Table 1-2.) around 95% of which is type II fibrillar collagen; it provides the tensile strength that is required to give articular cartilage its resistance to loading. Types IX and XI, present at around 1% and 3%<sup>33</sup>, act to stabilise or direct the

crosslinking of the type II collagen and are therefore found distributed within the collagen fibres throughout cartilage<sup>34</sup>. Type VI collagen, present at 1-2%<sup>33</sup>, has a role in the attachment of the chondrocytes to their immediate ECM and is found at high concentrations in the pericellular region<sup>35</sup>. Collagen fibres in the pericellular region are also typically finer than those in the territorial and inter-territorial regions<sup>29</sup>. Type X collagen is found in the calcified, hypertrophic regions of the cartilage and can be considered a marker of hypertrophic chondrocytes<sup>36</sup>. Type I collagen is the primary collagenous component of bone tissue and fibrocartilage and is also considered a marker of inappropriate matrix production although type I collagen has also been found to be expressed by cells in freshly isolated, non-calcified cartilage tissue<sup>37</sup>.

**Table 1-2. Types of collagen and their role within articular hyaline cartilage.** (Adapted from data in Ross & Pawlina 2006 ch. 6<sup>38</sup> and Wu et al 2010<sup>39</sup>.)

	<b>Primary Role</b>	<b>Polypeptide Chains</b>
<b>Type II</b>	Fibrillar collagen, represents the bulk of the structural collagen in cartilage	$[\alpha 1(\text{II})]_3$
<b>Type III</b>	Fibrillar collagen, also found in other tissues, in cartilage forms a mesh crosslinked with other type III fibres and type II fibres	$[\alpha 1(\text{III})]_3$
<b>Type VI</b>	Pericellular fibrillar collagen (“chain and bead” structure), assists in attaching chondrocytes to ECM	$[\alpha 1(\text{VI})]_2 \alpha 2(\text{VI})$ or $\alpha 1(\text{VI}) \alpha 2(\text{VI}) \alpha 3(\text{VI})$
<b>Type IX</b>	Fibril Associated Collagens with Interrupted Triple helices (FACIT) cartilage, associated with type II fibres, facilitates fibril interaction with proteoglycans	$\alpha 1(\text{IX}) \alpha 2(\text{IX}) \alpha 3(\text{IX})$
<b>Type X</b>	Organises collagen fibrils into three dimensional (3D) hexagonal lattice, typical of hypertrophic cartilage	$[\alpha 1(\text{X})]_3$
<b>Type XI</b>	Regulates collagen fibril size	$[\alpha 1(\text{XI})]_2 \alpha 2(\text{XI})$ or $\alpha 1(\text{XI}) \alpha 2(\text{XI}) \alpha 3(\text{XI})$

#### 1.4.2 Articular cartilage proteoglycans and glycosaminoglycans

Proteoglycans consist of one or more GAGs covalently linked to protein cores forming highly negatively charged proteoglycans. In the articular cartilage ECM the major proteoglycan by mass is aggrecan, a large aggregating proteoglycan formed from numerous chondroitin sulphate and keratan sulphate GAG chains attached to an aggrecan specific protein core. These aggrecan monomers further attach via the hyaluronan binding domain of their protein core to the GAG hyaluronan, a connection that is stabilized by the presence of a link protein. These extremely large aggregates ensure that aggrecan is retained within the matrix and act to prevent the loss of smaller molecules<sup>40</sup>. The keratan and chondroitin sulphated (s)GAGs contain multiple negatively charged sulphate and carboxylate functional groups all of which repel each other creating a 'bottlebrush' structure at both the individual aggrecan molecule (Figure 1-6) and the aggregate scale.

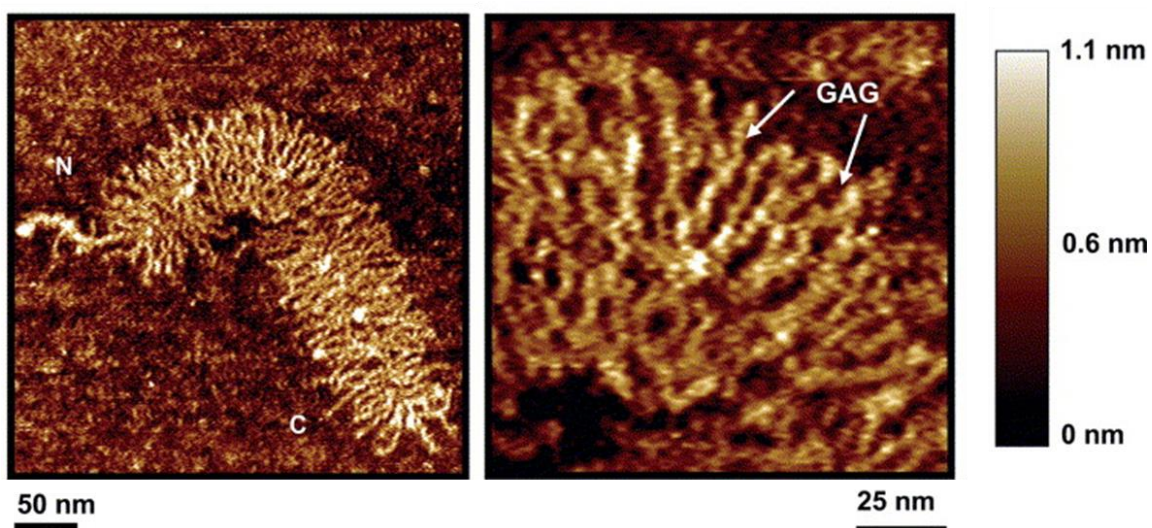


**Figure 1-6. Atomic force microscopy (AFM) height images of foetal epiphyseal aggrecan.** Low and high resolution AFM images of an aggrecan monomer showing the attached GAGs.

Reproduced from Ng *et al*, 2003<sup>41</sup> with permission from Elsevier.

The accumulation of negative charge conferred by proteoglycans serves to attract cations which then cause water to enter the tissue to maintain the osmotic balance with the surrounding synovial fluid<sup>42</sup>. It is this hydrostatic pressure within the tissue that maintains the ECM collagen fibres in tension, particularly when the tissue bulk is under the influence of compressive forces and the pressure is further increased. There is significant resistance to fluid flow within the tissue when a force is rapidly applied such as that found during joint loading due to the low porosity of the tissue and the charge interactions between water and proteoglycans allowing the tissue to withstand extremely high forces as these are largely borne by the water component of the tissue. With aging the average molecular mass of aggrecan has been found to decrease resulting in an increase in its molar concentration. There is also an accumulation of non- or poorly glycosylated protein from the hyaluronan binding region of the protein core reflecting a change in synthesis or degradation rates<sup>40</sup>.

A second large aggregating chondroitin sulphate proteoglycan – versican - has also been identified in cartilage. Typically having a wider tissue distribution than aggrecan, versican can also interact with hyaluronan and may have a role during joint development at the interzone, possibly by restricting innervation and vascularisation of the tissue<sup>43,44</sup>.

### **1.4.3 Small leucine-rich repeat proteoglycans**

In addition to aggrecan articular cartilage contains the small leucine-rich repeat proteoglycans (SLRPs) decorin, biglycan, fibromodulin and lumican. These SLRPs represent only a small proportion of proteoglycan by mass; however, they are present in a comparable molar quantity to that of aggrecan. Decorin and biglycan contain the sGAG chondroitin/dermatan sulphate, lumican and fibromodulin both contain keratan sulphate. The SLRP proteoglycans decorin, fibromodulin and lumican are often found associated with collagen fibrils and are believed to have a regulatory role in fibril synthesis and matrix interaction, they are also known to interact with non-fibrillar collagens found in the ECM<sup>42</sup>.

The cartilage ECM structure and organisation ensures that the tissue meets the demands placed upon it by joint motion: however, the ECM serves more than a mechanical role, influencing cellular function. Proteoglycans in the matrix can sequester growth factors with the potential to maintain a reservoir of the factor in proximity to the cells, and to modulate their influence upon the cells. Decorin can bind TGF- $\beta$ , a promoter of proteoglycan synthesis<sup>45</sup>, and in doing so can modulate its effects providing both a feedback mechanism and an ECM reservoir of growth factor to control proteoglycan synthesis and possibly cartilage remodelling<sup>42</sup>. Heparan sulphate binds numerous growth factors including basic fibroblast growth factor (bFGF), acidic fibroblast growth factor (aFGF), granulocyte macrophage colony stimulating factor (GM-CSF), interleukin-3 (IL-3) and interferon gamma (IFN $\gamma$ )<sup>42</sup>.

#### **1.4.4 Glycosaminoglycans**

By far the most abundant sGAG within the articular cartilage is chondroitin sulphate, accounting for 80% of the sGAG present it is a polysaccharide consisting of repeating glucuronic acid (GlcA) and *N*-acetylgalactosamine (GalNAc) disaccharide units. The disaccharide can be sulphated at the GlcA C2 position, the GalNAc C4, GalNAc C6 or both GalNAc C4 and C6 with sulphation at C4 or C6 being most common<sup>46</sup>. The chain length, terminal saccharide and extent and position of sulphation have been found to vary with age, with an overall decrease in C4 sulphation and an increase in sulphation at C6 from birth to 20 years<sup>46</sup>. Relatively lower sulphation has been found within the linkage region than the main body of the chain<sup>47</sup>. Zonal variations have also been noted corresponding to variation in tissue depth and topographical location<sup>46</sup>. Changes in sulphation have also been noted when cartilage is in a diseased state with reductions in the terminal residue sulphation from 60% to 30%<sup>48</sup>.

A further 5-20% of the sGAG content is keratan sulphate, with repeating disaccharides of galactose (Gal) and *N*-acetylglucosamine (GlcNAc). Keratan sulphate can also be sulphated to varying degrees at the C6 position of one or both of the monosaccharide units and like

chondroitin sulphate has also been found to exhibit changes in chain length and the degree of sulphation with tissue age<sup>42</sup>, with an increase in the proportion of keratan sulphate with increasing age<sup>40</sup>. The extent and positioning of sulphation in both chondroitin and keratan sulphate confer different properties upon the GAGs affecting their interaction with chondrocytes and other matrix molecules.

Hyaluronan is found in both the synovial fluid and in the articular cartilage and is a polysaccharide made up of repeating disaccharide sub-units of GlcA and GlcNAc. In synovial fluid it is present at approximately 3.1-4.1 mg/mL with a weight average molecular weight of 6-7 MDa<sup>3</sup>. In the articular cartilage hyaluronan represents 1-10% of the total GAG and it is present both as a free GAG and as the backbone for aggrecan aggregation where up to one hundred aggrecan molecules attach to a single hyaluronan chain<sup>49</sup>. There is evidence that the hyaluronan content becomes reduced with increasing age<sup>47</sup> although this is in contrast to previous evidence that it increased to age 30 then remained largely static<sup>50</sup>.

## **1.5 Cartilage ageing, damage and degeneration**

### **1.5.1 Ageing**

The structure of cartilage is not static throughout the lifetime of an individual; following tissue maturation there is constant activity by the chondrocytes to maintain the structure of the cartilage by interstitial growth and to replace cartilage that is degraded at the articulating surface despite the low co-efficient of friction. However, the level of ECM molecule synthesis declines with increasing age of the individual, possibly as a result of reduced responsiveness of chondrocytes to anabolic growth factors like insulin like growth factor 1 (IGF1)<sup>51</sup>, which along with a reduction in cellularity<sup>52</sup> leads to a reduction in the chondroitin sulphate and aggrecan content of the cartilage and a concomitant reduction in the water content. Not only is there a reduction in the overall GAG content, there are changes in the GAG structures including the extent and position of sulphation. The collagen within the ECM becomes increasingly cross-linked, increasing

the cartilage stiffness<sup>52</sup>. These changes in the ECM reduce the ability of the cartilage to resist the forces placed upon it and this is reflected in a gradual degeneration of the cartilage structure. This frequently progresses to the degenerative disease state osteoarthritis.

### **1.5.2 Damage and degeneration**

The avascular, aneural, and hypocellular nature of the cartilage tissue is detrimental when the tissue sustains physical damage, often due to sports related injuries. It was noted in 1743<sup>53</sup> based on observation and historical reports that once damaged the cartilage within joints was intractable to treatment, and this remains the case today. Damaged mature cartilage, particularly partial thickness chondral defects, will have a negligible healing response to injury although interestingly experimental animal models demonstrate that foetal cartilage will completely heal partial thickness defects with little to distinguish the healed tissue from the normal undamaged tissue<sup>54</sup>. There are few warning signs of early tissue damage as no pain is felt until the injury progresses to the subchondral bone with its associated nerves, and injuries are not generally repairable due to the low intrinsic metabolic rate and cellular and ECM turnover.

Arthritic and rheumatic diseases, mainly osteoarthritis and rheumatoid arthritis, plus a number of much less common diseases that affect the joints, are the most common cause of disability in the United States<sup>55</sup>. Osteoarthritis is by far the most prevalent and is responsible for 80% of cases in the UK<sup>56</sup>, with US based estimates suggesting that symptomatic osteoarthritis affects 12% of individuals over the age of 24 increasing to 33% for those over 60<sup>57</sup> and around 50% by 85. The risk further increases with an increase in body mass index<sup>58</sup>.

Osteoarthritic joints (Figure 1-7) are characterised by thinning, fibrillation, damage, and loss of the hyaline cartilage. As a whole-joint disease, there is also formation of bony spurs called osteophytes at the joint periphery, bony sclerosis, and some inflammation affecting the synovium. Surrounding muscles may be weakened and ligaments may develop laxity<sup>59</sup>. The

aetiology of the disease or, in fact, whether there is a single disease process, is unclear and it is likely that the disease may be as a result of combined systemic and extrinsic causes.

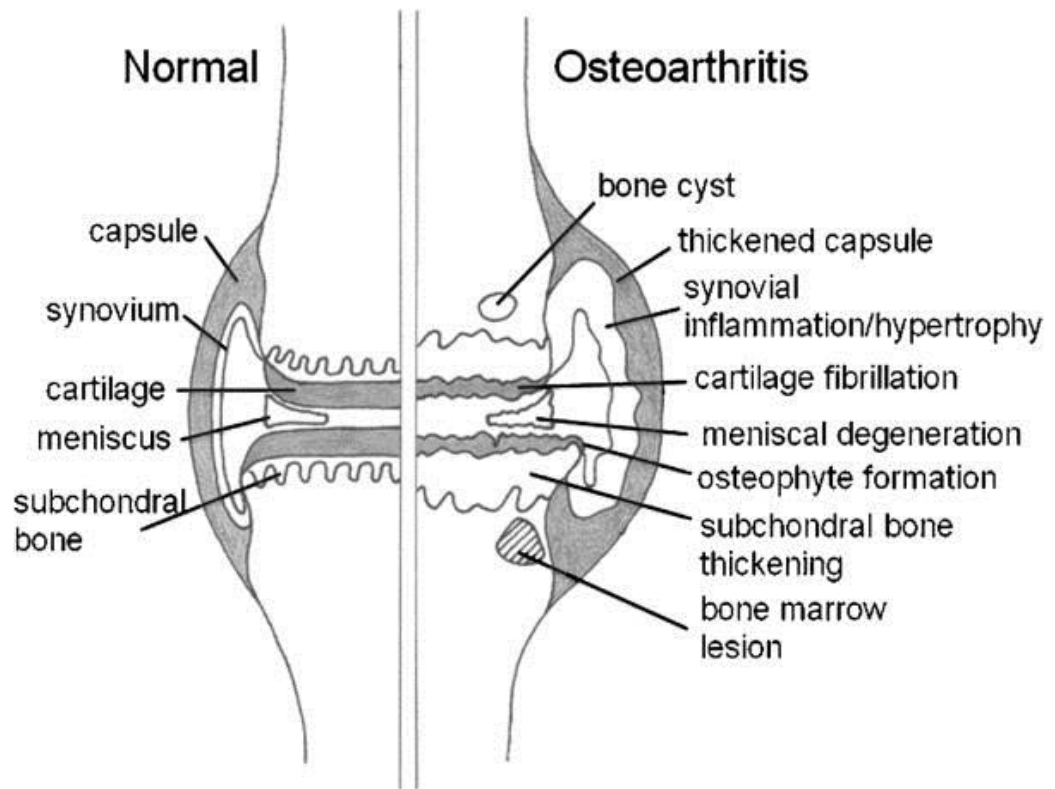


**Figure 1-7. Pathology of osteoarthritis.** The osteoarthritic joint is characterized by degradation and loss of the articular cartilage, thickening of the subchondral bone accompanied by formation of bone marrow lesions and cysts, osteophytes at the joint margins, variable degrees of synovitis with synovial hypertrophy, meniscal degeneration (knee), and thickening of the joint capsule.

Reproduced from Loeser 2010<sup>60</sup> with permission from Elsevier.

The cartilage in osteoarthritic joints is subjected to increased enzymatic degradation by a number of different matrix degrading enzymes<sup>61</sup> as a result of an imbalance of anabolic and catabolic processes (Figure 1-8) resulting in altered tissue properties. The disease causes chronic pain in affected joints and can lead to reduced mobility and a significantly impacted quality of life<sup>62</sup>.

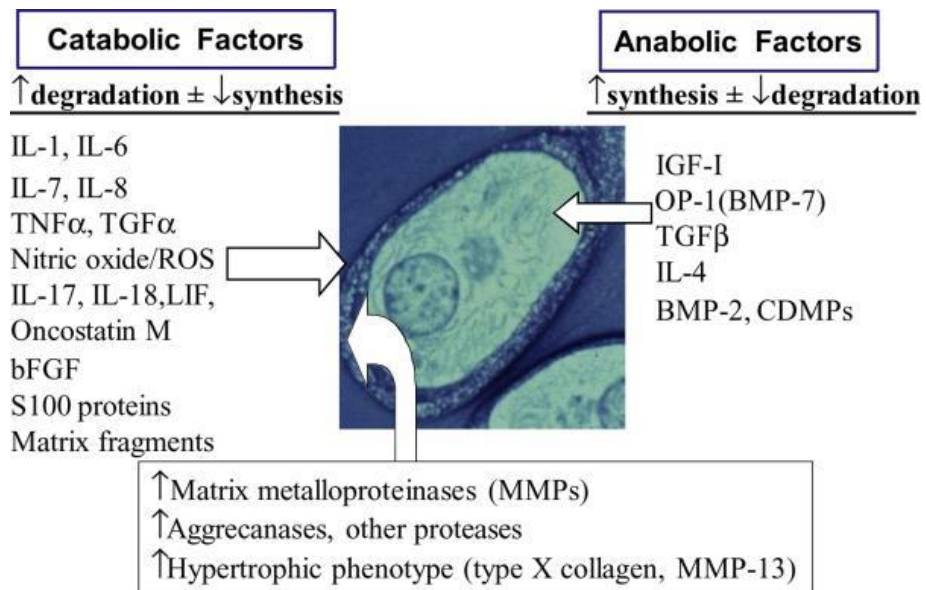


**Figure 1-8. Catabolic and anabolic factors that regulate chondrocyte function.** A host of factors, produced locally by articular chondrocytes, regulate matrix synthesis and degradation in articular cartilage. As osteoarthritis develops, catabolic activators overwhelm anabolic factors resulting in an imbalance in matrix synthesis and degradation. Matrix degradation is mediated by MMPs, aggrecanase, and other proteases produced by the chondrocyte in response to the catabolic factors. A change in the chondrocyte phenotype to a hypertrophic phenotype also occurs, likely in response to one or more of the catabolic factors.

Reproduced from Loeser 2010<sup>60</sup> with permission from Elsevier.

Other less common conditions can also lead to the formation of chondral or osteochondral lesions which may further cause osteoarthritis including osteochondritis dissecans where the damage is caused by an insufficient blood flow in the subchondral bone progressing to necrosis and cartilage delamination<sup>63</sup>.

The treatment options for arthritic joints remain limited, the UK body NICE (National Institute for Health and Care Excellence) recommend exercise, oral or topical analgesia, in some cases arthroscopic lavage and debridement and finally a joint replacement<sup>64</sup>, with osteoarthritis alone being responsible for more than half of all replacements in the US<sup>61</sup>. In Europe this procedure is performed every 1.5 minutes, again mainly due to osteoarthritis<sup>65</sup>, with 15% of joint replacement surgeries being performed on those under 60 in the UK<sup>66</sup>. Whilst a joint replacement can be a good option for elderly patients, it is not suited to younger patients where the lifetime of the

artificial joint is inadequate leading to the need for a second replacement joint, a more difficult procedure, later in life.

Alternative, more experimental treatment options whereby attempts are made to induce tissue regeneration or at the very least repair fall within the purview of the emerging field of regenerative medicine.

## **1.6 The role of regenerative medicine**

Regenerative medicine, either through the replacement of tissue with an *in vitro* engineered alternative or a cell therapy to support *in vivo* cellular activity aims to reproduce tissue with the anatomy and physiology of the native tissue<sup>67</sup>. Regeneration rather than the formation of scar tissue is the desired outcome, returning full function to the tissue or organ in question.

The limited treatment options along with an aging population and a higher incidence of injury within the younger population make articular cartilage tissue an ideal target for regenerative medicine therapies. To date progress in the area of musculoskeletal therapies has been relatively rapid in comparison to other body systems, with numerous clinical trials of treatments having been undertaken over the last thirty years, despite this long term outcomes remain uncertain.

Early techniques to promote repair included damaging the subchondral bone surface, beginning in 1959 with bone drilling<sup>68,69</sup> and microfracture<sup>70</sup> of the bone to induce bleeding and the formation of a fibrin clot in the defect. These procedures are believed to recruit stem cells from the underlying bone marrow. After 4-6 months the clot is replaced by a fibrocartilaginous tissue and the defect is filled<sup>71</sup>. Fibrocartilage tissue is more commonly associated with the menisci of the knees or the intervertebral discs<sup>49</sup>, rather than the hyaline articular cartilage, and is less suited to the mechanical demands placed upon it at the articulating surfaces. Alternative techniques aim to promote hyaline cartilage over fibrocartilage and include mosaicplasty also known as osteochondral autograft transplant system (OATS) whereby plugs of osteochondral tissue from a healthy non-load bearing region of cartilage are transplanted to the lesion. This technique does

lead to functional improvement but the size of the defect to be treated may be limited by available donor tissue<sup>71</sup>. Allogeneic transplants of osteochondral tissue can also be performed, particularly for larger defects where there is insufficient autologous tissue, but have the additional risks of disease transmission and rejection of the transplant<sup>72</sup>.

### **1.6.1 Autologous chondrocyte implantation**

Autologous chondrocyte implantation/transplantation (ACI/ACT) relies upon the implantation of *in vitro* expanded autologous chondrocytes to a cartilage lesion site which is covered with a patch to retain the cells (Figure 1-9). First performed in man by Brittberg *et al*<sup>73</sup> in the early 1990s the procedure requires the acquisition of a small cartilage biopsy from a macroscopically healthy, non-load bearing region of the joint. The biopsy is subjected to enzymatic digestion to dissociate the cells from the ECM and the resulting cells are cultured *in vitro* for 10-20 days. Following this period of expansion the cells are re-implanted to the defect site under a suitable patch, originally periosteal tissue. The Brittberg patient cohort generally reported improvements in function and a reduction in pain in response to the treatment and all had tissue rich in type II collagen filling the defect. Despite this, the resultant tissue was not always well anchored, varied with the transplant location and the quality of the tissue determined by biopsy and histological assessment was variable with frequent incidences of fibrocartilage rather than hyaline cartilage<sup>73</sup>.

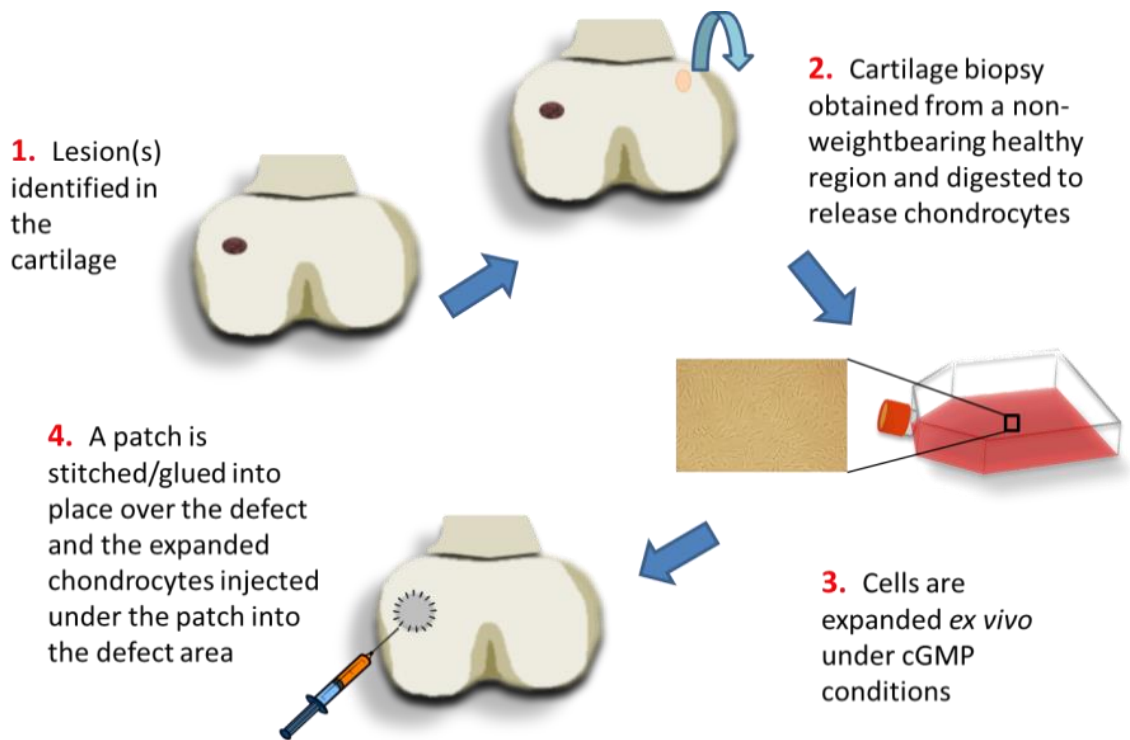


**Figure 1-9. The steps involved in the ACI procedure.**

As with the Brittberg study many trials of ACI report the production of fibrocartilage alone or a hyaline/fibrocartilage mix at the defect site<sup>74</sup>. Other problems noted on follow-up have included limited cellular and matrix distribution and organisation, tissue overgrowth and delamination of the new tissue from the subchondral bone<sup>74</sup>. The use of the periosteum as the patch is also in question as it may contribute to hypertrophy at the tissue surface<sup>75</sup>. Alternative sealing patches, particularly of collagen (e.g. chondrogide), are now undergoing assessment with a reduction, although not a complete elimination, in tissue hypertrophy apparent when assessed 1-2 years post-operatively<sup>76</sup>. Studies frequently have only a small number of participants and a limited follow-up duration (commonly 1-5 years<sup>74</sup>) making a long-term assessment of the results to date difficult, there are also constraints in monitoring repair as only very limited numbers of biopsies are practicable<sup>77</sup>. In addition to the uncertain outcome, ACI has other associated disadvantages including the requirement for two surgical procedures and thus an increased risk of surgical complications including infection and the potential for donor site morbidity.

As well as modifying ACI with the use of a collagen membrane rather than periosteum further alterations of the ACI technique have been attempted to improve the outcome including the use of 3D spheroids<sup>78</sup> that are entirely cell based and the introduction of biocompatible materials as carriers or scaffolds, seeded with cells prior to implantation to a defect site. Many of these are currently under investigation for commercial clinical application (Table 1-3)<sup>79</sup>.

**Table 1-3. Biomaterials intended for use as cell carriers for cell implantation for cartilage repair.**

(From Marlovits *et al*, 2006<sup>79</sup> and Nehrer and Brix, 2014<sup>80</sup>)

Technique	Product	Company
<b>1<sup>st</sup> Generation - Cell suspension with periosteum</b>	ACT-Biotissue	BioTissue
	Carticel	Genzyme
	ChondroCelect	Tigenix
	Chondrotransplant	Codon
	Novocart	Tetec
<b>2<sup>nd</sup> Generation - Cell suspension with collagen membrane</b>	Artrocell	Cellgenix/Geistlich/Ormed
	CACI	Verigen
<b>3<sup>rd</sup> Generation - Cell-Biomaterial</b>		
Hyaluronan polymer	Hyalograft	FAB
	Hyaff-11-S	Fidia, Anika Therapeutics
Collagen gel	CaReS-Collagen type I hydrogel	Ars Arthro
Collagen-membrane	ArthroMatrix	Arthrex/Orthogen
	MACI	Verigen/Genzyme
	MACT	Igor/André
Polymer	BioSeed-C – Fibrin/polygalactin /polydioxanone	BioTissue

Matrix induced autologous chondrocyte implantation/transplantation (MACI/MACT) introduced in 1999<sup>81</sup>, is a third generation ACI technique, involves culturing the chondrocytes on a collagen membrane prior to implantation, addressing both problems with cell retention at the defect site and associated with the use of a periosteal patch<sup>82</sup>. The cells are obtained from a 200-400 mg

cartilage biopsy and cultured for 3 days on the membrane prior to being re-implanted to the defect site with the cultured cells apposed to the prepared defect site<sup>80</sup>.

The substitution or a comparison of chondrocytes with MSCs is also increasingly common as bone marrow aspirate (BMA) harvest is relatively simple in comparison to obtaining a cartilage biopsy for chondrocyte expansion. Variations on this include the implantation of 'activated' of bone marrow aspirate concentrate (BMAC), with the advantage of requiring only a single surgery reducing patient risk and cost, the BMAC is pasted into the defect improving cell retention and can still be used with a scaffold material if desired. Early outcomes are similar to those of the MACI technique<sup>83</sup>.

Many of these modified techniques appear promising, but again will require long-term follow up to determine overall efficacy. Furthermore although these interventions are a viable alternative for the treatment of focal defects they are less efficacious in patients with osteoarthritis, the major cause of joint problems<sup>84</sup>.

## **1.7 Cells with prospects for use in cell therapies**

With the exception of microfracture techniques where cells are recruited from the sub-chondral bone the therapies described in the previous section rely upon an exogenous source of cells. This is largely as a result of the poor migratory capacity of cells within cartilage, which are in any case present in only limited numbers. There are several possible cell types which may be utilised each with differing properties.

### **1.7.1 Autologous chondrocytes**

Despite the hypocellularity of hyaline cartilage autologous chondrocytes can usually be isolated and expanded to sufficient numbers for treatment as is currently the case for ACI and associated therapies. However, there are factors that may be deleterious to chondrocyte recovery and expansion. In particular, chondrocytes obtained from older donors may not express either a

sufficient quantity, or the correct mix of ECM molecules to reproduce the mature hyaline cartilage matrix that is necessary for tissue regeneration<sup>85</sup>.

Primary chondrocytes are typically cultured *in vitro* in monolayer for expansion purposes; however, during monolayer culture cellular morphology digresses from the expected spherical cell to a more flattened appearance resembling a fibroblast. Associated with this change in cell morphology is a switch towards type I collagen production rather than type II and a tendency to produce increased amounts of smaller proteoglycans and reduced aggrecan<sup>86</sup>. This process is labelled as cell de-differentiation and has been an acknowledged issue with chondrocytes for decades<sup>87</sup>. Whilst 3D culture can restore some of the features of the chondrocytic phenotype it is also associated with a much slower rate of proliferation<sup>37</sup> with the maximum size of the cellular aggregate limited by the need for sufficient nutrient diffusion to prevent cell death in the centre of the mass. Collagen type I which should be absent in hyaline cartilage is still also frequently expressed<sup>88</sup>.

Additionally, as adult, committed lineage cells chondrocytes inherently have a limited proliferative capacity before the cells undergo senescence, a state that is associated with considerable changes in the cell phenotype and an absolute cessation of proliferation. Chondrocyte senescence is discussed further in section 1.8.

### **1.7.2 Stem cells**

Stem cells are defined as those cells with the ability to self-renew and undergo asymmetric division, i.e. to maintain a population of undifferentiated progeny identical to themselves and, under the influence of the appropriate cues, to differentiate into multiple cell types<sup>89</sup>. The totipotent zygote is the only cell with the ability to differentiate into all cell types including the extra-embryonic cells of the trophoblast<sup>90</sup>. Stem cells resident in *in vivo* niches serve as a self-renewing pool of cells for the regular replacement or repair of tissues as required<sup>91</sup>. Research is on-going using a variety of stem cells of different origin with variable proliferative and

differentiation capacities including hESCs, MSCs and tissue specific stem cells at both the fundamental and clinical application levels.

#### **1.7.2.1 Mesenchymal stem cells**

Whilst it is possible to use relatively mature autologous somatic cells in tissue engineering, for example, in ACI procedures, the cells may prove to be less than ideal due to potential donor site morbidity, poor proliferative potential and a loss of cell phenotype. This has led to the investigation of the use of adult MSCs as a cell source for regenerative medicine therapies. These cells have been shown to have a higher proliferative capacity in culture than somatic cells and to retain their differentiation potential over multiple passages; however, these features do not persist indefinitely<sup>92,93</sup>.

The existence of fibroblastic cells in the bone marrow was suggested first in 1867 by Cohnheim<sup>94</sup> and later confirmed by the work of Friedenstein in the 1970s<sup>95</sup>. Specifically adult stem cells capable of producing tissues of the mesenchymal germ layer (i.e. mesenchymal stem cells) were found within the plastic adherent bone marrow cell population that formed 'colony forming units-fibroblasts' and had the ability to proliferate extensively and to become a range of differentiated cell types<sup>95</sup>. Since then MSCs, or MSC-like cells, have been described in multiple tissue types including: peripheral blood<sup>96</sup>, muscle<sup>97</sup>, dermis<sup>98</sup>, dental pulp<sup>99</sup>, periosteum<sup>100</sup>/perichondrium<sup>101</sup>, adipose tissue<sup>102</sup> and the various birth associated tissues including UCB<sup>103</sup>, Wharton's jelly tissue<sup>104,105</sup>, amniotic fluid<sup>106</sup>, placenta<sup>107</sup> and synovial membranes<sup>108</sup>.

MSCs, alternatively described as bone marrow stromal cells (BMSCs), mesenchymal stromal cells or bone marrow stem cells, can be obtained with relative ease from aspirates of bone marrow, typically from the iliac crest<sup>38</sup>. Aspirated marrow consists of a heterogeneous mixture of haematopoietic and non-haematopoietic bone marrow cells, within the non-haematopoietic fraction is a mixture of cells including those with multi, tri, bi and unipotential characteristics<sup>109,110</sup>. Some cells have relative maturity and can form only a very limited range of

cell types for example those which appear to be committed osteoprogenitors, whilst others retain a more varied potentiality and can become a range of cell types including adipocytes, chondrocytes, osteoblasts and myoblasts *in vitro* when exposed to appropriate culture media and/or the application of physical forces<sup>111</sup>. MSCs have a well-established capacity for mesodermal differentiation pathways and additionally their differentiation to cells with features of other germ layers has also been described suggesting that the cells have trans-differentiation capacity or greater plasticity than first thought<sup>112</sup>. The fraction of bone marrow cells believed to be MSCs is low, reportedly 0.01 to 0.001%<sup>93,113</sup>. The isolation of MSCs from BMA can be achieved by simple plastic adherence to tissue culture plastic with the remaining non-adherent cells discarded during subsequent media changes. This simple approach appears to yield the greatest number of cells, although arguably a more heterogeneous cell population than the application of sorting techniques such as density, magnetic or flow cytometry based cell sorting<sup>114</sup>.

Confirmation of the identity of the recovered cells as MSCs remains challenging due to their lack of unique characteristics. They are therefore identified on the basis of being plastic adherent, having multipotent differentiation capacity as a population and by the expression of a range of cell surface markers. Typically those used are as proposed by the Mesenchymal and Tissue Stem Cell Committee of the International Society for Cellular Therapy and are the positive expression of CD73, CD90 and CD105 and the absence of expression of CD45, CD34, CD14 or CD11b, CD79a or CD19 and HLA-DR<sup>115</sup>, see Table 1-4 for more information on these markers. Other surface markers have also been described for MSCs including CD44, CD106, CD146, CD166, CD271 and STRO-1<sup>116</sup>, see Table 1-5 for a more extensive list of MSC positive and negative markers.

**Table 1-4. Mesenchymal and Tissue Stem Cell Committee of the International Society for Cellular Therapy recommended MSC markers.**

<b>Marker</b>	<b>Description</b>	<b>Location</b>	<b>Present(+)/absent (-) on MSCs</b>
<b>CD14</b>	55 kDa glycoprotein lipopolysaccharide (LPS, endotoxin) pattern recognition receptor (PRR) <sup>117</sup>	Monocyte/macrophage lineage marker	-
<b>CD19</b>	Regulatory B cell antigen receptor <sup>118</sup>	B lymphocyte marker	-
<b>CD34</b>	115 kDa transmembrane phosphoglycoprotein <sup>119</sup>	Considered to be a haematopoietic cell marker, also present on other populations including early MSCs	-
<b>CD45</b>	Leukocyte common antigen transmembrane glycoproteins <sup>120</sup>	Expressed on all nucleated cell of the haematopoietic lineage	-
<b>HLA-DR</b>	MHC class II receptor <sup>121</sup>	Expressed on 'professional' antigen presenting cells (macrophages, dendritic cells)	-
<b>CD73</b>	Ecto-5-prime-nucleotidase involved in marrow stromal interactions <sup>122</sup>	Expressed on MSCs	+
<b>CD90</b>	25–30 kDa glycosyl-phosphatidylinositol-linked membrane glycoprotein <sup>123</sup>	Expressed on MSCs	+
<b>CD105</b>	Endoglin - TGF-beta receptor III <sup>122,124</sup>	Expressed on MSCs	+

**Table 1-5. Expression of a range of markers in hMSCs.** Adapted from Batsali et al, 2013<sup>125</sup> with additional markers from \*Niehage et al 2011<sup>126</sup>. N.B. some markers are not universally positive.

Marker		-/+ expression
<b>CD11b</b>	Integrin $\alpha_M$	-
<b>CD31</b>	Platelet endothelial adhesion molecule 1 (PECAM1)	-
<b>CD33</b>	Sialic acid binding Ig-like lectin 3	-
<b>CD38</b>	Adenosine diphosphate (ADP)-ribosyl cyclase-1	-
<b>CD49d</b>	Integrin $\alpha_3$	-
<b>CD50</b>	Intercellular adhesion molecule 3 (ICAM3)	-
<b>CD53</b>	Tetraspanin-25	-
<b>CD56</b>	NCAM1	-
<b>CD80</b>	CD28 ligand	-
<b>CD86</b>	Activation B7-2 antigen	-
<b>CD117</b>	C-kit receptor	-
<b>CD133</b>	AC133 (prominin)	-
<b>CD144</b>	VE-cadherin	-
<b>CD235<math>\alpha</math></b>	Glycophorin	-
<b>SOX2</b>	Transcription factor SOX2	-
<b>CD10</b>	Neutral endopeptidase	+
<b>CD13</b>	Aminopeptidase N	+
<b>CD26</b>	Dipeptidylpeptidase 4	+
<b>CD29</b>	Integrin $\beta_1$	+
<b>CD40</b>	Tumour-necrosis factor receptor superfamily 5	+
<b>CD44</b>	Hyaluronan receptor	+
<b>CD49a</b>	Integrin $\alpha_1$	+
<b>CD49b</b>	Integrin $\alpha_2$	+
<b>CD49c</b>	Integrin $\alpha_4$	+
<b>CD49e</b>	Integrin $\alpha_5$	+
<b>CD51</b>	Integrin $\alpha_v$	+
<b>CD54</b>	ICAM1	+
<b>CD58</b>	Lymphocyte function associated antigen 3 (LFA3)	+
<b>CD71</b>	Transferrin receptor	+
<b>CD106</b>	Vascular cell adhesion molecule 1 (VCAM1)	+
<b>CD140<math>\alpha</math></b>	Platelet-derived growth factor receptor $\alpha$ (PDGFR $\alpha$ )	+
<b>CD140<math>\beta</math></b>	PDGF-R $\beta$	+
<b>CD146</b>	Melanoma-cell adhesion molecule (MeICAM)	+
<b>CD166</b>	Activated lymphocyte cell adhesion molecule (ALCAM)	+
<b>CD325</b>	N-cadherin	+
<b>HLA-I</b>	Human leukocyte antigen I (A, B, C, G)	+

<b>STRO-1</b>	STRO-1 cell surface antigen	+
<b>SSEA4</b>	Stage-specific embryonic antigen 4	+
<b><math>\alpha</math>-SMA</b>	$\alpha$ -smooth muscle actin	+
<b>NANOG</b>	Transcription factor	+
<b>OCT4</b>	Octamer-binding transcription factor 4	+
<b>GD2</b>	Ganglioside	+
<b>CD9</b>	Tetraspanin-29	+*
<b>CD46</b>	Membrane co-factor protein	+*
<b>CD47</b>	Leukocyte surface antigen	+*
<b>CD59</b>	Protectin	+*
<b>CD61</b>	Integrin $\beta_3$	+*
<b>CD63</b>	Lysosomal associated membrane protein(LAMP)-3	+*
<b>CD81</b>	Tetraspanin-28	+*
<b>CD95</b>	Fas antigen	+*
<b>CD97</b>	Leukocyte antigen 97	+*
<b>CD98</b>	Solute carrier family 3	+*
<b>CD99</b>	E2 antigen	+*
<b>CD109</b>	Platelet-specific Gv antigen	+*
<b>CD112</b>	Polio virus receptor related 2 protein	+*
<b>CD147</b>	Basigin	+*
<b>CD151</b>	Tetraspanin-24	+*
<b>CD155</b>	Polio virus receptor	+*
<b>CD172a</b>	Signal regulatory protein alpha	+*
<b>CD239</b>	Basal cell adhesion molecule (BCAM)	+*
<b>CD248</b>	Endosialin	+*
<b>CD276</b>	B7 homolog 3	+*
<b>CD304</b>	Neuropilin-1	+*
<b>CD316</b>	Ig superfamily member 8	+*
<b>CD325</b>	Cadherin 2	+*

Under the influence of the TGF- $\beta$  growth factors MSCs can be readily induced to produce markers of chondrogenesis *in vitro* including collagen type II and aggrecan<sup>127</sup>. Culture of the MSCs in the form of micromass pellets to allow 3D interactions leads to a phenotype more typical of the *in vivo* chondrocyte<sup>128</sup>; however, this approach may not be practical for cell therapy purposes.

Unsurprisingly, given the results of treatments like microfracture that result in fibrocartilaginous matrix, MSCs, even in pellet culture progress to a hypertrophic phenotype, producing copious amounts of type I and type X collagen in addition to the desired type II collagen<sup>128</sup>.

Whilst MSCs have a well-documented ability to differentiate into chondrocytes the mechanism by which they achieve improvements in clinical applications is unclear. Improvements may be a result of direct differentiation of cells; alternatively MSCs are believed to secrete trophic factors (bioactive molecules) contributing to changes mediated by cells *in situ*<sup>91,129</sup>. It is through this mechanism that haematopoiesis is supported in the bone marrow via the secretion of haematopoietic growth factors and cytokines<sup>91</sup>. MSCs can also respond to inflammatory signals secreted during tissue damage and migrate to the damaged area. It may be that both differentiation and trophic factors combined are necessary to achieve regeneration.

In addition to their utility based upon their differentiation capacity and the secretion of trophic factors MSCs can also modulate the immune response<sup>130</sup> greatly reducing the T-cell response to their, and other allogeneic cells' presence<sup>131</sup>. The immune modulation capabilities *in vitro* and *in vivo* are not yet well characterised and to assist with this attempts are underway to standardise experiments investigating these features of MSCs<sup>132</sup>. Alongside cartilage's somewhat immune-privileged status<sup>133</sup> due to its avascular nature these immunomodulatory effects may make MSCs a suitable source for an allogeneic treatment. An equine trial of injections of allogeneic MSC into articular cartilage resulted in some inflammatory response; however, this was no different than the response promoted by autologous injection<sup>134</sup>.

Unfortunately, the incidence and recovery of MSCs from bone marrow decreases with the age of the donor; this depletion in MSCs in bone marrow being responsible for the increased healing time of bone fractures in the elderly<sup>131</sup>. With increased time in culture the cells may also lose some of their differentiation potential beginning with a loss of adipogenic, then chondrogenic and lastly osteogenic differentiation capacity<sup>135</sup>. The term stem cell may also be a misnomer as so far the cells have not conclusively been shown to renew indefinitely in culture, becoming senescent probably due to their lack of telomerase activity<sup>136</sup>.

Interestingly MSCs have also been identified, by co-expression of two MSC markers: CD105 and CD166, in adult articular cartilage in both a normal and osteoarthritic state. Predictably, the expression of CD105 (endoglin), a TGF- $\beta$  receptor, was widespread within the cartilage; however, CD166 and co-expression of CD105 and CD166 was limited to smaller sub-populations of cells. The CD105/CD166 positive cells were found to be multipotent and demonstrated adipogenic, osteogenic and chondrogenic differentiation capacity. The presence of CD166 on perichondrial cells also appears to be a marker for a multipotent progenitor population<sup>137</sup>. Distribution of the cells throughout the cartilage is not uniform and they are predominantly located in the superficial and upper transitional zones<sup>138</sup>. The presence of these progenitor cells in adult cartilage may confer a much greater capacity for regeneration than that appreciated to date; however, it is clear from the inadequate tissue response that this cannot be exploited effectively during the natural response to injury. The incidence of CD105/CD166 positive cells was also found to be higher in osteoarthritic tissue than normal tissue<sup>137</sup> so the use of these cells, as with all MSCs due to their multilineage potential, must be approached with caution as it is likely that careful regulation of their activity is necessary to produce the required hyaline tissue.

### 1.7.2.2 Umbilical cord blood stem cells

The original source of MSCs as previously discussed is the bone marrow, and this remains the most commonly used; however, alternative sources may have benefits, including somewhat different proliferation and differentiation capacities, and a greatly increased ease of access.

Isolation of MSCs from bone marrow is reliable with several well supported methods relying on simple plastic adherence, either alone or in conjunction with density separation of mononuclear cells (MNCs), described in the literature; nevertheless, there are significant drawbacks associated with bone marrow aspiration. Typically marrow is aspirated from the iliac crest of the pelvic bone, with donor pain and donor site morbidity being of particular concern. Recovery and quality of the cells recovered from marrow have also been found to vary with donor age<sup>135</sup>. As such, postnatal tissues from even a fraction of the approximately 700,000 births annually in the UK alone<sup>139</sup>, and that would otherwise be considered as waste and discarded, represents a desirable and under-utilised pool of stem cell donor material.

Since the first report in 2000<sup>140</sup>, which detailed the recovery of MSC-like cells in 24% of the UCB samples tested, MSCs have been successfully isolated from UCB using methods similar to those described for bone marrow recovery. However, across many studies the rates of successful recovery of MSCs from UCB have generally been found to be much lower (e.g. 29%<sup>141</sup>, 34%<sup>142</sup>, 43%<sup>143</sup>) than with bone marrow, which rarely fails to yield MSCs. Rapid recovery (<2 hours), and a volume of blood in excess of 90 mL has been associated with a reported success rate increased to 90%<sup>144</sup> which compared to other reports to date is unusually high. UCB-MSCs have similar morphology, greater proliferative capacity than bone marrow-derived MSCs and surface marker analysis yields similar, although not identical, results. Cells from either source have been shown to be negative for the haematopoietic markers CD14, CD34, and CD133 and positive for CD29, CD44, and CD73. However, UCB-MSCs have 30% lower CD105 expression and 30% higher CD166 expression. CD90 expression also varied with most (≥95%) cells from either source positive for the

marker but at a lower fluorescence intensity in UCB-MSCs<sup>103</sup>. The greater proliferative capacity of UCB-MSCs may be attributed to longer telomeres in UCB-MSCs compared to bone marrow MSCs<sup>143</sup>, this characteristic could potentially support further scale up, therefore larger numbers of cells, before they are no longer clinically useful. The immune system modulatory effects may also be greater in MSCs isolated from neonatal tissues<sup>145</sup> making the cells a more suitable source for allogeneic transplants.

Differentiation of UCB-MSCs following typical protocols has shown good osteogenic and chondrogenic differentiation capacity; however, UCB-MSCs have frequently been found to have limited capacity to differentiate into adipocytes with little to no lipid accumulation even with extended culture<sup>103</sup>. Contrastingly some authors have reported that UCB- MSCs represent cells with a less restricted differentiation capacity with the potential for differentiation down endodermal or ectodermal pathways<sup>143</sup>. Conflicting reports of varying degrees of success when attempting to isolate and differentiate UCB-MSCs indicate that the ideal isolation and *in vitro* conditions may not yet have been elucidated. This is further supported by reports of similar gene expression profiles from different donors isolated in the same conditions, compared to the same donor isolated in differing culture conditions<sup>142</sup>.

Interestingly there is evidence of a small population of primitive cells that express ESC markers and support both haematopoietic and non-haematopoietic therapies. These cells are reside within the lineage negative population (CD45-, CD33-, CD7-, glycophorin A<sup>146</sup>) or more simply the CD133+ population of UCB MNCs.

As a readily available cell source with an established banking system resulting in over 600,000 units of UCB stored in public banks<sup>147</sup> and more than 780,000 privately stored units<sup>148</sup> UCB-MSCs may have advantages over bone marrow MSCs including wider differentiation capacity, greater proliferation and reduced immune response that would make these cells an ideal choice for regenerative medicine therapies.

### 1.7.2.3 Embryonic stem cells and their derivatives

Beyond the four-cell stage of embryonic development the ability of isolated cells to form a complete organism, i.e. totipotency, is lost. Cells become specified to either the extra-embryonic tissues, or the inner cell mass that will continue to develop into the embryo. The cells of the inner cell mass retain the capacity to form all the cell types required to form a complete organism but can no longer support implantation and development<sup>90</sup>. This capacity to form endoderm, ectoderm and mesoderm is pluripotency and is a defining feature of embryonic stem cells (ESCs). ESCs, cells essentially halted at the pluripotent stage of embryonic development, were isolated from mice in 1981<sup>149,150</sup> and subsequently from non-human primates<sup>151,152</sup>. hESCs were first isolated from the inner cell mass of a surplus *in vitro* fertilisation (IVF) blastocyst and successfully cultured *in vitro* by Thompson *et al* in 1998<sup>153</sup>. Under the proper *in vitro* conditions these cells appear capable of indefinite self-renewal and retain their pluripotency as evidenced by the formation of teratomas when cells are transplanted to immune compromised mice<sup>153</sup>. Combined, the properties of pluripotency and unlimited expansion make hESCs a tool with exceptional potential in the study of developmental biology and for regenerative medicine therapies.

As expected of pluripotent cells, hESCs will differentiate down the chondrogenic lineage; during the formation of *in vivo* teratomas or via the production in suspension culture of embryoid bodies a cartilage like tissue can be observed, in conjunction with other tissue types<sup>154</sup>. hESC chondrogenic differentiation has been induced by a variety of factors often used in a complex cocktails and at different time points including TGF- $\beta$ , activin A, BMA4, bFGF, BMP receptor inhibitor dorsomorphin, Wnt3a, follistatin, GDF5, neurotrophin 4, chondrocyte conditioned media, and hypoxic pre-conditioning<sup>155-159</sup>. In an attempt to avoid the formation of multiple contaminating cell types, a major barrier to the therapeutic use of hESCs, a stepwise differentiation of hESCs may be favoured with the formation and selection of more lineage restricted MSC-like cells followed by chondrogenic differentiation, with selection being based

upon the previously identified MSC markers<sup>160,161</sup>. *In vivo* studies using hESCs for chondrogenesis have only resulted in partial success with reports of heterogeneous cartilage, insufficient cartilage and teratoma formation<sup>161</sup>. To successfully produce only chondrogenic cells in sufficient numbers protocols are likely to be extremely complex and require rigorous selection procedures.

Despite the potential evidenced by hESCs, and the cells derived from them, exploiting them remains challenging. Issues of practicality, ethical concerns associated with the destruction of viable embryos and safety concerns with respect to teratogenesis persist. Despite these issues clinical trials have been initiated using two hESC derived cell types. The first, a clinical trial by the biopharmaceutical company Geron Corporation for the treatment of spinal cord injury using oligodendrocyte progenitor cells derived from hESCs<sup>162</sup> has since been halted due to cost considerations<sup>163</sup>. However, Advanced Cell Technology continue trialling the use of derived retinal pigmented epithelial cells for degenerative eye conditions<sup>164,165</sup>.

#### **1.7.2.4 Induced pluripotent stem cells**

A major advancement in hESC technology was the development of the technique inducing pluripotency in previously differentiated somatic cell types to create induced pluripotent stem cells (iPSCs). The conversion of adult somatic cells to iPSCs involves the transfection of cells with a number of key genes that re-programme the cell phenotype so that it resembles that of ESCs. This was first achieved in mice in 2006 by Takahashi *et al*<sup>166</sup> who, following reductionist screening of 24 candidate genes by transduction, identified the inductive gene combination of *Oct3/4*, *Sox2*, *c-Myc*, and *Klf4*<sup>166</sup>. This was quickly followed in 2007 by successful reprogramming of human cells by both Takahashi *et al* using the same 4 defined factors<sup>167</sup> and by Yu *et al* with the Thomson group again using *OCT3/4*, and *SOX2* but in combination with *NANOG* and *LIN28*<sup>168</sup>. The elimination of *C-MYC* from the protocol is an important improvement as the gene is oncogenic and Takahashi *et al* followed their publication soon after with a modification which excluded the *C-MYC* gene completely without replacement, they were still able to generate iPSC colonies, albeit

with reduced speed and efficiency<sup>169</sup>. In all of the protocols the resulting cells were found to strongly resemble hESCs.

The potential to use iPSCs rather than hESCs circumvents two established issues of hESCs. Firstly, the immunogenicity of allogeneic hESCs derived cells, as no hESCs are available from autologous sources, and secondly bypass of the ethical concerns surrounding the destruction of human embryos for hESC production. There is also the possibility of generating iPSCs from abnormal cells with the possibility of studying those disease causing cells and using them in disease models for therapy screening. Combining iPSC technology with protocols for differentiation towards specific tissue types raises the prospect of therapies where practically unlimited numbers of cells can be generated which can then thereafter can be used for numerous autologous therapies in any individual with no ethical concerns. As with hESCs, iPSCs can be differentiated into MSC-like cells that gain an MSC immunophenotype and differentiation capacity although this is altered compared to bone marrow MSCs, particularly with regard to adipogenesis<sup>170</sup>. Chondrogenesis in these cells has also now been demonstrated<sup>171,172</sup>.

The plasticity of hESCs and iPSCs is extensive; however, they cannot be used alone to re-create a whole organism due to the lack of differentiation to extra-embryonic tissues that arise from the trophoctoderm, i.e. they are not totipotent. Recent research with mouse cells suggests that cell differentiation state can be further reversed to the totipotent stage and this may lead to cells with an even more naïve phenotype and further improved plasticity<sup>173</sup>.

## **1.8 Cell Senescence**

The onset of cellular senescence where cells irreversibly cease proliferation and undergo a number of phenotype changes is a major barrier to their *in vitro* study, meaning only limited numbers of investigations can be performed on a relatively small scale before the finite cell supply is exhausted.

### 1.8.1 Replicative senescence

From 1910 onwards Alexis Carrel and colleagues published work asserting that normal vertebrate somatic cells were capable of undergoing an infinite number of cell divisions and were therefore immortal in culture, maintaining that they had established an immortal culture of chick embryonic heart cells and later alleging that this culture was grown continuously for 34 years. The failure of other researchers to successfully grow normal cells indefinitely was ascribed entirely to inadequate culture conditions<sup>174</sup>. This remained the prevailing opinion until 1961 with the publication of work by Leonard Hayflick demonstrating that, unless they were genetically abnormal, cells *in vitro* could be cultured only for a limited number of divisions and that this was an intrinsic property of the cells<sup>175,176</sup>. This phenomenon of replicative senescence whereby cells are only able to undergo a finite number of mitotic divisions before replicative potential is exhausted and proliferation ceases has since been termed the 'Hayflick limit'. It is now believed that cells undergo replicative senescence when, due to a gradual loss with each cell division, their telomeres are shortened beyond a critical minimum length required for DNA replication both *in vitro* and *in vivo*<sup>177-179</sup>.

The presence of telomeres was identified at the end of the 1930s when it was determined that chromosome termini had specialised structures that were key to successful separation of chromatids during cell division without fusion events<sup>180</sup>. Building on the subsequent discoveries of DNA structure<sup>181</sup> and DNA polymerase<sup>182</sup> Olovnikov recognised that incomplete synthesis of DNA during replication would lead to residual single stranded DNA at the ends of chromosomes which would shorten with each replication cycle (the 'end replication problem'), and that this may be the cause of the limited *in vitro* lifespan of somatic cells<sup>183</sup>. Human telomeres consist of approximately 5-15 kb of repeats of the nucleotide hexamer TTAGGG<sup>184</sup> the 3' terminal telomere ends have a single stranded overhang of between 100 to 300 bases, this overhang in association with various telomere binding proteins (Shelterin complex) form a protective T-loop structure believed to prevent the activation of the DNA damage response<sup>185,186</sup>. The progressive loss of the

telomere overhang region that enables the formation of the T-loop and the resultant chromosomal capping may be the key structure controlling the onset of senescence rather than the overall telomere length<sup>187</sup>. The senescence response acts as an essential mechanism to the uncontrolled proliferation of abnormal cells thereby preventing cancerous growths. This is increasingly apparent from the close relationship between tumour suppressor genes, senescence and cancer<sup>188</sup>.

The defining feature of senescence is irreversible growth arrest; however, senescent cells *in vitro* frequently also undergo changes in morphology, in particular becoming larger and flatter; additionally there are other markers of senescence including the accumulation of senescence associated  $\beta$ -galactosidase (SA $\beta$ Gal)<sup>189</sup>. This enzyme accumulates in the lysosomes of cells presumed to be undergoing senescence<sup>190</sup> and as such is used as an *in vitro* marker of cell senescence. SA $\beta$ Gal is also detectable in cells in tissues where there is a correlation between increasing age and increased amounts of SA $\beta$ Gal<sup>191,192</sup>.

Senescence can also be induced in cells by alternative mechanisms that are generally not intrinsically linked to the Hayflick limit but rather are environmental<sup>193</sup>. These environmental stressors can also be linked in chondrocytes with reduced synthesis of the vital ECM components type II collagen and aggrecan and a reduced response to growth factors including insulin-like growth factor<sup>191</sup> TGF $\beta$ 1, bFGF and platelet-derived growth factor  $\beta\beta$  (PDGF $\beta\beta$ )<sup>85</sup>, and epidermal growth factor (EGF)<sup>194</sup>. Other changes in cell secretion also occur during senescence that are collectively described as the senescence-associated secretory phenotype (SASP) which leads to a chronic pro-inflammatory state<sup>195</sup>. In chondrocytes the acquisition of a SASP results in changes that may lead to the onset of, or contribute to osteoarthritis<sup>196-198</sup>.

Whatever the causative mechanism involved, chondrocyte senescence is highly likely to impact upon the tissue's ability to regenerate with increased age and may play a significant role in the development of degenerative disease as evidenced by a report that cells with a higher SA $\beta$ Gal

content have been found to be concentrated in areas in closer proximity to osteoarthritic damage whilst cells further from lesions have a lower SA $\beta$ Gal content<sup>199</sup>.

### 1.8.2 Telomerase enzyme

In a limited number of cell types telomere shortening and therefore replicative senescence is innately avoided by the maintenance of telomere length by via the actions of the ribonucleoprotein telomerase reverse transcriptase. Restricted to only a few cell types with a rapid turnover, some stem cells and cancer cells<sup>200</sup> the enzyme consists of an RNA template component TERC, the catalytic component TERT and telomerase associated protein-1 (TEP1)<sup>201</sup> with both TERC and TEP1 expressed constitutively<sup>202,203</sup>. Following fertilisation telomerase is active throughout the human embryo through the first trimester of development and is gradually lost from various tissue compartments thereafter<sup>200</sup>.

The canonical role of the telomerase enzyme is the maintenance or extension of telomeres via the synthesis of new telomere repeats extending the overall telomere length; however, the enzyme has additional non-telomere related functions. The TERT component of the telomerase complex acts in canonical Wnt transcriptional regulation via complexation with  $\beta$ -catenin and NF- $\kappa$ B signalling by binding with p65<sup>204</sup>, post-transcriptional gene silencing via the production of siRNA that can modulate cell proliferation and regulation of apoptosis via mechanisms that are unclear but are mitochondrial rather than nuclear responses<sup>205</sup>. It is also involved in the DNA damage response again by unknown mechanisms (reviewed in<sup>206</sup>).

It has been demonstrated that *in vitro* replicative senescence can be avoided, despite extensive proliferation, by the re-expression and activity of *hTERT*<sup>200,207,208</sup>. In several cell types this strategy has supported the maintenance of telomere length and enhanced proliferation, or even resulted in immortalisation, whilst also preserving or potentially enhancing cell function<sup>209</sup>. This strategy of telomerase re-introduction or re-expression may be a valuable tool for increasing the availability

of cells that would otherwise only be available in limited numbers and would particularly enable much more extensive studies.

## 1.9 Hypoxic culture

The three primary cell types under investigation in this thesis have previously been investigated for chondrogenic potential in both standard 21% O<sub>2</sub> culture and in reduced oxygen culture at 2% and 0.2% O<sub>2</sub> with some benefits described at the lower 2% O<sub>2</sub> level<sup>210,211</sup>. As such, the work described herein is predominantly carried out in a 2% O<sub>2</sub> environment. The *in vitro* culture of cells in an environmental oxygen level that is below the ambient 21% level is often referred to as hypoxia; however, with bone marrow oxygen tensions reportedly as low as 1-2%<sup>212</sup>, the mammalian reproductive tract ranging from 1.5-8%, foetal circulation at approximately 5%<sup>213</sup> a mean arterial level of 12% and a mean tissue level of 3%<sup>214</sup> culture of cells under standard *in vitro* conditions at atmospheric oxygen levels (21% O<sub>2</sub>) exposes them to greatly increased amounts of oxygen compared to physiological norms. This is particularly relevant to articular cartilage which has been reported to have an oxygen tension of <1% due to its avascular nature<sup>215</sup>.

Oxygen functions as both a metabolite for energy production and as a signalling molecule, thus oxygen tensions can have wide ranging effects upon cell behaviour including at the transcriptional level. At low O<sub>2</sub> levels hypoxia inducible factor (HIF), usually rapidly degraded when oxygen is abundant, accumulates within cell nuclei activating those genes that have hypoxia response elements (HREs)<sup>216</sup>. These changes in gene expression in low O<sub>2</sub>, often referred to as the hypoxic response, are important during periods of O<sub>2</sub> deprivation that lead to pathological changes but also have a significant non-pathological role in tissues where lower O<sub>2</sub> levels are the physiological norm. During early embryonic development the lack of vasculature within the embryo severely limits the available oxygen and following the establishment of early vasculature significant regions of hypoxia remain. Evolution in the presence of this non-pathological hypoxia has resulted in a significant regulatory role for oxygen level during embryonic morphogenesis. Hypoxia is

implicated in the formation of mesenchymal condensations, the earliest stage of joint formation, and the switch from chondrocyte proliferation to hypertrophy. A number of genes well known for their role in chondrogenesis and endochondral ossification are regulated via a HIF pathway including *SOX9* and *VEGF* by direct activation and *RUNX2*, required for bone formation, subjected to inhibition by *SOX9*<sup>217</sup>.

Culture of cells in hypoxic (i.e. oxygen levels below the 21% O<sub>2</sub> found in ambient air) conditions has generally been reported to be beneficial to cell recovery and proliferation, differentiation status and matrix production depending upon cell type<sup>218–223</sup>. This improvement in recovered cell numbers, proliferation and maintenance of a stem cell state has been noted in hESCs, bone marrow MSCs and MSCs recovered from birth associated tissues, e.g. UC tissue/Wharton's jelly MSCs cultured in 2% O<sub>2</sub> displayed more rapid population doubling times and greater proliferative capacity whilst retaining their immunophenotype and differentiation potency<sup>213,224</sup>. Although the balance of the evidence is generally in favour of hypoxic culture there are conflicting reports<sup>225</sup>. These variations in results may be due, at least in part to the wide variation in the conditions of culture.

Chondrocytes that could be considered to be de-differentiated after expansion in monolayer culture that were then cultured in 3D culture systems at reduced O<sub>2</sub> tensions demonstrated an increase in cell numbers, along with significantly increased collagen deposition and GAG content over 20% O<sub>2</sub> controls<sup>86,226</sup>. The improved chondrocytic phenotype achieved in studies like these by the use of a 3D culture system were greatly enhanced by the use of reduced O<sub>2</sub> levels and appeared to be regulated at least in part by hypoxic modulation of the transcription factor *SOX9*<sup>86</sup>. Gene expression analysis of chondrocyte samples using microarray has demonstrated that all of the common cartilage ECM molecules are upregulated in response to hypoxic conditions. The mode of action of hypoxia in maintaining the desired phenotype appears to involve both *SOX9* mediated pathways and *SOX9* independent pathways and also extend to down-regulation of the genes associated with hypertrophy<sup>155,227,228</sup>.

## 1.10 Summary and hypotheses

The poor healing capacity and limited treatment options available for cartilage damage and degeneration results in an opportunity to resolve these issues using strategies arising from the emerging field of regenerative medicine, with potential contributions from tissue engineering and cell therapies. Strategies employed to date have largely involved the transplantation of autologous cells, particularly chondrocytes and MSCs, to damaged areas and have resulted in significant improvements in patient quality of life. Nevertheless, despite this success more detailed examination of the repair tissue reveals sub-optimal fibrocartilage tissue rather than the desired hyaline cartilage tissue. It is possible that these inferior results are due to the application of an unsuitable cell type or a lack of understanding of chondrogenesis and joint development processes. Further study is clearly warranted; however, extensive *in vitro* investigation is hampered by the process of replicative senescence and the accompanying changes that cells inevitably undergo due to their inherent lack of the telomerase enzyme.

The work described in this thesis employs several strategies, namely the use of a more physiologically relevant O<sub>2</sub> environment to compare chondrogenesis in three different cell types with potential for application in cartilage repair strategies. This is further extended to attempt to resolve the issues encountered with extensive *in vitro* cell expansion by using a strategy of re-introduction of the *hTERT* gene, with changes in the cell phenotype of the resulting progeny following considerable expansion assessed. The potential of using an alternative source of tissue in the form of UCB rather than bone marrow to recover MSCs was also considered with an emphasis on the use of physiological hypoxia to improve cell recovery.

These strategies tested two key hypotheses:

- The application of a physiologically relevant 2% O<sub>2</sub> environment improves the numbers of colonies and MSC cells recovered from UCB (Chapter 3).

- Re-expression of *hTERT* in cells with relevance to cartilage tissue engineering (chondrocytes, MSCs and ESC-derived cells) is sufficient to extend the proliferative capacity of the cells whilst concomitantly maintaining the primary cell phenotype and the chondrogenic differentiation capacity (Chapters 4-6).



Keele University

---

# **Chapter 2**

---

## ***Materials and methods***

## 2.1 Materials

Unless otherwise indicated materials were sourced from the manufacturer or their distributor within the United Kingdom.

**Table 2-1. List of materials, catalogue numbers and suppliers.**

	<b>Catalogue number</b>	<b>Supplier</b>
3,3'-Diaminobenzidine (DAB)	D8001	Sigma-Aldrich
3-aminopropyltriethoxysilane (APES)	A3648-100mL	Sigma-Aldrich
3-isobutyl-1-methylxanthine (IBMX)	I7018	Sigma-Aldrich
ABC immunoperoxidase staining system: anti-mouse anti-goat anti-rabbit	SC-2017 SC-2023 SC-2018	Santa Cruz Biotechnology
Acetic acid	A6283	Sigma-Aldrich
Acetone	A/0560/17	Fisher Scientific
Agarose	BP1356-500	Fisher Scientific
Alcian blue	A3157	Sigma-Aldrich
Alizarin red S	A5533	Sigma-Aldrich
Ammonium acetate	A2706	Sigma-Aldrich
Ascorbic acid phosphate	A8960	Sigma-Aldrich
Basic Fibroblast growth factor (bFGF)	100-18B	Peprotech
Bovine serum albumin (BSA)	BP9703-100	Fisher Scientific
CD45 coated microbeads	130-045-801	Miltenyi Biotec
Citric acid	C0759	Sigma-Aldrich
Cryopreserved human bone marrow mononuclear cells (MNCs)(isolated from human bone marrow aspirate)	2M-125B	Lonza
4',6-Diamidino-2-phenylindole (DAPI)	D9542	Sigma-Aldrich
Dexamethasone	D2915	Sigma-Aldrich
Dimethyl methylene blue (DMMB)	341088	Sigma-Aldrich
DirectLoad Wide Range DNA Marker	D7058	Sigma-Aldrich
Dimethylsulphoxide (DMSO)	D2650	Sigma-Aldrich
DPX mounting medium	360294H	Analar
Dulbecco's Modified Eagle Medium (DMEM) – 4.5 g/L glucose	BE12-709F	Lonza
Eosin	SLBJ6425V	Sigma-Aldrich
Ethanol (absolute)	E0650/17	Fisher Scientific
Ethidium bromide	E1510	Sigma-Aldrich
Ethylene diaminetetraacetic acid (EDTA)	BP2482-1	Fisher Scientific

FBS (foetal bovine serum)	DE14-801F (Lot#1SB020) FB-1001G/500 (Lot#11484)	Lonza  Biosera
Fibronectin	F0895	Sigma-Aldrich
Ficoll-Paque Premium (1.077 ± 0.001 g/mL at 20 °C)	17-5442-02	GE Healthcare
Fresh human bone marrow aspirate (BMA)13	1M-125	Lonza, US
FuGENE 6 Transfection reagent	E2691	Roche
G418	G418-RO	Sigma-Aldrich
Gel Loading Buffer (0.05% bromophenol blue, 40% sucrose, 0.1 M EDTA, 0.5% SDS)	G2526	Sigma-Aldrich
Glucose	G7021	Sigma-Aldrich
Glycine	50046	Sigma-Aldrich
Haematoxylin (Gill's Number 2)	GHS216	Sigma-Aldrich
Human chondrocytes (OK3)	C12710	Promocell
Hydrochloric acid (HCl)	320331	Sigma-Aldrich
Hydrogen peroxide	BPE2633-500	Fisher Scientific
Immunohistochemistry antibodies: Collagen I Collagen II Collagen VI Collagen X Aggrecan	AB90395 AB3092 AB6588 AB49945 AF1220	Abcam Abcam Abcam Abcam R&D Systems
Indomethacin	I7378	Sigma-Aldrich
Industrial methylated spirits (99%)	I99050	Genta Medical
Insulin	I9278	Sigma-Aldrich
Insulin, Transferrin, Selenium (ITS)	I3146	Sigma-Aldrich
Isopropanol	P/7500/17	Fisher Scientific
Knockout DMEM	10389172	Fisher Scientific
Knockout serum replacement	10828-028	Fisher Scientific
LD MACS columns	130-042-901	Miltenyi Biotec
L-Glutamine	BE17-605E	Lonza
L-Proline	P5607	Sigma-Aldrich
Magnesium sulphate	M2773	Sigma-Aldrich
Matrigel	354234	SLS/BD Biosciences
Methanol	M/3900/17	Fisher Scientific
Non-essential amino acids	BE13-114E	Lonza
Oil Red O	O0625	Sigma-Aldrich
Paraffin-Histoplast	6774060	Thermo Scientific
Paraformaldehyde	P/0840/53	Fisher Scientific
Penicillin, streptomycin, amphotericin B	BE17-745E	Lonza
Phosphate buffered saline (Mg <sup>2+</sup> and Ca <sup>2+</sup> free)	BE17-516F	Lonza
Phycoerythrin conjugated antibodies: CD14 CD19 CD34	130-098-167 130-098-168 130-098-140	

	CD45	130-098-141	Miltenyi Biotec
	HLA-DR	130-098-177	
	CD73	130-097-943	
	CD90	130-097-932	
	CD105	130-098-906	
	IgG <sub>1</sub>	130-098-845	
	IgG <sub>2a</sub>	130-098-849	
	PicoGreen double stranded DNA assay	P11496	Fisher Scientific
	Picric acid	P6744	Sigma-Aldrich
	Polybrene (Hexadimethrine bromide)	H9268	Sigma-Aldrich
	Proteinase K	P2308	Sigma-Aldrich
	QIAshredder minispin columns	79656	Qiagen
	RNase Zap	R2020	Sigma-Aldrich
	RNeasy mini kit	74104	Qiagen
	Senescent cells histochemical staining kit	CS0030	Sigma-Aldrich
	Silver nitrate	S/1280/46	Fisher Scientific
	Sirius red/Direct red 80	365548	Sigma-Aldrich
	Sodium bicarbonate	10247	Analar
	Sodium chloride	S7653	Sigma-Aldrich
	Sodium citrate	S4641	Sigma-Aldrich
	Sodium hydroxide	301677P	Analar
	Sodium pyruvate	S8636	Sigma-Aldrich
	SuperScript III One-Step RT-PCR System with Platinum <i>Taq</i> High Fidelity DNA Polymerase kit	12574030	Life Technologies/ Fisher Scientific
	SuperScript III Platinum SYBR Green One-Step qPCR Kit	11588656	Life Technologies/ Fisher Scientific
	Toluidine blue	10506271	Fisher Scientific
	Transforming growth factor $\beta$ 3 (TGF $\beta$ 3)	100-36E	Peptotech
	Tris-Acetate-EDTA (TAE) buffer (50X) (2 M Tris Acetate, 100 mM Na <sub>2</sub> EDTA)	EC-872	National Diagnostics
	Tris-HCl	T5941	Sigma-Aldrich
	Trypan blue	T8154	Sigma-Aldrich
	Trypsin	15090	Life Technologies
	Trypsin/Versene (EDTA)	BE02-007E	Lonza
	Tween 20	66368	Analar
	Ultrapure distilled water DNase RNase free	10977-035	Gibco
	Xylene	X/0250/17	Fisher Scientific
	$\beta$ -glycerophosphate	G5422	Sigma-Aldrich
	$\beta$ -mercaptoethanol	10368072	Fisher Scientific

## **2.2 General cell culture techniques**

To maintain sterility all cell culture procedures were carried out in a class II microbiological safety cabinet using disposable sterile plastic consumables. Except where indicated all cells and pellets were cultured in humidified, 2% oxygen, tri-gas controlled incubators with 5% CO<sub>2</sub> and 93% N<sub>2</sub> as we have previously demonstrated that this is beneficial to all of our cells during recovery, expansion or chondrogenesis<sup>210,221,229,230</sup>.

### **2.2.1 Enzymatic sub-culture with trypsin**

As necessary cells were sub-cultured enzymatically at confluence using 0.05% (w/v) trypsin/0.02% (w/v) ethylenediaminetetraacetic acid (EDTA) (5 g/L trypsin and 2 g/L EDTA diluted 1 in 10 in calcium and magnesium free PBS). To trypsinise to a single cell suspension media was aspirated from cells and the monolayer washed thoroughly with PBS until all traces of culture media were removed. Sufficient trypsin/EDTA was added to cover cells and culture vessels were incubated at 37 °C until cells began to detach. Flasks were tapped to encourage cell detachment and once this was complete, approximately 3 volumes of the cell-relevant maintenance media (MM) added to halt the trypsin activity. Cell suspensions were then transferred to an appropriately sized centrifuge tube and pelleted at 250 g. The supernatant was aspirated and cells re-suspended in media in preparation for seeding.

### **2.2.2 Haemocytometer cell counting**

Cells to be counted were trypsinised as described in 2.2.1 to obtain a uniform, single cell suspension, if trypan blue viability was to be ascertained a small aliquot of the suspension was diluted and mixed 1 in 2 with trypan blue. A Neubauer haemocytometer was prepared by exhaling on the haemocytometer and using gentle pressure to adhere the haemocytometer coverslip to the resulting condensate. Approximately 10 µL of suspension was introduced by capillary action under the adhered coverslip of the Neubauer haemocytometer, cells were then counted under a microscope. A mean count was determined from the 4, 1 mm<sup>2</sup> corner regions to give the number

of cells per 0.1  $\mu\text{L}$ . To determine the number of cells/mL and the total cells the mean number of cells/0.1  $\mu\text{L}$  was multiplied by  $10^4$  and the total number of mL of cell suspension respectively. If trypan blue was used the dilution factor was also taken into account in the calculation.

### **2.2.3 Cryopreservation of cells**

For long term storage, as necessary, cells were detached from flasks with trypsin/EDTA as described in 2.2.1, re-suspended in FBS supplemented with 10% (v/v) dimethyl sulphoxide (DMSO) and immediately transferred to cryovials and placed in an isopropanol filled Mr Frosty freezing container for controlled cooling to  $-80\text{ }^\circ\text{C}$  before being transferred to liquid nitrogen storage dewars.

### **2.2.4 Cell counting using the Millipore Scepter cell counter**

The Millipore Scepter hand-held cell counter (Figure 2-1) uses the principle of Coulter counting to determine cell count and cell size, producing a cell distribution histogram that can be gated by cell diameter or volume<sup>231</sup>. To count, cells were re-suspended in PBS or if already suspended in media, diluted in PBS to a volume of 200  $\mu\text{m}$ . The ideal working concentration range for the Cell Scepter lies between approximately  $1 \times 10^4$  to  $5 \times 10^5$  cells/mL, when the cell concentration is above the working range this is indicated on the Cell Scepter and the count is void. On any occasion that this was the case a more dilute sample was re-counted. To use the counter a single use cartridge was inserted into the Cell Scepter and then submerged in the cell suspension. The plunger of the counter was depressed and released to sample the suspension after which the cell count was displayed on the Scepter screen and was gated by cell size as required. For analysis data was downloaded from the Cell Scepter and analysed using the proprietary software package Scepter Software Pro.

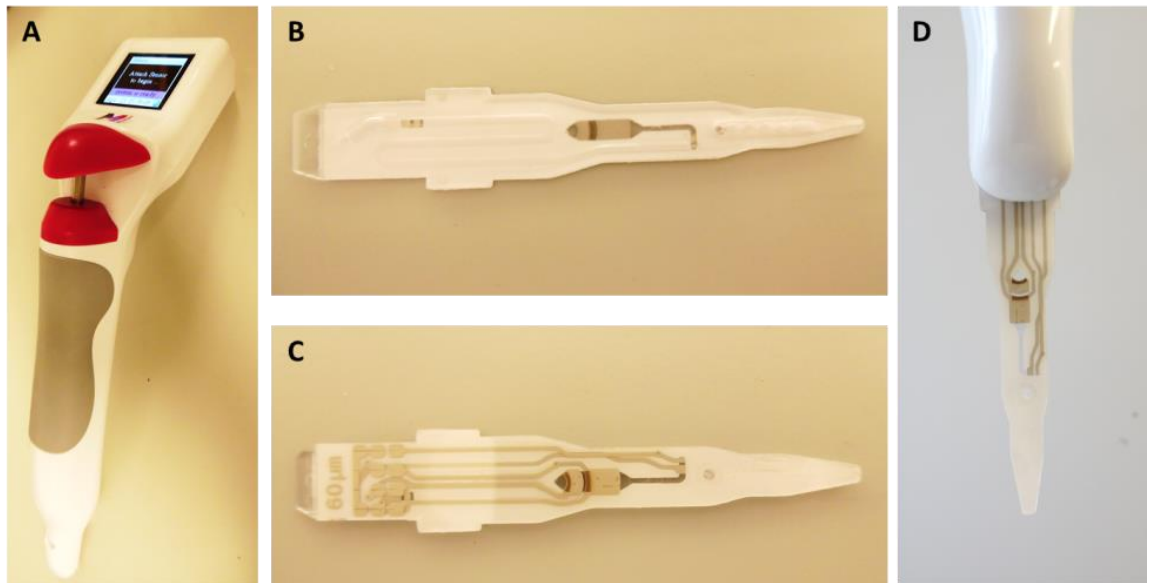


**Figure 2-1. Hand held Cell Scepter counter.** The hand held Cell Scepter (A), single use, disposable counting cartridges (B) and (C) and a cartridge loaded into the Scepter (D).

## 2.3 Isolation and culture of cells

### 2.3.1 Isolation and culture of bone marrow mesenchymal stem cells from bone marrow aspirate

MSCs were isolated from whole BMA by a modification of the plastic adherence technique described by D'Ippolito *et al*<sup>232</sup> and as refined in Kay *et al*<sup>230</sup>.

Commercially sourced whole human BMA, retrieved from the bilateral iliac crests of healthy consenting donors and supplemented with approximately 100 U of heparin/mL bone marrow, was seeded within 48 hours of aspiration at a density of  $1 \times 10^5$  MNCs/cm<sup>2</sup> in 75 cm<sup>2</sup> tissue culture flasks according to the MNC count provided with the aspirate by the supplier. Culture flasks were pre-coated with 10 ng/ml fibronectin diluted in PBS for a minimum of one hour at room temperature after which the fibronectin solution was aspirated and the BMA seeded in coated flasks in Dulbecco's Modified Eagle Medium (DMEM) (4.5 g/L glucose) supplemented with 5% (v/v) FBS, 2 mM L-Glutamine (L-Glut), 1% (v/v) non-essential amino acids (NEAA) and 1% (v/v) penicillin, streptomycin, amphotericin B (PSA) (100 U/mL penicillin, 100 µg/mL streptomycin,

0.25 µg/mL amphotericin B) and cultured for one week. A 50% media change was then performed and cells incubated for a further week after which a 100% media change was performed removing the majority of the remaining non-adherent leukocytes and erythrocytes.

Following isolation prophylactic antibiotic/antimycotic treatment with PSA was ceased and routine media changes were carried out twice weekly with maintenance media (MM) consisting of DMEM supplemented with 10% (v/v) FBS, 2 mM L-Glut, 1% (v/v) NEAA and 4 ng/mL bFGF to enhance cell proliferation<sup>233</sup>. The isolated adherent cells were designated BMA13. As an accurate population doubling (PD) was not determined during recovery, starting PD was designated as PD1 at passage 1.

### **2.3.2 Isolation and culture of bone marrow mesenchymal stem cells from bone marrow mononuclear cell preparations**

Vials of commercially available, density separated, cryopreserved, human bone marrow MNCs were stored in liquid nitrogen until required for MSC isolation. When required, vials of cells were transferred from liquid nitrogen to a 37 °C water bath and submerged until almost thawed. Cells and freezing media were then transferred to a centrifuge tube of complete media (as for hMSC isolation from bone marrow, 2.3.1) and centrifuged for 3 minutes at 250 g. The supernatant was then aspirated and cells re-suspended in complete media. Cells were then plated at  $1 \times 10^5$  MNCs/cm<sup>2</sup> and treated as for human BMA, 2.3.1.

### **2.3.3 Culture of human chondrocytes**

Commercially available primary human articular (knee) chondrocytes OK3 (Promocell) originally from a 71 year old female donor were routinely cultured in a MM of DMEM (4.5 g/L glucose) supplemented with 10% (v/v) FBS, 2 mM L-Glut, 1% (v/v) NEAA and 4 ng/mL bFGF. Cells were supplied cryopreserved at P2 and banked at P4, this was designated PD4 as earlier PD could not be accurately determined and future PD were determined from that point. During culture a

complete media change was performed twice weekly and cells were sub-cultured enzymatically at confluence using trypsin/EDTA as described in 2.2.1.

#### **2.3.4 Culture of embryonic stem cell derived progenitor cells**

hESC clonally derived progenitor cells 9C12H and 1C6 were previously clonally isolated and expanded from the H9 or H1 ESC lines respectively, as described by Forsyth *et al*<sup>234</sup>. PD was previously determined and was continued from the previously calculated point. Cells were routinely cultured in MM consisting of Knockout DMEM (KO-DMEM) supplemented with 10% (v/v) FBS, 2 mM L-Glut, 1% (v/v) NEAA, 4 ng/mL bFGF and 100 nM dexamethasone. A complete media change was performed twice weekly and cells were sub-cultured enzymatically at confluence using trypsin/EDTA as per section 2.2.1.

#### **2.3.5 Culture of human embryonic stem cell line H1**

H1 hESCs were cultured using mouse embryonic fibroblast (MEF) conditioned media on a Matrigel coated substrate. Cells were enzymatically sub-cultured with trypsin/EDTA as necessary.

##### **2.3.5.1 Conditioning of media on mouse embryonic fibroblasts**

CBA and C57BL/6 mice were mated and the females sacrificed by cervical dislocation twelve days after the observation of a vaginal plug. To retrieve embryos, the mouse abdomen was thoroughly swabbed with alcohol and opened with sterile scissors. If pregnant, the embryonic horns were removed from the mouse and the placental sacks opened. The embryo heads' were removed to ensure that they were euthanized and to remove neural tissue and the remaining tissue transferred to a 50 mL centrifuge tube containing 1% (v/v) PSA in PBS. Samples were then transferred to a biological safety cabinet for processing.

Any visible vascular tissue was removed and the tissue minced before being transferred to 0.05% (w/v) trypsin/0.02% (w/v) EDTA and placed in an incubator at 37 °C for 15-20 minutes with vortexing every 5 minutes. Larger tissue fragments were then allowed to settle and the

supernatant removed and added to complete culture media (DMEM (4.5 g/L), 10% (v/v) FBS, 2 mM L-Glut, 1% (v/v) NEAA and 1% (v/v) PSA) and distributed across an appropriate number of tissue culture flasks and placed in a humidified incubator at 37 °C, 5% CO<sub>2</sub>, ambient oxygen levels. When approaching 100% confluency MEFs were either sub-cultured enzymatically or cryopreserved as per section 2.2.1 or 2.2.3. Following the initial isolation cells were subsequently cultured in the absence of prophylactic antibiotics and antimycotics.

To produce conditioned media cells were expanded until approximately 70% confluency before their culture media was removed, cells washed with PBS and unconditioned hESC media added. This media consisted of KO-DMEM, 20% (v/v) Knockout serum replacement, 2 mM L-Glut, 1% (v/v) NEAA, 4 ng/mL bFGF, 0.1 mM β-mercaptoethanol. After conditioning overnight, media was removed to sterile bottles and frozen until required. As needed, media was thawed and filtered through a 0.2 µm filter before being supplemented with a further 4 ng/mL bFGF and stored at 4 °C.

#### **2.3.5.2 Matrigel coating of tissue culture flasks**

As required one 0.5 mL aliquot of Matrigel was thawed at 4 °C and diluted 1 in 50 in chilled KO-DMEM. Diluted Matrigel was used to cover the growth surface of tissue culture flasks for a minimum of 1 hour at room temperature. Any flasks that were not to be used immediately were stored at 4 °C. Immediately prior to use the Matrigel solution was aspirated from the flasks.

## **2.4 Umbilical cord blood collection**

Ethical approval was obtained for a pilot study to collect UCB from 12 elective caesarean section patients, REC reference number 13/NE/0045. This study was performed in collaboration with the Royal Stoke University Hospital, University Hospital of North Midlands NHS Trust (previously University Hospital of North Staffordshire) and approval was also obtained from Keele University, and the Trust Research and Development Office as required. Patients were considered eligible for

the study if they were due to undergo non-emergency elective caesarean sections at >37 weeks gestation, were over the age of 18 and deemed capable of giving informed consent.

UCB was collected following informed consent, babies were delivered by the obstetrician as per usual practice and the umbilical cord (UC) clamped and cut. Following delivery venous and arterial samples were taken routinely by medical staff to determine cord blood gas saturation values after which the placenta and cord were available for cord blood collection.

Initially it was intended that samples would be obtained under gravity; however, the requirement to clamp the cord, deliver the placenta and take blood gases delayed access for around 10 minutes, sometimes longer. As such, clotting was already beginning, leading to poor drainage of blood from the cord. Therefore, blood was aspirated using a needle and syringe, firstly from the cord and then from the large visible blood vessels in the placenta (Figure 2-2) above the uppermost clamp. Collected blood was transferred to sterile 50 mL centrifuge tubes with sterile acid citrate dextrose (ACD) anticoagulant (85 mM sodium citrate, 78 mM citric acid, 111 mM glucose) at an approximate ratio of 5 mL per 30 mL blood. Collected blood was transferred to the Guy Hilton Research Centre for processing in sterile conditions; all UCB samples were processed immediately after collection.

## **2.5 Density separation of cord blood**

MNCs were isolated from some cord blood samples using density gradient separation (Figure 2-3). Prior to blood collection Ficoll-Paque was transferred from 4 °C to room temperature to equilibrate.

15 mL of Ficoll-Paque was pipetted to 50 mL centrifuge tubes and the cord blood, diluted 1 in 4 in PBS supplemented with ACD, layered carefully above the Ficoll. Tubes were then centrifuged for 40 minutes at 400 g with the centrifuge brake set to minimal levels.

Around 80% of the upper layer (plasma) was aspirated and interface layer containing MNCs transferred to fresh tubes. Cells were then washed twice with PBS centrifuging for 15 minutes at 200 g after each wash. Isolated cells were then either plated on 10 ng/mL fibronectin coated flasks in both 2% and 21% oxygen, or separated using MACS cell separation followed by plating, and treated as per bone marrow MSC isolation (section 2.3.1).

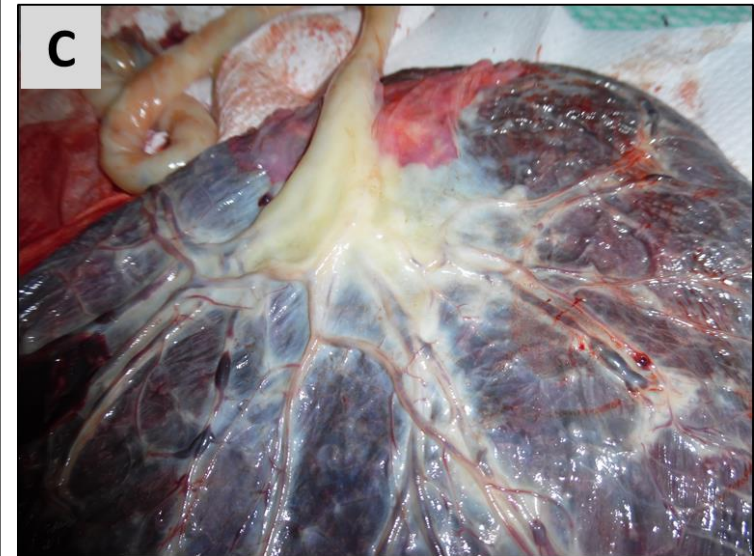
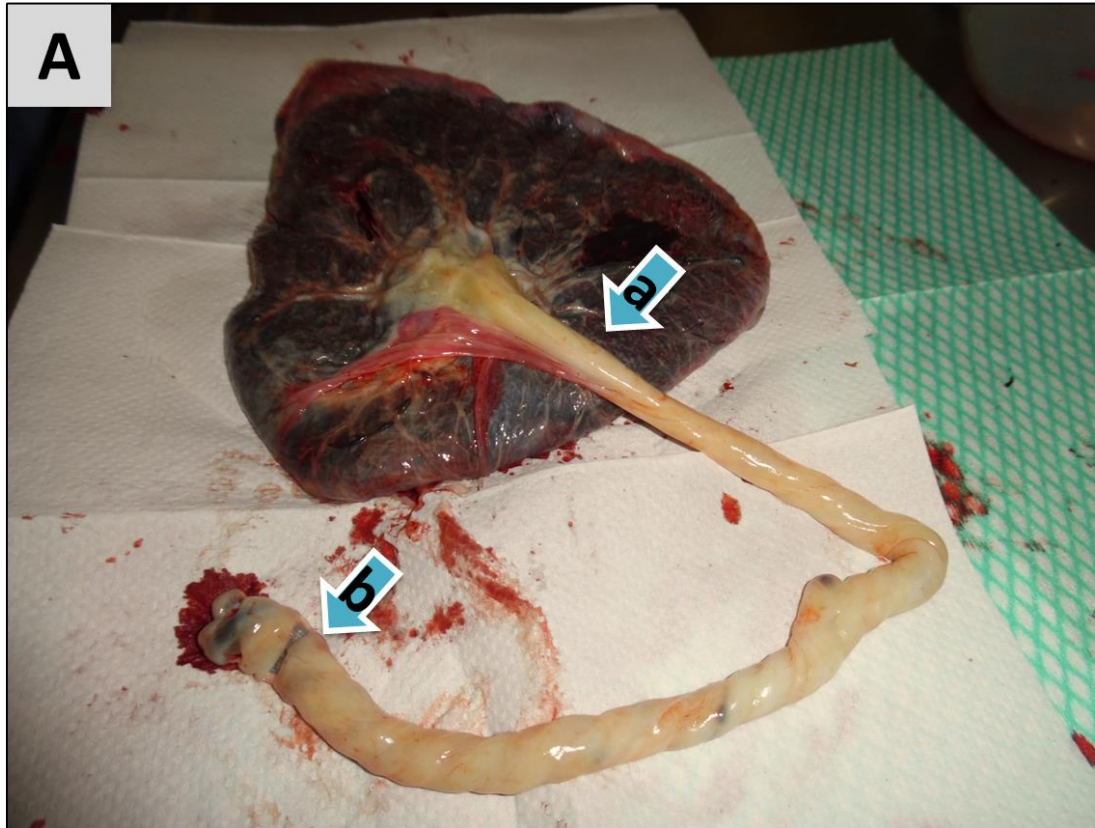


**Figure 2-2. Cord and placental blood collection.** (A) Placenta and UC, a and b show positions of crushing clamps applied during delivery, note the damage evident at position b, on this occasion no clamp had been applied at position a. (B) Crushing clamp still applied to the UC. (C) Close-up view of placental vessels used to maximise blood collection (vessels are drained in this image and are more prominent prior to this).

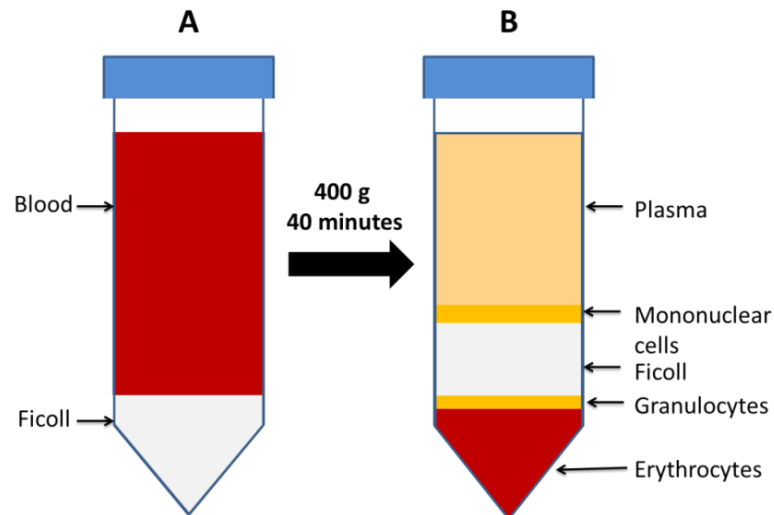


**Figure 2-3. Density gradient separation of blood.** (A) Blood is carefully layered over Ficoll-Paque (density of 1.077 g/mL) and centrifuged for 40 minutes at 400 g leading to (B) separation of the components of blood into layers isolating the MNCs.

## 2.6 MACS cell separation

Magnetic separation of CD45<sup>+</sup> cells was carried out using Miltenyi Biotec's MACS system with anti CD45 magnetic micro beads.

### 2.6.1 Labelling cells with beads

Prior to cell isolation a buffer of PBS with 0.5% bovine serum albumin (BSA) and 2 mM EDTA was prepared, sterile filtered and stored at 4 °C. Following MNC isolation cells were counted using a Millipore Scepter cell counter and cells re-suspended in 80  $\mu$ L of buffer/ $10^7$  cells. 20  $\mu$ L of CD45 beads were added, mixed with gentle flicking and cells were incubated for 15 minutes at 4 °C.

Following incubation cells were washed with approximately 2 mL buffer/ $10^7$  cells and centrifuged at 300 g for 10 minutes, the supernatant removed and cells re-suspended in 0.5 mL buffer.

### 2.6.2 Separating cells

Cells were separated using LD columns. The column was removed from the packaging and inserted into a magnetic separator. Prior to the addition of labelled cells 2 mL of buffer

(described in 2.6.1) was added to the column and allowed to run through. A fresh collection tube was then placed below the column and the labelled cells added and allowed to run through before washing through with 2 x 1 mL aliquots of buffer. This fraction contained any un-labelled cells which were plated in two 10 ng/mL fibronectin coated T25 flasks, 1 in 2% O<sub>2</sub> and 1 in 21% O<sub>2</sub>. The labelled cell fraction was then collected separately by removing the column from the magnet and flushing the contents out with 2 x 3 mL of buffer using the supplied plunger. This cell fraction was plated in 2 x T150 fibronectin coated flasks, 1 in 2% O<sub>2</sub> and 1 in 21% O<sub>2</sub>. Both fractions were then treated as per bone marrow MSC isolation section 2.3.1 excepting an increase in FBS to 10% (v/v).

## **2.7 Retroviral transduction of cells with *hTERT***

Retroviral transduction was performed using the Phoenix-A (Amphotropic) system. Target cells for the transduction were BMA13, OK3 and 1C6. BMA13 and OK3 cells were seeded at 5x10<sup>4</sup> cells/well and 1C6 at 2.5x10<sup>4</sup> cells/well in 6-well culture plates and cultured for 48 hours prior to retroviral infection.

The Phoenix system is available as both an ecotropic (only capable of infecting murine or rat cells) and an amphotropic variant (capable of infecting most mammalian cells). As human cells were being infected the Phoenix-A variant was used. See Figure 2-4 for an explanation of the Phoenix-A system and Figure 2-5 for a summary of the transduction protocol. As the use of an amphotropic vector incorporating *hTERT* represents a potential biological genetically modified organism (GMO) safety risk all transduction work was performed at the Blizzard Institute, Barts and The London School of Medicine and Dentistry, using their Class II GMO laboratory facility.

The Phoenix-A system utilises a readily transfectable human embryonic kidney (HEK) 293T-based packaging cell line that has been stably transfected with the Moloney murine leukaemia virus (MMLV) *gag*, *pol* polyprotein genes under the influence of the human respiratory syncytial virus (RSV) promoter, and separately with the *env* gene under the influence of a cytomegalovirus

promoter (CMV). Thus these cells can produce the proteins required for retroviral packaging. Following the transient transfection of a gene of interest flanked by the MMLV LTR promoter, and under the influence of the *cis*-acting RNA packaging signal  $\Psi^{235}$ , proteins produced by the packaging cell are used to package the gene of interest to produce complete virions capable of infecting and stably transducing cells. These virions themselves are still lacking the *gag*, *pol* and *env* genes so are not replication competent.

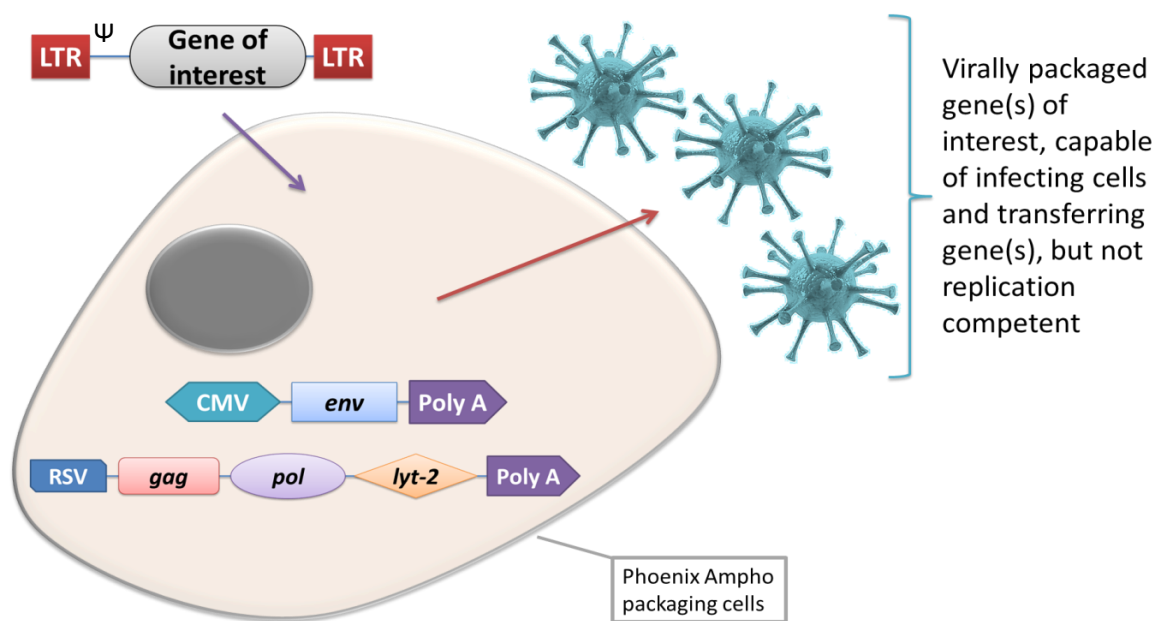


**Figure 2-4. The Phoenix-A system for retroviral vector production.** Phoenix-A HEK packaging cells, containing viral packaging genes on two different constructs, can be transfected with a further construct containing the gene(s) of interest flanked by long terminal repeats. The gene of interest is then packaged under the influence of the *cis*-acting regulatory element  $\Psi$ , using proteins produced by the packaging cells. These virions are then capable of transducing most mammalian cells with the gene of interest but are not themselves replication competent.

Phoenix-A packaging cells were seeded in 10 cm culture dishes at a density of  $2.5 \times 10^5$  cells/cm<sup>2</sup> and cultured for 24 hours in DMEM supplemented with 10% FBS, 1% NEAA, 1% L-Glut and 1% PSA. After 24 hours, for each dish of cells, 25  $\mu$ L of Fugene was added dropwise to 550  $\mu$ L of serum free DMEM and mixed gently before being incubated at room temperature for 5 minutes, after which 10  $\mu$ g of DNA with *hTERT*/G418 (pBABE-hTERT) resistance, G418 resistance alone (pBABE) (provided by Professor E. K. Parkinson, Blizard Institute, QMUL) was added to the Fugene/DMEM, mixed gently and incubated at room temperature for 20 minutes. This was then added dropwise to the Phoenix-A cell dishes with gentle swirling to mix and cells incubated for a further 24 hours. Phoenix-A medium was then replaced with medium suitable for the target cell transduction and cells incubated for 24 hours at 32°C for optimal virus production.

Supernatants containing virus were collected with a syringe and filtered with a 0.45  $\mu$ m syringe filter, fresh medium was added to the Phoenix-A dishes for further viral supernatant collection and cells returned to an incubator at 32 °C. The collected supernatant was divided to 1 mL aliquots and kept on ice. To prepare target cells for infection media was removed and replaced with 1 mL of media supplemented with polybrene at 5  $\mu$ g/mL and cells incubated at 37 °C for 15 minutes. For the infection of target cells a mixture of 1 mL of viral loaded supernatant and 1 mL of culture medium supplemented with polybrene at 5  $\mu$ g/mL was prepared for each well and added as appropriate. Control plates that received no DNA were also prepared. Plates were then sealed with parafilm and centrifuged at 300 rpm for 1 hour before being returned to the incubator. After 6 hours the infection process was repeated with fresh viral supernatant.

Selection of successfully transduced cells was begun 24 hours after infection with medium supplemented with G418 at 1 mg/mL and continued for 2 weeks, cells were sub-cultured once during selection. Following selection surviving resistant cells were trypsinised and cryopreserved.

## Phoenix A Retroviral Transfection

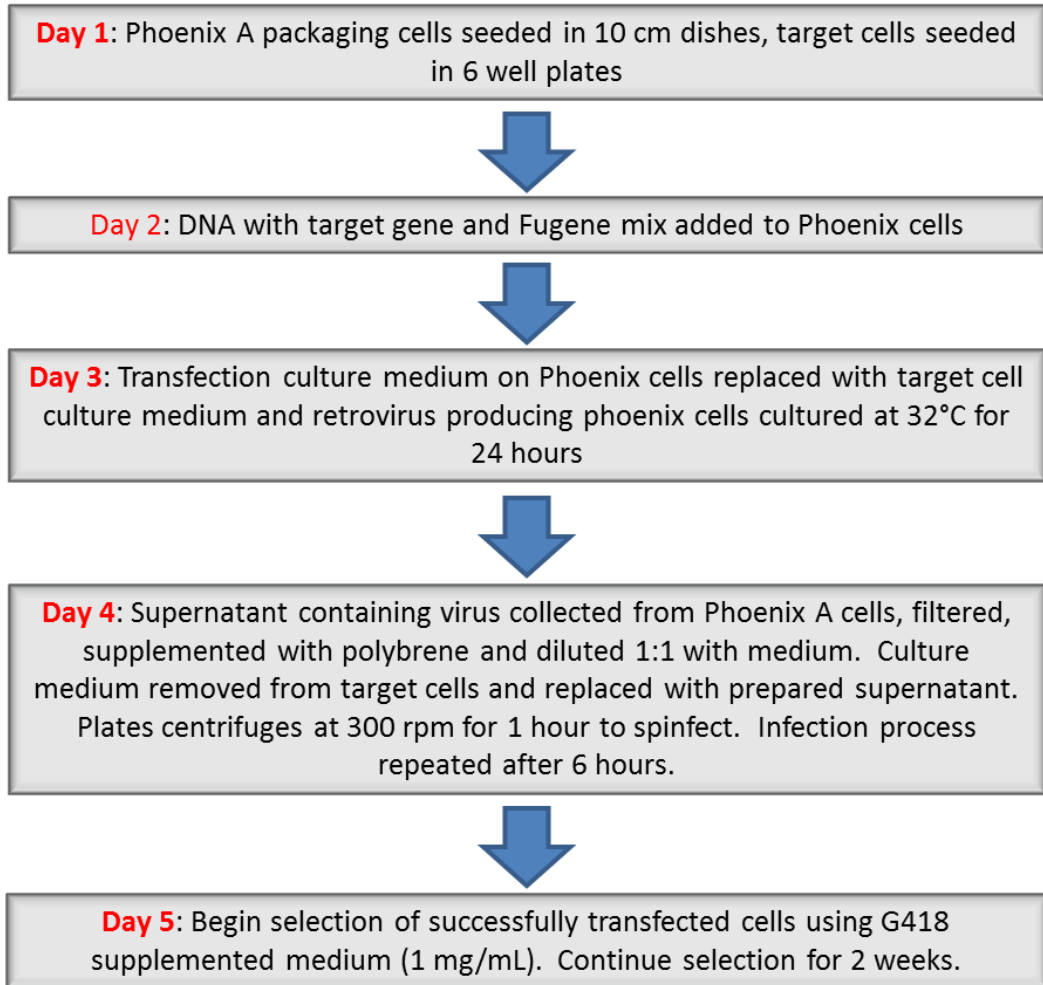


Figure 2-5. Summary of the protocol for Phoenix-A transduction of target cells.

### 2.8 Longitudinal proliferation study

The ability of ectopic *hTERT* expression to prevent functional replicative senescence was determined by monitoring the proliferation of transduced cells in comparison to non-transduced cells. Cells were maintained in continuous culture following transduction in parallel with non-transduced cells, all cells were enzymatically sub-cultured at confluence with the split ratio used to maintain approximately one sub-culture per week. Population doublings (PD) of cells were estimated based upon the split ratio of cells at sub-culture (i.e. 1:2 equals 1 PD, 1:4 equals 2 PD, 1:8 equals 3 PD etc.<sup>175,176</sup>), cells were assumed to be senescent when the cumulative PD

plateaued. Cell counts were also performed at sub-culture using a haemocytometer to determine the number of cells/cm<sup>2</sup> at confluence.

## 2.9 Senescence associated $\beta$ -Galactosidase staining

Cells were expanded to the limit of their proliferative capacity, when cells were no longer actively proliferating or, in the case of transduced cells, had greatly exceeded the capacity of control cells senescence was confirmed by SA $\beta$ Gal staining<sup>190</sup> using a SA $\beta$ Gal histochemical staining kit. If  $\beta$  galactosidase is present in the cells the enzyme cleaves the glycosidic bond present in X-Gal (5-bromo-4-chloro-3-indolyl-beta-D-galactopyranoside) to yield galactose and 5-bromo-4-chloro-3-hydroxyindole which then dimerises to form an insoluble blue precipitate<sup>236</sup>.

To detect SA $\beta$ Gal media was aspirated and cells washed twice with PBS before being fixed using the formaldehyde based fixation buffer supplied with the kit (2% formaldehyde, 0.2% glutaraldehyde, 0.704 mM Na<sub>2</sub>PO<sub>4</sub>, 0.147 mM KH<sub>2</sub>PO<sub>4</sub>, 0.137 M NaCl, 0.268 mM KCl) for 10 minutes at room temperature. Fixed cells were then either stored under PBS at 4 °C or stained immediately. To prepare the staining mixture solution, reagent B (400 mM Potassium ferricyanide), reagent C (400 mM Potassium ferrocyanide), X-Gal solution (40 mg/mL), and ultrapure water (final ratio 1:0.125:0.125:0.25:8.5) was prepared and filtered with a 0.22  $\mu$ m syringe filter. PBS was removed and a sufficient volume of staining mixture added to each well to cover the cells. Plates were then incubated at 37 °C with atmospheric CO<sub>2</sub> levels for 16 hours. The reaction must be maintained at pH6 therefore incubation must not be carried out in an incubator with increased CO<sub>2</sub> levels.

The staining mixture was then removed and the cells washed with PBS.

SA $\beta$ Gal stained cells were counterstained with haematoxylin for 10 minutes followed by washing in tap water. A final wash in acetic acid acidified water was carried out to ensure that haematoxylin remained red rather than blue for good contrast. Photomicrographs were then

obtained under brightfield. Total cells and SA $\beta$ Gal positive cells from 4 different fields were manually quantified using the Fiji distribution of ImageJ<sup>237</sup>.

## **2.10 Tri-lineage differentiation**

To determine differentiation potential cells were seeded at  $5 \times 10^4/\text{cm}^2$  in standard proliferation media overnight to allow attachment after which media were changed to differentiation media.

Cells were then cultured in the appropriate differentiation media for 20 days with media changes twice weekly.

### **2.10.1 Chondrogenic differentiation**

Chondrogenic differentiation was induced in monolayer and in pellets using pro-chondrogenic media (PChM) which consisted of basal media with reduced FBS (1% (v/v)) further supplemented with, 1% (v/v) ITS, 1% (v/v) sodium pyruvate, 0.1  $\mu\text{M}$  dexamethasone, 50  $\mu\text{M}$  ascorbic acid phosphate, 40  $\mu\text{g}/\text{mL}$  L-proline (Sigma-Aldrich) and 10  $\text{ng}/\text{mL}$  TGF- $\beta$ 3. Cells for staining in monolayer were fixed with 95% methanol for 10 minutes, washed with PBS and stored at 4  $^\circ\text{C}$  under PBS until staining with alcian blue, section 2.11.1. Cells for glycosaminoglycan and DNA quantification were not fixed and were processed as described in section 2.14.

### **2.10.2 Osteogenic differentiation**

Osteogenesis was induced in cells using media supplemented with 50  $\mu\text{M}$  ascorbic acid phosphate, 10  $\text{mM}$   $\beta$ -glycerophosphate and 0.1  $\mu\text{M}$  dexamethasone for 20 days before monolayers were fixed with 95% methanol for 10 minutes, washed with PBS and stored at 4  $^\circ\text{C}$  under PBS until staining with alizarin red S for calcium deposits as per section 2.11.2.

### **2.10.3 Adipogenic differentiation**

Adipogenesis was induced with 0.5  $\mu\text{M}$  dexamethasone, 0.5  $\text{mM}$  3-isobutyl-1-methylxanthine, 10  $\mu\text{g}/\text{mL}$  insulin and 0.1  $\text{mM}$  indomethacin. Cells were fixed with 4% (w/v) paraformaldehyde in

PBS for approximately 20 minutes, washed with PBS and stored at 4 °C under PBS until staining with Oil Red O for intracellular lipid droplets as described in 2.11.3.

## **2.11 Histological staining of differentiated monolayers**

### **2.11.1 Alcian blue monolayer staining**

Fixed monolayers were stained with Alcian blue to detect sulphated glycosaminoglycans. 1% (w/v) alcian blue was prepared in 0.1 M aqueous HCl and paper filtered. This results in a stain with a pH of 1.0, which has improved specificity for sGAGs over preparations made in acetic acid, as the higher pH results in more weakly acidic groups (e.g. carboxylated residues) remaining protonated and therefore un-stained. To stain monolayers the PBS under which monolayers were stored were removed and the cells washed before being covered with the Alcian blue stain overnight. The stain was then removed and the well washed gently under running tap water until clear. Stained monolayers were imaged as soon as possible thereafter.

### **2.11.2 Alizarin red S monolayer staining**

Fixed monolayers were stained with alizarin red S to detect mineralised calcium nodules. An aqueous solution of 2% (w/v) of alizarin red S was prepared in distilled water (dH<sub>2</sub>O) and paper filtered. To stain monolayers PBS was removed and the cells washed before being covered with alizarin red S solution for 10 minutes. Stain was then removed and monolayers washed gently under running tap water until clear. Wells were then allowed to dry before image acquisition.

### **2.11.3 Oil Red O monolayer staining**

Fixed monolayers were stained with Oil Red O for intracellular lipid droplets. An Oil Red O stock solution was prepared as a saturated solution using 300 mg of Oil Red O in 100 mL of 99% (v/v) isopropanol, to ensure maximum saturation of the solution it was left at least overnight before being used. The working solution was prepared fresh immediately prior to staining; to prepare, a small volume of stock solution was diluted to 60% (v/v) in dH<sub>2</sub>O and the resultant solution filtered

using a 0.22  $\mu\text{m}$  syringe filter. PBS covering the wells was removed and the cell monolayer washed rapidly with a small amount of 60% isopropanol and covered with the filtered Oil Red O working solution for 5 minutes after which the stain was removed, the well rapidly washed once with 60% isopropanol before imaging immediately.

## **2.12 Flow cytometry**

Cells were trypsinised, counted and re-suspended in flow cytometry buffer (PBS with 0.5% (w/v) BSA and 2 mM EDTA) for 15 minutes and approximately  $1 \times 10^5$  cells aliquoted into 1.5 mL microcentrifuge tubes, centrifuged at 300 g for 10 minutes and the supernatant discarded. Phycoerythrin conjugated antibodies (CD14, CD19, CD34, CD45, CD73, CD90 and CD105, HLA-DR, IgG<sub>1</sub> and IgG<sub>2a</sub> isotype controls) diluted in flow cytometry buffer were used to re-suspend cell pellets followed by incubation in the dark at 4 °C for 10 minutes. Buffer was added to stained cells to a volume of approximately 1 mL and cells centrifuged at 300 g for 10 minutes, supernatant discarded and the cells re-suspended in 300  $\mu\text{L}$  of flow cytometry buffer. At least 50,000 events were acquired on a Beckton Dickinson FC500 flow cytometer. Data were analysed using the freely available Flowing Software (version 2.1) supported by Flow Explorer 4 to produce coloured density plots of forward and side scatter. Percentage positive events were determined using gates to exclude 99% of the appropriate isotype control events. (IgG<sub>1</sub>: CD19, CD73, CD90 and CD105, IgG<sub>2a</sub>: CD14, CD34, CD45, HLA-DR.)

## **2.13 Preparation of monolayer samples for DMMB and PicoGreen analysis**

### **2.13.1 Preparation of cell monolayers**

Chondrogenic differentiation was induced using PChM as described in section 2.10.1.

Cells were seeded in MM at approximately  $5 \times 10^4/\text{cm}^2$  in 24 well tissue culture plates in triplicate wells for control and pro-chondrogenic condition assessment at days 0, 5, 10 and 20 and incubated overnight to allow attachment. Media was then replaced with either fresh MM or

PChM as appropriate and changed regularly throughout the experiment; all media were collected for DMMB sGAG analysis.

At days 0, 5, 10 and 20 the media was removed and cells covered with 125 µg of proteinase K in 100 µL of 100 mM ammonium acetate. After approximately 5 minutes the contents of the well were repeatedly pipetted to dislodge all cells and the contents transferred to a 1.5 mL microcentrifuge tube. Wells were washed with a second aliquot of 100 µL of proteinase K solution and this was added to the initial material. Tubes were capped and incubated overnight at 60 °C; all samples were vortexed at least twice during incubation.

Following digestion 1 mL of ice cold absolute ethanol was added to each digest and samples were left to precipitate at -20 °C overnight, centrifuged at 17,000 g to pellet the precipitate and the ethanol supernatant discarded. Pellets were dried by speed-vac for ten minutes then re-dissolved in 125 µL of 100 mM ammonium acetate for PicoGreen and DMMB analysis, dissolution was slow so samples were left overnight at 4 °C to maximise this.

### **2.13.2 Preparation of media**

Due to evaporation of media from wells during cell culture collected media volumes had to be restored to the correct volumes with dH<sub>2</sub>O, volumes for correction were determined by mass. Following volume adjustment where necessary, aliquots of 333 µL of collected spent media were aliquoted and treated with 25 µL of 2.5 mg/mL proteinase K at 60 °C overnight. Samples were cooled, 1 mL of ice-cold ethanol was added and samples precipitated at -20 °C overnight. The precipitate was pelleted by centrifugation at 17,000 g for 15 minutes and the ethanol supernatant discarded before the pellet was dried and re-dissolved in 125 µL of 100 mM ammonium acetate for DMMB analysis. Aliquots of all media types were also processed and prepared to correct media DMMB reading as media, particularly MM with 10% FBS, gave significant positive values.

## **2.14 DMMB sulphated GAG quantification**

Samples dissolved in 100 mM ammonium acetate were used for DMMB sGAG quantification, 50 µL of each sample was aliquoted in duplicate to a 96 well microplate; plates were then transferred to a Synergy 2 plate reader. An automated dispense unit was used to dispense 200 µL of DMMB solution (16 mg DMMB, 0.76 g glycine, 0.595 g NaCl, 23.75 mL 0.1 M HCl, dH<sub>2</sub>O to 250 mL) to a single well followed by determination of the absorption at 530 nm. All wells were processed in this manner to maximise reproducibility and minimise the potential for precipitation of the DMMB-GAG complex.

## **2.15 PicoGreen double stranded DNA assay**

The Quant-iT PicoGreen double stranded DNA assay was carried out on ethanol precipitated cell digests re-dissolved in 125 µL of 100 mM ammonium acetate according to the manufacturer's protocol. Double stranded DNA standards were prepared from the kit Lambda DNA standard at concentrations of 20, 10, 5, 2.5 and 1.25 µg/mL in 100 mM ammonium acetate. Duplicate sample aliquots and standards (10 µL) were diluted 1 in 10 in TE buffer in a 96 well microplate. PicoGreen working solution was prepared by diluting 1 in 200 in TE buffer immediately before use; 100 µL of the working solution was added to each sample or standard and incubated for two minutes before being read using a Synergy 2 plate reader (excitation 480 nm, emission 520 nm). Concentrations were determined using a calibration curve with linear regression; samples were normalised using 10 mM ammonium acetate in TE buffer.

## **2.16 Cell pellet creation**

For each set of pellets created cells were trypsinised and counted to determine the total number of cells and therefore pellets that could be formed. The total cell suspension was divided in two to allow the creation of pellets in both MM and PChM. The cell suspensions were then centrifuged at 250 g for 3 minutes to pellet cells and the trypsin/media supernatant removed.

Cells were re-suspended in either MM or PChM to a concentration of  $2.5 \times 10^5$  cells/mL. 1 mL of cell suspension then pipetted to the requisite number of 1.5 mL microcentrifuge tubes. Tubes were capped and centrifuged at 300 g for 3 minutes before being transferred to an incubator.

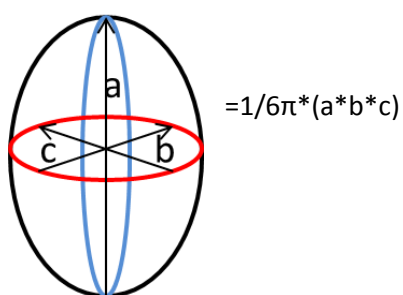
Cell pellets for day 0 DMMB and PicoGreen analysis had the media removed from the pellet and transferred to an additional microcentrifuge tube and both cells and media were stored at  $-20^\circ\text{C}$  until needed. Cell pellets for day 1 histology were cultured overnight before the media was removed and approximately 0.5 mL 4% buffered paraformaldehyde added for 24 hours at room temperature. The paraformaldehyde was then removed and replaced with PBS before storing at  $4^\circ\text{C}$  until required. Day 20 cell pellets continued to receive media changes twice weekly with the appropriate medium type and were then frozen or fixed as described.

## 2.17 Pellet size

Fixed cells were imaged and photomicrographs used for pellet size determination in ImageJ.

Pellets were measured in ImageJ with the pixel/mm ratio determined using a stage micrometer.

Pellets were generally spheroidal; however, as some were more ellipsoidal a measurement of diameter was taken on both the long and short axis. A volume for each pellet was then estimated using the equation for the volume of an ellipsoid:



As the measurements are taken from a two dimensional image b and c are assumed to be equal.

## 2.18 Micro computed tomography

### 2.18.1 Sample scanning

Samples were stored in PBS prior to scanning. To scan samples were blotted briefly to remove excess liquid and placed on polystyrene packed into a 0.5 mL microcentrifuge tube. The microcentrifuge tube was then slotted into the smallest sample holder provided with the  $\mu$ CT 40 (Scanco Medical)  $\mu$ CT scanner before being sealed with Parafilm. The sample holder was then slotted into position in the  $\mu$ CT scanner and the door sealed (Figure 2-6).

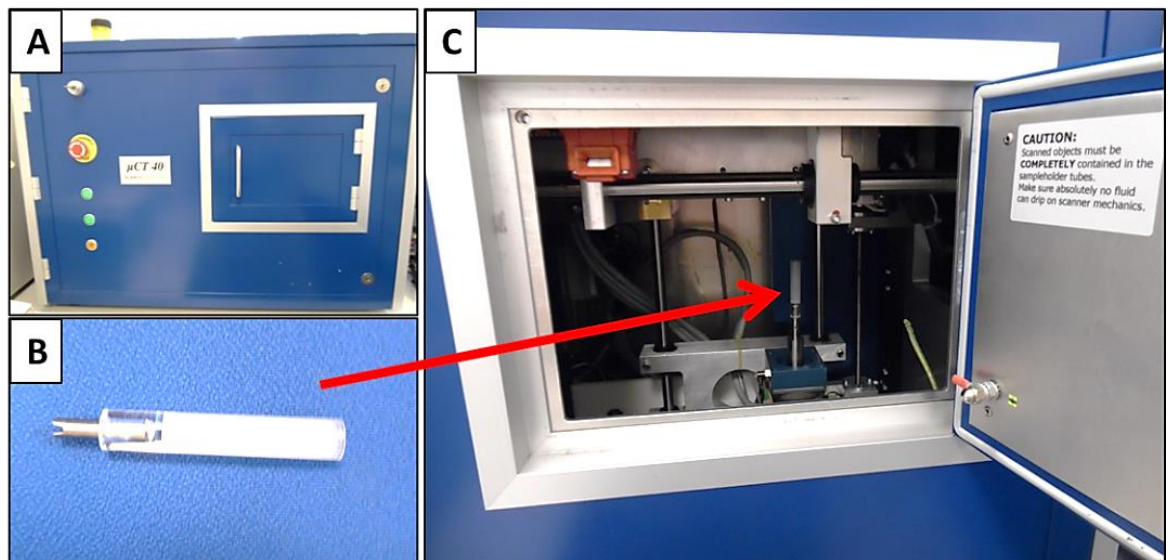


**Figure 2-6. Scanco Medical  $\mu$ CT 40 scanner.** External view of scanner (A), sample holder used for all samples (B) and internal mount for samples (C).

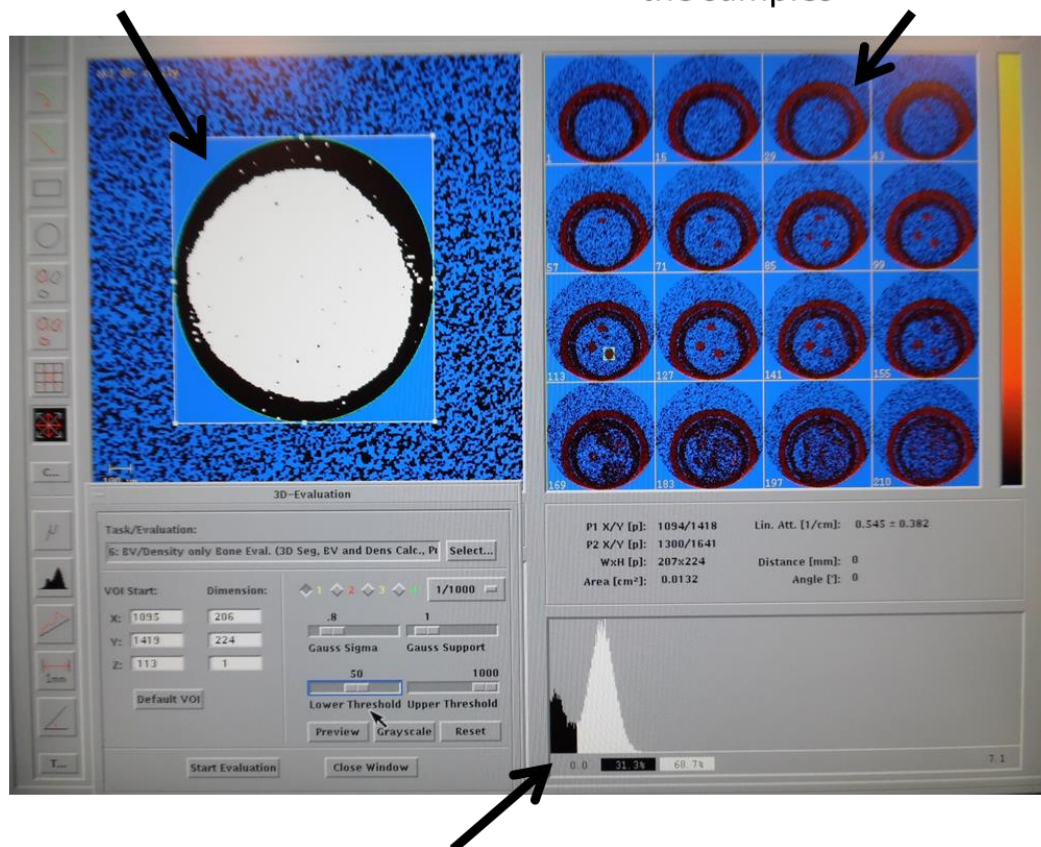
A 'Scout-view' scan was performed to locate the samples and specify the region to be scanned; reducing this to the minimum required reduces the total scanning time. All scans were performed with  $\mu$ Ct settings of 45 kVp/176  $\mu$ A. Following scan acquisition samples were immediately removed and returned to PBS. Porcine cartilage was also scanned for comparison.

### 2.18.2 Sample processing

Following scan acquisition the scan is automatically compiled after which it is available for processing. Compiled scans were opened and individual samples isolated by contouring selected scans and applying the contouring to the entire scan. Each sample was then analysed to determine relative volume and density based on a threshold which effectively separated the sample from background noise, in this case 50 (Figure 2-7).

Contoured sample thresholded at 50

Selected scans through the samples



Histogram of signal, thresholding at 50 isolates the majority of the sample (white) and removes the majority of the background signal

**Figure 2-7. Analysis of  $\mu$ CT scanned samples.** Following scanning each sample was analysed using the scanner's proprietary software. The sample was isolated by drawing a contour to encompass all section after which it was thresholded at 50/1000 for analysis of volume and density.

## **2.19 Cell lysis and homogenisation**

### **2.19.1 Lysis of monolayers and trypsinised cells**

Cells were lysed using the RLT lysis buffer provided with the RNeasy mini kit following the manufacturer's protocol. Prior to lysis cell monolayers were washed with PBS after which 350  $\mu$ L of RLT buffer supplemented with 10  $\mu$ l/ml  $\beta$ -mercaptoethanol was added. A cell scraper or vigorous pipetting was used to ensure cells were detached from the culture flask and the resulting lysate was transferred to a QIAshredder minispin column for homogenisation and removal of insoluble material. This was centrifuged at for 2 minutes at 17000 g before the minispin column was removed and discarded and the tube capped; cell lysates were either processed for RNA extraction immediately or were stored at -80 °C until required.

### **2.19.2 Lysis of cell pellets**

After 20 days in culture, particularly in the presence of PChM, all cell pellets were extremely resistant to lysis, as such the RNeasy mini kit was used with some modifications to the manufacturers protocol.

Prior to lysis pellets were washed in PBS and frozen. Each pellet was then physically disrupted using a disposable, single use, DNase, RNase free pestle in the presence of a small amount of RLT lysis buffer supplemented with 10  $\mu$ L/ml  $\beta$ -mercaptoethanol. Pellets were homogenised in this way in the tube in which they were cultured to ensure any cells not in the main body of the pellet were also lysed. RLT lysis buffer was then added in 2 aliquots over the pestle to wash off any cellular material to a total volume of 350  $\mu$ L and the tube vortexed. To further disrupt proteinaceous material 150  $\mu$ L of 2.5 mg/mL proteinase K<sup>238</sup> was then added to the lysis buffer and incubated for 20 minutes at 57 °C with vortexing half way through and at the end. Lysate was then added to a QIAshredder column and centrifuged at 17,000 g before the minispin column was removed and discarded and the tube capped. All pellet lysates were then immediately processed for RNA extraction.

## 2.20 RNA extraction

Prior to RNA extraction all pipettes and surfaces were treated with RNase ZAP. Total RNA extraction was carried out using the RNeasy mini kit. Lysates from pellets were processed immediately after lysis; frozen lysates were defrosted and placed on ice.

One volume of 70% ethanol was added to the lysate and the resulting solution transferred to an RNeasy mini spin column. This was centrifuged for 15 seconds at 17,000 g and the flow-through discarded leaving total RNA bound to the column membrane. To wash the membrane, buffer was added and the tube centrifuged repeatedly at 17,000 g, following each centrifugation the flow-through was discarded (700 µL of buffer RW1, 15 seconds centrifugation, 500 µL of buffer RPE, 15 seconds centrifugation, 500 µL of buffer RPE, 2 minutes centrifugation). The used collection tube was discarded and replaced with a fresh tube. The mini spin column was then centrifuged at 17,000 g to remove any residual fluid. The collection tube was discarded and replaced with a final 1.5 mL lidded collection tube. To elute the RNA from the membrane 10-25 µL of RNase free water was added to the column and allowed to soak the membrane for one minute, after which the column was centrifuged for 1 minute at 17,000 g. The eluent was re-pipetted onto the membrane and the column centrifuged a final time at 17,000 g for 1 minute. Extracted RNA was quantified using a Nanodrop 2000 spectrophotometer (Thermo Scientific) and stored at -80 °C until required.

## 2.21 Reverse transcription – polymerase chain reaction

RNA extracts were diluted in ultrapure RNase/DNase free dH<sub>2</sub>O to a concentration of 25 ng/µL for *hTERT* expression analysis. Reverse transcription-polymerase chain reaction (RT-PCR) was carried out in one step using a SuperScript III One-Step RT-PCR Platinum *Taq* HiFi kit. These kits contain Superscript III reverse transcriptase enzyme for cDNA synthesis, Platinum *Taq* DNA polymerase for amplification and the proofreading enzyme *Pyrococcus* species *GB-D* polymerase to improve amplification fidelity. This system also uses 'hot start' technology, which is the incorporation of

*Taq* DNA polymerase antibodies to block enzyme activity until they are denatured by the first melting cycle at 94 °C, to prevent premature and non-specific amplification.

One µL (25 ng) of each diluted RNA sample was aliquoted to chilled 0.2 mL PCR tubes and kept on ice, a master mix of 6.25 µL 2x reaction mix, 1 µL of each relevant primer (10 µM) and 3 µL RNase/DNase free water per sample was prepared. Immediately prior to transfer to the thermal cycler, 0.25 µL per sample of SuperScript III RT/Platinum *Taq* High Fidelity enzyme mix was added to the master mix, 11.5 µL of master mix added to each sample and the tubes capped; if necessary the tube strip was briefly centrifuged and then transferred to a SensoQuest Labcycler (Geneflow) thermal cycler. The thermal cycler was programmed as follows:

- One cycle of 50 °C for 30 minutes (reverse transcription step)
- One cycle of 94 °C for 2 minutes (denature hot start antibodies and DNA melting)
- 40 cycles of:
  - 94 °C for 15 seconds (DNA melting)
  - Annealing temperature as appropriate for primer pair for 30 seconds
  - 68 °C for 1 minute (DNA extension)
  - One cycle of 68 °C for 5 minutes
  - 15 °C ∞

Following completion of amplification samples were either fractionated immediately on agarose gels or stored at 4 °C prior to fractionation.

### **2.21.1 Primer Sequences**

RT-PCR was carried out with custom primers (Life Technologies) for the housekeeping gene  $\beta$ -*Actin* and *hTERT* with primer sequences as listed in Table 2-2.

**Table 2-2. RT-PCR primer sequences.**

Gene name (protein product)	Sense sequence (5' to 3')	Antisense sequence (5' to 3')	Annealing Temperature (°C)	Product size (bp)
<b>ACTB</b> (Actin, cytoplasmic 1)	GCCACGGCTGCTCCAGC	AGGGTGTAACGCAACTAAGTC	55	477
<b>TERT</b> (telomerase reverse transcriptase)	GCAGCTCCCATTTTCATCAGC	CAGGATGGTCTTGAAGTCTG	58	343

## 2.22 Agarose gel electrophoresis

Following RT-PCR amplification samples were fractionated by agarose gel electrophoresis. Gels were poured approximately 1hour prior to use and consisted of 2% agarose in 1X tris-acetate-EDTA (TAE) buffer (40 mM Tris Acetate, 2 mM Na<sub>2</sub>EDTA) with 0.7 µg/mL ethidium bromide.

Ethidium bromide is a fluorescent DNA dye that intercalates with the double stranded DNA helix whereupon fluorescence emission following UV excitation (Figure 2-8A) is increased compared to non-complexed ethidium bromide allowing the visualisation of ethidium bromide-complexed DNA bands within the gel.

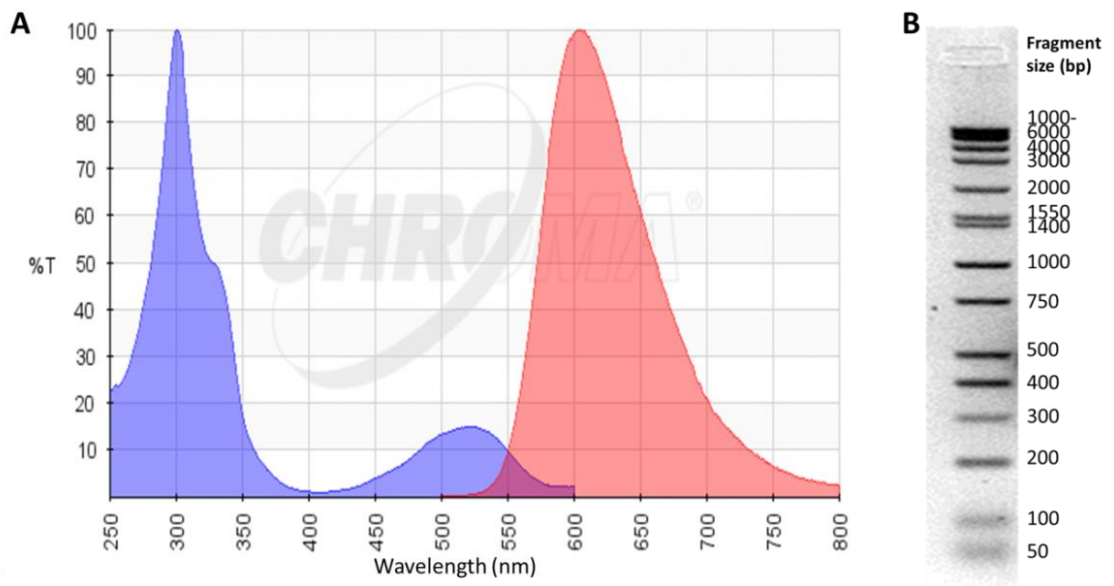


**Figure 2-8. Ethidium bromide gel electrophoresis.** (A) Ethidium bromide absorption (blue) and emission (red) spectra. (Chroma Spectra Viewer, <https://www.chroma.com/spectra-viewer>). (B) Direct load wide range DNA ladder. Fragment size (base pairs (bp)) indicated. The top 3 bands are not fully resolved at this percentage gel and these electrophoresis settings.

Prior to loading each sample was mixed with a 2  $\mu$ L aliquot of gel loading buffer and then carefully pipetted into the gel wells. To allow the determination of fragment size DirectLoad wide range DNA marker (Figure 2-8B) was also run. All gels were run for 1 hour at 100 V in 1X TAE buffer and were visualised by fluorescence at 254 nm in a UV transilluminator (Syngene); gel images were captured with Syngene Genesnap software.

### 2.23 Quantitative reverse transcription-polymerase chain reaction

Relative gene expression in cell pellets at day 0 and after 20 days in either MM or PChM was assessed using quantitative reverse transcription-polymerase chain reaction (qRT-PCR) using SuperScript™ III Platinum™ SYBR™ Green One-Step qPCR Kits. Sybr green is a DNA binding cyanine dye that exhibits greatly enhanced (>1000 fold increase) fluorescence when bound to double stranded DNA. qRT-PCR allows the determination of the abundance of the product during the course of amplification, with the product specified by the primer pair. As the product is amplified a fluorescent signal is generated which is measured at the end of each PCR cycle. At the end of

the PCR run the relative abundance of product in each sample can be determined by comparison of the cycle number that each sample has accumulated sufficient fluorescence to cross an arbitrary threshold. This threshold is determined by the thermal cycler and is set to be above background levels and lies within the exponential phase of product amplification for all samples. The cycle at which the threshold is passed ( $C_T$ ) was normalised for all samples and all PCR runs using the  $C_T$  value for the housekeeping gene *GAPDH* (glyceraldehyde 3-phosphate dehydrogenase) and relative expression calculated using the  $2^{-\Delta\Delta C_T}$  method.

RNA extracts were diluted in ultrapure RNase/DNase free dH<sub>2</sub>O to a concentration of 7.5 ng/ $\mu$ L for expression analysis. Samples were prepared by aliquoting 1  $\mu$ L (7.5 ng) of each diluted RNA sample to chilled 0.2 mL PCR tubes that were kept on ice, a master mix of 6.25  $\mu$ L 2x reaction mix, 1  $\mu$ L of each relevant primer (10  $\mu$ M), 0.025  $\mu$ L ROX and 3  $\mu$ L RNase/DNase free water per sample was prepared. Immediately prior to transfer to the thermal cycler, 0.25  $\mu$ L per sample of enzyme mix was added to the master mix and the master mix thoroughly mixed and 11.5  $\mu$ L of master mix added to each sample and the tubes capped; if necessary the tube strip was briefly centrifuged and then transferred to a Stratagene MX3005P real time thermal cycler. The thermal cycler was programmed as follows and as shown in Figure 2-9:

- One cycle of 50 °C for 15 minutes (reverse transcription step)
- One cycle of 95 °C for 5 minutes (denature hot start antibodies and DNA melting)
- 40 cycles of:
  - 95 °C for 15 seconds (DNA melting)
  - Annealing temperature as appropriate for primer pair for 30 seconds
  - 68 °C for 30 seconds (DNA extension)
    - Fluorescence determination
  - One cycle of 40 °C for 1 minute
  - Pre-programmed melt curve:
    - 96 °C for 1 minute
    - 55 °C for 30 seconds

- 95 °C for 30 seconds
  - Fluorescence determination as temperature increased incrementally from 55 °C to 95 °C

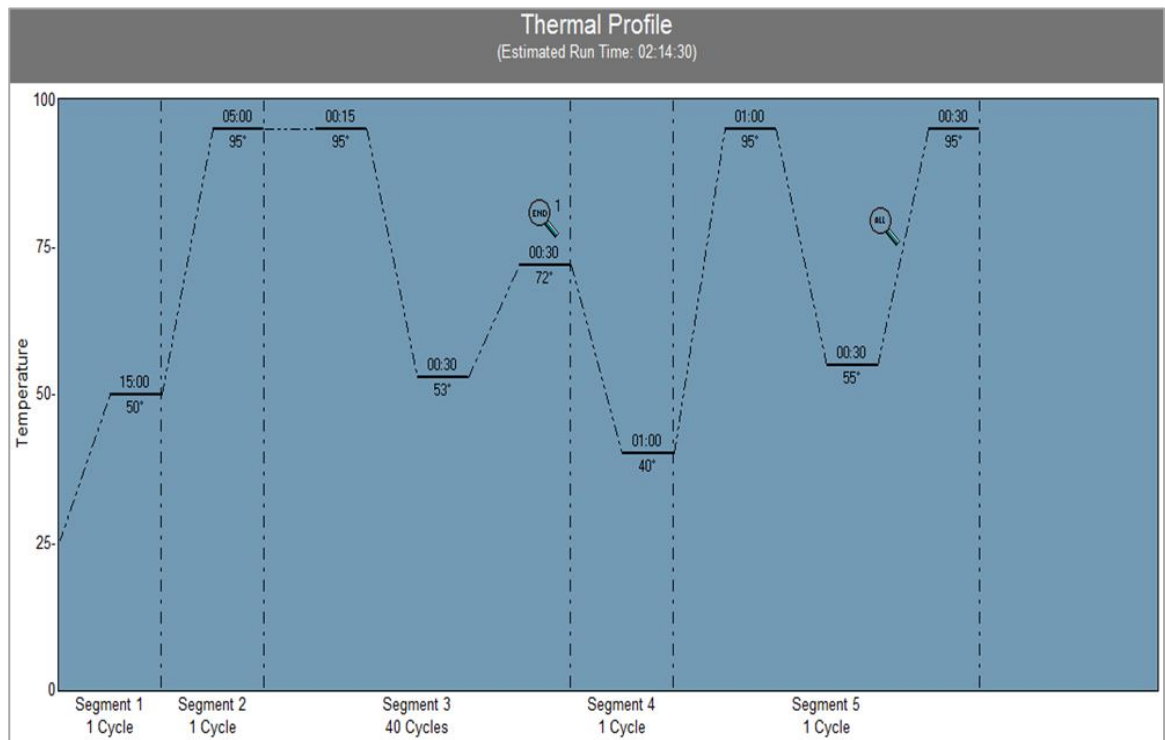


**Figure 2-9. qRT-PCR thermal cycle programme.** Segment 1 corresponds to the reverse transcription step, segment 3 to amplification of the product and segment 5 to the melt curve.

### 2.23.1 qRT-PCR primer sequences

Primers were designed using Primer3 primer designing tool<sup>239,240</sup> from NCBI EntrezGene Reference sequence gene sequences. The exon coding sequence was identified from the whole gene sequence and a region of the exon coding sequence used in Primer3. Where possible all primers were designed to be exon spanning and preferably located on an exon/exon junction. Primer sequences are listed in Table 2-3.

**Table 2-3. qRT-PCR primer sequences.**

Gene name (protein product)	Sense sequence (5' to 3')	Antisense sequence (5' to 3')	Annealing Temperature (°C)	Product size (bp)
<b>GAPDH</b> (Glyceraldehyde 3-phosphate dehydrogenase)	GACTTCAACAGCGACACC	TTCTCTTGTGCTCTTGC	53	196
<b>COL1A2</b> (Collagen alpha- 2(I) chain)	GACTTTGTTGCTGCTTGC	CAAGTCCAACCTCTTTCC	51	242
<b>COL2A1</b> (Collagen alpha- 1(II) chain)	TGTCCTTCGGTGCAGG	GTCAGTTGGCAGATGG	54	220
<b>COL3A1</b> (Collagen alpha- 1(III) chain)	AAGGACACAGAGCTTCG	CTGGTTGACCATCACTGC	52	210
<b>COL6A3</b> (Collagen alpha- 3(VI) chain)	CTTTGACTTTGACGAGTACC	TGAATGACCACCTTCACG	51	150
<b>COL10A1</b> (Collagen alpha- 1(X) chain)	TTCATGGAGTGTTTTACGC	GTCCAGGACTCCGTAGC	55	222
<b>ACAN</b> (Aggrecan core protein)	TCTGAGGGTCATCACTGC	CTTCTCCTTGGACACACG	56	217
<b>COMP</b> (Cartilage oligomeric matrix protein)	GGGAACTGCAGGAAACC	GCTCTCCGTCTGGATGC	57	215
<b>SOX9 (SRY (Sex Determining Region Y)-Box 9)</b> (Transcription factor SOX9)	CCGAGCTCAGCAAGACG	CTTGAAGATGGCGTTGG	55	218

Following design, lyophilised primers were obtained from Life Technologies custom primer service and dissolved in RNase/DNase free water to 100 µM stock solutions and 10 µM working solutions and stored at -20 °C.

### 2.23.2 qRT-PCR data analysis

Relative gene expression in the form of  $2^{-\Delta\Delta CT}$  fold change values were calculated<sup>241</sup> using the software REST-2009<sup>242</sup>. Rest determines  $2^{-\Delta\Delta CT}$  values from input  $C_T$  values obtained from the thermal cycler MXPro QPCR software; it also performs statistical analysis using a randomisation

algorithm. The REST-2009 software reports expression changes in the form of box and whisker plots where the box represents the interquartile (middle 50%) values and the whiskers the outer quartiles with a dotted line at the median.

#### **2.23.2.1 Hierarchical clustering**

The previously calculated fold change values were used to produce heat maps of gene expression with the associated hierarchical clustering dendrograms of both samples and genes. Hierarchical clustering was performed within cell type, within transduced and parental cell type and across all data. The clustering was performed using the Hierarchical clustering algorithm in Gene Cluster 3.0<sup>243</sup> with associated data viewed in Java TreeView<sup>244</sup>. To produce a clustered data set fold change values were saved as a tab de-limited file which was then loaded into Gene Cluster 3.0. Data were first log transformed after which hierarchical clustering was done using an un-centred correlation similarity metric and average linkage clustering. Cluster 3.0 output files were then viewed in Java TreeView, heat map images exported and the correlation co-efficient for each cluster noted.

### **2.24 Pellet and tissue histology and immunohistochemistry**

#### **2.24.1 Porcine tissue control samples**

Porcine cartilage and tendon tissue samples were obtained to be used as a positive controls for histological and immunohistological staining. Full depth articular cartilage cores were removed from a porcine knee joint (provided by Dr Hareklea Markides) using a bone marrow biopsy Jamshidi needle, tendon tissue was excised from the same joint using scissors and a scalpel. Tissue was fixed overnight in 4% (w/v) paraformaldehyde at room temperature, washed in PBS and stored at 4 °C prior to paraffin embedding.

#### **2.24.2 Embryonic chick femur control samples**

A fixed and paraffin embedded embryonic chick femur at E11 was kindly provided by Michael Rotherham to use as a tissue control.

#### **2.24.3 Paraffin embedding**

Pellets and tissue samples were dehydrated by alcohol series, firstly by immersing in 70% IMS for at least 1 hour followed by 90%, 100% and 100% isopropanol for 1 hour each before being transferred to melted paraffin wax at 60 °C in a wax embedder (Thermo Shandon) overnight. Isopropanol rather than ethanol was used as the primary dehydration agent as this removed the requirement for a clearing agent such as xylene or HistoClear as isopropanol, unlike ethanol, is fully miscible with melted paraffin wax. Following overnight incubation in wax, samples were transferred to fresh paraffin wax in an embedding mould, a labelled cassette added and transferred to the wax embedder cooling plate to solidify.

#### **2.24.4 3-Aminopropyltriethoxysilane coating of slides**

Standard Superfrost glass microscope slides were treated with 3-aminopropyltriethoxysilane (APES)<sup>245</sup> to improve section adhesion prior to being used. To coat, clean slides were soaked in acetone for 2 minutes to remove any trace residues and air dried. Dry slides were then submerged in freshly prepared 2% (v/v) APES in acetone for a further 2 minutes. APES coated slides were then washed in 2 changes of dH<sub>2</sub>O and dried in an oven at 60 °C before being stored dust-free until needed.

#### **2.24.5 Paraffin embedded sample sectioning**

Prior to sectioning tissue blocks were trimmed to remove excess paraffin. Blocks were then located in the rotary microtome and sectioned at 10 µm; 2-3 discontinuous sections approximately 130 µm apart were taken from each pellet for each slide. Sections were carefully transferred to a tissue float bath with dH<sub>2</sub>O at approximately 50 °C and picked up on APES coated

Superfrost slides. Slides with sections were placed in an oven at 60 °C overnight and stored at room temperature prior to staining.

#### **2.24.6 Section de-paraffinisation**

Immediately prior to staining (histological or immunohistochemical) slides were de-paraffinised. Slides were warmed to 60 °C in an oven and immediately transferred to 100% xylene for 10 minutes followed by fresh 100% xylene for a further 10 minutes to remove the infiltrated paraffin wax. To rehydrate, slides were exposed to 100%, 100%, 90%, 70%, and 50% IMS for 3 minutes each and then transferred to dH<sub>2</sub>O before staining immediately.

#### **2.24.7 Haematoxylin and eosin staining**

Deparaffinised and rehydrated tissue sections were immersed in Gill's number 3 haematoxylin for 30 seconds followed by washing with tap water until the effluent ran clear. If haematoxylin had not blueed at this stage sections were immersed briefly in Scott's tap water substitute and then dipped in eosin x 10 followed by washing and dehydration in 2 changes of absolute alcohol, clearing in 100% xylene and mounting in DPX mounting medium.

#### **2.24.8 Toluidine blue staining**

Deparaffinised and rehydrated tissue sections were immersed in 0.04% toluidine blue in a 0.2 M sodium acetate buffer for 10 minutes at room temperature followed a tap water wash until effluent ran clear. Slides were transferred to a drying oven to remove any trace of water and mounted using DPX mounting medium<sup>246,247</sup>.

#### **2.24.9 Picrosirius red staining**

Deparaffinised and rehydrated tissue sections were immersed in 0.1% picrosirius red in saturated aqueous picric acid for 1 hour at room temperature followed by washing in 2 changes of acidified water. Stained sections were then dehydrated in 90% and 100% IMS for 30 seconds before

transfer to 100% xylene and mounting with DPX mounting medium. Images were acquired under brightfield and cross-polarised light.

## **2.25 Immunohistochemistry**

### **2.25.1 Heat induced epitope retrieval**

Deparaffinised and rehydrated slides (2.24.6) were transferred to citrate buffer pH6 in a staining dish at 90 – 100 °C. This was placed in a vegetable steamer to maintain the temperature for 20 minutes. The slides and staining dish were then removed from the steamer and allowed to cool for 20 minutes before washing with PBS. Slides were laid flat in a humidification chamber and the areas around the sections carefully blotted, sections were then isolated with a hydrophobic pen to localise fluids to the tissue sections during later steps.

### **2.25.2 Enzymatic antigen retrieval**

Slides were de-paraffinised, rehydrated and the samples isolated with a hydrophobic pen before being laid flat in a humidification chamber. Approximately 25 µl of 0.1% trypsin in PBS was pipetted directly onto each section and the humidification chamber transferred to an oven at 37 °C for 20 minutes. Slides were then washed 3 times for 5 minutes each with PBS.

### **2.25.3 Primary antibody staining**

Following antigen retrieval (heat induced or enzymatic) excess PBS was blotted from around sections and blocking buffer consisting 1% BSA was carefully pipetted onto sections and incubated at room temperature for 1 hour.

Excess blocking buffer was then carefully blotted from sections to receive primary antibody staining (buffer was left undisturbed on sections to be used as secondary antibody only controls). Antibody (collagen I, collagen II, collagen VI, collagen X and aggrecan) diluted in blocking buffer was then carefully pipetted onto tissue sections and the humidification chamber transferred to

4 °C overnight. As slides had to be stained in multiple batches a slide with porcine cartilage (chick femur for collagen X) was included with each batch to assess staining reproducibility.

#### **2.25.4 Secondary antibody staining**

Following primary antibody staining slides were washed thoroughly with PBS for 3 x 5 minutes after which all sections were flooded with 3% (v/v) hydrogen peroxide in methanol for 10 minutes to quench any endogenous peroxidase activity. Slides were again washed in PBS for 3 x 5 minutes and the appropriate biotinylated secondary antibody from either an anti-mouse, anti-rabbit or anti-goat ABC staining system kit, diluted as directed by the manufacturer, pipetted onto the sections and incubated at room temperature for 1 hour.

After approximately 45 minutes the AB enzyme reagent from the kit was prepared by mixing 50 µL of avidin, 50 µL of biotinylated horse radish peroxidase (HRP) and 2.5 mL of PBS. This mixture was allowed to stand for 30 minutes to allow the formation of the avidin-biotin complex before it was used.

After 1 hour slides were washed thoroughly with PBS for 3 x 5 minutes before being treated with the pre-mixed avidin-biotinylated HRP complex for 30 minutes, after which slides were again washed in PBS.

#### **2.25.5 Staining with the diaminobenzidine substrate.**

Stock 3,3'-diaminobenzidine (DAB) was prepared as a 1% (w/v) solution in 10 x mL of dH<sub>2</sub>O and 3-5 drops of 12 M HCl added before being shaken for approximately 10 minutes to ensure complete dissolution. This was aliquoted and stored at -20 °C until required.

Immediately prior to staining a working solution of DAB was prepared consisting of 250 µL of 1% DAB, 250 µL of 0.3% (v/v) hydrogen peroxide and 5 mL PBS.

To stain sections slides were washed briefly in dH<sub>2</sub>O, the excess blotted and sections covered with the DAB working solution for 1-3 minutes (timing was kept consistent for each antibody). DAB was

then removed immediately, the whole slide immersed in dH<sub>2</sub>O before dehydrating in 90% (v/v), followed by 100% alcohol, clearing in xylene and mounting with DPX mounting medium.



Keele University

---

## **Chapter 3**

---

***Pilot study to determine the  
viability of human umbilical cord  
blood as a source of MSCs***

### 3.1 Introduction

Bone marrow aspirates are still in widespread use for MSC isolation; however, MSC like cells have also been isolated from a number of alternative tissues including adipose tissue, dental pulp, synovium and synovial fluid, peripheral blood, a number of foetal tissue and birth associated tissues including the placenta, UC and UCB<sup>125</sup>. Isolation of MSCs from bone marrow is a reliable process with several well supported methods usually relying on simple plastic adherence; however, there are significant drawbacks associated with bone marrow aspiration. Typically marrow is aspirated from the iliac crest of the pelvic bone, with significant pain and potential donor site morbidity being of particular concern.

Considered to be biological waste products and therefore usually discarded after delivery, the birth associated tissues including the UCB represent a desirable and underused stem cell source. With the first successful UCB transplant for a haematological disorder (Fanconi's anaemia) in 1988<sup>248</sup> and with greater than 30,000 transplants carried out to date<sup>147,249</sup> UCB is a readily available source of cells with a well-established banking system. UCB units can now be used to treat in excess of 85 conditions<sup>250</sup> and its availability has been particularly valuable for patients from ethnic minority groups<sup>251</sup> due to the reduced stringency of HLA matching required with UCB compared to bone marrow. The use of UCB is also associated with a reduced incidence of viral transmission in comparison to bone marrow<sup>252</sup>.

In addition to the HSCs, MSCs have been successfully isolated from UCB; however, the rates of successful recovery of MSCs from UCB are extremely variable and are generally much lower (29%<sup>141</sup>, 34%<sup>142</sup>, 40%<sup>253</sup>, 43%<sup>143</sup>, 48%, 50%<sup>254</sup>, 90%<sup>144</sup>) than those achieved with bone marrow. UCB-MSCs have been found to have a similar morphology to bone marrow MSCs, are sometimes reported to have a greater proliferative capacity than bone marrow MSCs, and surface marker analysis as with many of the varied MSC sources yields similar, although not identical, results.

With bone marrow oxygen tensions reportedly between 1-8%, the mammalian reproductive tract ranging from 1.5-8% and foetal circulation at approximately 5%<sup>213</sup> culture of cells under standard *in vitro* conditions exposes them to greatly increased oxygen levels compared to physiological norms. Culture of stem cells in environmental oxygen levels below the 21% O<sub>2</sub> found in ambient air, often referred to as hypoxic conditions, is more representative of the *in vivo* environment, or physiologically normoxic state. Reduced oxygen culture has been reported to be beneficial to both cell recovery and proliferation<sup>218</sup>. This includes those MSCs recovered from birth associated tissues, e.g. Wharton's jelly MSCs cultured in 2% O<sub>2</sub> displayed more rapid population doubling times and greater proliferative capacity whilst retaining their immunophenotype and differentiation potency<sup>213,224</sup>. However, again there is a conflicting report where it was determined that reduced O<sub>2</sub> made no difference to recovery<sup>144</sup>.

UCB-MSCs may have advantages over bone marrow MSCs including wider differentiation capacity, greater proliferation and reduced immune response that would make these cells an ideal choice for regenerative medicine. However, low recovery rates may have hindered research into their application as there are relatively few reports in the literature compared to alternative sources of MSCs.

The work described in this chapter tests the hypothesis that UCB is a suitable source material for MSC recovery and that a 2% O<sub>2</sub> environment leads to improved MSC recovery as assessed by cell and colony number.

### **3.2 Aim**

The primary aims of this chapter were to:

- Obtain ethical approval for a pilot study collecting UCB from 12 donors undergoing elective caesarean section at the Royal Stoke University Hospital.
- Determine whether isolation of cells in a more physiological oxygen level (2% O<sub>2</sub>) relative to physiological hyperoxia (21% O<sub>2</sub>) is beneficial to cell recovery rates.

- Determine whether UCB is a viable source of MSCs for use in *in vitro* studies of MSC chondrogenesis.

### 3.3 Methods

The sequence of experiments for this chapter is summarised in Scheme 1.

Following informed consent UCB was collected from the UC and placenta of 12 donors undergoing elective caesarean sections, as described in section 2.4, and transferred to the Guy Hilton Research Centre for processing in sterile conditions. The MNC count of the UCB was determined using the Millipore hand-held Cell Sceptor (section 2.2.4) and samples were plated in 10 ng/mL fibronectin coated tissue culture flasks as whole blood in DMEM (4.5g/L glucose) supplemented with 1% v/v L-Glut, 1% v/v NEAA and 1% v/v PSA. Seeding density (based on MNC/cm<sup>2</sup>), medium FBS content (% v/v) and O<sub>2</sub> tension were the experimental variables as summarised in Table 3-1.

**Table 3-1. Summary of the UCB plating conditions.**

	FBS (v/v)		O <sub>2</sub> (%)		Seeding density				
	5%	10%	2%	21%	1x10 <sup>4</sup> /cm <sup>2</sup>	1x10 <sup>5</sup> /cm <sup>2</sup>	1x10 <sup>6</sup> /cm <sup>2</sup>	2x10 <sup>6</sup> /cm <sup>2</sup>	1x10 <sup>7</sup> /cm <sup>2</sup>
UCB1-3	✓	✓	✓	✓	✓	✓	✓	✓	✓
UCB4-6		✓	✓	✓				✓	
UCB7-9		✓	✓	✓	All MNCs divided equally between 2% and 21% O <sub>2</sub>				
UCB10-12		✓	✓	✓	All MNCs divided equally between 2% and 21% O <sub>2</sub>				

To remove the majority of the erythrocytes UCB7-9 were Ficoll density separated as described in section 2.5, after which recovered MNC were plated evenly between 2% and 21% O<sub>2</sub> culture in 10% FBS supplemented medium. UCB10-12 were also Ficoll density separated followed by MACS separation of the cells based on CD45 antigen expression as described in section 2.6. Separated

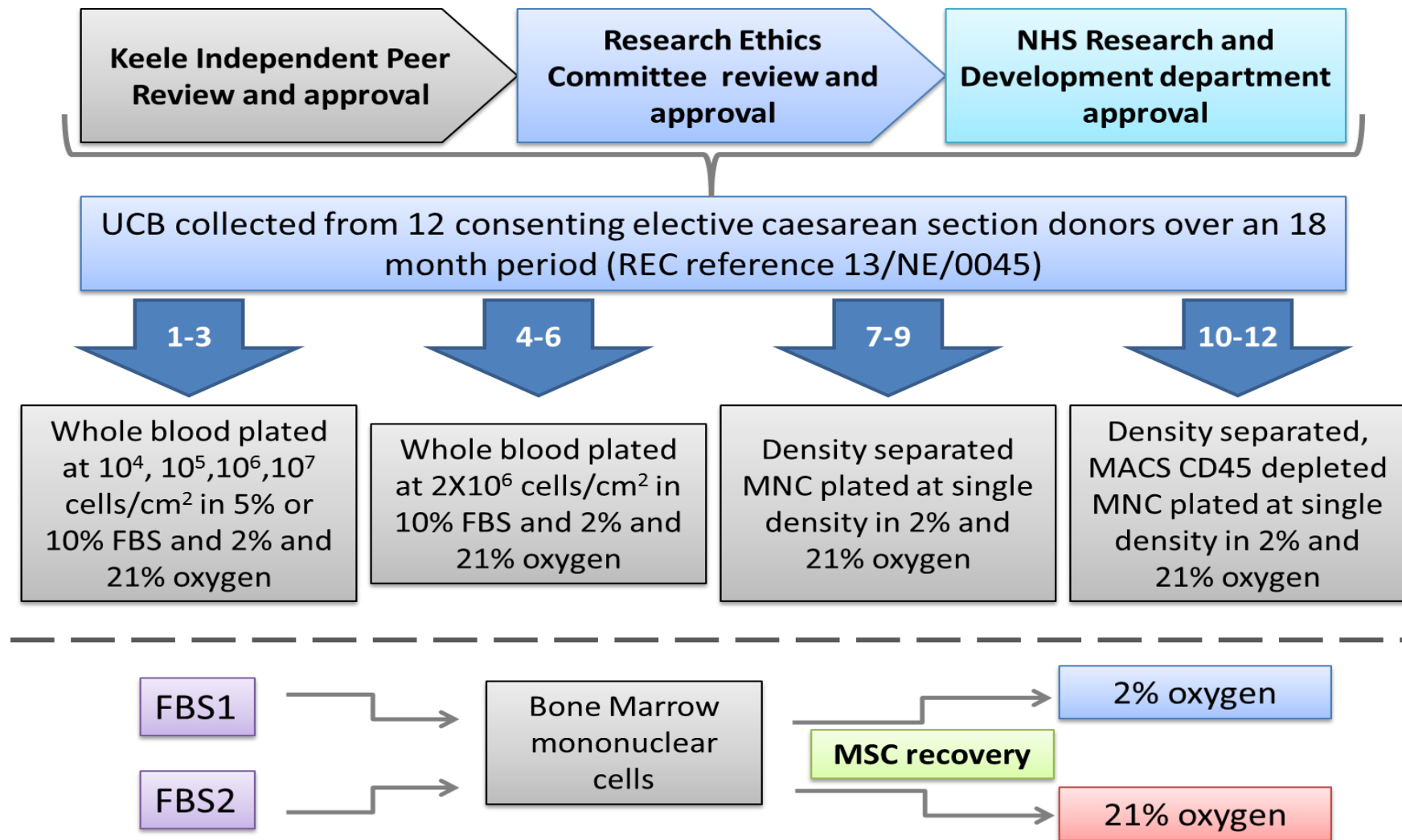
CD45+ cells were plated in 10% FBS supplemented medium in T150s in 2% and 21% O<sub>2</sub>, CD45- cells were plated in T25s in 2% and 21% O<sub>2</sub>. UCB7-12 MNCs were also all plated on 10 ng/mL fibronectin coated tissue culture flasks. In all cases flasks received a 50% media change after 7 days and 100% after 14 days with twice weekly media changes thereafter.

Early results indicated that FBS batch may have been a key variable in the recovery of MSCs from UCB samples. To determine the influence of the FBS batch on MNC recovery commercially available, Ficoll separated human bone marrow MNC were plated as described in section 2.3.2. Cells were plated at  $1 \times 10^5$  cells/cm<sup>2</sup> in 10 ng/mL fibronectin coated flasks and 6-well plates in DMEM (4.5 g/L glucose) supplemented with 1% (v/v) L-Glut, 1% (v/v) NEAA and 1% (v/v) PSA in either 10% (v/v) FBS1 or FBS2 in both 2% and 21% O<sub>2</sub>. Flasks and plates received a 50% media change after 7 days and 100% after 14 days with twice weekly media changes thereafter. After a three week recovery period the 6-well plates were fixed with 95% (v/v) methanol for 10 minutes, washed and stained with haematoxylin and allowed to dry. Dry plates were scanned and the MSC-like colonies counted. Flasks were trypsinised (section 2.2.1) and cells were counted and sized using the Cell Scepter as described in 2.2.4. Cell morphology of cells in colonies was also examined.

### **3.3.1 Statistical analysis**

Colony area, colony number, cell recovery, cell volume and cell size were all compared using two-way ANOVA with Tukey's multiple comparisons test to determine pairwise statistical significance,  $p \leq 0.05$  was considered significant. Analysis was performed using Graphpad Prism V6.01.

Unless otherwise stated all values quoted in the results are mean  $\pm$  standard deviation.



Scheme 1. Summary of the methodology adopted in Chapter 3.

### **3.4 Results**

As indicated in the experimental plan the ethical approval of several bodies had to be gained prior to the collection of any samples. This process involved firstly getting approval for the study following review by the Keele University Joint Independent Peer Review Committee. Once granted the project was submitted to a NHS Research Authority Research Ethics Committee, and once REC approval was gained (REC reference 13/NE/0045) the project proposal was submitted to the Research and Development department of the University Hospitals of North Midlands NHS Trust (previously University Hospital of North Staffordshire NHS Trust). Final project approval was granted and the collections commenced in October 2013 and were completed in March 2015.

In total informed consent was obtained from 15 donors with sample collection from 12 donors. The remaining 3 consenting donors delivered prior to the scheduled date for their elective caesarean section and UCB was therefore not collected from those potential donors.

In accordance with the ethically approved protocol, all samples were acquired without any modification to the medical care that donors received. All prospective donors were identified and consent obtained by a single obstetrics Consultant; however, the surgery was performed by whichever surgeon was scheduled to be performing obstetric surgery on the scheduled date. As a result of this surgical practice, with regards to clamping and placental delivery, varied and led to a variable sample collection outcome. In particular, it was found retrospectively that some samples were collected following delayed cord clamping which led to a large reduction in the volume of blood that could be obtained (Table 3-2). For example UCB2 and UCB10, with total collection volumes of only 12.5 mL and 20 mL respectively, were both found retrospectively to have been collected following delayed cord clamping reducing the available volume of blood and increasing the extent of clotting prior to sample acquisition. Additionally the cord from UCB2 was also cut very close to the placenta resulting in a very short cord and corresponding loss of blood volume.

**Table 3-2. Details of the 12 UCB samples obtained.** Quoted volumes are inclusive of ACD anticoagulant at approximately 5 mL/30 mL blood. \*Cords confirmed retrospectively to have delayed cord clamping.

11/10/2013	UCB1	35 mL
26/11/2013	UCB2*	12.5 mL
07/01/2014	UCB3	40 mL
26/02/2014	UCB4	40 mL
09/05/14	UCB5	35 mL
13/05/2014	UCB6	70 mL
03/06/2014	UCB7	30 mL
08/07/2014	UCB8	40 mL
30/09/2014	UCB9	40 mL
17/10/2014	UCB10*	20 mL
24/03/2015	UCB11	60 mL
27/03/2015	UCB12	65 mL

The mean volume obtained was  $41 \pm 17$  mL with a minimum of 12.5 mL and a maximum of 70 mL (Figure 3-1); collected volumes followed a normal distribution as assessed by the D'Agostino and Pearson omnibus normality test.

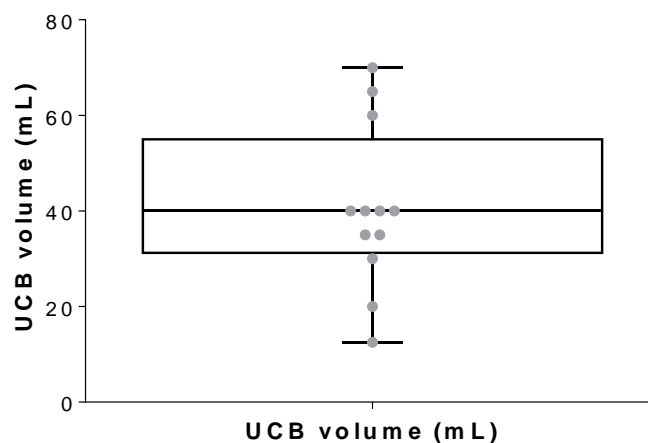


**Figure 3-1. Box and whisker plot of UCB samples.** Whiskers indicate minimum and maximum values, box area the interquartile range with the median indicated by the horizontal mid-point line. Volumes from all samples (N=12) are shown.

### 3.4.1 UCB1-3

UCB1 was plated systematically in T25 flasks as described at four alternative seeding densities, in media containing 5% or 10% FBS at 2% or 21% O<sub>2</sub>. By the 100% media change at two weeks stage none of these systematically plated samples appeared to contain any attached cells and no colonies were observed to develop over the subsequent weeks. However, there was a volume of residual blood remaining after all T25 flasks had been seeded and this was also plated into tissue culture flasks rather than discarding valuable material.

Firstly residual blood was plated at  $2 \times 10^6$  cells/cm<sup>2</sup> on fibronectin coated T150 flasks in 2% and 21% O<sub>2</sub>. The 2% O<sub>2</sub> flask was found to contain a single colony of cells that had the typical MSC morphology of elongated cells growing at high density (Figure 3-2A and B). At 30 days this colony had expanded to have an approximate diameter of 2 cm and was enzymatically passaged into a T12.5 flask. Following passage the cells underwent no further proliferation, instead adopting an enlarged, flattened morphology typical of senescent cells (Figure 3-2C). As these cells did not expand, further characterisation could not be carried out.

The final volume of blood was placed into a single T150 tissue culture flask at  $1.5 \times 10^7$  cells/cm<sup>2</sup> in a in 2% O<sub>2</sub>, 10% FBS without fibronectin. This flask yielded approximately 5 small colonies containing around 10-20 cells and 1 larger colony as shown in Figure 3-2D-F. The cells in these colonies appeared to be relatively loosely attached to the substrate, as shown by the number of cells that are rounded up and only partially attached to the flask, and did not have the morphology typical of MSCs. Over the subsequent weeks increasing number of cells detached from the flask.

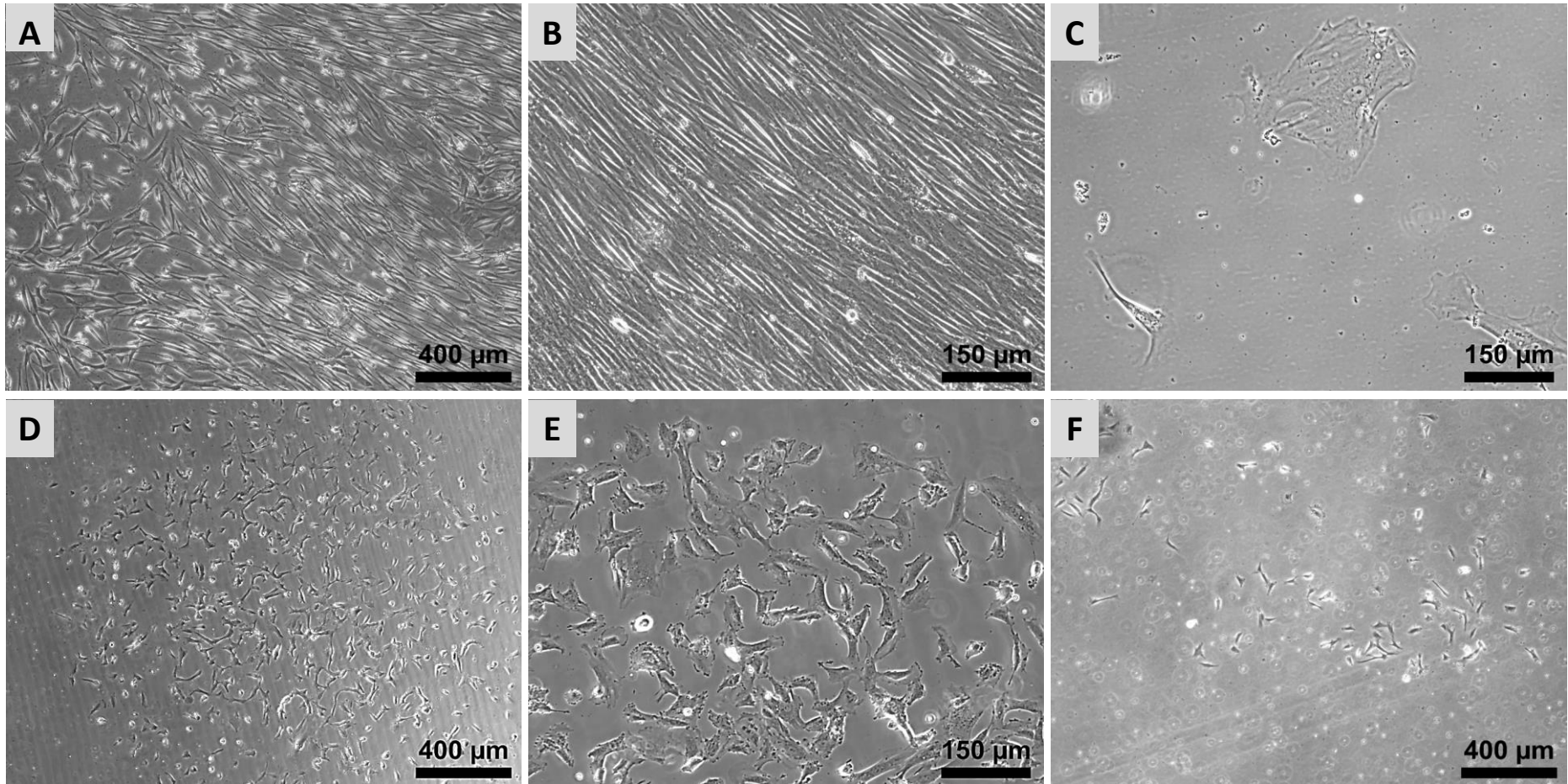


**Figure 3-2. UCB1 recovered cell morphologies.** Phase contrast micrographs showing the single colony of MSC like cells (A) and (B) that appeared senescent following passage (C). (D), (E) and (F) show small colonies of non-MSC like cells that subsequently detached from the flask.

Due to an unavoidable supplier change all subsequent UCB samples had to be plated with a different batch of FBS.

UCB2 did not yield any colonies of MSC like cells in any condition, instead only occasional rounded (Figure 3-3A) or irregularly shaped cells that were frequently granular and multinucleated were observed; these cells also appeared to have the potential to be somewhat proliferative *in vitro* as evidenced by loose colony formation Figure 3-3B and C).

UCB3 had no adherent cells, instead containing only clusters of erythrocytes (Figure 3-3D) with the exception of one potential colony of cells at the periphery of a single flask (Figure 3-3E and F) seeded at  $10^5$  cells/cm<sup>2</sup>, 21% O<sub>2</sub>, 10% FBS, these cells did not appear to be fully attached with a rounded appearance and were insufficiently flattened to observe the cell morphology. As with colonies in UCB1 these cells did not proliferate and were lost over time.

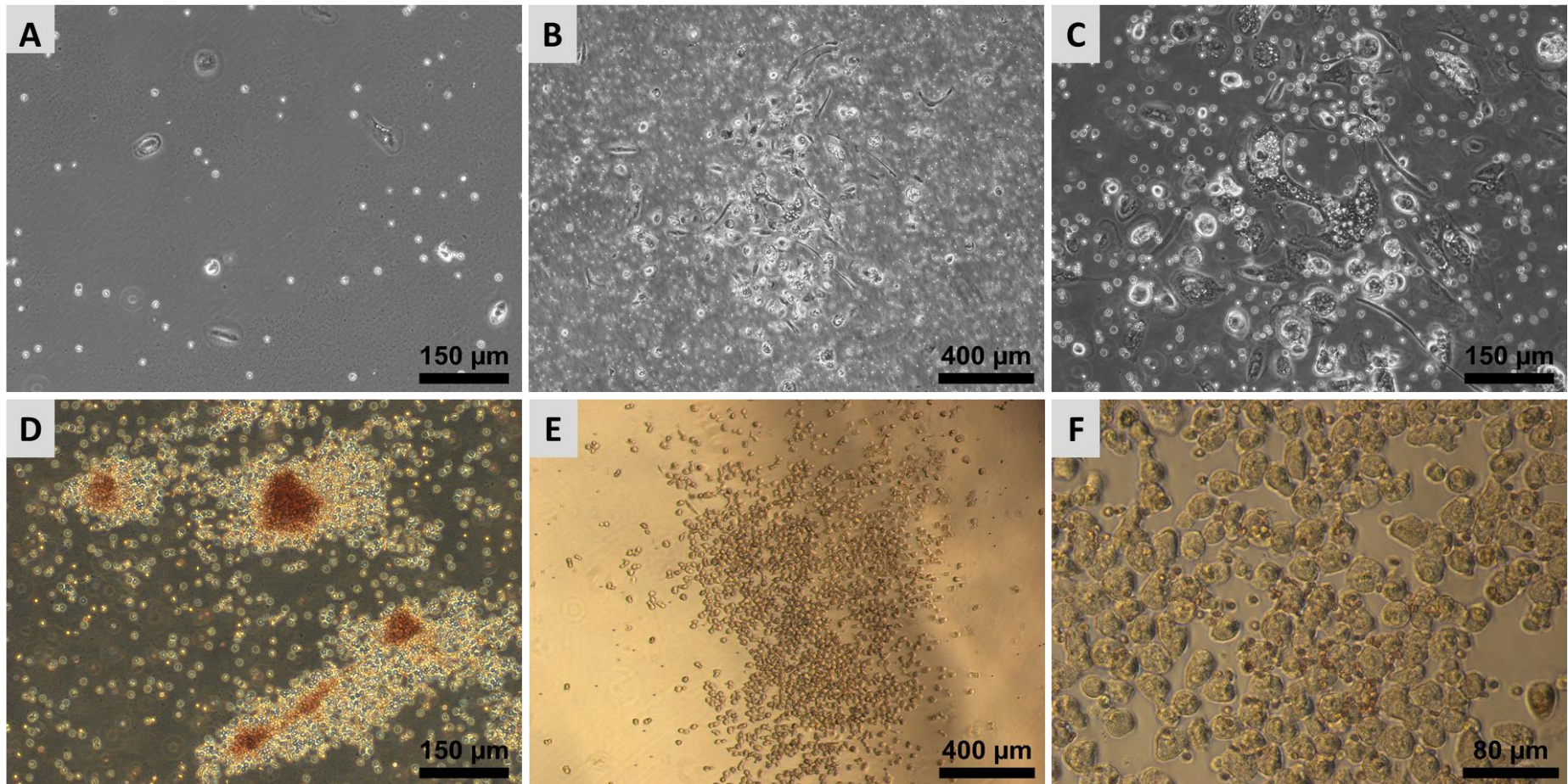


**Figure 3-3. Cells from UCB2 and UCB3.** Phase contrast micrographs of the occasional rounded cells observed from UCB2 (A) and the small colony of irregularly shaped cells (B) and (C). UCB3 yielded only clumped erythrocytes (D) with the exception of one possible colony (E) and (F); however, cells were not fully attached or flattened.

### **3.4.2 UCB4-6**

As the only MSC like colony from UCB1-3 was obtained from blood plated at  $2 \times 10^6$  cells/cm<sup>2</sup>, cords 4-6 were plated at this density only, the % FBS variable was also removed with all cells being plated only in a standard 10% FBS supplemented medium. This allowed scale up of the cell plating to T150 flasks to maximise the recovery potential. Blood was still plated in both 2% and 21% O<sub>2</sub>.

Despite this scale up, UCB4-6 failed to yield any adherent cells in any condition. It was observed that the plating of whole blood led in some cases to the deposition of a dense layer of debris and erythrocytes, as this may have hindered cell adherence, UCB7-9 were separated by density centrifugation over Ficoll and the isolated MNCs plated rather than the whole blood.

### **3.4.3 UCB7-9**

Plating of isolated MNCs from UCB7-9 resulted only in the isolation of the rounded adherent cells that went on to produce cells with varied morphologies (Figure 3-4). These cells were particularly numerous in UCB8, where there appeared to be substantial proliferation resulting in confluent flasks. Therefore characterisation of the immunophenotype of these cells was performed on half of the cells against the panel of antibodies to identify MSCs, whilst the remainder were re-plated. Cells were found to be extremely resistant to trypsinisation, requiring mechanical cell scraping to remove them from the tissue culture plastic surface. Following re-plating only small numbers of cells attached and they were no longer proliferative.

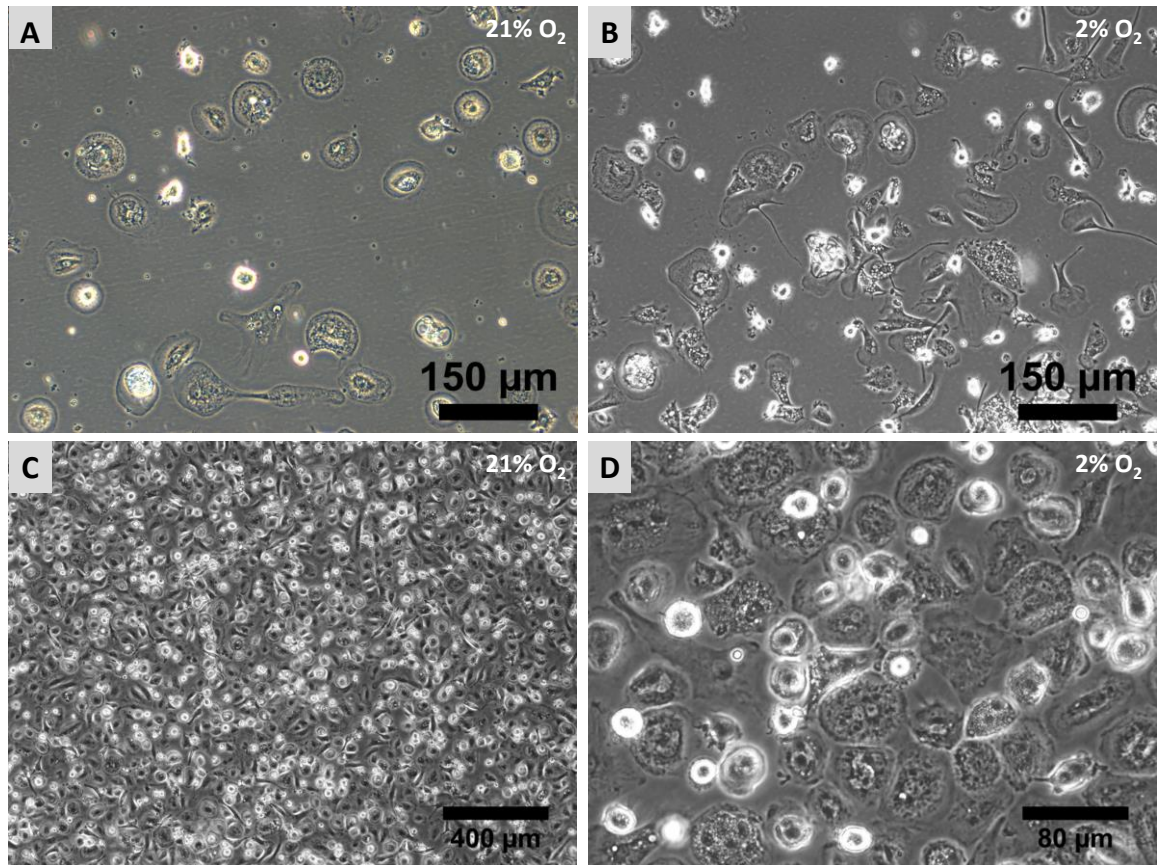


**Figure 3-4. Cells recovered from UCB7 and UCB8.** Phase contrast micrographs of cells recovered from UCB7 (A) and (B) and UCB8 (C) and (D) 14 days after plating UCB.

Flow cytometry of UCB8 against a panel of markers used to identify MSCs (Figure 3-5) showed that in 2% O<sub>2</sub> cells were very strongly positive for CD14 (81.0%), CD45 (92.7%) and HLA-DR (89.8%), the typical MSC markers CD73, CD90 and CD105 were negative. In 21% O<sub>2</sub> cells were also strongly positive for CD14 (78.5%), CD45 (95.5%) and HLA-DR (90.0%). In addition to this a small subset of the population were also positive for CD90 (18.0%) and CD105 (21.2%) indicating a possible MSC sub-population; however, there was no evidence of this following re-plating of the cells in culture.

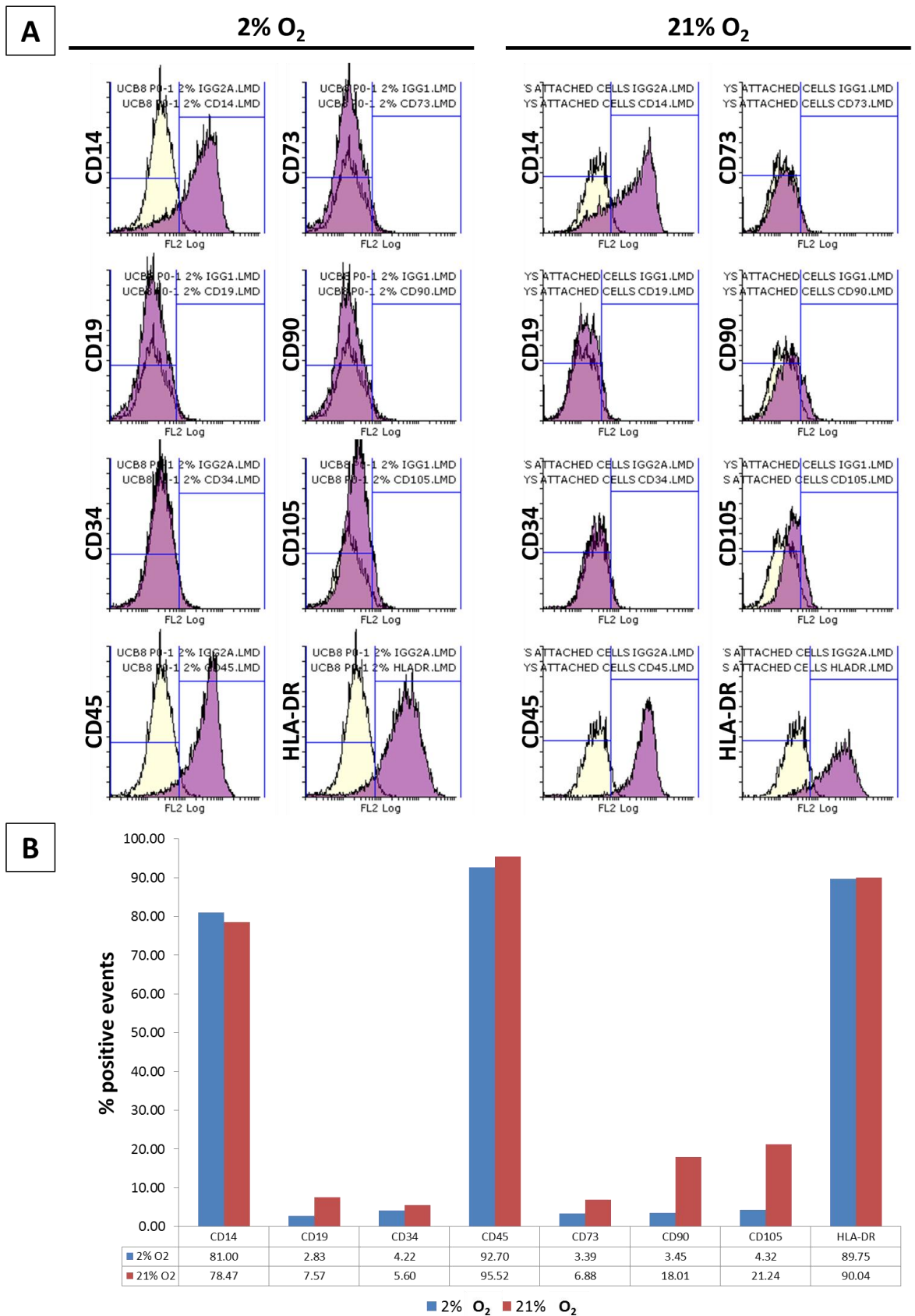


**Figure 3-5. Immunophenotyping of cells from UCB8.** Cells recovered in 2% and 21% O<sub>2</sub> were assessed by flow cytometry against the panel of markers used to identify MSCs. (A) Overlay histograms of each antibody marker, (B) percentage positive cells compared to staining with the relevant isotype control.

#### 3.4.4 UCB10-12 CD45 depletion using MACS technology

As UCB7-9 yielded a population of cells strongly positive for leukocyte antigens CD14, CD45 and HLA-DR, with a possible population of MSCs detectable only by flow cytometry, UCB10, 11 and 12 were subjected to CD45 positive cell depletion using magnetic separation with CD45 beads to separate all leukocytes from potential MSCs. Following isolation both the CD45 positive and negative cell fractions were plated on fibronectin coated plates in 2% O<sub>2</sub> and 21% O<sub>2</sub>.

Separation using the MACS system resulted in a pellet from the CD45- fraction that was primarily residual erythrocytes which pass freely through the column and a CD45+ fraction that was primarily leukocytes that are initially retained in the column plus small numbers of physically trapped erythrocytes resulting in a pinkish colour to the pellet (Figure 3-6). Any MSCs should be present in the CD45- population.

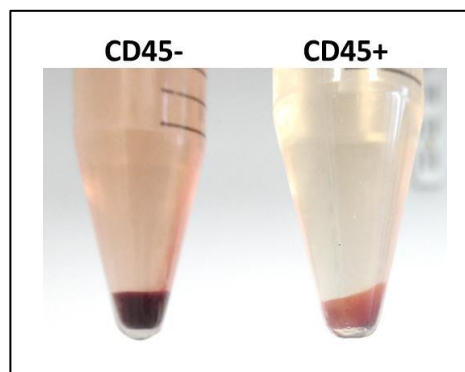


**Figure 3-6. UCB12 sample following MACS separation.** Ficoll density separated MNC samples were separated using MACS CD45 beads. The CD45- fraction contains the majority of the residual erythrocytes and any MSCs as these pass through the separation column freely due to a lack of CD45 whilst the CD45+ fraction is primarily leucocytes.

Using the UCB10 sample at the 50% media change cells were checked by flow cytometry for CD45 expression (Figure 3-7). The CD45+ fraction were 97.2% positive (using 99% gating of the relevant isotype control) for CD45 while the CD45- fraction, which at this point consisted almost entirely of

erythrocytes, was CD45 negative (0.5% positive events) demonstrating effective separation of the CD45 positive cells using the magnetic separation kit.

Despite CD45 depletion for all three UCB samples no MSC cells appeared to be present in either the CD45- flask, that contained only debris and erythrocytes, or the CD45+ flask which continued to yield rounded, attached cells that became granular, irregularly shaped and sometimes multinucleated as found with UCB7-9 (Figure 3-8).

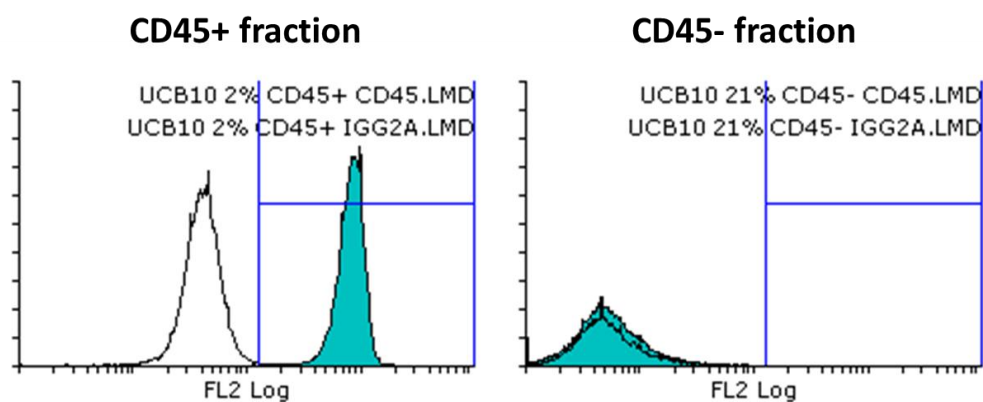


**Figure 3-7. CD45 expression of CD45 MACS separated cells.** The unfilled histogram is the IgG<sub>2a</sub> isotype control, the filled histogram is CD45.

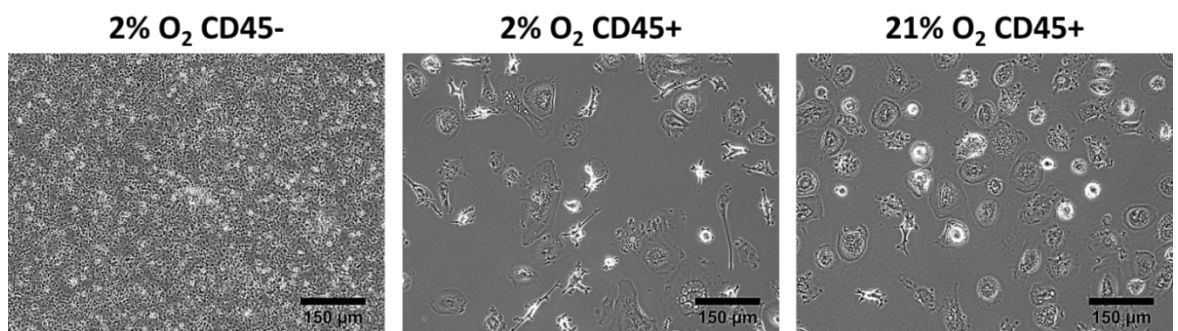


**Figure 3-8. Cell morphology following CD45 MACS separation.** Phase contrast micrographs of cells in the CD45- fraction and CD45+ fraction of CD45 MACS separated UCB MNCs after two weeks in culture.

Of the twelve UCB samples collected and plated only the first sample yielded a visually identifiable colony of MSC like cells; as UCB1 was recovered with FBS1 (supplied by Lonza) whilst the later samples had to be recovered with FBS2 (supplied by Biosera) this change in FBS was investigated

as a possible causative factor in the lack of MSC cell recovery concomitant with the recovery of large numbers of non-MSC-like cells..

#### **3.4.5 The influence of FBS batch on MSC recovery from MNC preparations**

Prior to selection of the new FBS batch (FBS2) several options were batch tested for bone marrow MSC cell proliferation and the selected batch was found to be the most optimal of those available (Appendix B, Supplementary figure 1). FBS2 has also been used for MSC recovery from whole BMA with no unusual results. As all UCB samples with ethical approval had been collected at this point this investigation was performed using commercially available MNC isolated from BMA and a small reserve of FBS1. Following recovery, colony counts, cell counts, and cell size and morphology were all determined.

##### **3.4.5.1 Colony recovery**

Following a three week recovery period cells were fixed and stained with haematoxylin (Figure 3-9), the plates were then scanned and both the percentage area occupied by stained cells and the number of colonies recovered were determined by image analysis in ImageJ.

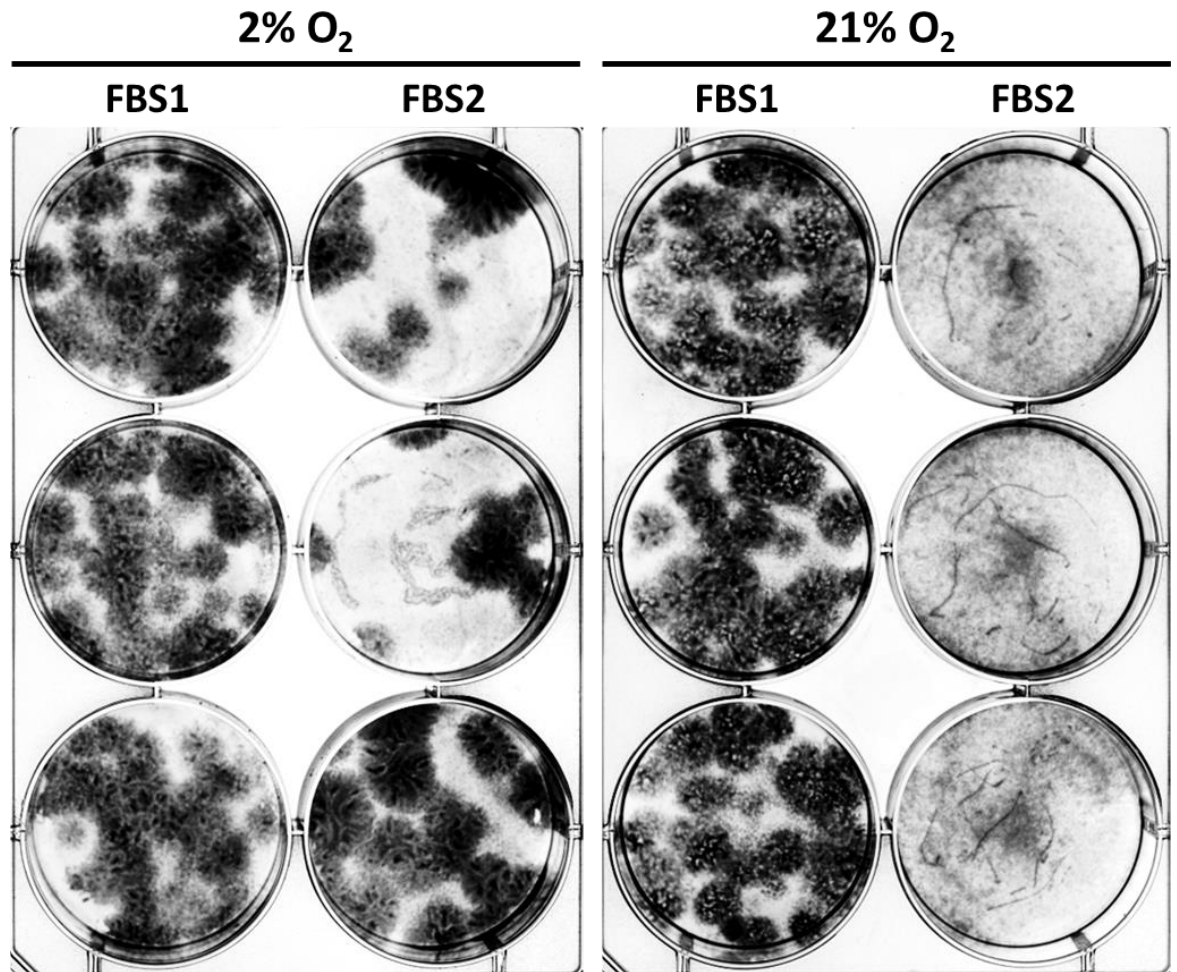


**Figure 3-9. CFU-F recovery of MSCs from MNCs.** MSC CFU-F recovery from bone marrow MNCs in two alternative FBS batches, in both 2% and 21% O<sub>2</sub>. Cells are fixed and stained with haematoxylin.

As a percentage of the total area cells from FBS1 occupied  $89.5 \pm 2.7\%$  in 2% O<sub>2</sub> and  $85.3 \pm 3.3\%$  in 21% O<sub>2</sub> whilst FBS2 covered only  $54.0 \pm 24.7\%$  of the available area in 2% and  $47.7 \pm 6.9\%$  in 21% O<sub>2</sub>. The difference between recoveries in FBS1 versus FBS2 was significant ( $p \leq 0.05$ ) in both 2% and 21% O<sub>2</sub>. As shown in Figure 3-9 there were no dense, isolated colonies found with culture in 21% with FBS2, although more generalised cell staining was present. As a result colony counts (Figure 3-10) for FBS1 were  $24.3 \pm 2.5$  in 2% O<sub>2</sub> and  $23.3 \pm 3.5$  colonies in 21% O<sub>2</sub> whilst FBS2 yielded  $10.3 \pm 3.5$  colonies in 2% O<sub>2</sub> and 0 colonies in any well at 21% O<sub>2</sub>. All results excepting colony recovery in FBS1 in 2% and 21% oxygen were statistically significant to at least the  $p \leq 0.01$  level.

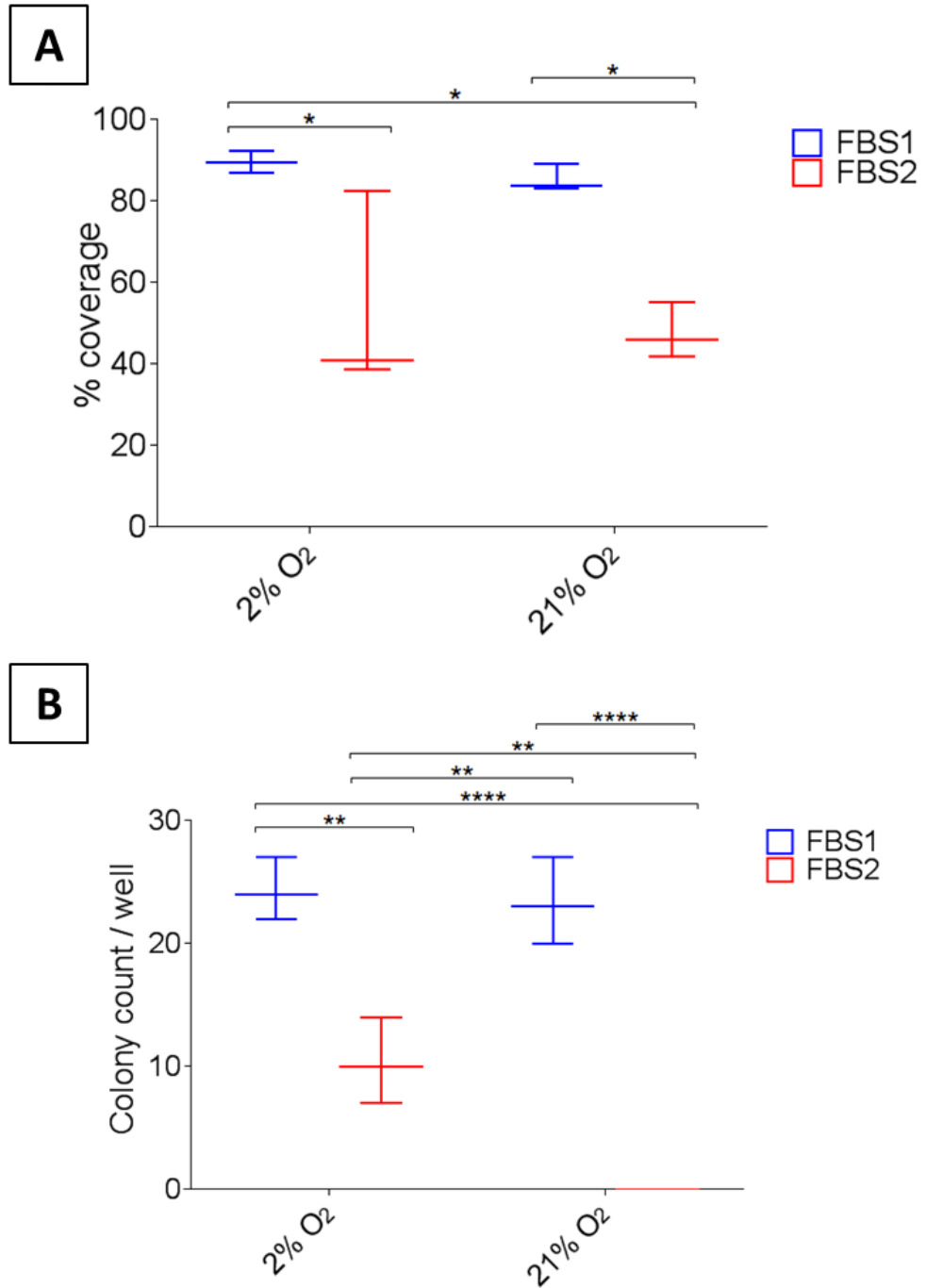


**Figure 3-10. CFU-F formation.** Colony formation in 2% and 21% O<sub>2</sub> with FBS1 and FBS2 was assessed both by percentage area covered by stained cells (A) and by colony count (B). Data are expressed as mean ± standard deviation, N=3, \*p≤0.05, \*\*p≤0.01, \*\*\*\*p≤0.0001.

#### **3.4.5.2 Cell morphology following recovery**

The morphology (Figure 3-11) of the majority of the cells recovered in FBS1 in 2% or 21% O<sub>2</sub> was consistent with that of MSCs, with elongated, bipolar, colony forming cells. Recovery in FBS2 at 21% O<sub>2</sub> resulted in very few MSC like cells with most cells being rounded and of various sizes consistent with the cells frequently seen with recovery from MNC cord blood preparations. Even where MSC like cells were present in FBS2 they appeared unable to form high density colonies although more dispersed clusters were occasionally found. This effect was less severe in 2% O<sub>2</sub> with cultures in FBS2 containing a mixture of both cell types with MSCs that were able to form high density cell colonies.

#### **3.4.5.3 Cell recovery**

Cell number at recovery was also determined by counting using the Millipore Cell Sceptor that also provides information on cell size (diameter and volume). MSC like cells were much more easily trypsinised than other cells resulting in the majority of the cells counted being MSC like cells. FBS1 yielded similar numbers of cells in both 2% and 21% O<sub>2</sub> at 29,400 and 27,000 ± 2,000 cells/cm<sup>2</sup>. FBS2 cell yield was significantly (p≤0.05) improved over FBS1 in 2% at 46,800 ± 6,321 cells/cm<sup>2</sup> but significantly reduced compared to both FBS1 in 2% O<sub>2</sub> (p≤0.01) and FBS2 in 2% O<sub>2</sub> (p≤0.0001) with only 9,710 ± 2,683 cells/cm<sup>2</sup> recovered (Figure 3-12).

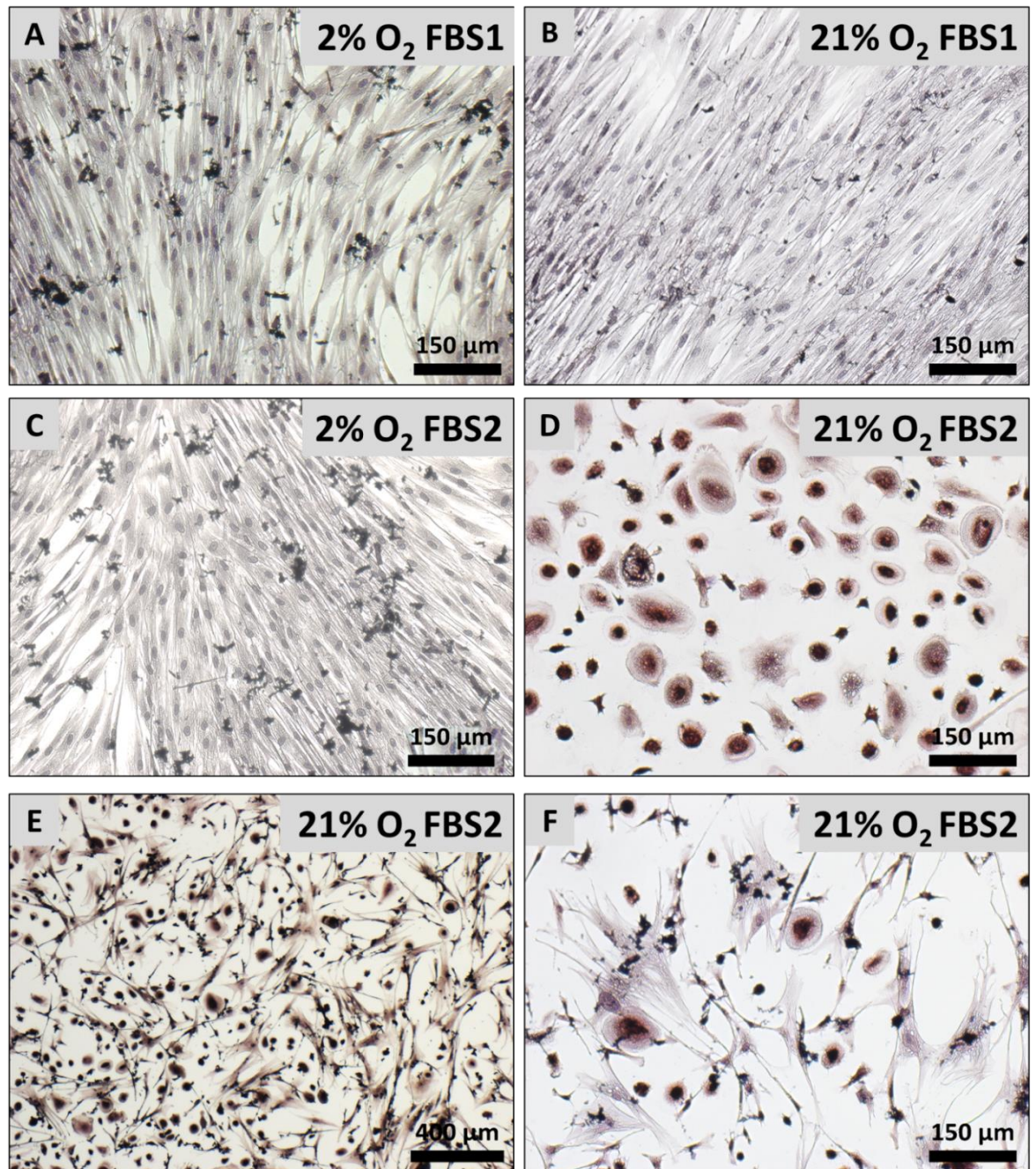


**Figure 3-11. CFU-F cell morphology.** Representative brightfield micrographs of cells isolated in 2% (A) and (C) or 21% O<sub>2</sub> (B), (D), (E) and (F) in FBS1 (A) and (B) or FBS2 (C-F). Cells are fixed and stained with haematoxylin.

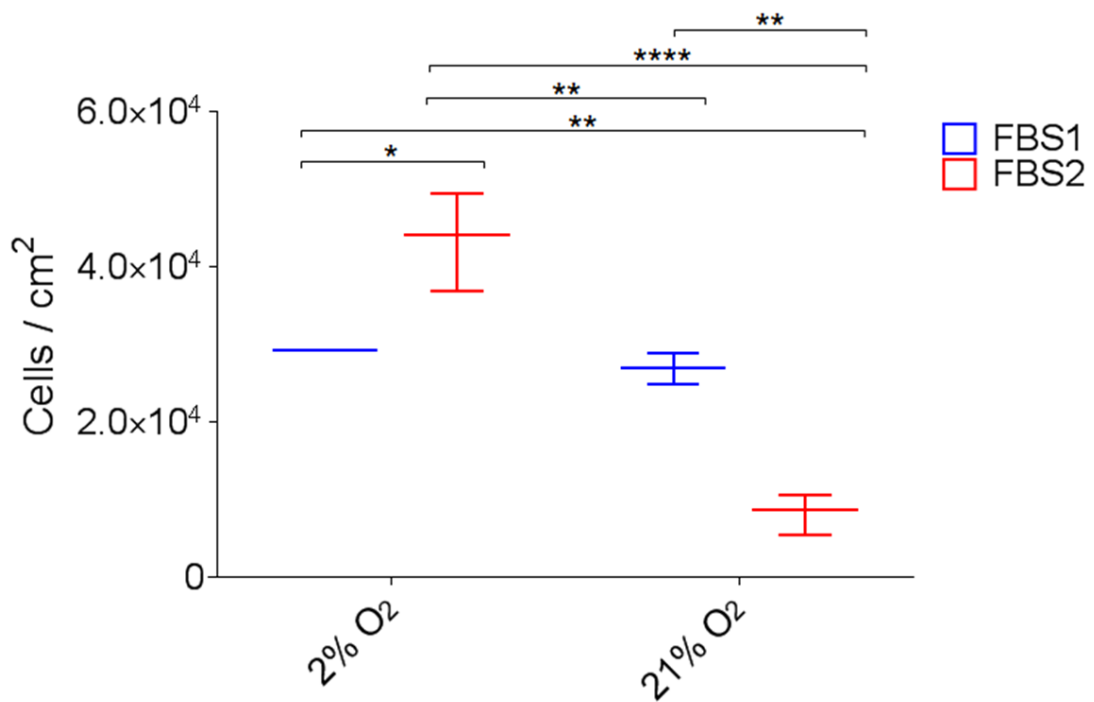


**Figure 3-12. Cell recovery in FBS1 and FBS2 in 2% or 21% O<sub>2</sub>.** Cells were trypsinised and counted using the Millipore cell Sceptor. Data are expressed as mean ± standard deviation, N=3, \*p<0.05, \*\*p<0.01, \*\*\*\*p<0.0001.

Cells recovered in FBS2 were smaller than in FBS1 at both 2% O<sub>2</sub> (18.12 ± 0.08 μm/3.12 ± 0.04 pL compared to 20.88 ± 0.13 μm/4.77 ± 0.08 pL, p<0.001) and 21% O<sub>2</sub> (19.77 ± 0.55 μm/4.05 ± 0.34 pL compared to 21.78 ± 0.40 μm/5.42 ± 0.30 pL, p<0.01). Using either FBS batch cells were larger in 21% O<sub>2</sub> than the corresponding cells in 2% O<sub>2</sub>, significantly so with FBS2 (p<0.01) (Figure 3-13).

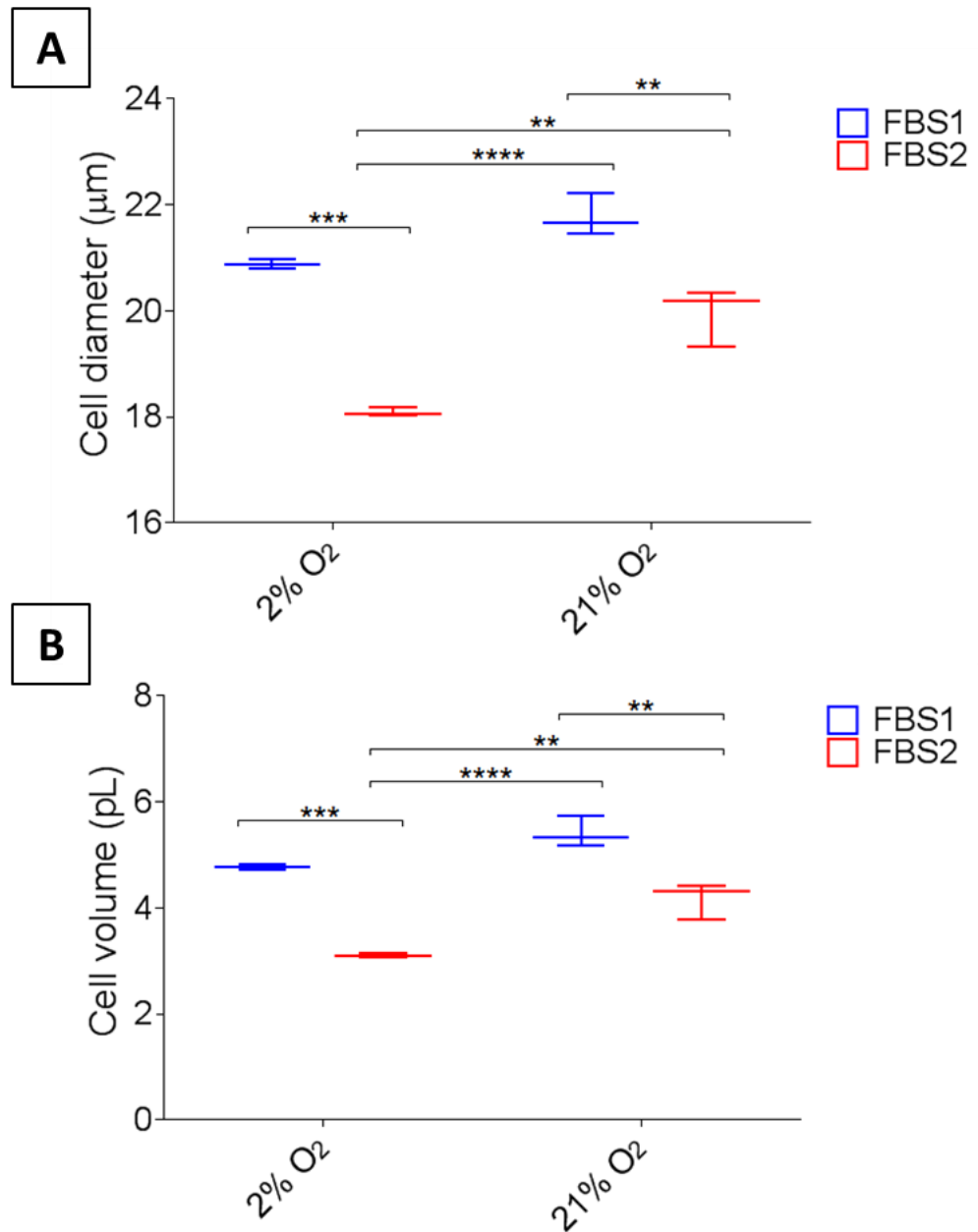


**Figure 3-13. Cell size following recovery from MNCs.** Following recovery cell size was characterised by diameter (A) and volume (B). Data are expressed as mean  $\pm$  standard deviation, N=3, \*\* $p \leq 0.01$ , \*\*\* $p \leq 0.001$ , \*\*\*\* $p \leq 0.0001$ .

### 3.5 Discussion

The use of UCB for MSC isolation is an attractive prospect due to the established banking processes in place for UCB HSC transplantation and supposed naivety of the cells<sup>255</sup>; however, there is a limited body of literature available in support of the reliable and reproducible isolation of MSCs from UCB. One possible option for improving success rates is the application of a more physiologically relevant oxygen level during isolation and culture; an approach that has seen improvements in cell recovery and proliferation in other stem cell types<sup>221,230,220</sup>. Physiological compared to ambient oxygen levels (2% compared to 21%), along with variable FBS concentration (5% and 10%) and initial seeding density ( $1 \times 10^4$  MNCs/cm<sup>2</sup> to  $1 \times 10^7$  MNCs/cm<sup>2</sup>) were factors investigated in the pilot study described in this chapter.

There were several logistical issues identified with the blood collection protocol that are likely to have had a deleterious impact on the study. The collected blood volume was very variable and was particularly limited where cord clamping and cutting had been delayed by the obstetric surgeon, a process that is recommended by the World Health Organisation (recommend clamping and cutting “not earlier than 1 minute after birth”)<sup>256</sup>. Delayed cord clamping and cutting is the process whereby following delivery the UC is not clamped or cut for between one to five minutes or potentially until the UC stops pulsing. A recent Cochrane review of the practice found that it made no difference to primary maternal outcomes e.g. the likelihood of severe post-partum haemorrhage; however, it is advocated by some as it increases blood volume and haemoglobin concentration in neonates as a result of placental transfusion (blood from the placenta is returned to the neonate circulation) and is associated with reduced iron deficiency in three to six month old infants<sup>257</sup>. Delaying clamping and cutting of the UC by three minutes results in a reduction of approximately 70% in the residual placental blood volume<sup>258</sup>. Total UCB sample volume has been identified as a key factor in the later successful isolation of MSCs with the suggestion that  $\geq 90$  mL is required for effective isolation<sup>144</sup>. This volume was not achieved in any sample taken herein and

other studies suggest that this would be unusually high for UCB collection. Katsares *et al* as part of an UCB characterisation study recovered 2,000 units of UCB immediately after delivery, with the placenta *in utero* and still only obtained an average volume of  $60.64 \pm 25.47$  mL<sup>259</sup> similar to Jones *et al* with a mean of  $72.0 \pm 0.27$  mL<sup>260</sup> from 9,205 collections carried out in varied circumstances. In addition to the lower volumes the necessary delay in accessing the UC due to the requirement to obtain blood for blood gas measurements often meant that blood had begun to clot before collection was completed, or in the case of samples with delayed clamping, started. As with blood volume evidence of clotting has been found to be deleterious to MSC isolation with no recovery from samples with evidence of either clotting or haemolysis<sup>103</sup>.

The initial approach involving the plating of whole blood was one that has previously proved to be successful for the reliable isolation of MSCs from BMA samples<sup>230</sup>, and by the conclusion of the study (N=12) was the only technique that yielded any adherent cells that resembled MSCs (Figure 3-2). However, problems with erythrocyte sedimentation and the resultant coating of the flask with a film of cells and cellular debris were encountered with some samples due to the necessity of plating the higher volumes of blood required to counter the lower incidence of MSCs described in UCB. As this debris layer may have provided a physical barrier to MSC adherence subsequent UCB samples were plated from Ficoll density separated MNC preparations. This variation of the initial protocol resolved the problem of high numbers of contaminating erythrocytes; however, it also resulted in a high incidence of isolation of rounded, strongly attached cells that in no way resembled MSCs. Finally, in an attempt to remove contaminating cell populations MNC preparations were depleted of CD45+ cells using immunomagnetic separation. The cell separation was successful; however, no MSCs were recovered from the CD45- fraction, whilst the CD45+ fraction continued to yield rounded strongly adherent cells.

The contaminating cells that were frequently recovered in samples, particularly following Ficoll density separation, had a rounded morphology in early cultures which changed as cultures aged,

resulting in a diverse population of cells including granular cells and very large multinucleated cells; these are all very strongly adhered to the culture flask, being highly resistant to trypsinisation. The strong expression of CD14, CD45 and HLA-DR along with the mononuclear cell fraction origin and the morphology of these cells indicates that the cells are highly likely to be monocytes and later, their differentiated progeny macrophages and dendritic cells<sup>261-263</sup>.

Monocytes are part of the innate immune response resulting in inflammation and phagocytosis. The cells develop initially in the bone marrow from common myeloid progenitor cells and migrate to the blood, in adult peripheral blood they constitute approximately 7-10% of total leukocytes<sup>264,265</sup> and in circulating blood have a half-life of one to three days<sup>261</sup>. Circulating monocytes can be divided into three sub-types based on immunophenotype as shown in Table 3-3.

**Table 3-3. Human monocyte sub-types.** Adapted from Yang *et al*, 2014<sup>261</sup>.

<b>Monocyte sub-type</b>	<b>% of monocytes</b>	<b>Surface marker expression</b>	<b>Function</b>
<b>Classical</b>	80-95	CD14++ CD16-	Phagocytosis High levels of peroxidases and IL-10
<b>Intermediate</b>	2-11	CD14++ CD16+	Pro-inflammatory Low levels of peroxidases and high IL-1 $\beta$ and TNF $\alpha$
<b>Non-classical</b>	2-8	CD14+ CD16++	Patrolling High IL-1 $\beta$ and TNF $\alpha$ , respond to DNA and RNA molecules

Monocyte/macrophage-like cell recovery has been described frequently in studies endeavouring to isolate MSCs from UCB and their presence in cultures where MSC isolation is being attempted

has been recognised as a problem, with no successful recovery of MSCs where adherent monocytes were present<sup>103,266</sup>.

In the first study successfully isolating UCB MSCs Erices *et al*<sup>140</sup> nevertheless recovered a heterogeneous population of non-MSC cells in 74% of the units they tested. Following further characterisation they described the cells they found as osteoclast-like as they were strongly positive for tartrate resistant acid phosphatase (TRAP), CD45 and CD51/61 (integrin  $\alpha_v\beta_3$ /vitronectin integrin receptor complex<sup>267</sup>) positive whilst lacking expression of CD64 (macrophage marker<sup>268</sup>). CD14 positive cells were present but the percentage of cells expressing this reduced from 53% at 3 weeks to 26% at 5 weeks<sup>140</sup>. This reduction in CD14 expression can be seen with changes in the monocyte differentiation status<sup>269</sup>. Similarly, in what they identified as their most optimal condition, Perdikogianni *et al* recovered cells with an MSC like morphology in 25% of samples; they also recovered adherent haematopoietic cells. The MSC-like cells that they did obtain were slow growing and could only be briefly expanded. Despite successfully isolating some MSC-like cells these were found to have limited proliferative capacity meaning that insufficient cell numbers could be cultured for differentiation experiments<sup>270</sup>. The results seen with the experiments in this chapter were less promising, more closely mirroring those described by Alvarez-Viejo *et al*<sup>271</sup> where only round cells with the appearance of monocytes were isolated from twenty UCB donors and Zeddou *et al*<sup>272</sup> where despite assessing multiple culture conditions and trying both CD271+ and CD133+ enrichment and CD3, CD19, CD14 and CD38 immunodepletion only 1 of 15 UCB samples yielded any MSC-like cells. They also describe isolating primarily strongly attached rounded cells presumed to be macrophages along with more elongated cells which were nevertheless CD73, CD90 and CD105 negative<sup>272</sup>.

Other attempts to improve recovery rates have used both positive and negative immunoselection techniques to directly isolate MSCs or to remove contaminating haematopoietic cells. An approach using immunodepletion of committed lineage cells based on CD7, CD19, CD38 and glycoporphin A expression was successful for Lee *et al* (although overall recovery rates are not

stated)<sup>273</sup>; however, the same approach made little difference in the study by Zeddou *et al*<sup>272</sup>. The recovery of MSCs from the pilot study herein was not improved by immunodepletion of haematopoietic cells using the CD45 common leukocyte antigen which would be expected to resolve the problem of contaminating monocytes if that was the only, or main issue impacting on recovery.

Positive immunoselection might be expected to be a more successful approach, for example selection based on CD271 (low affinity nerve growth factor receptor (LNGFR)) is successful with bone marrow and adipose tissue MSCs and appears to select for cells that undergo improved tri-lineage differentiation<sup>274</sup>, has also been attempted with UCB. Selection by CD271 of a clearly rare cell population would be extremely desirable for UCB, particularly for cells destined for musculoskeletal therapies; however, CD271 appears to be absent from cells from UCB with no positive population identifiable by flow cytometry or magnetic immunoselection<sup>270</sup>.

In the wider context these results are less surprising, early bone marrow culture methods using Dexter-long term cultures were established and optimised to maximise haematopoiesis. These cultures described the formation of a confluent layer of adherent cells, the stromal layer, that supported the haematopoietic process<sup>275</sup>. Subsequently the cells isolated to form a marrow stromal layer have been compared to cells recovered in conditions optimised more towards MSC recovery, with the resulting MSCs comprising a much more homogeneous population of cells in comparison to the mixed stromal cells, where fibroblastic cells were present alongside adhered haematopoietic cells. A sub-population of the cells from the stromal layer, and most of the MSCs were positive for CD105 and CD166, both recognised as MSC markers. Additionally stromal layers contained cells positive for CD14 and CD45 i.e. monocytes/macrophages and similar Dexter long term cultures prepared from UCB appear to favour the isolation of monocytes and macrophages<sup>275</sup>. Both the MSCs and the mixed stromal cells had the capacity to support haematopoiesis although this capacity was more variable in MSCs compared to stromal cells, particularly from some donors<sup>276</sup>. The different cell populations isolated were primarily as a result

of alterations in media composition, the marrow stromal layer prompted to form in the presence of 12.5% FBS plus 12.5% horse serum supplemented with hydrocortisone whilst more a more homogeneous population of MSCs was recovered in 10% FBS only supplemented medium<sup>276</sup>. It is clear from this that factors present in various sera can significantly impact on the cells recovered from blood and bone marrow products. Furthermore, plastic adherence is one method used for the isolation of monocytes for *in vitro* work with monocytes, macrophages and dendritic cells, as monocytes will typically adhere readily to both endothelial cells or to plastic surfaces. Various sources of monocytes are used for this purpose including peripheral blood, bone marrow and UCB, with UCB being a good choice due to the high incidence of CD34+ cells from which dendritic cells can also be generated<sup>277</sup>.

FBS batch variability was identified as a candidate likely to be at least partially responsible for the poor MSC recovery with FBS2 seemingly promoting recovery of monocytes to the detriment of MSC recovery compared to FBS1. FBS is a staple of cell and tissue culture systems providing a complex and variable mixture of vitamins, minerals, hormones, attachment/ECM proteins, growth factors and cytokines although these are variable and poorly characterised<sup>278</sup> (see Appendix C for manufacturer Certificates of Analysis for FBS1 and FBS2). Although characterisation of low molecular weight proteins has rarely been attempted FBS has been found to contain a variety of factors that may influence cells' behaviour including bFGF, IGF-II, glial growth factor (GGF) and TGF- $\beta$ 1 with these bovine growth factors having an effect on human cell types<sup>279</sup>.

Although it could not be directly assessed on UCB MNC samples the FBS batch variability was found to be a crucial factor affecting successful recovery from Ficoll isolated bone marrow MNCs. Whilst experimental confirmation would be required the results from the bone marrow MNCs are likely to be translatable to UCB MNC preparations. Results from bone marrow MSCs may in fact represent a more conservative model of the situation as the monocyte content of adult peripheral blood at 39% of the total MNCs, was found to be much higher than that of bone marrow at 18% of the total MNC count, bone marrow cells are also likely to be less mature<sup>280</sup>. UCB monocyte

content in particular may also tend to be higher than that of adult peripheral blood with the UCB average monocyte count ( $0.8 \pm 1.2 \times 10^3$  cells/ $\mu\text{L}$ ) lying at the top end of the normal range for adults ( $0.1\text{-}1.0 \times 10^3$  cells/ $\mu\text{L}$ )<sup>259</sup>. It should be noted that although there are strong similarities between adult monocytes and UCB monocytes, there are nevertheless differences that could have impacted on the results<sup>281</sup>.

Cell adhesion and differentiation of monocytes occurs in the presence of FBS and is typically enhanced using a variety of cytokines, most commonly M-CSF<sup>282</sup>, and a combination of GM-CSF and IL-4 that more commonly directs the differentiation towards dendritic cells<sup>283</sup>. These cytokines can be considered activating and thus pro-survival factors that cause the cells to undergo maturation and differentiation in the absence of which monocytes undergo apoptosis<sup>284</sup>. Supplementation of serum free culture media with a number of different cytokines (GM-CSF, M-CSF, IL-4, IL-10, LPS, IFN $\gamma$ ) has been previously noted to cause changes in monocyte adhesion<sup>285</sup>. GM-CSF has previously been shown to increase the adherence of monocytes to plastic surfaces and endothelial cells as well as increasing monocyte viability<sup>286</sup>. Similarly IL-3 increases endothelial and plastic adhered monocyte cell numbers while the converse is seen with IL-4 decreasing cell attachment<sup>287</sup>.

The attachment of cells to substrates is mediated by a number of attachment factors including the integrins, cell membrane spanning heterodimers of variable  $\alpha$  and  $\beta$  subunits. Integrins are responsible not only for adhesion but also transmit information from the cell surroundings, including the ECM, and activate intracellular signalling cascades affecting cell behaviour; multiple factors are known to affect integrin expression on cells. On monocytes TGF- $\beta$ 1 causes increased expression of both  $\alpha$  and  $\beta_1$  integrin subunits, specifically  $\alpha_3\beta_1$  (VLA-3 (very late antigen-3)) and  $\alpha_5\beta_1$  (VLA-5 (very late antigen-5)). Upregulation of  $\alpha_3\beta_1$  can lead to increased cell adhesion to the ECM proteins laminin, type IV collagen and fibronectin and  $\alpha_5\beta_1$  to fibronectin<sup>288</sup>. The flasks used in this study were fibronectin treated as this has been found to enhance recovery of MSCs from bone marrow and also from equine UCB samples<sup>289</sup>. This treatment may have been detrimental in

our study if changes such as those described with TGF- $\beta$ 1 treatment of monocyte cultures were induced in the UCB samples promoting monocyte recovery. However, the majority of UCB studies have not used fibronectin and nevertheless experienced significant monocyte contamination issues possibly due to their higher availability in UCB.

There was a clear differential response to the FBS batch variation in 2% compared to 21% oxygen cultures of bone marrow MNCs, with physiological hypoxia moderating the deleterious impact of FBS2. Colonies of MSCs successfully developed in FBS2, albeit at much lower frequency than in FBS1 in 2% O<sub>2</sub> whereas no colonies developed in FBS2 in 21% O<sub>2</sub>. MSC recovery has previously been shown to be enhanced in 2% O<sub>2</sub> compared to 21% O<sub>2</sub><sup>230</sup>, although this was not the case in FBS1; however, if this was occurring in FBS2 then the higher number of MSCs earlier in culture could themselves moderate the number of monocytes that become attached during recovery. MSCs have been found to inhibit the differentiation of monocytes via secreted factors including IL-6<sup>290</sup>. The converse situation may also be true where enhanced recovery of monocytes had a direct, detrimental effect on MSC recovery. As noted in Table 3-3, as part of the innate immune response they can produce reactive oxygen species (ROS), nitric oxide, myeloperoxidase, inflammatory cytokines and initiators of angiogenesis. The various monocytes can produce a range of cytokines such as IL-1 $\beta$ , IL-6, IL-10 and TNF- $\alpha$ <sup>261,291</sup> the effects on MSCs from these would likely be many and varied.

Cell numbers recovered in cultures in FBS2 were also greatly reduced in 21% O<sub>2</sub> but in contrast were significantly enhanced compared to FBS1 in 2% O<sub>2</sub>. A large proportion of this difference is likely to be a result of more rapid proliferation in FBS2 once colonies had become established. This resulted in larger, denser colonies in 2% O<sub>2</sub> FBS2 compared to FBS1 cultures, increased proliferation in FBS2 acted to offset the reduced CFU-F recovery rate, the increased proliferation from FBS2 was previously noted during FBS batch testing (Appendix B, Supplementary figure 1). Although increased proliferation, i.e. larger colonies, may give rise to the required cell numbers for cell therapies more rapidly, in practice these cells will have undergone mitosis more frequently

and thus represent an 'older' cell population. In comparison samples with higher initial CFU-F recovery of MSCs increasing the starting cell population numbers will require fewer population doublings and correspondingly cells will be 'younger'. Furthermore both culture time, cell density and thus cell-cell contact, and various combinations thereof have been identified as factors affecting the subsequent differentiation capacity of MSCs<sup>292,293</sup>. The situation is further complicated by the possibility that oxygen tension can modulate multiple cell processes by both direct and indirect action for example changing the expression of cell attachment factors, cytokine receptors and any genes with HREs. Oxygen can also result in indirect effects for example as a result of changing the oxidative balance within the culture<sup>220,294-305</sup>.

Taken together, although the mechanisms of action are unclear and remain topics for future studies, the results strongly support the removal of FBS from the culture system. There would be considerable benefits associated with the removal of FBS from the culture system including the removal of xenogeneic proteins and the risk of xeno-pathogen contamination. There are multiple possible options to replace FBS including defined media<sup>306</sup>, human serum, platelet rich plasma, platelet lysate or cord blood serum or plasma<sup>307</sup>, where use could be either on an autologous<sup>308</sup> or pooled basis as appropriate. Inevitably there would still be batch variation with all of these biological products. Ultimately, particularly when trying to isolate rare populations of cells, only the identification of the components key to successful isolation, expansion and differentiation and the subsequent preparation of a defined medium alongside fully controlled procedures will reliably eliminate the problems described in this chapter.

### **3.6 Conclusion**

There has been a flurry of clinical trials investigating the applicability of MSC therapies for a multitude of indications including their potential utility in cartilage repair therapies. Early studies used bone marrow MSCs; however, similar cells have since been identified in a multitude of different tissue types including the birth associated tissues that are typically discarded. With pre-

existing and established facilities for UCB banking this tissue may prove to be an under-utilised pool of donor material. Unfortunately as described herein and extensively in the literature the isolation of MSCs from UCB is currently unreliable due most probably to both an intrinsically low presence of the cells within UCB, and sub-optimal conditions for their isolation. This Pilot study attempted to address this unreliability by modifying the culture conditions to include a physiologically relevant oxygen tension for the *in vitro* recovery steps.

In this study only a single MSC-like cell colony was recovered from 12 donor samples, instead contamination of cultures with monocytes was the more common outcome and immunodepletion of CD45 positive cells did not improve recovery rates. FBS batch variability was identified as a particularly relevant culture variable and the batch in question was found to impact significantly and negatively on the isolation of MSCs from bone marrow MNCs which would usually be relatively reliable. The effect of FBS batch was also found to be further modulated by a varied oxygen environment with 2% O<sub>2</sub> moderating the negative effects and being more permissive to MSC recovery. These observations on the potentially devastating influence of certain FBS batches have wide-ranging implications not only for isolation of MSCs from UCB but for the cell culture industry in general. They strongly support of the use of FBS free and ideally human serum free conditions for cell culture whenever possible. Furthermore this work highlights the extensive changes in outcome that can occur with oxygen modulation, a less frequently considered cell culture variable.

Despite the issues encountered, as UCB is usually discarded its potential as a source of stem cell donor material should not be completely overlooked and continued work is required to improve upon current techniques. However, until refinements are made or unless very large numbers of UCB units are available the use of UCB is not practicable in a small laboratory setting. Alternative sources of MSCs from other birth associated tissues may prove to be more practical options with an increasing focus on UC tissue cells which reliably produce much larger numbers of cells with MSC characteristics such as surface marker expression and immune modulation<sup>309</sup>.

As the recovery rate of UCB MSC cells was so poor no cells could be carried forward for the investigation of their chondrogenic capacity and the following chapters use bone marrow aspirate derived MSCs.



Keele University

---

# **Chapter 4**

---

## ***Characterisation of cells following transduction with hTERT***

## 4.1 Introduction

As discussed in Chapter 1 cartilage damage and degeneration are common problems, becoming increasingly relevant in the western world due to an aging population<sup>65</sup>. Once tissue integrity has been compromised this avascular, alymphatic and aneural tissue, which contains only a small numbers of largely quiescent resident cells<sup>310</sup>, fails to heal naturally, leading to long-term tissue degradation<sup>24</sup>. Treatments other than prosthetic joint replacements have limited efficacy, so when a joint replacement is not appropriate, for example due to patient age, only the option of long-term pain management strategies remains. The large number of affected individuals combined with the apparent simplicity of the tissue has made the prospect of tissue regeneration via regenerative medicine strategies including cell therapies and tissue engineering highly attractive. As a result cartilage was one of the earliest targets of regenerative medicine strategies, beginning in the early 1970s<sup>311</sup>.

Despite the numerous advances that have been made and the undoubted quality of life improvements for many patients<sup>312</sup> the desired outcome of well integrated, hyaline-only cartilage has yet to be reliably achieved<sup>313</sup>. Arguably this may be as a result of the use of a non-optimal cell type or inadequate cell culture conditions, as many of the proposed therapies are reliant on an *ex vivo* cell expansion step. However, the *in vitro* study of key biological cellular processes, an understanding of which is likely to be vital to eventual clinical success, is difficult due to an inherent property of all somatic cells: replicative senescence<sup>189</sup>.

Described and characterised by Leonard Hayflick in the 1960s, replicative senescence occurs *in vitro* after a fixed number of cell divisions<sup>176</sup>. Upon achieving this maximum, cells undergo characteristic changes including enlargement, altered secretory profiles, changes in tumour suppressor gene expression and SA $\beta$ Gal activity, and most importantly irreversible proliferation arrest. Additionally with every passage or population doubling of a cell population there can be changes in cell phenotype. Some of these changes are well described in the two cell types most

used for cartilage therapies: primary cartilage chondrocytes and MSCs. When cultured *in vitro*, particularly in a two dimensional environment, primary chondrocytes undergo a process of de-differentiation becoming less responsive to pro-chondrogenic influences<sup>314</sup>. Chondrocyte senescence is increasingly implicated in the disease pathology with increased SA $\beta$ Gal activity in cells surrounding articular cartilage lesions, reduced mitotic activity and reduced telomere lengths, all correlating with increasing age<sup>315</sup>.

As an alternative to chondrocytes, multipotent<sup>93</sup> mesenchymal stem/stromal cells, as described by Friedenstein *et al*<sup>316</sup>, offer potentially greater proliferation, a more flexible response to differentiation cues and the prospect of an allogeneic therapy due to their immunomodulatory properties<sup>317</sup>. Unlike chondrocytes, MSCs are also available from numerous tissues including several that would otherwise be discarded<sup>318</sup>, removing the requirement for invasive surgery and healthy tissue removal. Both cell types have an adequate proliferative capacity for autologous cell therapies but show widespread variation in proliferation and then efficacy of differentiation potential between donors<sup>319</sup>, particularly as the donor age increases<sup>320</sup>. hESCs have greater still proliferative and differentiation possibilities, due to their properties of self-renewal and pluripotency<sup>153</sup>. However, numerous technical challenges concerning uniformity of differentiation and purity of cell populations must be resolved before these cells can be used safely due to the inherent capacity of undifferentiated cells to form teratomas. Despite these difficulties hESC derived cells are now entering early phase clinical trials<sup>164</sup>.

Studies have suggested that the re-introduction of *hTERT* expression prevents continued telomere erosion to critically short lengths that causes cells to become senescent as a result of DNA damage signalling events<sup>321</sup>. Telomere regions have also been proposed to contain numerous irreparable DNA double strand breaks<sup>322,323</sup> with ectopic telomerase expression reportedly resolving the DNA lesions by an as yet unknown mechanism<sup>324</sup>. *In vivo*, endogenous telomerase expression is detectable only in stem and early progenitor cells, somatic cells in some rapidly renewing tissues and in cancerous cells. *In vitro* expression appears more restricted and is only

consistently found in hESCs and cancer cells<sup>325</sup>. It has been demonstrated that replicative senescence can be avoided by the re-expression and activity of the telomerase reverse transcriptase catalytic subunit, *hTERT*<sup>200,207,208</sup> which can support the maintenance of telomere length whilst also preserving or even enhancing cell function<sup>209</sup>.

The work in this chapter tests the hypothesis that the re-expression of hTERT in cells with relevance to cartilage tissue engineering is sufficient to extend the proliferative capacity of the cells whilst maintaining the primary cell phenotype.

## 4.2 Aims

The aims of the work described in this chapter were:

- Using a retroviral vector transduce primary chondrocytes, MSCs and hESC derived MSC-like cells with *hTERT*.
- Establish that *hTERT* is then stably expressed.
- Investigate the effect of the transduction on:
  - Replicative capacity: determine whether the re-introduction of *hTERT* could firstly prevent the onset of replicative senescence in these cells and,
  - Determine whether *hTERT* affects the cell phenotype compared to that of the primary cells.

## 4.3 Methods

The sequence of experiments for this chapter is summarised in Scheme 2 and all materials and methods are described in full in Chapter 2.

Primary human MSCs BMA13 were recovered from human BMA as described in section 2.3.1; recovered BMA13, commercial human chondrocytes OK3, and hESC-derived MSC-like 1C6 cells were retrovirally transduced with the catalytic subunit of telomerase *hTERT* or EV as described in section 2.7. Successfully transduced cells were selected using G418 with selected resistant cells

creating the cell lines BMA13H, BMA13EV, OK3H, 1C6H and 1C6EV. All cells were cultured in a 2% O<sub>2</sub> environment prior to transduction and a 21% O<sub>2</sub> environment during transduction and selection. All cells were then stored in liquid nitrogen until required for experiments. All subsequent cell culture steps were performed in a 2% O<sub>2</sub> tri-gas incubator.

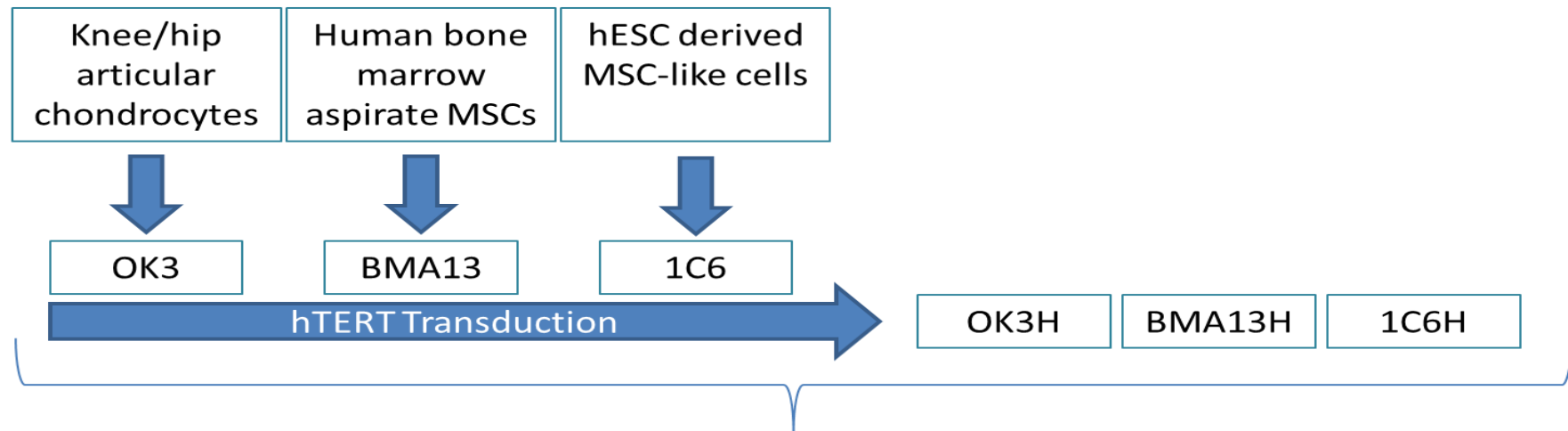
*hTERT* expression at early and later time points was assessed by RT-PCR in all cells and cell-lines as described in sections 2.19-2.22. To determine the effects of *hTERT* transduction the proliferative capacity of the *hTERT* transduced, parental, and EV cells was determined as described in section 2.8 by long-term cell culture to senescence, changes in the cell morphology were observed throughout the culture period and at early and late PD levels cells were assessed for SA $\beta$ Gal activity as per section 2.9.

The forward scatter (relative size), side scatter (relative cell granularity/complexity) and the immunophenotype of transduced cells was determined by flow cytometry against an accepted hMSC marker panel as described in 2.12 (typically positive: CD73, CD90, CD105, typically negative: CD14, CD19, CD34, CD45, HLA-DR) and compared to that of the parental cell types. Similarly tri-lineage differentiation capacity was assessed by inducing osteogenic, chondrogenic and adipogenic differentiation as described in sections 2.10-2.11.3 followed by histological staining with alizarin red S, alcian blue and Oil Red O as per sections 2.11.1-2.11.3.

#### **4.3.1 Statistical analysis**

The percentage of SA $\beta$ Gal positive cells and flow cytometry forward scatter and side scatter were compared using one-way ANOVA with Tukey's multiple comparisons test to determine pairwise statistical significance,  $p \leq 0.05$  was considered significant. Analysis was performed using Graphpad Prism V6.01.

Unless otherwise stated all values quoted in the results are mean  $\pm$  standard deviation.



- RNA extracted from parental and transduced cells to detect the presence/absence of hTERT expression using RT-PCR and gel electrophoresis.
- Cells expanded continuously to determine whether hTERT expression has extended proliferative capacity.
  - Tri-lineage differentiation capacity tested for all cell types.
  - Cell immunophenotype determined using flow cytometry.
    - Cells stained for the senescence marker SA- $\beta$ Gal.

Scheme 2. Summary of the methodology adopted in Chapter 4.

## 4.4 Results

Three primary cell types underwent retroviral transduction with the *hTERT* gene as described in section 2.7. The pBABE-*hTERT* construct used confers resistance to G418 antibiotic treatment alongside insertion of the *hTERT* gene. Following gene transduction and selection with G418 pBABE-*hTERT* and pBABE only empty vector (EV) transduced plates for OK3 (OK3H and OK3EV) and BMA13 (BMA13H and BMA13EV) and 1C6 (1C6H and 1C6EV) all retained cells resistant to the antibiotic treatment, control untreated plates were completely cleared during the same time period with the G418 treatment. Only small numbers of cells were retained following transduction in BMA13H/BMA13EV and particularly with OK3H/OK3EV, somewhat larger numbers were available with 1C6H and 1C6EV. Due to the very low cell numbers available and the extensive proliferation necessary to recover from this, insufficient cells were available from the OK3EV population to compare the phenotype of these cells with OK3H. However, some comparisons could be performed with BMA13EV and 1C6EV. As the aim of the introduction of *hTERT* was to attempt to arrest changes in the cell phenotype it was deemed more appropriate to compare transduced cells with early population doubling, non-transduced cell populations.

### 4.4.1 Ectopic *hTERT* expression in transduced cells

Following transduction, cells were expanded in 2% O<sub>2</sub> and banked for future use. RNA was then isolated from both parental and transduced cell types to determine whether transduction had resulted in the expression of the *hTERT* transcript. This is essential as the pBABE-*hTERT* construct used does not contain a reporter gene to confirm successful transduction, although resistance to antibiotic selection is an indicator of this. *β-Actin* (*ACTB*) was included as a housekeeping gene to confirm the presence of amplifiable RNA, particularly relevant in samples where *hTERT* expression was absent.

As shown in Figure 4-1, as expected the parental cell types, including the H1 hESC derived 1C6, did not express the *hTERT* transcript. In contrast all three of the transduced cell types clearly

expressed *hTERT*. RNA isolated from H1 hESC and the previously transduced and characterised 9C12H cell line (Forsyth *et al*<sup>234</sup>), both cell types known to express *hTERT*, were included as positive controls.

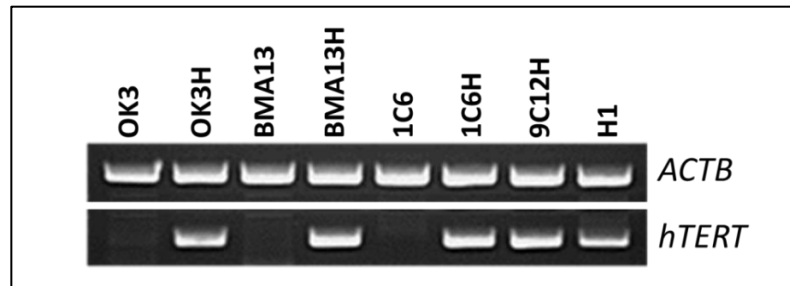


**Figure 4-1. RT-PCR determination of *hTERT* expression.** *hTERT* is expressed in transduced cells and is not present in non-transduced parental cell types. 9C12H and H1 are cell types known to express *hTERT* and are included as positive controls. ACTB confirmed the presence of amplifiable RNA in all samples.

RNA was then isolated from cell cultures at a range of passages/PD to confirm that *hTERT* expression was maintained in daughter cell populations without a requirement for further periods of antibiotic selection and was stable as cells were continuously expanded. RNA isolated from the two available EV cell types was also included to confirm *hTERT* expression resulted from specific gene insertion not as a result of the transduction process (Figure 4-2).

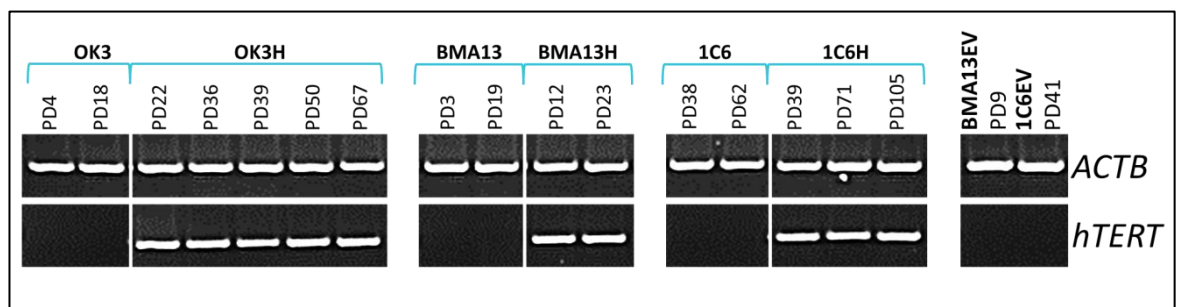


**Figure 4-2. RT-PCR determination of *hTERT* expression stability.** Continued *hTERT* expression is maintained across many passages/population doublings in all transduced cell lines. Neither the parental cell types nor the EV cells BMA13EV or 1C6EV express *hTERT*. ACTB confirms the presence of amplifiable RNA in all groups.

All of the created cell line populations maintained *hTERT* expression across multiple passages representing months of continuous expansion. In contrast no expression was detected in parental cell types at multiple time points, or in the two available EV cell populations. In *hTERT* negative cells *ACTB* expression confirmed the presence of amplifiable RNA.

#### **4.4.2 Cell proliferative capacity**

The introduction and expression of *hTERT* has the capability to extend the proliferative capacity, or even to immortalise, cells. To determine whether this had been achieved in OK3H, BMA13H or 1C6H the cells were maintained in continuous culture, in 2% O<sub>2</sub>, in their respective MM alongside their non-transduced counterparts and the BMA13EV and 1C6EV cells until they had either undergone cessation of proliferation (failure to achieve confluence after ≥ 30 days) or, where proliferative capacity was extended, they had clearly exceeded the proliferative capacity of the non-telomerised cells (. Cell growth curves).

OK3 cell proliferation continued for 24 PD after which cells no longer achieved confluency. The rate of growth prior to growth arrest was relatively stable with growth arrest occurring relatively abruptly. OK3H also exhibited a relatively stable growth rate that was comparable to that of OK3; however, growth slowed dramatically from PD35. This very slow growth rate was maintained for a prolonged period, with only 4 PD achieved over 172 days. Following this crisis period cell growth resumed at a rate similar to that prior to the growth crisis, continuing to PD55 whereupon cells were removed from culture having already achieved 31 PD more than the primary cell counterpart.

BMA13 cells underwent 18 PD at a consistent rate before growth began to slow, with cells failing to reach confluence beyond PD23. EV transduced cells displayed similar growth characteristics, slowing from PD18 and ceasing at PD22. BMA13H underwent an additional 9 PD beyond the capacity of BMA13 before growth in these cultures also ceased. BMA13H cells recovered from

liquid nitrogen that had been banked at an earlier time point (PD8) on the growth curve initially proliferated well but ceased growth at a reduced PD23, comparable to non-transduced cells.

1C6 cells had a rapid growth rate initially undergoing 20 PD in 40 days before slowing significantly with the subsequent 11 PD taking 104 days and proliferation ceasing at PD65. Cells transduced with the empty vector (1C6EV) had a reduced capacity in comparison, ceasing at PD45. In contrast 1C6H demonstrated a greatly increased proliferation capacity, being expanded to PD115 before being removed from culture with no sign of proliferation slowing. Initial growth rates were slightly reduced compared to 1C6; however, remained very consistent throughout.

Due to very slow growth rates following recovery from liquid nitrogen post-transduction all cells were supplemented with the mitogen bFGF. Growth curves for BMA13 both in both the presence and absence of bFGF are shown in Figure 4-4 and clearly show that, at least in this cell type, bFGF supplementation had the effect of slightly increasing the growth rate of the cells and extending the total proliferative capacity by 8 PD.

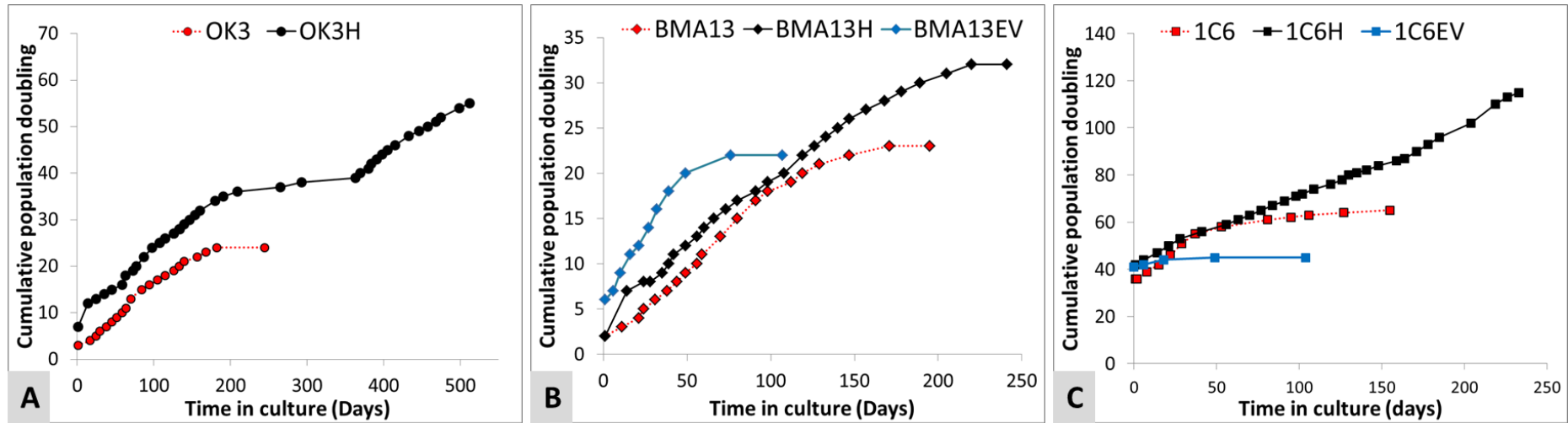


**Figure 4-3. Cell growth curves.** Cells were serially passaged until proliferation ceased or until growth capacity had exceeded that of the relevant parental cell type. Curves are shown for primary chondrocytes OK3 and transduced OK3H (A), hMSCs BMA13, transduced BMA13H and empty vector BMA13EV (B) and ESC derived 1C6, transduced 1C6H and empty vector 1C6EV (C).

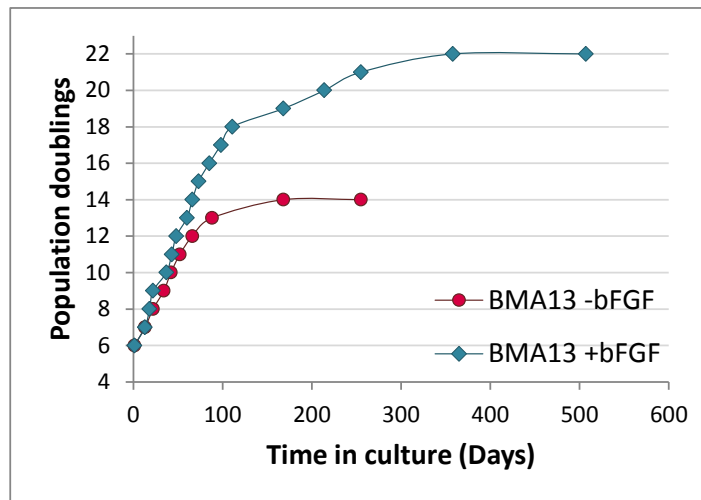


**Figure 4-4. Growth curve of BMA13 in the presence and absence of bFGF.** From PD5 bFGF was withdrawn from a culture of BMA13 at sub-culture and cells were subsequently cultured in the presence or absence of 4 ng/mL bFGF until senescence.

#### 4.4.3 Cell morphology

Cell morphology was monitored throughout the proliferation period to record visible changes associated with both the transduction and with cell aging. Phase contrast photomicrographs were taken throughout the growth period and are shown at early, intermediate and late PD levels (exact PD as indicated) and with 4x (upper) and 10x (lower) objective lenses (Figure 4-5, Figure 4-6 and Figure 4-8). All transduced cell populations, whether the transduction was performed with *hTERT* or EV, retained a morphology consistent with that of their parental cell population at early population doublings. Late PD primary non-transduced cells underwent changes in morphology that are consistent with a senescent phenotype including cell enlargement, an increase in cell processes and greater number of poorly attached/detaching cells.

OK3 and OK3H (Figure 4-5) had a bi- or tri-polar appearance initially. During the OK3H crisis period that OK3H cells had in growth the morphology became much more irregular with multiple cell processes and intracellular vesicles. Many of the cells rounded up and detached from the flasks. Following the recovery from crisis the cells regained and retained morphology similar to the early PD cells.

BMA13H and BMA13EV like BMA13 (Figure 4-6) had predominantly bipolar cells that formed closely aligned colonies that at high cell densities gained a whorled appearance typically seen in hMSC colonies (Figure 4-7). At late PD levels both BMA13 and BMA13EV had more diverse cell morphologies with cells generally being larger, much more irregularly shaped and often only poorly attached to the culture plastic. In contrast, BMA13H cells at late PD were large and had a tendency to become much more polygonal, later appearing as highly refractive stellate cells (Figure 4-6L inset).

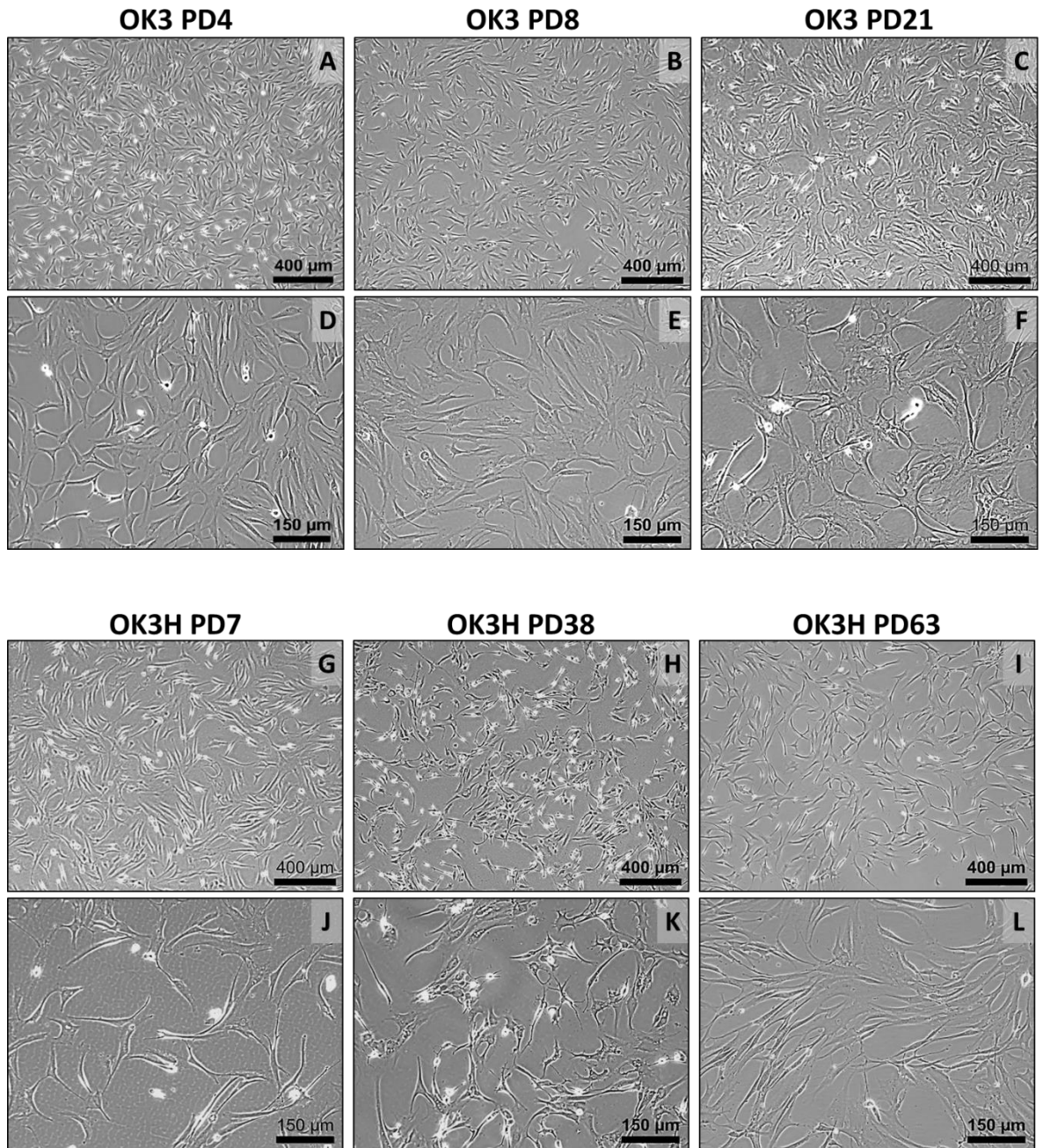


**Figure 4-5. OK3 and OK3H cell morphology.** Phase contrast micrographs of OK3 (A-F) and OK3H (G-L). Images were acquired at early (A, D, G, H), mid (B, E, H, K) and late (C, F, I, L) PD. The categorisation of 'early', 'mid' and 'late' time points are relative to each cell type's individual growth curve and exact PD are as indicated.

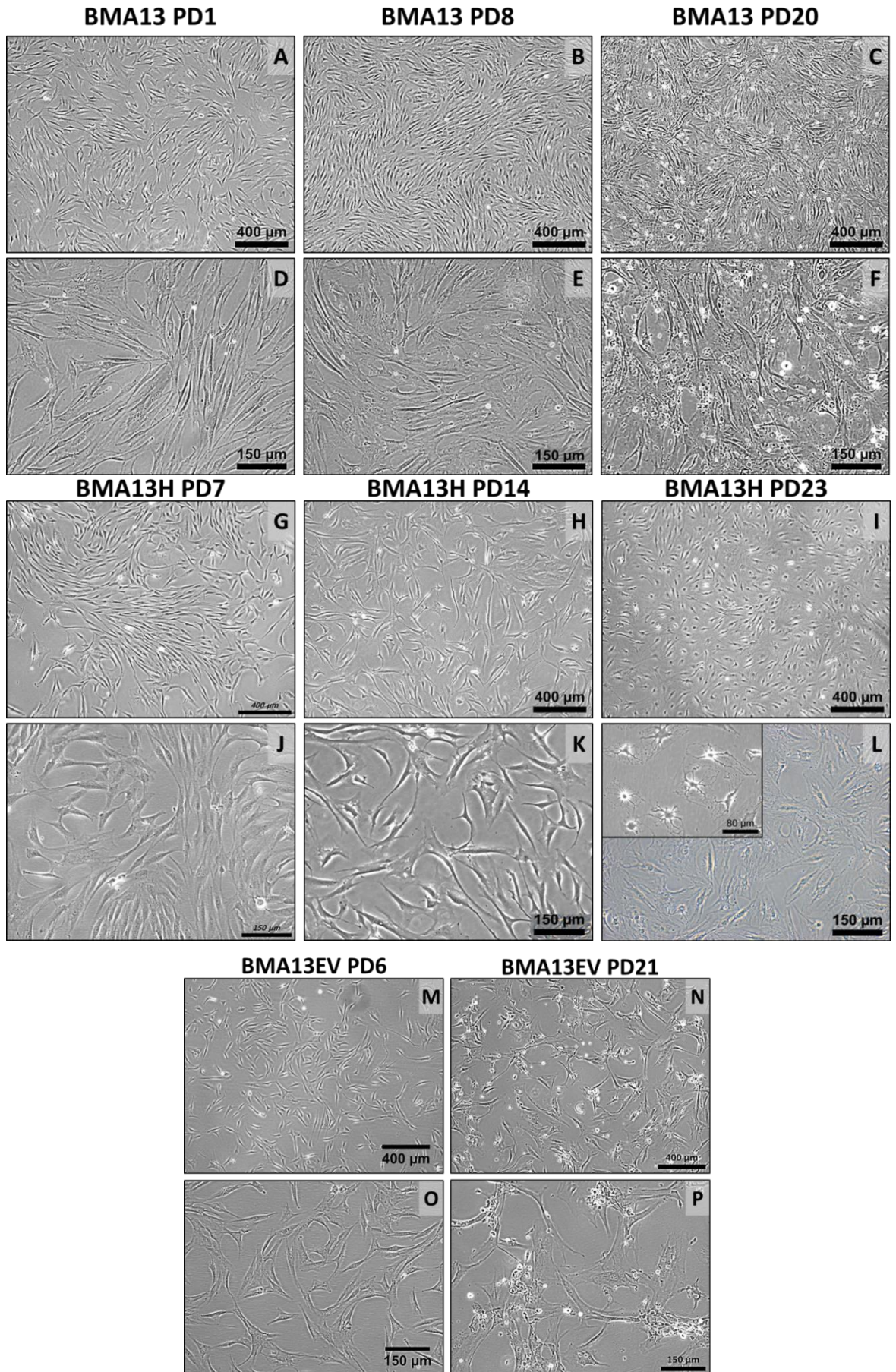


**Figure 4-6. BMA13, BMA13H and BMA13EV cell morphology.** Phase contrast photomicrographs of BMA13 (A-F), BMA13H (G-L) and BMA13EV (M-P). BMA13 and BMA13H images were acquired at early (A, D, G, H), mid (B, E, H, K) and late (C, F, I, L) population doublings. BMA13EV images were acquired at early (M, O) and late (N, P) PD. The categorisation of ‘early’, ‘mid’ and ‘late’ time points are relative to each cell type’s individual growth curve and exact PD are as indicated.

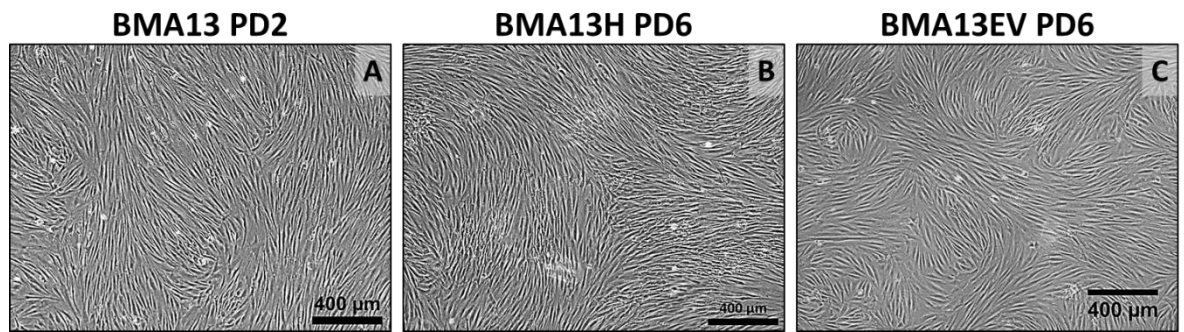


**Figure 4-7. Confluent BMA13, BMA13H and BMA13EV.** Phase contrast photomicrographs of confluent BMA13 (A), BMA13H (B) and BMA13EV (C) at early PD demonstrating the whorled patterns typically seen with hMSCs at confluence.

1C6 and 1C6H and 1C6EV were small, elongated cells. These cells always proliferated to form high density irregular colonies. At senescence 1C6 and 1C6EV cells often became much larger, colony areas contained considerable numbers of cells detaching from the culture plastic and an increased amount of cellular debris. In contrast 1C6H had little variation from the original morphology over a time period encompassing 75 PD.

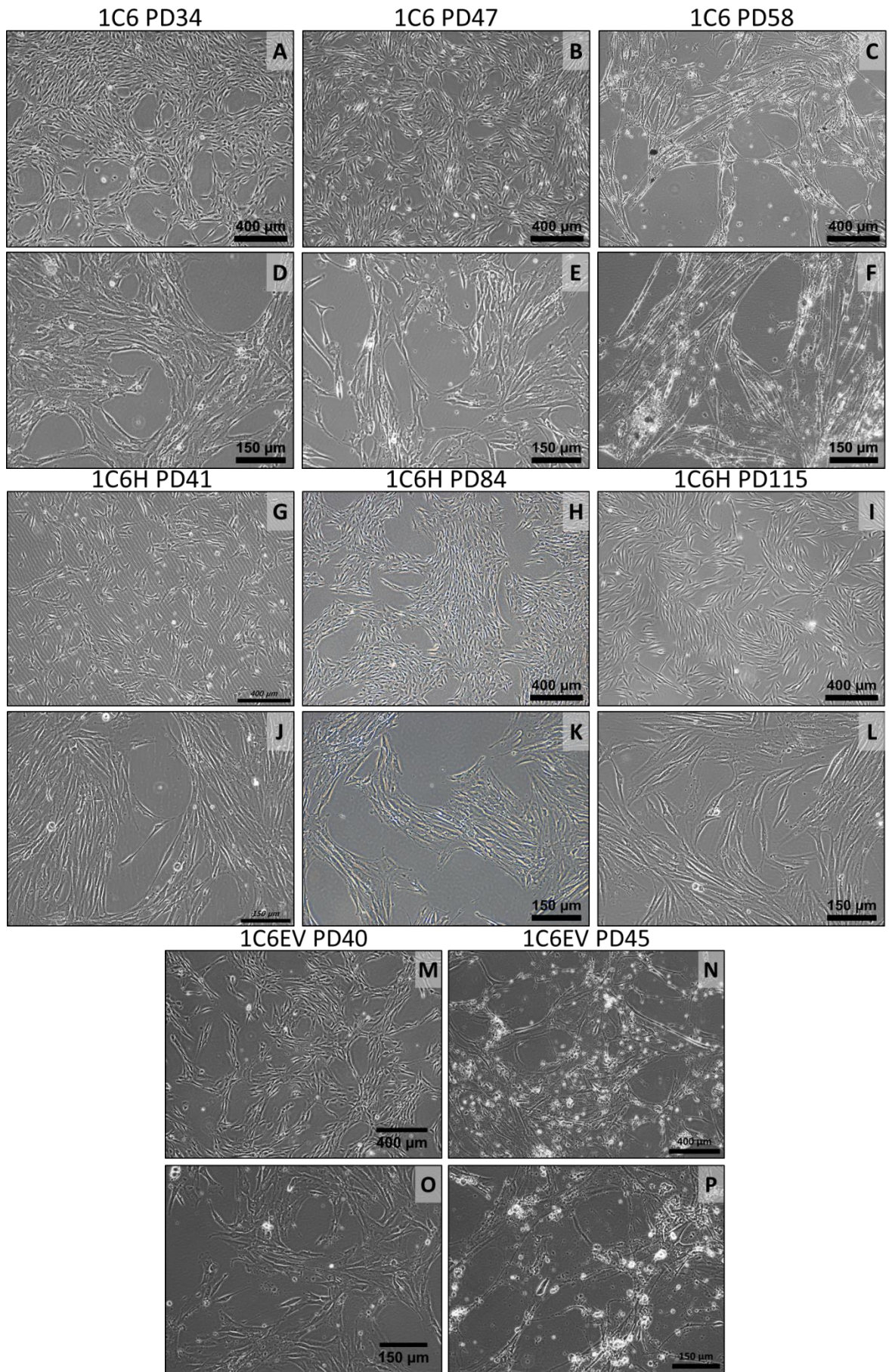


**Figure 4-8. 1C6, 1C6H and 1C6EV cell morphology.** Phase contrast photomicrographs of 1C6 (A-F), 1C6H (G-L) and 1C6EV (M-P). 1C6 and 1C6H images were acquired at early (A, D, G, H), mid (B, E, H, K) and late (C, F, I, L) population doublings. 1C6EV images were acquired at early (M, O) and late (N, P) PD. The categorisation of 'early', 'mid' and 'late' time points are relative to each cell type's individual growth curve and exact PD are as indicated.

#### 4.4.4 SA $\beta$ Gal activity

The presence of SA $\beta$ Gal in cells is considered to be an indicator that the cells are undergoing senescence. Primary cells that were judged to be at relatively early and late PD, determined from the growth curves, and their transduced counterparts were stained for SA $\beta$ Gal activity. SA $\beta$ Gal staining was peri-nuclear spreading out into the cytoplasm and ranged in intensity from a mild to moderate, to an intense degree of staining (Figure 4-9). For the purpose of quantification cells exhibiting any level of staining were counted as SA $\beta$ Gal positive cells.

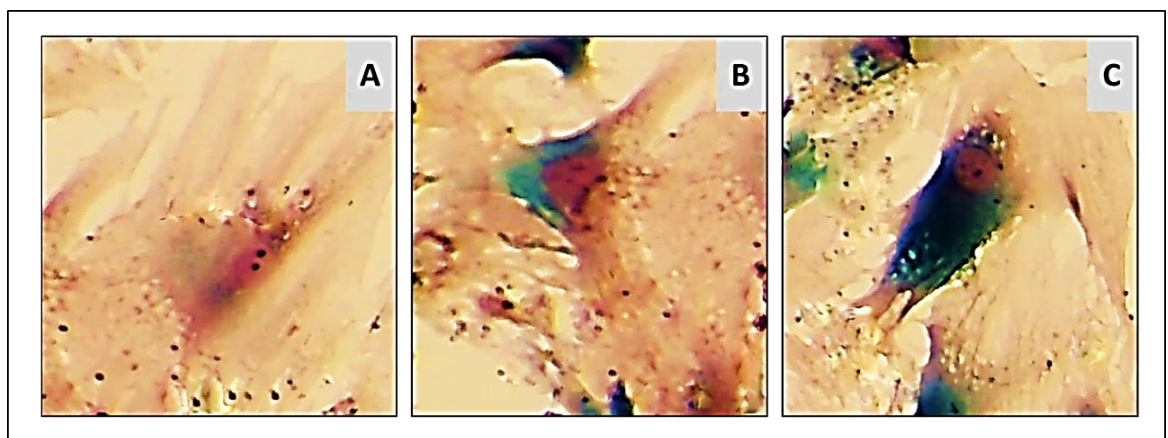


**Figure 4-9. SA $\beta$ Gal staining of cells.** Staining intensity ranged from mild (A), moderate (B) to intense (C) and surrounded the nucleus extending out into the cell cytoplasm. Brightfield images from a single field of view obtained with a 20x objective lens. Cells are counterstained with haematoxylin.

Upon staining, all primary cells at low PD had relatively low levels of SA $\beta$ Gal activity. (Figure 4-10 and Figure 4-11). Where cells were positive it was most frequently with mild levels of staining although occasional cells did stain more intensely. The BMA13 culture contained the greatest number of SA $\beta$ Gal positive cells ( $29.3 \pm 4.9\%$ ) followed by OK3 ( $20.7 \pm 7.9\%$ ) with 1C6 having the

lowest SA $\beta$ Gal positive cell count ( $9.1 \pm 2.8\%$ ). BMA13EV and 1C6EV empty vector transduced cells at low PD were not significantly different to low PD parental cells at  $26.1 \pm 4.6\%$  and  $11.2 \pm 2.6\%$  for BMA13EV and 1C6EV respectively.

At higher PD all parental cells had significantly ( $p \leq 0.0001$ ) increased levels of staining compared to low PD cells, with OK3 levels highest at  $85.1 \pm 7.2\%$  and BMA13 at  $81.7 \pm 6.3\%$ . 1C6 was somewhat lower at  $39.2 \pm 6.3\%$  of cells stained; however, this still represents a mean 4.3 fold increase in the number of cells stained, comparable to BMA13 at a 2.8 fold increase and OK3 with a 4.1 fold increase. BMA13EV at late PD was again not significantly different to the non-transduced population with  $86.8 \pm 3.8\%$  cells stained positively whereas 1C6EV was significantly elevated at  $62.7 \pm 9.7\%$  ( $p \leq 0.001$ ).

BMA13H and 1C6H remained at levels comparable to early PD parental cells ( $25.6 \pm 4.4\%$  and  $12.3 \pm 2.5\%$ ). OK3H levels were significantly increased ( $42.3 \pm 3.0\%$ ,  $p \leq 0.01$ ) over early PD OK3 but remained significantly lower ( $p \leq 0.0001$ ) than late PD parental cells.

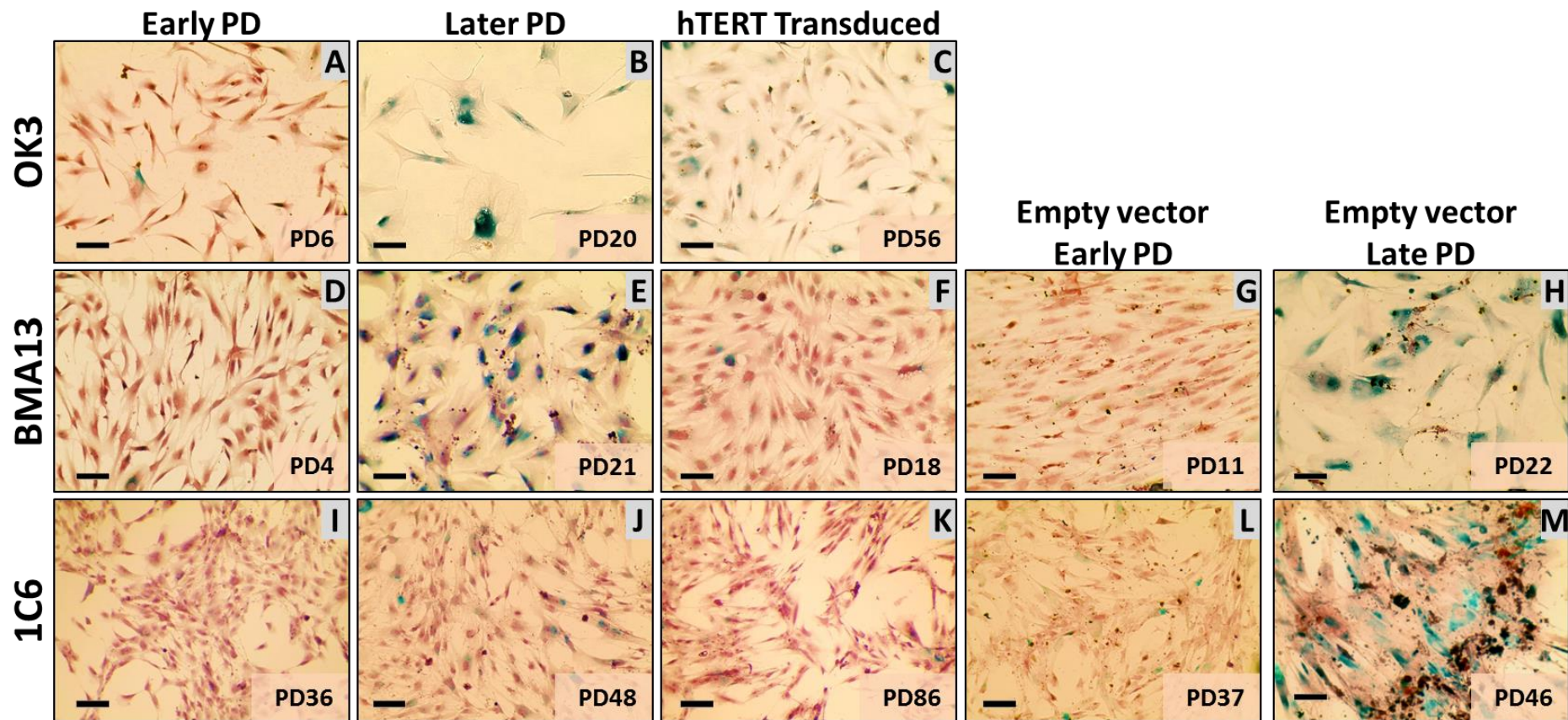


**Figure 4-10. SA $\beta$ Gal staining.** Brightfield micrographs of SA $\beta$ Gal staining of primary, mortal cells at early (A), (D) and (I), and late PD (B), (E) and (F), alongside *hTERT* transduced late PD cells (C), (F) and (K). Empty vector cells BMA13EV and 1C6EV at early PD (G) and (L) and late PD (H) and (M) are also shown. Scale bar = 100  $\mu$ m.

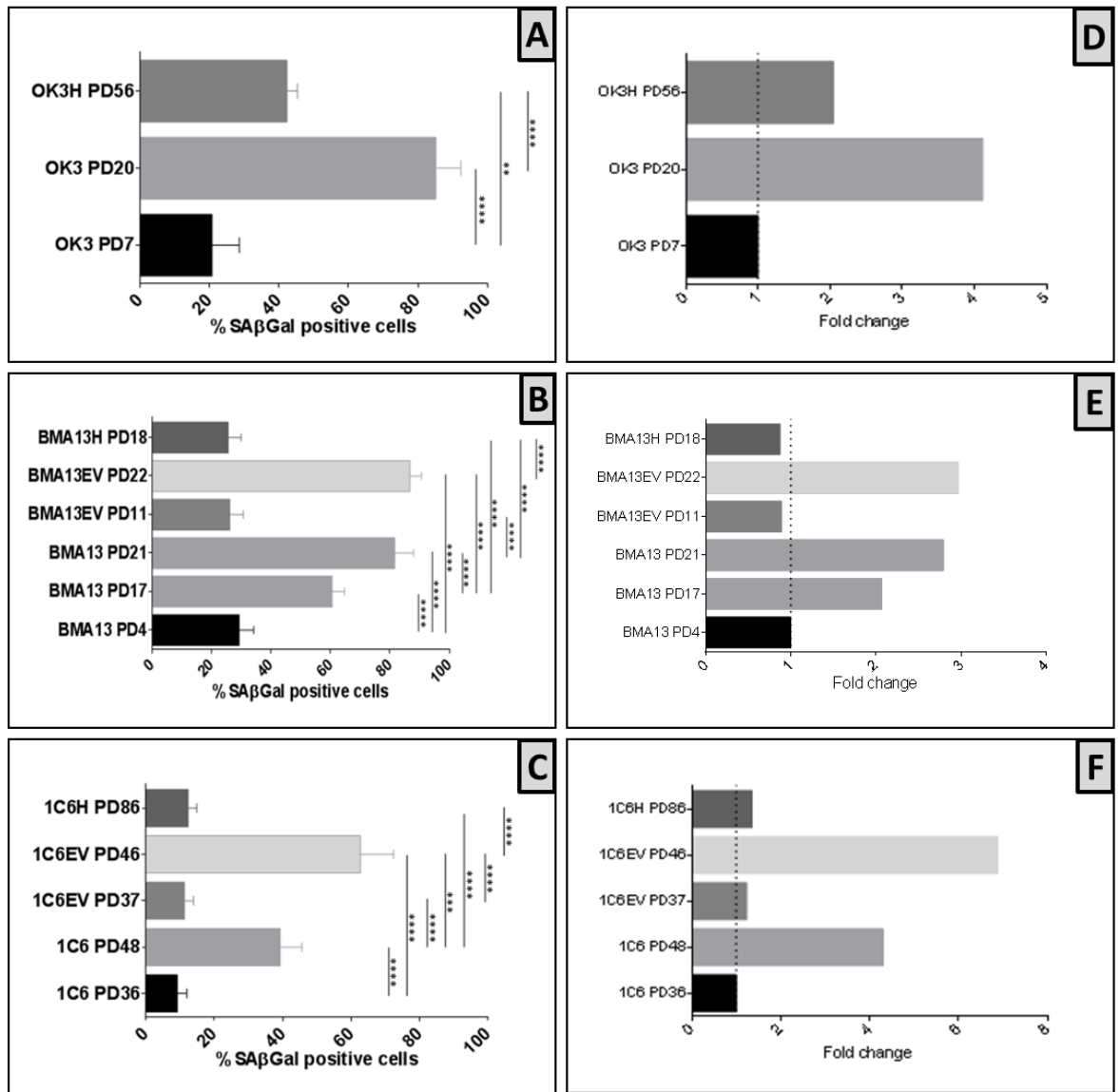


**Figure 4-11. Quantification of cells with SAβGal activity.** SAβGal positively stained cells as a percentage of the total cell number (A-C) and expressed as a fold change relative to the matched early PD primary cells. Data in (A-C) are expressed as mean ± standard deviation, N=4, \*\*p≤0.01, \*\*\*p≤0.001, \*\*\*\*p≤0.0001.

#### 4.4.5 Tri-lineage differentiation capacity

The tri-lineage differentiation capacity of non-telomerised and *hTERT* transduced cells was determined and images of differentiated cells are shown in Figure 4-12. The ability to undergo tri-lineage differentiation is a defining property of MSCs therefore was essential to confirm this property in primary cells and observe any changes in transduced cells. Control wells cultured in

MM for the duration of the experiment had no positive staining with alizarin red S or Oil Red O; however, some staining was apparent with alcian blue for sGAG particularly in 1C6 cells.

Following culture in osteogenic differentiation media there was no evidence of mineralisation in either OK3 or OK3H, evidenced by a lack of alizarin red S stained bone nodules; in contrast BMA13, 1C6 and 1C6H all had strongly stained mineralised regions. BMA13H also stained positively demonstrating a retained capacity to undergo osteogenesis; however, stained regions were much more infrequent and smaller than in BMA13 primary cell cultures.

Alcian blue staining for the sGAG produced during chondrogenesis was positive after culture in PChM in all but OK3H cells where there was no appreciable difference between culture in MM or PChM. Cells undergoing chondrogenesis often spontaneously fully (e.g. OK3 and BMA13H) or partly (e.g. BMA13 and 1C6) detached from the culture plastic and formed pellet like structures that were strongly positive for sGAG, this process is illustrated more clearly in Figure 4-13. Interestingly alcian blue staining in 1C6H, whilst still positive, appeared markedly reduced in comparison to 1C6 staining.

Intracellular lipid droplets produced by cells undergoing adipogenesis were stained with Oil Red O. BMA13 and 1C6 were expected to undergo adipogenesis and stained strongly with Oil Red O following culture in adipogenic media. Interestingly the OK3 and to a greater extent the OK3H cells also produced numerous lipid filled vesicles. The transduced cell types BMA13H and 1C6H both appeared to have reduced staining in comparison to BMA13 and 1C6 respectively.

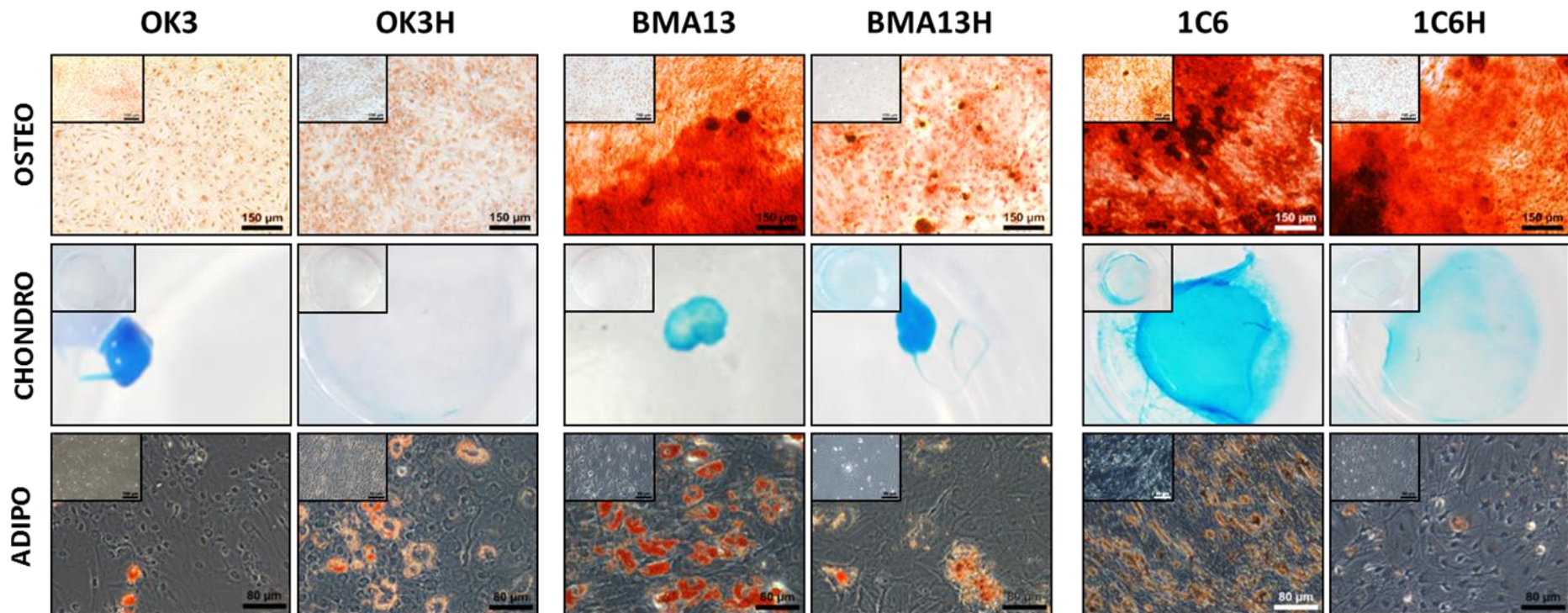


**Figure 4-12. Tri-lineage differentiation of parental and transduced cells.** Images of cells following culture in monolayer for 21 days in the presence of the appropriate pro-differentiation media supplements followed by fixation and staining. Osteogenic samples were stained with alizarin red S for calcium deposits, scale = 150  $\mu\text{m}$ . Chondrogenic samples were stained with alcian blue for SGAGs, images are from 1 well of a 24 well plate. Chondrogenic medium frequently caused cells to partially or fully separate from the substrate and contract into pellet-like structures. Adipogenic samples are stained with oil red O for lipid droplets, scale = 80  $\mu\text{m}$ . Images of controls cells cultured in standard maintenance media and stained as appropriate are inset for comparison.

PD level of cells was as follows: OK3 PD6, OK3H PD50, BMA13 PD6, BMA13H PD28, 1C6 PD36, 1C6H PD83.

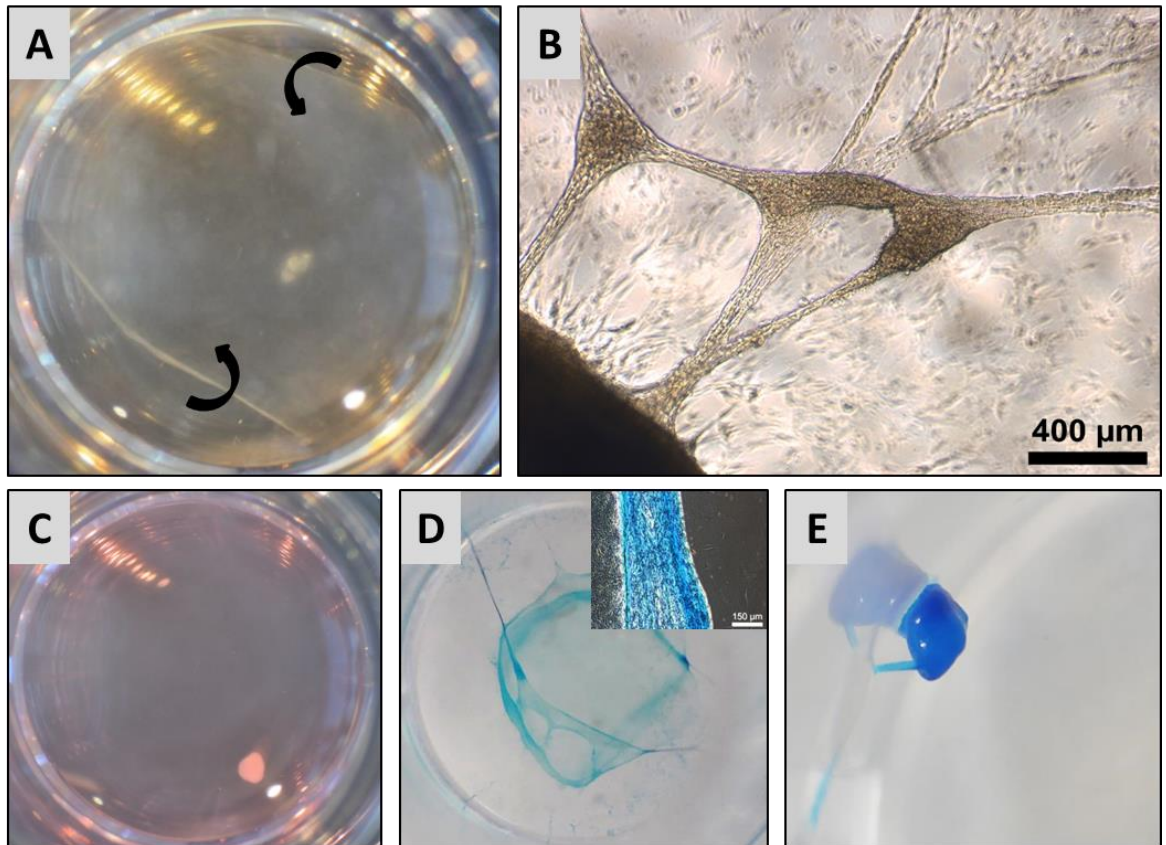


**Figure 4-13. Spontaneous pellet formation in monolayer chondrogenic cultures.** Highly confluent monolayer cultures spontaneously formed pellets, particularly in response to culture in PChM. Pellet-like structures would form when confluent monolayers initially rolled in from the edges of the well (A). They would often remain attached to the walls of the wells (B) and (D) and could partially (D) or fully detach (C) and (E).

#### 4.4.6 Flow cytometry analysis

Flow cytometry was performed to obtain information on cell size assessed by the forward scatter parameter, cell complexity or granulation assessed by the side scatter parameter and to compare the immunophenotype of all cell group against the MSC panel of markers specified by the International Society for Cellular Therapy <sup>115</sup>.

##### 4.4.6.1 Cell size and complexity

Forward and side scatter density plots showing relative size and complexity of all cell types are shown in Figure 4-14. Profiles of BMA13/BMA13H (Figure 4-14C and D) and 1C6/1C6H (Figure 4-14E and F) show similar, although not identical distributions with respect to both size and

complexity; however, OK3H (Figure 4-14B) is quite clearly distinct from OK3 (Figure 4-14A). Cell size (forward scatter) histograms show cell size relative to the signal obtained for 15  $\mu$ m control beads (Figure 4-14G, H and I).

Quantification of relative cell size (Figure 4-15) by forward scatter determined that all cell types were statistically different to all other cell types and that of the primary cells OK3 cells were largest with a mean value of  $262 \pm 9.3$  followed by BMA13 at  $203.6 \pm 4.4$  and finally 1C6 at  $179.3 \pm 2.3$ . Transduced cells were all dissimilar to primary cells where OK3H and 1C6H were smaller at  $190.5 \pm 3.4$  and  $162.4 \pm 1.6$  respectively and BMA13H was larger than BMA13 at  $239.6 \pm 9.6$ .

Relative cell complexity is indicated by the side scatter parameter and is plotted in Figure 4-16, all cells were different to all other cells excepting OK3 ( $209.9 \pm 2.8$ ) and BMA13 ( $202.1 \pm 9.9$ ). OK3H and BMA13H both had higher side scatter values than their parental cell types at  $295.2 \pm 9.8$  and  $254.8 \pm 9.2$  respectively. In contrast 1C6 had a higher measure of complexity at  $189.4 \pm 3.9$  than 1C6H at  $167.6 \pm 3.1$ .

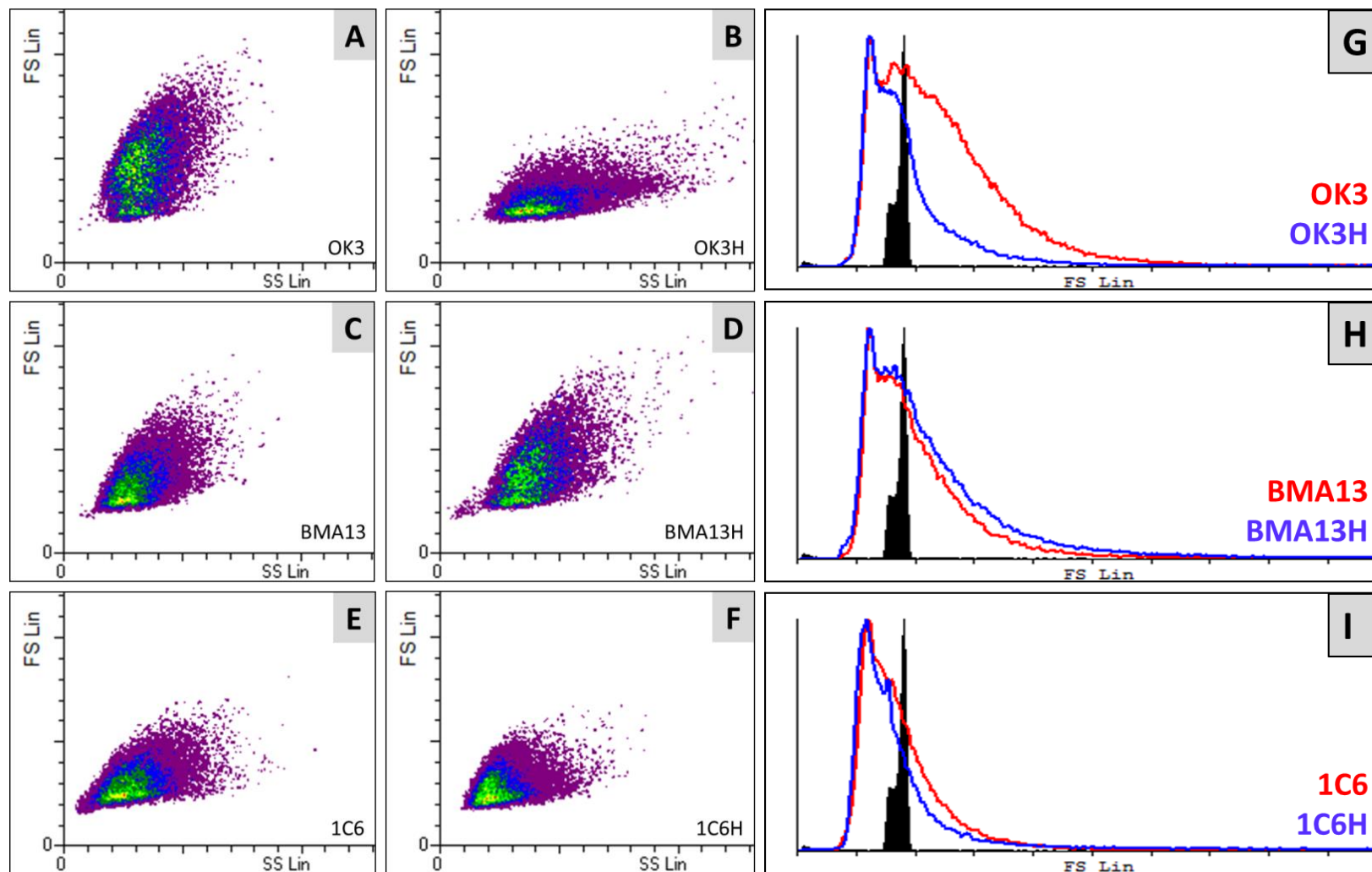


**Figure 4-14. Flow cytometry results.** Forward scatter (FS) and side scatter (SS) density plots for primary cells OK3 (A), BMA13 (C) and 1C6 (E) and transduced cells OK3H (B), BMA13H (D) and 1C6H (F). Cell size relative to 15  $\mu$ m beads is shown in FS histograms (G), (H) and (I). PD level was as follows: OK3 PD10, OK3H PD66, BMA13 PD6, BMA13H PD17, 1C6 PD44, and 1C6H PD118.

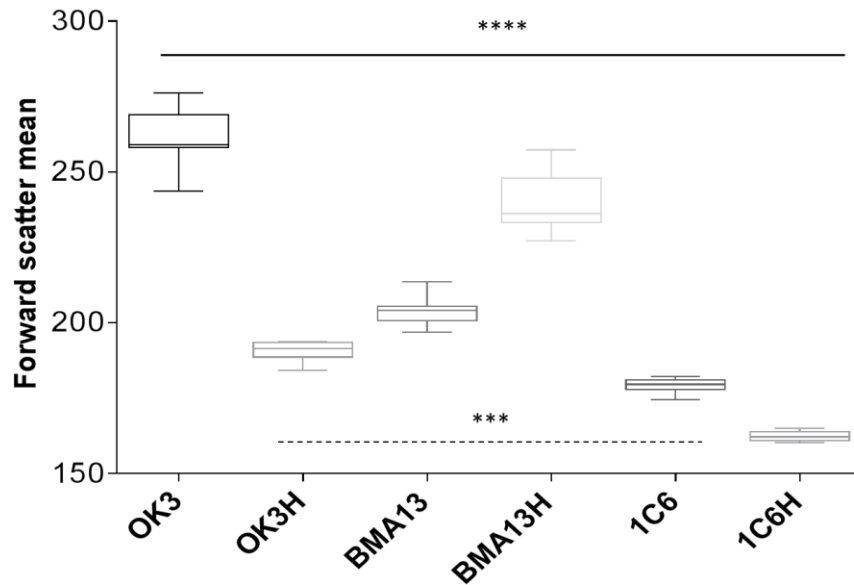


**Figure 4-15. Relative cell size.** Relative cell size box and whisker plots determined by flow cytometry forward scatter. The box indicates the interquartile range and the whiskers are minimum and maximum with the median indicated by horizontal line. All results are significant to all other results at \*\*\*\* $p \leq 0.0001$  except OK3H to 1C6 where \*\*\* $p \leq 0.001$ . PD level was as follows: OK3 PD10, OK3H PD66, BMA13 PD6, BMA13H PD17, 1C6 PD44, and 1C6H PD118.

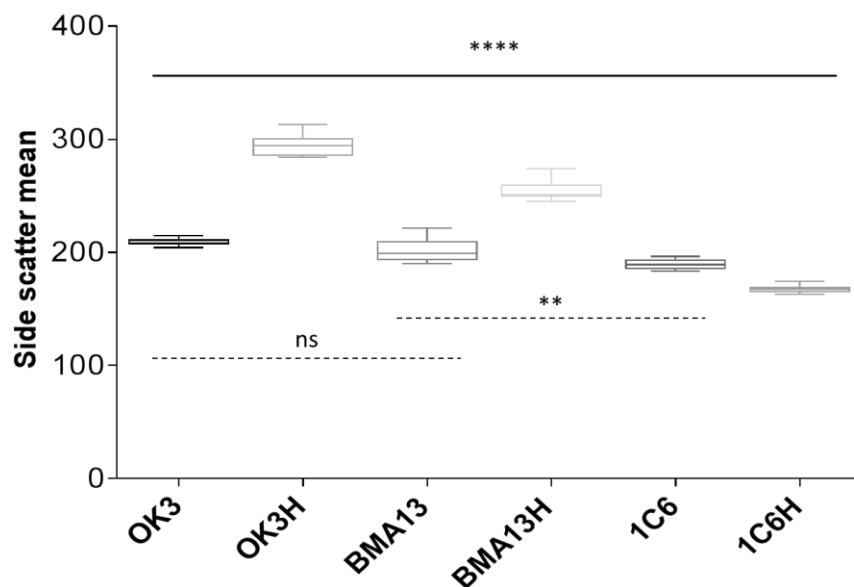


**Figure 4-16. Relative cell complexity.** Relative cell complexity box and whisker plots determined by flow cytometry side scatter. The box indicates the interquartile range and the whiskers are minimum and maximum with the median indicated by horizontal line. All results are significant to all other results at \*\*\*\* $p \leq 0.0001$  except BMA13 to 1C6 where \*\* $p \leq 0.01$  and OK3 to BMA13 where there is no significant difference (ns). PD level was as follows: OK3 PD10, OK3H PD66, BMA13 PD6, BMA13H PD17, 1C6 PD44, and 1C6H PD118.

#### 4.4.6.2 Cell immunophenotype

All cells were incubated with antibodies to CD14, CD19, CD34, CD45, HLA-DR, CD73, CD90 and CD105 a combination that is considered to be a marker panel for hMSCs<sup>115</sup>. Staining was compared relative to the recommended non-specific isotype control, either IgG<sub>1</sub> or IgG<sub>2a</sub> depending on the antibody. Histograms of fluorescence intensity for all markers are shown for OK3 and OK3H in Figure 4-17, for BMA13 and BMA13H in Figure 4-18 and 1C6 and 1C6H in Figure 4-19. The percentage of cells that were considered positively stained was determined by gating the stained population with a gate that excluded 99% of all isotype control events; results are plotted in Figure 4-20.

Both isotype controls stained equally across all cell types, also matching unstained cells demonstrating minimal non-specific fluorescence. CD19, CD34 and CD45, markers typically negative in MSCs were all considered negative in all cells at  $\leq 2\%$  positively stained cells indicating non-haematopoietic lineages. CD14 was slightly elevated in OK3 and OK3H at 12.1% and 5.7% and just barely elevated in BMA13 and BMA13H at 3.4% and 2.5% positive cells. HLA-DR was positive in 88.1% of cells for BMA13 but negative in all other cell types. The MSC positive markers CD73, CD90 and CD105 were positive in BMA13 in 99.9%, 88.1 and 99.1% of cells respectively. In BMA13H expression was comparable for CD73 at 99.9% but halved for CD90 with only 42.5% positive cells. CD105 remained strongly positive although at a slightly reduced 95.6% positive cells. Interestingly OK3 and OK3H were also strongly positive for both CD73 and CD90 at 99.8% and 98.8% for CD73 and 98.1% and 97.1% for CD90. Expression of CD105 was also present but at a reduced level of 52.0% in OK3 and 42.6% in OK3H.

1C6 is a hMSC-like cell type and as such would be expected to be positively stained with the hMSC markers. Cells stained positively for CD73 at 99.9% of cells but CD90 and CD105 were at reduced levels compared to the MSCs, with 66.0% positive cells with CD90 expression and only 11.7% positive cells with CD105 expression. CD73 expression was maintained at high levels (99.9%) in

1C6H but like BMA13H levels of CD90 were much lower, in this case almost completely removed at only 4.0%. However, CD105 expression increased somewhat to 18.8%.

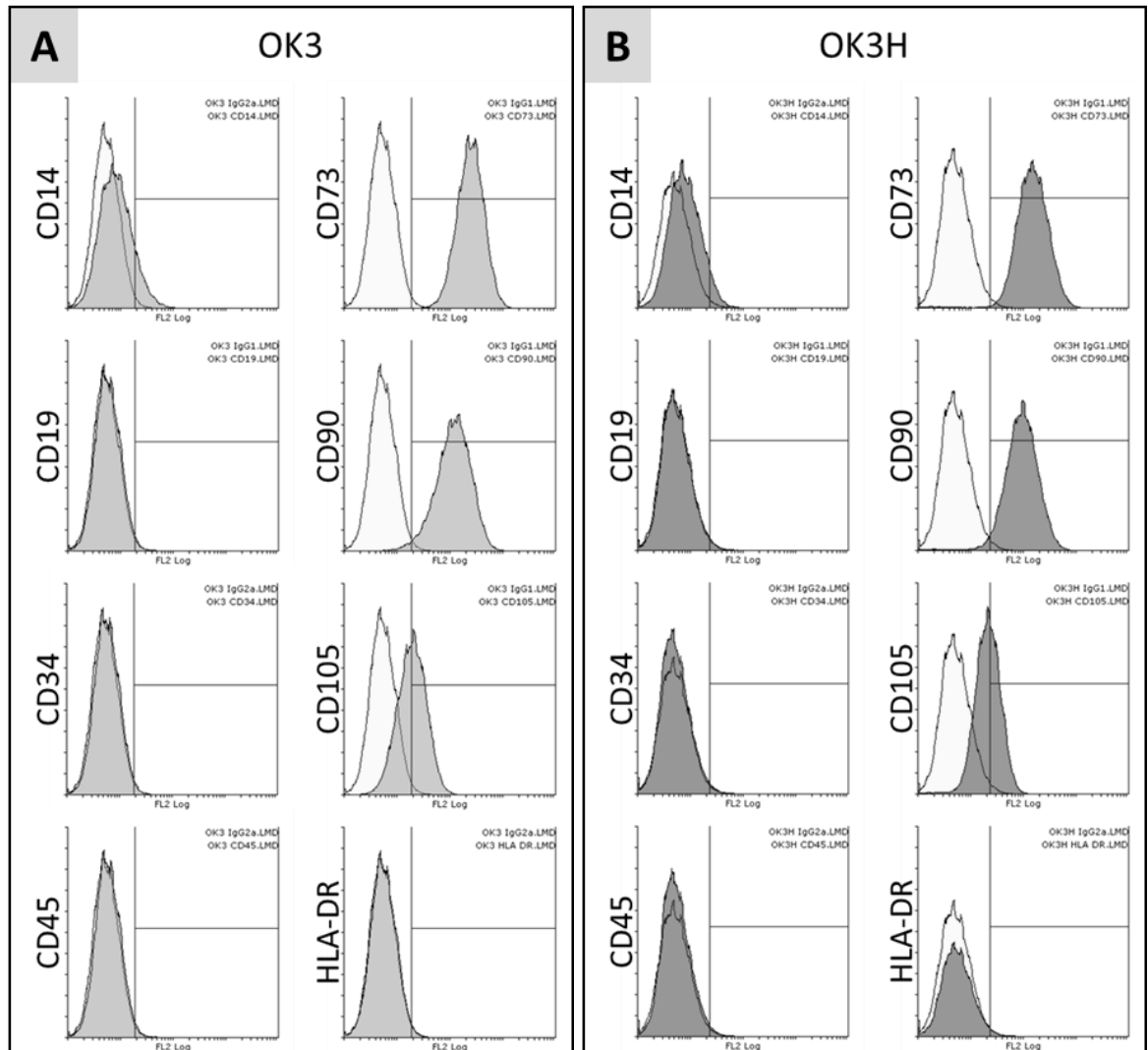


**Figure 4-17. Immunophenotype of OK3 and OK3H.** Expression of typically negative (CD14, CD19, CD34, CD45, HLA-DR) and typically positive (CD73, CD90, CD105) MSC markers in OK3 (A) and OK3H (B). Light fill = isotype control IgG<sub>1</sub> or IgG<sub>2a</sub>, dark fill = antibody marker. Histogram region set to exclude 99% of isotype control events. PD level was as follows: OK3 PD10, OK3H PD66.

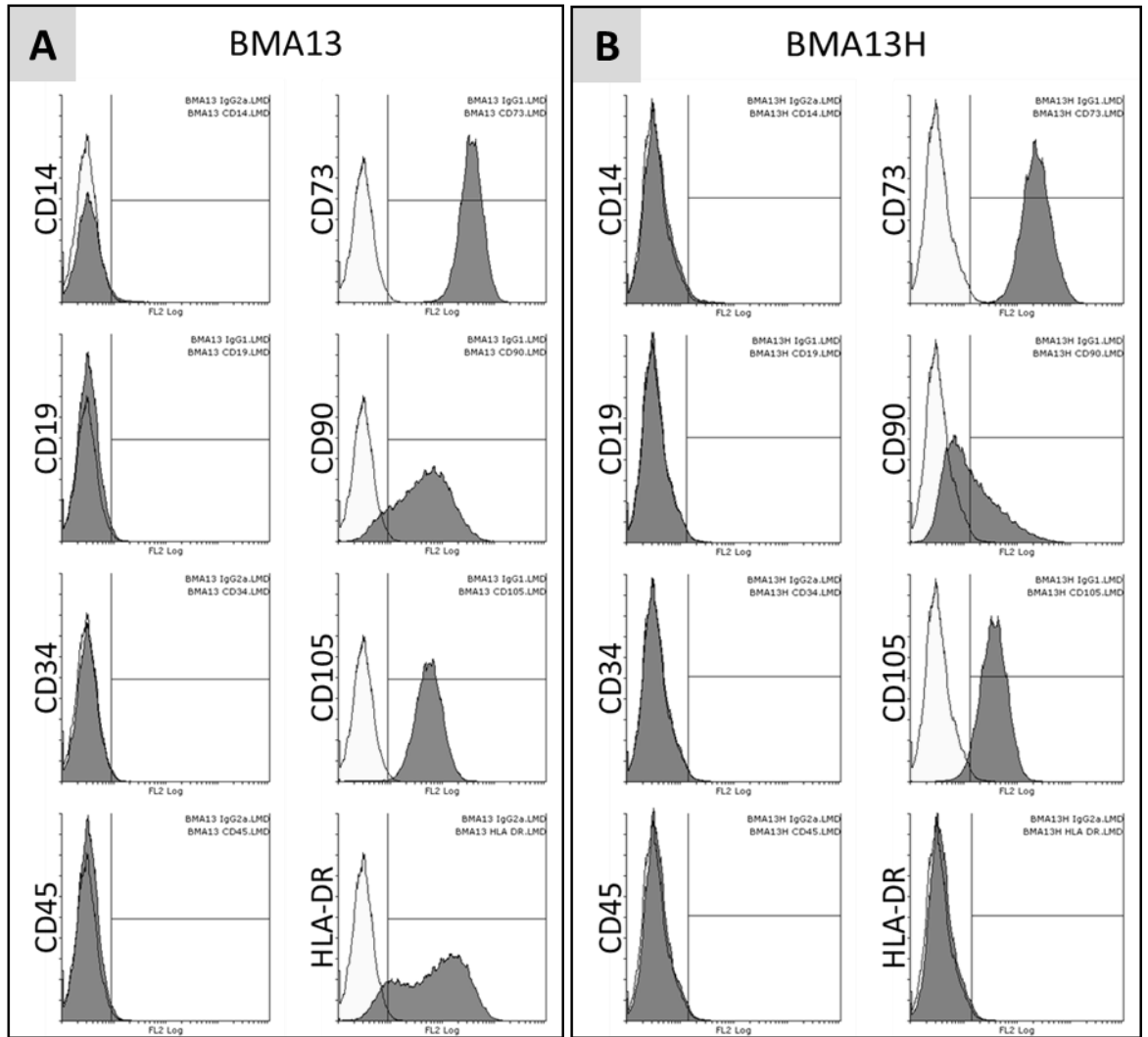


**Figure 4-18. Immunophenotype of BMA13 and BMA13H.** Expression of typically negative (CD14, CD19, CD34, CD45, HLA-DR) and typically positive (CD73, CD90, CD105) MSC markers in BMA13 (A) and BMA13H (B). Light fill = isotype control IgG<sub>1</sub> or IgG<sub>2a</sub>, dark fill = antibody marker. Histogram region set to exclude 99% of isotype control events. PD level was as follows: BMA13 PD6, BMA13H PD17.

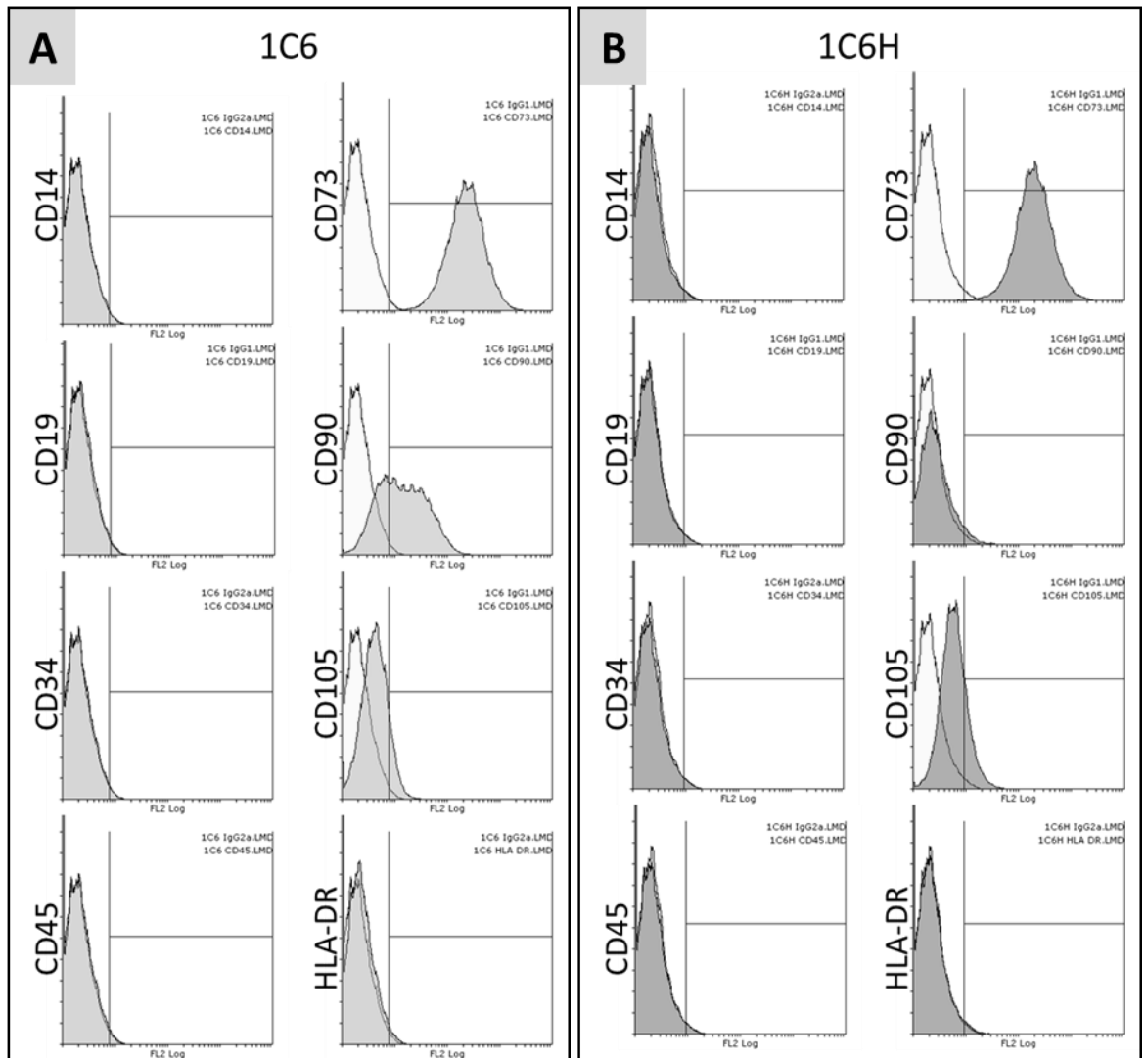


**Figure 4-19. Immunophenotype of 1C6 and 1C6H.** Expression of typically negative (CD14, CD19, CD34, CD45, HLA-DR) and typically positive (CD73, CD90, CD105) MSC markers in 1C6 (A) and 1C6H (B). Light fill = isotype control IgG<sub>1</sub> or IgG<sub>2a</sub>, dark fill = antibody marker. Histogram region set to exclude 99% of isotype control events. PD level was as follows: 1C6 PD44, 1C6H PD118.

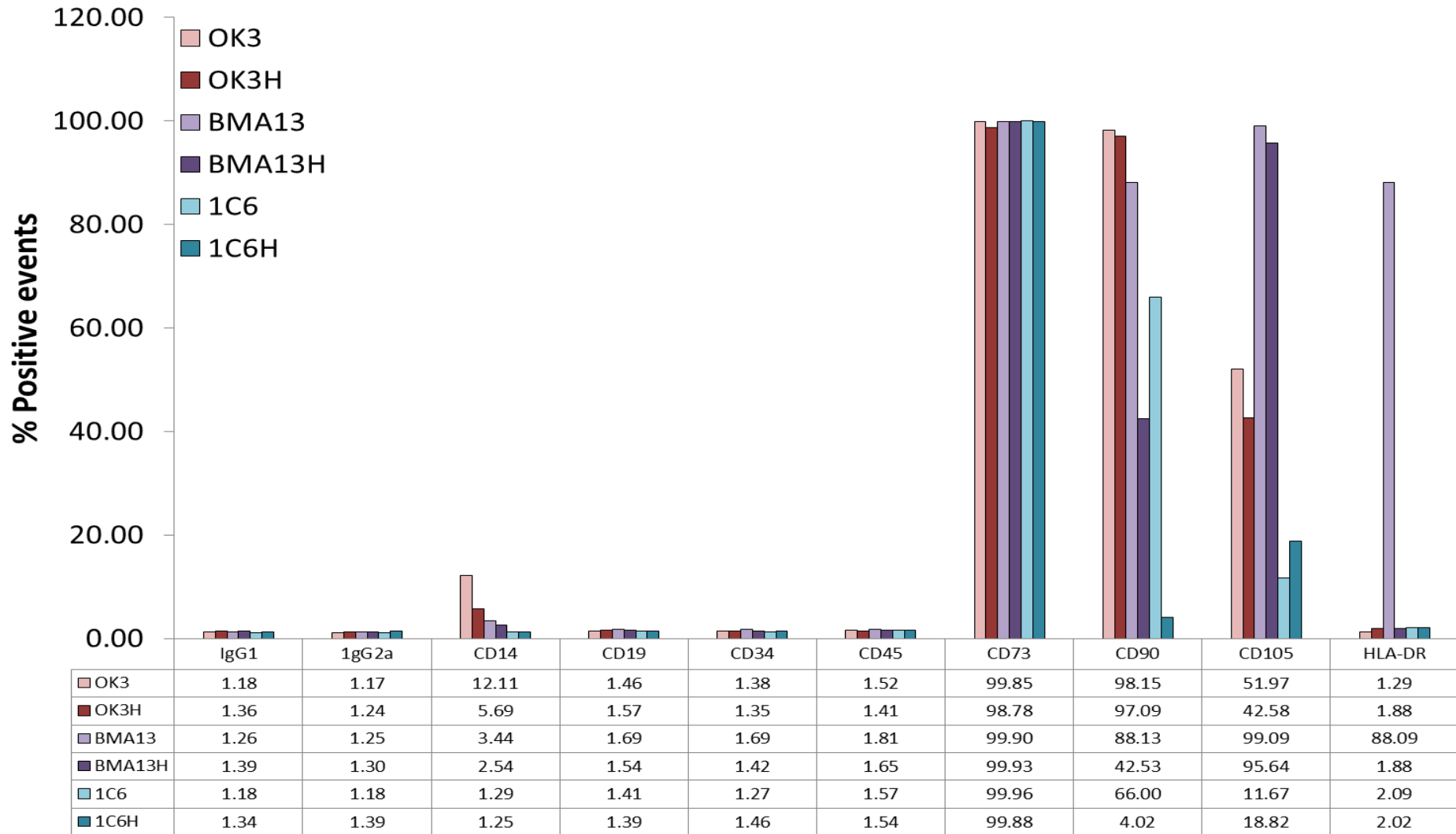


**Figure 4-20. Quantification of immunophenotype markers.** Percentage positive events relative to relevant isotype control marker IgG<sub>1</sub> or IgG<sub>2a</sub> with region set to exclude 99% of isotype control events. PD level was as follows: OK3 PD10, OK3H PD66, BMA13 PD6, BMA13H PD17, 1C6 PD44, and 1C6H PD118.

## 4.5 Discussion

Regenerative medicine offers new therapies for difficult to treat indications like cartilage damage, that frequently rely solely or partly upon a cellular component. Unfortunately many of the clinically relevant cell types are subject to de-differentiation and all primary somatic cells are eventually subject to replicative senescence. This makes any long term, reproducible study of a stable cell population impossible. Immortalisation of clinically relevant cells with the essential catalytic subunit of telomerase, *hTERT*<sup>326–328</sup> was investigated as a route to extend their *in vitro* longevity whilst simultaneously maintaining their differentiation capacity to extend their utility as a research tool. The re-expression specifically of the catalytic subunit, *hTERT*, rather than the other components of telomerase the *TERC* template RNA<sup>329</sup> or the *TEP1* protein has previously been determined to be the limiting step in telomerase activity, with a strong correlation between *hTERT* expression levels and telomerase activity<sup>330</sup>. This immortalization approach has particular applicability for cartilage based cell therapies as in addition to the phenomenon of replicative senescence, primary chondrocytes undergo rapid de-differentiation during *in vitro* culture with a corresponding loss of phenotype<sup>51,314</sup>. Importantly this includes the reduced expression of chondrocyte/chondrogenesis associated genes<sup>331</sup> and reduced responsiveness to pro-chondrogenic signals<sup>332</sup>, making any long term study of these cells towards cartilage repair therapies challenging.

Low levels of endogenous telomerase activity have occasionally been reported to be present in both human chondrocyte and MSC cell cultures<sup>333,334</sup>. Telomerase is active in hESCs; however, its activity is down-regulated as differentiation proceeds and cells accordingly undergo telomere shortening and eventually senescence<sup>202</sup>. As such it would not be expected to be constitutively active in the clonally derived MSC-like 1C6 cell population and cells should undergo senescence after extensive expansion in line with other somatic cells. The results described herein were in accordance with the majority of previous literature and telomerase expression was absent in the

primary non-transduced MSCs BMA13<sup>92,335-338</sup>, chondrocytes OK3<sup>339</sup>, and embryonic derived 1C6<sup>234</sup>. Cells underwent replicative senescence in line with previous reports with regards to both proliferation capacity and SA $\beta$ Gal activity<sup>221,340,341</sup>. *hTERT* transduction resulted in persistent *hTERT* expression in all three cell types even after extensive expansion. However, despite this, a variable response with respect to proliferative potential was noted where 1C6H was the only cell type to undergo prolonged, uninterrupted proliferation. The minimal changes in proliferative capacity seen in BMA13H are in contrast to other publications reporting successful immortalisation of MSCs<sup>338,342</sup>. The senescence of these cells may therefore be due to an alternative mechanism, particularly as the cells were exposed to atmospheric oxygen levels during transduction with *hTERT* having previously been isolated and cultured in 2% oxygen. Oxidative stress during exposure to higher ambient O<sub>2</sub> levels is a known risk factor for stress induced cellular senescence<sup>343</sup> and has been implicated as a causative factor in the lack of immortalisation following *hTERT* transduction in other cell types despite telomere elongation<sup>222</sup>.

To date there are only a very a limited number of reports published describing chondrocyte immortalisation, particularly in reference to human cells. Early experiments used viral proto-oncogenes including the simian vacuolating virus 40 large T antigen (SV40-Tag)<sup>344</sup> to immortalise cells and resulted in a variable impact on cell phenotype and a complex inverse relationship between cell proliferation and chondrogenic ECM synthesis, whereby only slowly proliferating cell populations exhibited ECM synthesis<sup>345,346</sup>. Immortalisation of chondrocytes with *hTERT* has also been described, with assessment of semi-quantitative changes in aggrecan and collagen II gene expression. However, ECM formation via the production and secretion of proteoglycan or proteins was not determined with the study relying only on semi-quantitative gene expression changes. Furthermore, although the cells appeared to retain some chondrogenic capacity aggrecan and collagen II expression were reduced in comparison to control chondrocytes<sup>339</sup>. However, the immortalisation process in chondrocytes may be more complex as others have determined a requirement for secondary transduction with human papillomavirus 16 oncogenes E6 and E7 in

addition to telomerase<sup>347</sup>. In low oxygen culture conditions similar to those employed here only one of three lines gained proliferative potential following *hTERT* transduction despite evidence of extended telomeres in all three<sup>348</sup>.

Following transduction of cells with *hTERT* and a subsequent period of proliferation it is not unusual for cells to undergo a period of slow growth coincident with an increase in tumour suppressor gene expression and cell death, this period is often termed 'crisis' and following the crisis cells may recover to earlier proliferation rates<sup>222</sup> (see Figure 4-21). These results where OK3H experienced an extended pause, or crisis period, suggest that a secondary event allowing bypass of key regulatory gene responses (e.g. pRb, p14<sup>ARF</sup>, p53, p21<sup>CIP1</sup>, or p16<sup>ink4a</sup>)<sup>349</sup> may have occurred in a sub-population of cells during OK3H culture. This along with the ectopic *hTERT* expression allowed continued proliferation beyond the M2 checkpoint and potentially completes the immortalisation process of the cells. Whilst the results for 1C6H are not as definitive as OK3H there was a slowing of cell proliferation coincident with the onset of senescence in 1C6 that may also have represented a crisis period but in this case cells recovered to earlier proliferation rates very rapidly, possibly as a result of the more rapid proliferation rates of 1C6H cells in general. It is tempting to speculate that BMA13H may also have entered the crisis period but that circumstances allowing the bypass of M2 either did not occur at all, or in a sufficient number of BMA13H cells to enable a population level recovery; further experiments would be required to confirm whether this is the case and whether 1C6H and OK3H are indeed immortalised. Larger scale cultures of BMA13H may enable a sufficient number of cells to recover from a potential crisis to result in an immortalised population.

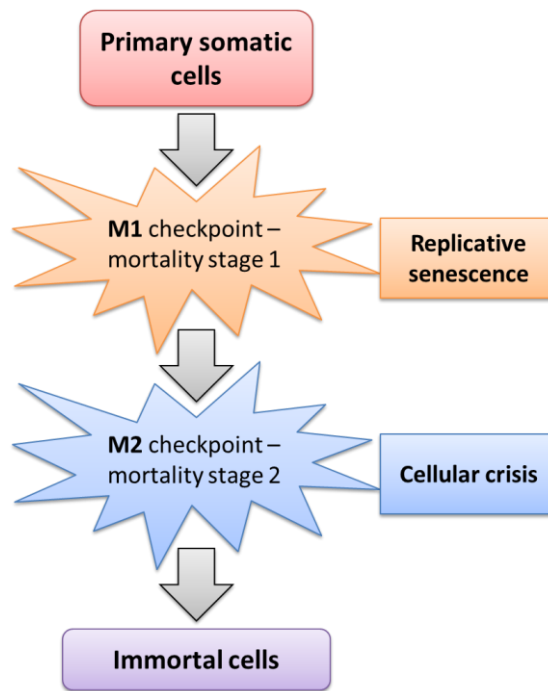


**Figure 4-21. Possible route to cell immortalisation.** Primary somatic cells are believed to pass through two ‘checkpoints’ where proliferation can be halted: M1 and M2. M1 may be bypassed by telomerase transduction; however, M2 may still prevent immortalisation or cause the cells to undergo a crisis period before immortal cells emerge. (Adapted from Choi and Lee, 2015<sup>349</sup>.)

SA $\beta$ GAL, a reported marker for senescent cells<sup>190</sup>, in our samples resulted in the expected higher level of staining of increasing numbers of cells in cultures approaching their maximum number of population doublings. However, it was observed that there was a low background level of activity in both earlier PD OK3 and BMA13, and more notably, high levels in OK3H although this was in conjunction with cells with no detectable SA $\beta$ Gal activity. It is possible that the OK3H is a mixed population with some cells undergoing senescence but alternatively there are multiple culture conditions where SA $\beta$ Gal, a lysosomal  $\beta$ -galactosidase<sup>350</sup>, is found in proliferating cell populations including cells proliferating under stress and in regions of cell confluence<sup>351,352</sup>. The presence of SA $\beta$ Gal activity despite ongoing proliferation is further evidence that mechanisms other than telomere length dependent replicative senescence are active in our cultures. Similar results were found by Zhu *et al*<sup>353</sup> transfection with both *hTERT* and cyclin-dependent kinase 4 (*CDK4*) and further optimisation of culture conditions was necessary to produced differentiation competent

immortalised muscle satellite cells<sup>353</sup>. It is possible that supplementation of the media with additional anti-oxidatives or performing the transduction in a more hypoxic environment would lead to more favourable outcomes.

There are currently no known, unique markers for the identification of cells as MSCs, therefore of necessity MSCs are most commonly defined by the expression or absence of expression of a collection of cell surface markers alongside specific physical/behavioural features. Specifically: plastic adherence, expression of the surface antigens CD73, CD90 and CD105 and concomitant with the lack expression of CD14 or CD11b, CD19 or CD79 $\alpha$ , CD34, CD45 and HLA-DR; and the presence of demonstrable tri-lineage mesodermal differentiation capacity confirming multipotency<sup>115</sup>.

In accordance with these requirements the BMA13 MSCs that were used in this study expressed CD73 (100%), CD90 (88%) and CD105 (99%) and lacked expression of CD14, CD19, CD34 and CD45; however, positive expression of HLA-DR (88%) was seen. Although surface expression of the HLA-DR antigen is typically negative on MSCs they have been shown to contain an intracellular reservoir of HLA-DR that becomes detectable at the cell surface following stimulation for example with IFN- $\gamma$ <sup>354</sup>. HLA-DR has also previously been reported by others on MSCs in the absence of inflammatory stimuli; particularly relevant to the results herein HLA-DR was observed more so when cells were isolated from whole BMA rather than separated MNCs, and particularly in response to exposure to bFGF<sup>355,356</sup>. Subsequent differentiation of the HLA-DR positive MSCs can also lead to a reduction in HLA-DR surface expression<sup>354</sup>. Although seemingly undesirable from a transplantation perspective increased expression of HLA-DR on MSC does not appear to present a barrier to their application clinically, even with potential allogeneic applications, as MSCs expressing HLA-DR, like their HLA-DR negative counterparts, still do not cause an *in-vitro* proliferative response in mixed lymphocyte cultures<sup>354</sup>.

Interestingly we found that OK3 chondrocytes also expressed CD73 (100%), CD90 (98%) and CD105 (52%), positive expression of MSC markers on chondrocytes has been reported previously<sup>314,357,358</sup> with a greatly increased expression of CD90 in response to monolayer culture<sup>314</sup>. Alternatively it has been proposed that these cells may be representative of a chondroprogenitor or MSC like cell type present within cartilage<sup>357,359</sup>. This is not strongly supported here as although OK3 appeared to readily accumulate the lipids associated with adipogenesis, there was no evidence of mineralisation under osteogenic conditions.

Changes in immunophenotype occurred in all three cell populations in response to *hTERT* transduction and subsequent expansion. CD90 expression was reduced in both BMA13H and 1C6H and CD105 was reduced in OK3H when compared to parental cells. CD73, CD90 and CD105 expression decreases with increased passage number in MSCs<sup>360</sup> so these changes may be indicative of a loss of MSC phenotype in BMA13H. High CD90 expression has also been linked to an enhanced osteogenic response in adipose derived MSCs<sup>123</sup>. The same group also found that low expression of CD105 also predisposed the cells to greater a greater osteogenic response; however, CD90 appeared to be the predominant factor<sup>123</sup>. Both BMA13H and 1C6H appeared qualitatively to have reduced osteogenic capacity following transduction, coincident with a reduced CD90 expression. Flow cytometry also identified that all three transduced cell lines differed in both relative size (FS) and granularity (SS).

#### **4.6 Conclusion**

The introduction of telomerase and sustained expression was confirmed in all three transduced cell types, successfully conferring enhanced proliferation and possibly immortality on both OK3H chondrocytes and 1C6H hESC derived cells. Despite reports from others that describe a stable cell phenotype and maintenance of differentiation capacity post transduction in a ranges of cell types, all three telomerised cell lines herein underwent measurable changes in phenotype. Differences included a reduction in cell surface marker expression, changes in cell size and a qualitative

reduction in differentiation capacity in comparison to the parental cell types. There is a paucity of comparators for chondrocyte immortalisation in the literature; the few reports that do exist also describe difficulties, with the process requiring changes in additional culture conditions or further genetic modification. MSC immortalisation is more common and typically more successful, suggesting that a feature of the culture and immortalisation protocol used in this study may be responsible for the poor results with BMA13H. Considering that all of the factors in this experiment with the exception of oxygen tension were not extraordinary, the most likely candidate for this is culture shock or oxidative stress. This may have been induced in the cells as a result of the necessity of performing the transduction in 21%, ambient oxygen conditions with cells that had previously been cultured in physiological hypoxia. As the genetic modification had to be performed at a different institution further investigation of the transduction process is out with the scope of this thesis but should be the subject of future studies of cell immortalisation.

As the primary focus of this thesis is a comparison of chondrogenic capacity, and this was only qualitatively assessed in this chapter, the next chapter determines and compares the primary and transduced cells' chondrogenic capacity quantitatively in a simple 2D environment.



Keele University

---

## **Chapter 5**

---

### ***Sulphated glycosaminoglycan production by cells in monolayer culture***

## 5.1 Introduction

There are several cell types currently under investigation for applications involved in the regeneration of damaged or degenerated articular cartilage. Presently indexed on ClinicalTrials.gov<sup>361</sup> there are 33 trials involving cartilage and MSCs with 14 listed as active, 43 with cartilage and stem cells with 18 active, and 48 involving cartilage and chondrocytes of which 18 are active (Figure 5-1). Despite studies like these having been ongoing for decades the therapies involved have yet to be recommended for routine clinical practice, for example the NICE recommendation for ACI is in favour of continued clinical research but not currently for routine clinical use (NICE Technology Appraisal TA89<sup>362</sup> (At the time of writing the NICE guidance is under appraisal). Patients undergoing these therapies often have significant symptomatic improvements but tissue regeneration is imperfect with fibrocartilage rather than hyaline tissue produced, impacting on long term treatment efficacy.

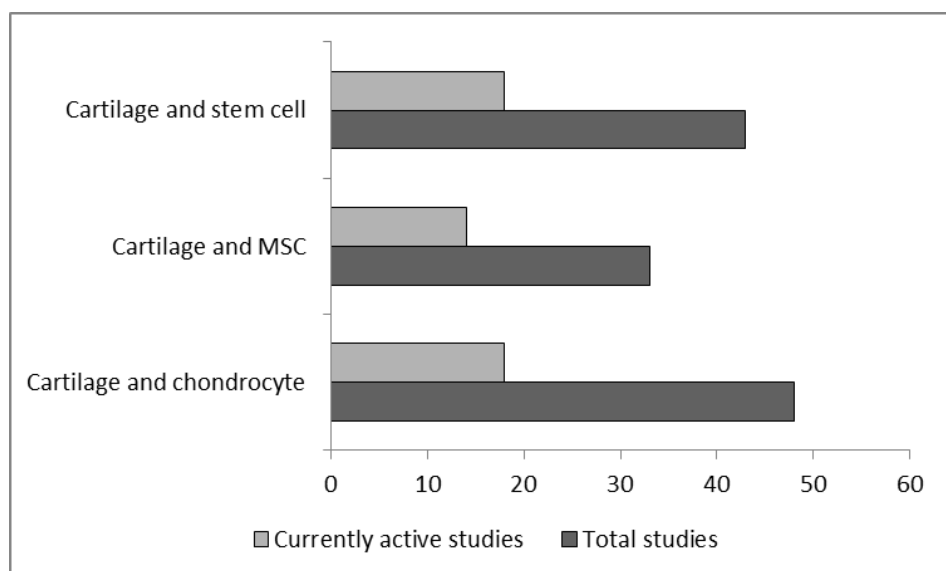


**Figure 5-1. Current clinical trials.** Total number, and the number of currently active clinical trial indexed at ClinicalTrials.gov using the search terms “cartilage and stem cell”, “cartilage and MSC” and “cartilage and chondrocyte”. Data retrieved 10/08/15.

Current treatments for cartilage problems largely revolve around the management of symptoms and include joint stabilisation with bracing, intra-articular steroid injections, pain management, treatment with non-steroidal anti-inflammatories and possibly joint debridement and lavage. These interventions assist in slowing continued degeneration and manage symptoms; however, they cannot reverse the damage done and ultimately disease progression often culminates with a prosthetic joint replacement<sup>363</sup>. In older and less active patient cohorts this may represent an acceptable outcome, although patients may have endured years of symptoms with the associated reduction in quality of life; however, for younger and more active cohorts total joint replacement is a less desirable outcome as the joint will frequently (9 % – 16%) require revision surgery within 10 years<sup>363</sup>. The prospect of improved tissue regeneration alongside a limited repertoire of current therapies continues to drive interest in regenerative medicine cartilage therapies. Current sub-optimal outcomes are possibly as a result of the application of a non-optimal cell type and further *in vitro* characterisation of the cells typically used: MSCs and chondrocytes would be beneficial.

Preliminary investigations of changes in cell phenotype are typically done in a simple monolayer system, with the changes being driven by the application of biochemical cues in the form of cell culture medium supplements, most significantly for chondrogenesis the use of TGF- $\beta$ .

*In vivo* the growth factor TGF- $\beta$  acts both as an early promoter of chondrogenesis at the condensation stage and also acts later to prevent the onset of a hypertrophic phenotype<sup>364</sup>.

During mesenchymal condensation TGF- $\beta$ 1 drives the production of N-cadherin and versican, key molecules in the cell-cell interactions during the condensation process. Later it inhibits numerous molecules associated with terminal differentiation and cartilage hypertrophy including type X collagen, VEGF, osteocalcin and MMP13<sup>13</sup>. To promote *in vitro* chondrogenesis supplementation of the culture media with members of the TGF $\beta$  superfamily is used, with either TGF- $\beta$ 1 or TGF- $\beta$ 3 used most commonly for inducing chondrogenesis at an optimal concentration of 10 ng/mL<sup>365</sup>. TGF- $\beta$ 1 and 3 have both been identified as effective promoters of chondrogenesis, particularly

when used in combination with the steroid dexamethasone<sup>366</sup>, although more limited there is also evidence that TGF- $\beta$ 2 can also promote chondrogenesis. In addition to TGF- $\beta$  and dexamethasone medium is usually further supplemented with ascorbic acid, an insulin, transferrin, and selenium mix, sodium pyruvate, and L-proline. This combination has been shown to be sufficient to promote chondrogenesis of cells in a monolayer, particularly in a low oxygen environment such as that employed for the work in this chapter<sup>367,368</sup>.

This chapter continues work from Chapter 4 and further examines in a more quantitative manner the hypothesis that *hTERT* expression maintains the low PD primary cell phenotype during chondrogenesis in monolayer despite extensive *in vitro* cell expansion.

## 5.2 Aims

The aim of the work described in this chapter was to characterise the parental and transduced cells with respect to their response in a simple *in vitro* environment to a pro-chondrogenic influence via supplementation of the culture medium with, in particular, TGF- $\beta$ 3. As the key aim of cartilage regenerative medicine therapies is the recapitulation of the ECM the production of sGAG is a responsive marker of chondrogenesis.

## 5.3 Methods

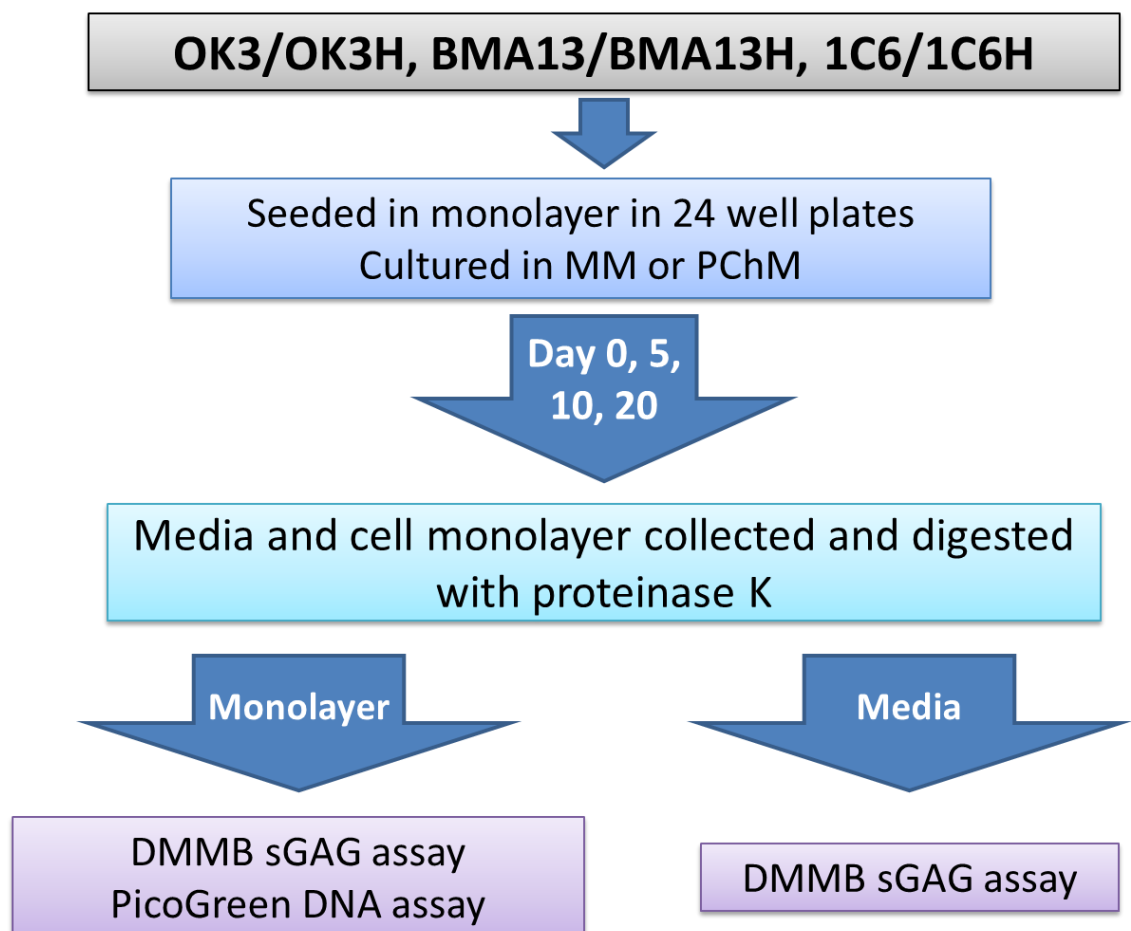
The sequence of experiments for this chapter is summarised in Scheme 3.

Parental, EV and transduced cells were all expanded in 2% O<sub>2</sub> and then seeded in multi-well plates in MM overnight to allow cell attachment after which they were cultured for a further 20 days in 2% O<sub>2</sub>, in the presence of either MM or PChM. Samples were acquired for digestion at days 0, 5, 10 and 20 for both the monolayer and spent culture media and processed as described in section 2.13. Stored spent culture media and cell digests were quantitatively assessed for sGAG content using the DMMB assay as described in section 2.14 and cell content of the monolayer determined via the PicoGreen DNA assay as described in section 2.15.

### 5.3.1 Statistical analysis

Absolute monolayer and media associated sGAG, normalised monolayer and media associated sGAG and monolayer DNA content were compared using two-way repeated measures ANOVA with pairwise comparisons with Bonferroni correction of MM to PChM at each time point to determine statistical significance,  $p \leq 0.05$  was considered significant. Analysis was performed using Graphpad Prism V6.01.

Unless otherwise stated all values quoted in the results are mean  $\pm$  standard deviation.



Scheme 3. Summary of the methodology adopted in Chapter 5.

## 5.4 Results

### 5.4.1 Monolayer associated sGAG

sGAG associated with the cell monolayers was quantified using the DMMB assay on cell digests at day 0 (after overnight cell attachment) and following 5, 10, and 20 days in culture in 2% O<sub>2</sub>, in either MM or PChM (Figure 5-2 and Figure 5-3). For all three primary cell types, culture in the pro-chondrogenic environment induced by the use of PChM resulted in the accumulation of large amounts of monolayer associated sGAG. This resulted in a maximal amount of sGAG by day 20 in OK3 ( $8.84 \pm 2.25 \mu\text{g}$ ) followed by BMA13 ( $5.61 \pm 0.150 \mu\text{g}$ ) and lastly 1C6 ( $5.24 \pm 0.237 \mu\text{g}$ ). This corresponded to fold changes relative to starting sGAG levels of 9.5 fold, 14.0 fold and 10.6 fold in OK3, BMA13 and 1C6 respectively. Primary cell cultures in MM also had increases, albeit smaller, in monolayer associated sGAG culminating, in day 20 quantities that were highest in 1C6 ( $3.68 \pm 0.377 \mu\text{g}$ ), followed similarly by OK3 ( $3.56 \pm 0.231 \mu\text{g}$ ) and lastly, at much lower levels, BMA13 ( $0.758 \pm 0.074 \mu\text{g}$ ) with corresponding fold changes relative to day 0 of 7.1 fold, 3.3 fold and 1.6 fold respectively. The larger increases seen in sGAG in PChM compared to MM resulted in significantly higher sGAG in PChM compared to MM by day 5 (mean difference of  $1.63 \mu\text{g}$ ,  $p \leq 0.05$ ) for BMA13 and day 10 for OK3 (mean difference of  $2.25 \mu\text{g}$ ,  $p \leq 0.05$ ). In contrast, 1C6 initially had significantly more sGAG in MM with mean differences of  $0.85 \mu\text{g}$  ( $p \leq 0.01$ ) at day 5 and  $1.20 \mu\text{g}$  ( $p \leq 0.0001$ ) but by day 20 1C6 also had more sGAG in PChM than MM. As a result of these changes, by day 20 differences were greatest in OK3 (mean difference of  $5.28 \mu\text{g}$ ,  $p \leq 0.0001$ ) followed closely by BMA13 (mean difference of  $4.85 \mu\text{g}$ ,  $p \leq 0.0001$ ) and smallest in 1C6 (mean difference of  $1.56 \mu\text{g}$ ,  $p \leq 0.0001$ ).

Similar results were seen in cultures of BMA13H and 1C6H with PChM day 20 cultures having significantly more monolayer associated sGAG than MM cultures. In BMA13H changes were insignificant until day 20 and the extent of the fold change compared to day 0 and the size of the difference between cultures in MM versus PChM for both cell types in PChM, and for 1C6H in

both MM and PChM were decreased at day 20 compared to those of the corresponding primary cells. This resulted in mean differences of 1.08  $\mu\text{g}$  ( $p \leq 0.0001$ ) for BMA13H and 1.364  $\mu\text{g}$  ( $p \leq 0.001$ ) for 1C6H. In contrast OK3H maintained an inverse relationship to all other cultures for all 20 days, with cells in MM having more monolayer associated sGAG than cultures in PChM resulting at day 20 in a mean difference 2.067  $\mu\text{g}$  ( $p \leq 0.0001$ ).

Data in Figure 5-3D-F, where fold changes are expressed relative to the previous time point, allow a more detailed examination of the temporal changes in sGAG production with each time interval. These indicate that more sGAG was produced in the first five days in the majority of cell types, followed by a decrease in the rate of change between day 5 and 10, followed by more conservative changes thereafter. The exceptions to this trend were 1C6 cells cultured in PChM where there was a steady increase in sGAG with each time period and OK3H which had reduced sGAG within the first 5 days followed by a slight recovery; however, overall this resulted in little net gain.

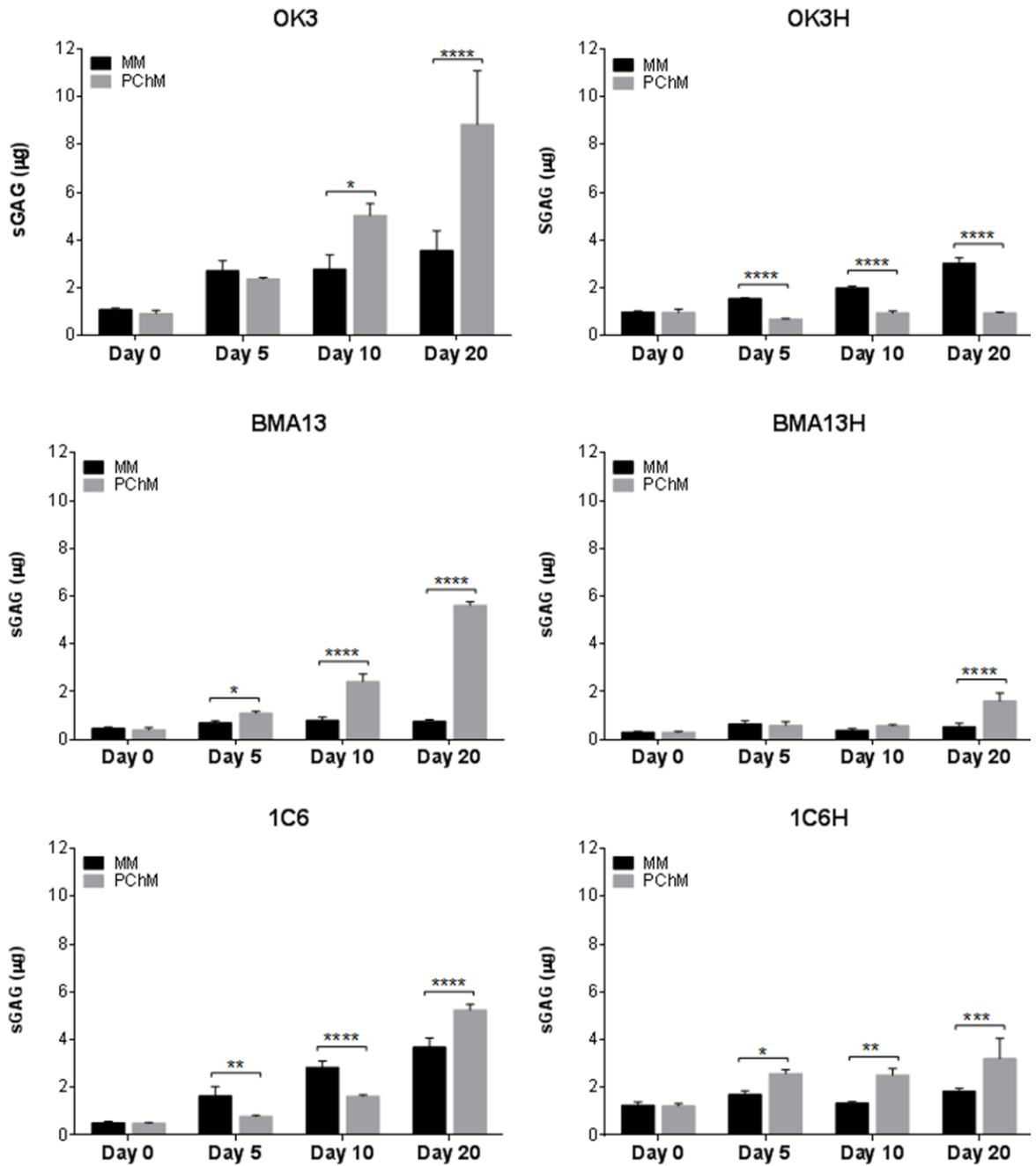


**Figure 5-2. Monolayer associated sGAG.** sGAG associated with cell monolayers was quantified using the DMMB assay at day 0, 5, 10 and 20 for all cells after culture in MM or PChM. Data are expressed as mean  $\pm$  standard deviation, N=3, \* $p < 0.05$ , \*\* $p < 0.01$ , \*\*\* $p < 0.001$ , \*\*\*\* $p < 0.0001$ . PD level was as follows: OK3 PD6, OK3H PD50, BMA13 PD6, BMA13H PD16, 1C6 PD42, 1C6H PD84.

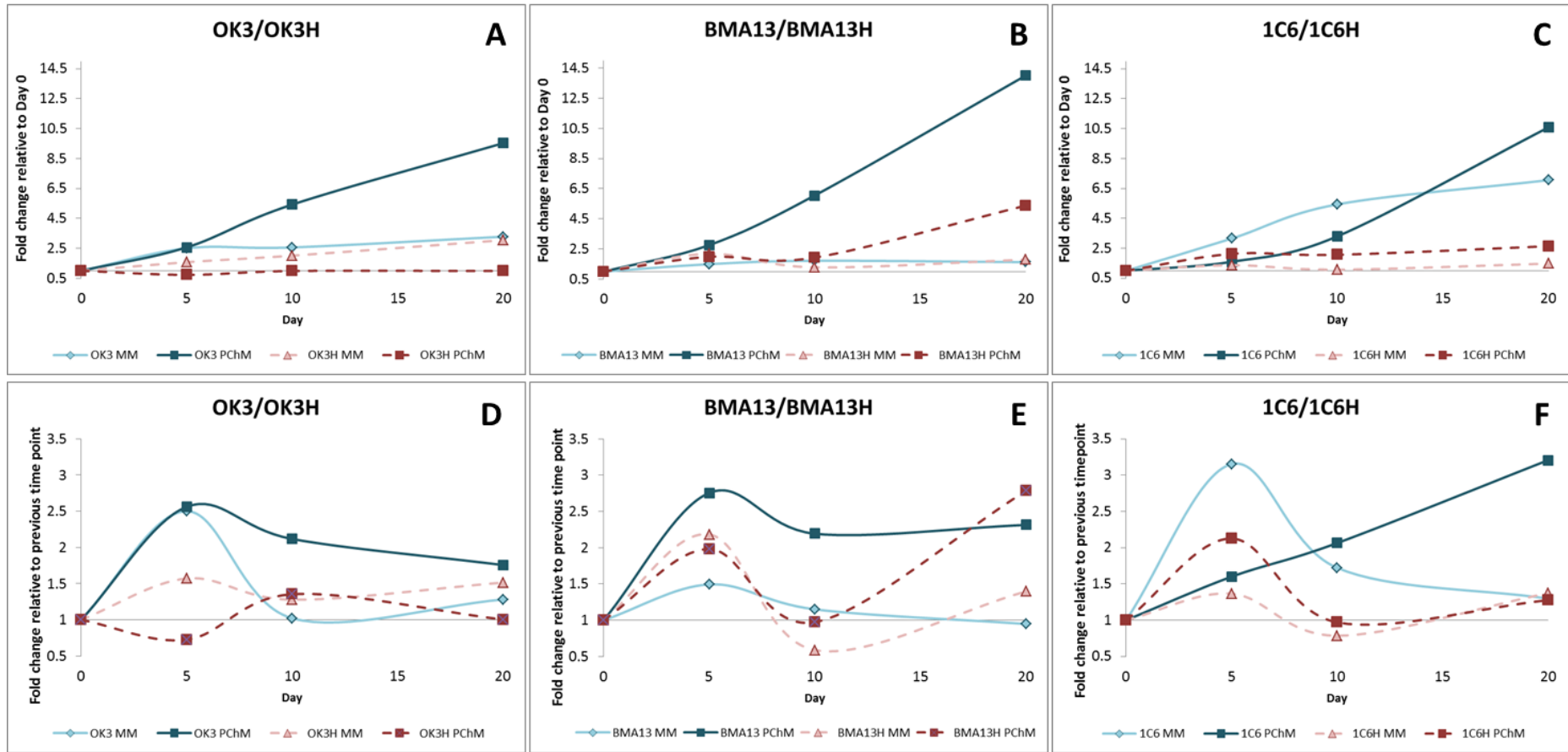


**Figure 5-3. Fold change in monolayer associated sGAG.** For comparison purposes data were expressed as mean fold change relative to the day 0 sGAG content of the monolayer (A-C) and relative to the previous timepoint (D-E). PD level was as follows: OK3 PD6, OK3H PD50, BMA13 PD6, BMA13H PD16, 1C6 PD42, 1C6H PD84.

#### 5.4.2 Media associated sGAG

sGAG associated with the spent cell culture media was also quantified using the DMMB assay at day 0 (after overnight cell attachment) and following 5, 10, and 20 days in culture in either MM or PChM. All data were first normalised using appropriate media controls and are expressed cumulatively with the earlier time points in line with monolayer associated sGAG (Figure 5-4).

As with monolayer associated sGAG, media sGAG increased over the course of the experiment, this increase occurred in all cell types and in both MM and PChM. Amounts at day 20 were largest by far in OK3 and OK3H MM cultures at  $113.28 \pm 1.026 \mu\text{g}$  and  $96.316 \pm 1.639 \mu\text{g}$ . This was followed by 1C6 at  $17.769 \pm 2.758 \mu\text{g}$  and BMA13 at  $14.978 \pm 1.745 \mu\text{g}$ . Again, as with monolayer associated sGAG, smaller amounts were identified in the media of transduced cells BMA13H and 1C6H at  $3.560 \pm 0.666 \mu\text{g}$  and  $5.445 \pm 0.403 \mu\text{g}$ . However, in contrast to monolayer associated sGAG which was usually higher in PChM, media sGAG from PChM cultures was reduced compared to MM. In OK3 and in 1C6 levels were significantly lower, and by day 20 were  $26.885 \pm 3.298 \mu\text{g}$  ( $p \leq 0.0001$ ) and  $6.549 \pm 0.376 \mu\text{g}$  or 0.24 and 0.37 times that in MM in OK3 and 1C6 respectively. BMA13H and 1C6H were also had significant reductions in PChM compared to MM with 0.61 fold ( $p \leq 0.05$ ) and 0.78 fold ( $p \leq 0.01$ ) differences. BMA13 on the other hand was significantly increased in PChM compared to MM at  $19.831 \pm 0.445 \mu\text{g}$  ( $p \leq 0.0001$ ) representing a 1.4 fold increase.

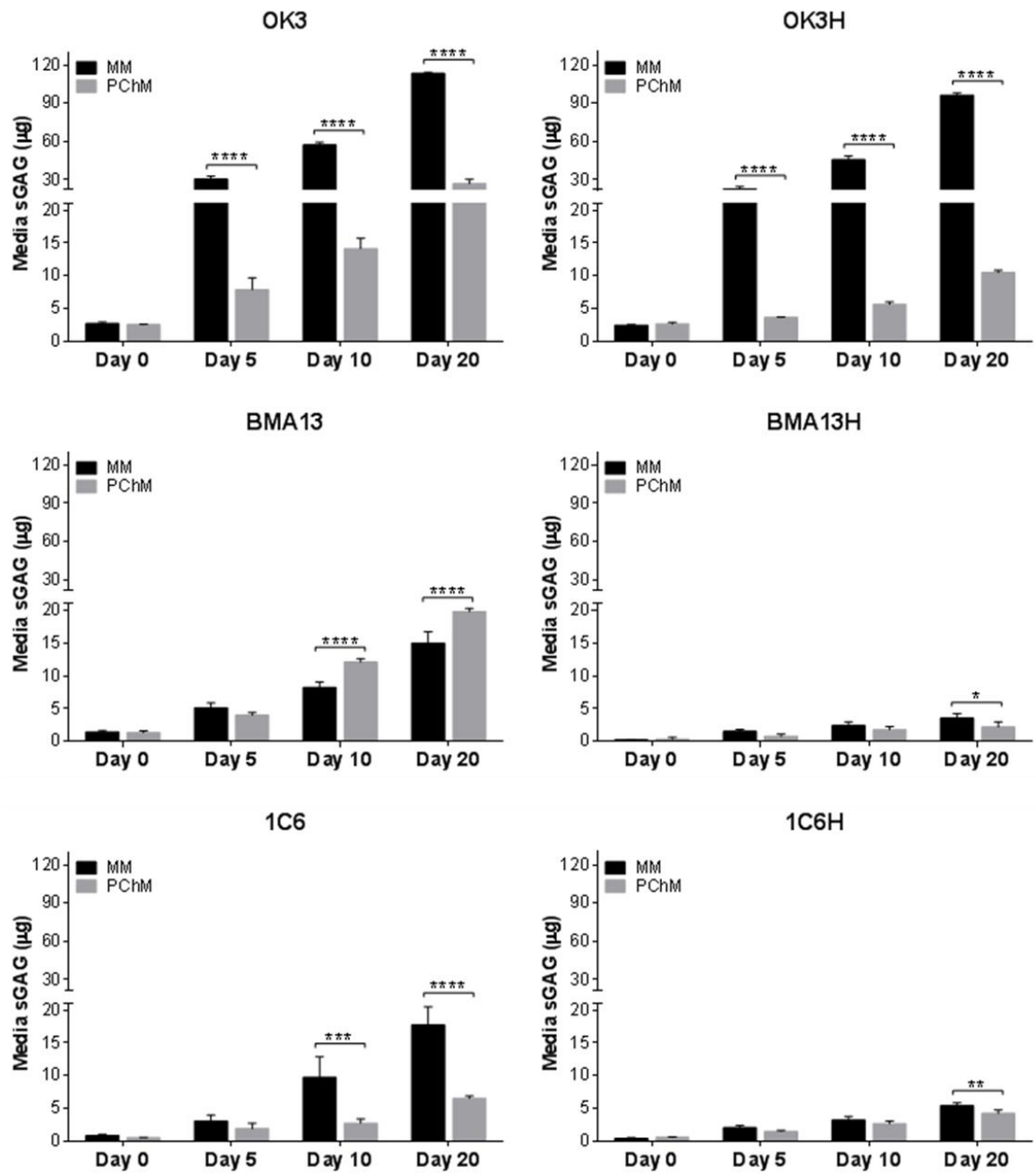


**Figure 5-4. Media associated sGAG.** sGAG associated with spent cell culture media were quantified using the DMMB assay at day 0, 5, 10 and 20 for all cells after culture in MM or PChM. Data are expressed as mean  $\pm$  standard deviation, N=3, \*p<0.05, \*\*p<0.01, \*\*\*p<0.001, \*\*\*\*p<0.0001. PD level was as follows: OK3 PD6, OK3H PD50, BMA13 PD6, BMA13H PD16, 1C6 PD42, 1C6H PD84.

### 5.4.3 Total sGAG changes

Total sGAG at day 20 as a result of the contributions from the monolayer associated sGAG and the media associated sGAG are shown in Figure 5-5, with the contribution from each fraction expressed as a percentage of the total amount of sGAG in Figure 5-6A and as total fold change in Figure 5-6B. Cultures of all cells had an overall increase in total sGAG after 20 days in culture compared to starting amounts irrespective of culture media conditions. Larger total increases were detected in MM than PChM in all cases excepting BMA13, with increases in sGAG in MM ranging from 4.4 fold over day 0 values in 1C6H to 30.9 fold in OK3. This is in comparison to increases in PChM from 3.1 fold in OK3H to 14.7 fold in BMA13. All three primary cell types had greater fold increases and total sGAG production than their corresponding transduced cell types. The proportion of total sGAG associated with the monolayer by day 20 ranged from 3.0% (OK3H) to 25.2% (1C6H) in MM and 8.4% (OK3H) to 44.45% (1C6) in PChM. Culture in PChM overall led to a decrease in total sGAG due to a reduced media associated fraction, but this was concomitant with an increase in monolayer associated sGAG.

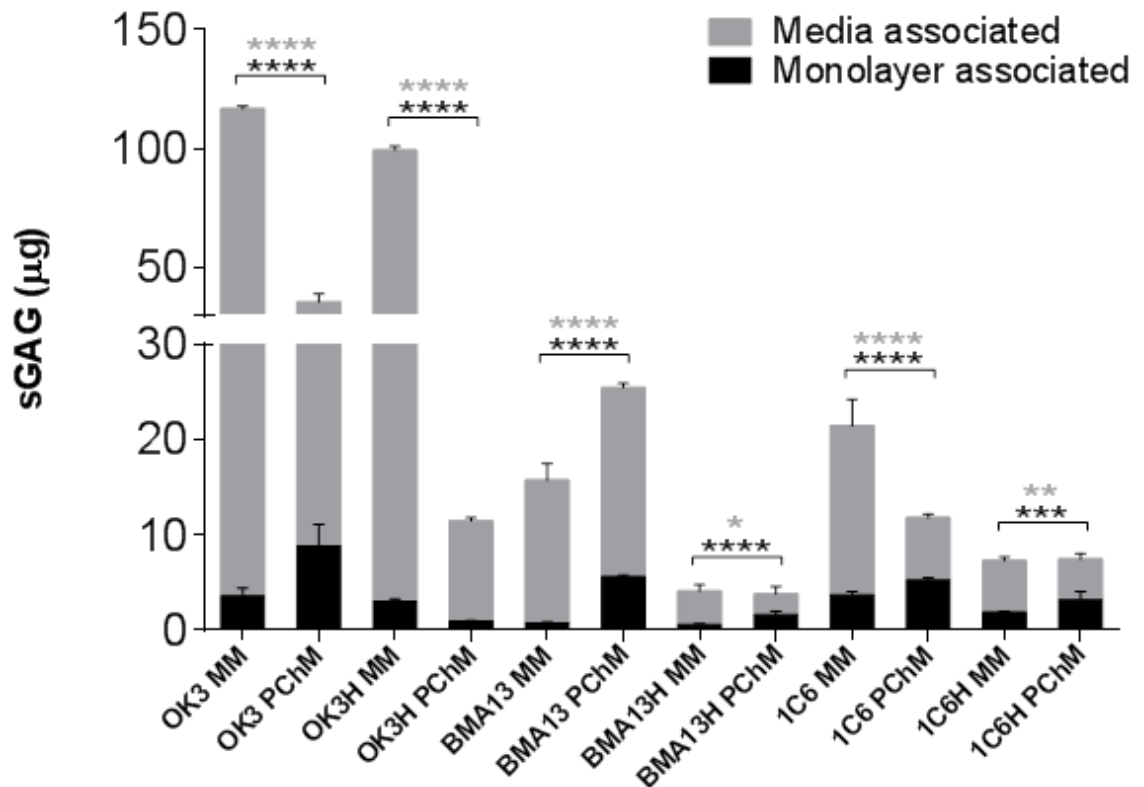


**Figure 5-5. Total sGAG at day 20.** Day 20 summary of total sGAG by both monolayer and media contribution at day 20. Data are expressed as mean  $\pm$  standard deviation, N=3, \* $p \leq 0.05$ , \*\* $p \leq 0.01$ , \*\*\*\* $p \leq 0.0001$ . Black asterisks indicate significance between monolayer associated sGAG; grey asterisks indicate significance between media associated sGAG. PD level was as follows: OK3 PD6, OK3H PD50, BMA13 PD6, BMA13H PD16, 1C6 PD42, 1C6H PD84.

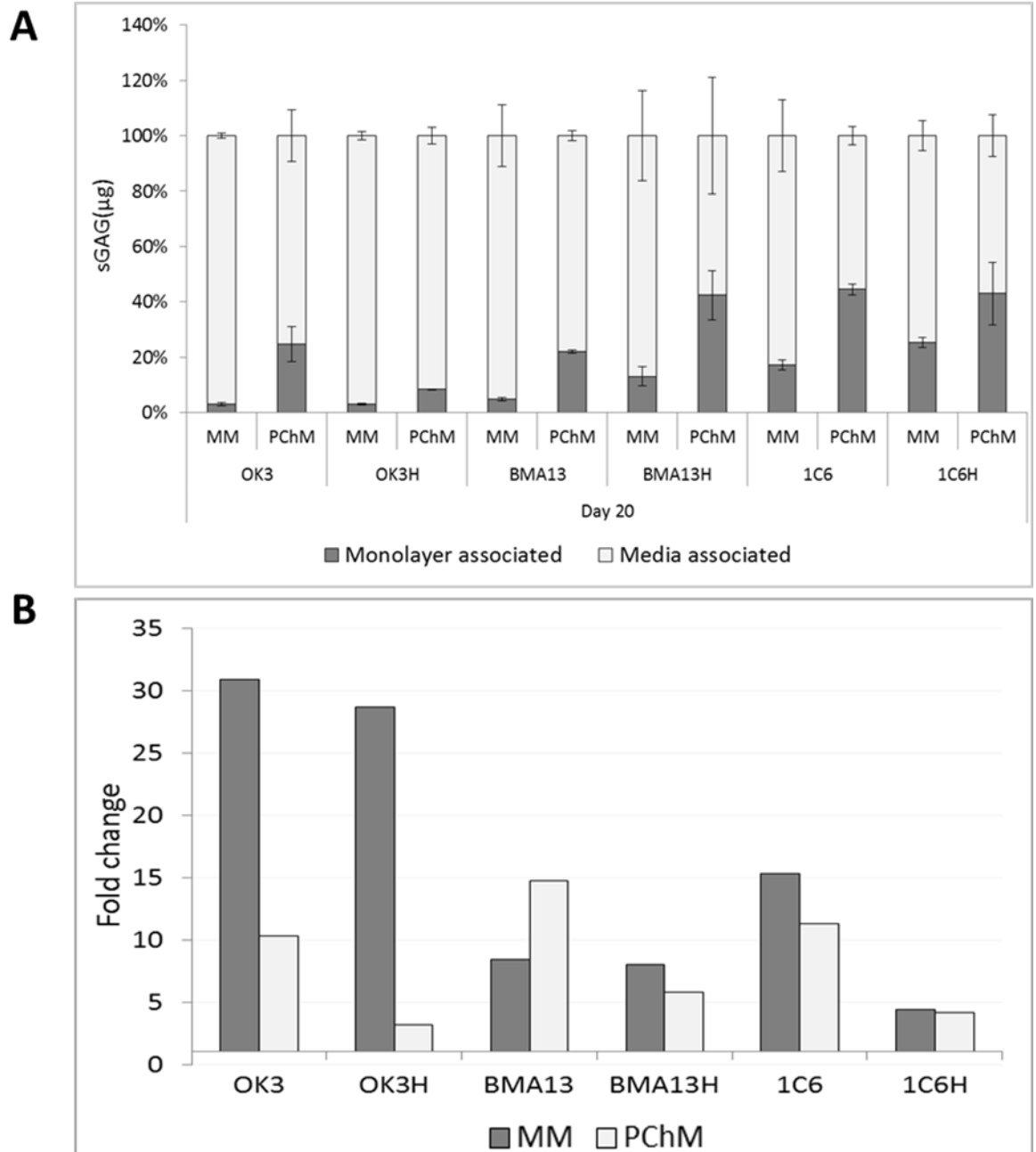


**Figure 5-6.Total sGAG.** (A) Percentage of total sGAG contributed by the monolayer and media associated fractions. (B) Total mean fold change at day 20 relative to day 0. PD level was as follows: OK3 PD6, OK3H PD50, BMA13 PD6, BMA13H PD16, 1C6 PD42, 1C6H PD84.

#### 5.4.4 DNA quantification

DNA in all cell monolayers was quantified from digests using the PicoGreen fluorescent DNA assay (Figure 5-7 and Figure 5-8). In OK3 and OK3H cell cultures there was significantly more DNA in cultures in MM than in PChM by day 5 with a mean difference of 0.529  $\mu\text{g}$  ( $p \leq 0.0001$ ) in OK3 cells and 0.354  $\mu\text{g}$  ( $p \leq 0.0001$ ) in OK3H. In OK3 this represents a 6.1 fold increase from day 0 in MM and 4.2 fold increase in PChM and in OK3H this is reduced to 2.6 fold and 1.5 fold increases in MM and PChM respectively. In OK3 by day 20 the difference between MM and PChM had narrowed to 0.353  $\mu\text{g}$  ( $p \leq 0.01$ ) due to a steady increase in DNA resulting in a day 20 total fold increase of 4.9 fold in PChM compared to a slight increase followed by a decrease in MM giving a day 20 total fold increase of 6.5 fold. In contrast to this, OK3H had a total fold increase of 3.7 in MM; however, there was no further increase beyond day 5 in PChM giving a total fold change of only 1.4.

BMA13 responded very differently to OK3 cells with the inverse relationship of much larger increases in DNA in PChM compared to MM, where DNA content remained relatively static after an increase to day 5. This difference was significant by day 10 with 1.01  $\mu\text{g}$  ( $p \leq 0.0001$ ) and increased at 20 to 1.67  $\mu\text{g}$  ( $p \leq 0.0001$ ). Total fold changes were 4.4 fold in PChM and 1.5 fold in MM. BMA13H behaved similarly to BMA13 in PChM but had a slightly higher increase in MM resulting in a final difference of 0.800  $\mu\text{g}$  ( $p \leq 0.05$ ).

Overall changes in DNA in 1C6 were more comparable to those in OK3 than BMA13, being more likely to have higher DNA in MM than in PChM, significantly so at day 5 (0.483  $\mu\text{g}$  difference,  $p \leq 0.001$ ) and 10 (0.432  $\mu\text{g}$ ,  $p \leq 0.001$ ). However, by day 20 due to a gradual decrease in DNA in MM from day 5, and a gradual increase in DNA in PChM from day 5 there was no longer a significant difference between culture in MM or PChM. 1C6H initially appeared to be following the same trend as 1C6 with a larger amount of DNA in MM than PChM by day 5; however, this was not statistically significant and at day 10 and day 20 DNA in both MM and PChM had decreased.

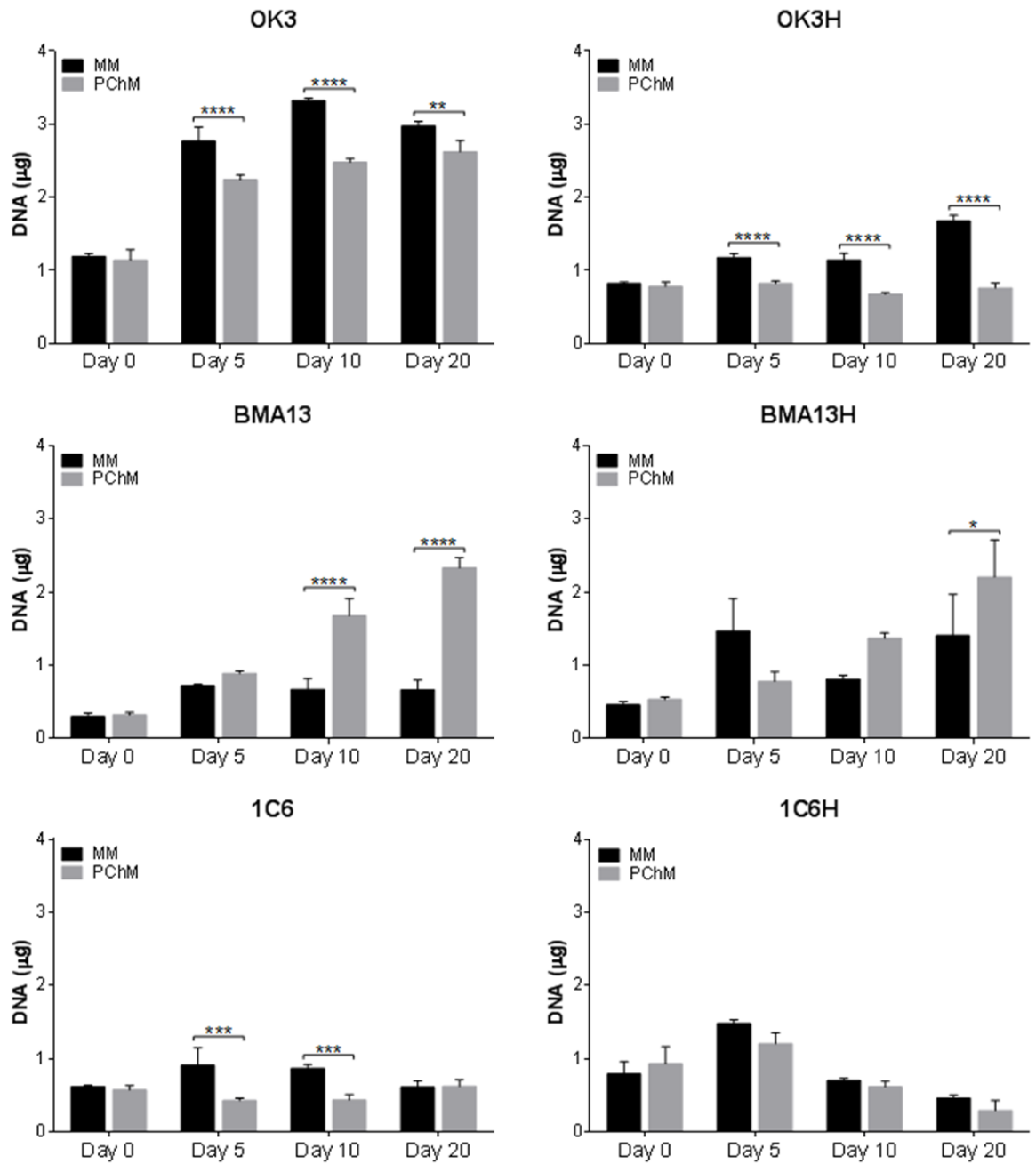


**Figure 5-7. Monolayer DNA content.** DNA associated with cell monolayers was quantified using the PicoGreen assay at day 0, 5, 10 and 20 for all cells after culture in MM or PChM. Data are expressed as mean  $\pm$  standard deviation, N=3, \* $p \leq 0.05$ , \*\* $p \leq 0.01$ , \*\*\* $p \leq 0.001$ , \*\*\*\* $p \leq 0.0001$ . PD level was as follows: OK3 PD6, OK3H PD50, BMA13 PD6, BMA13H PD16, 1C6 PD42, 1C6H PD84.

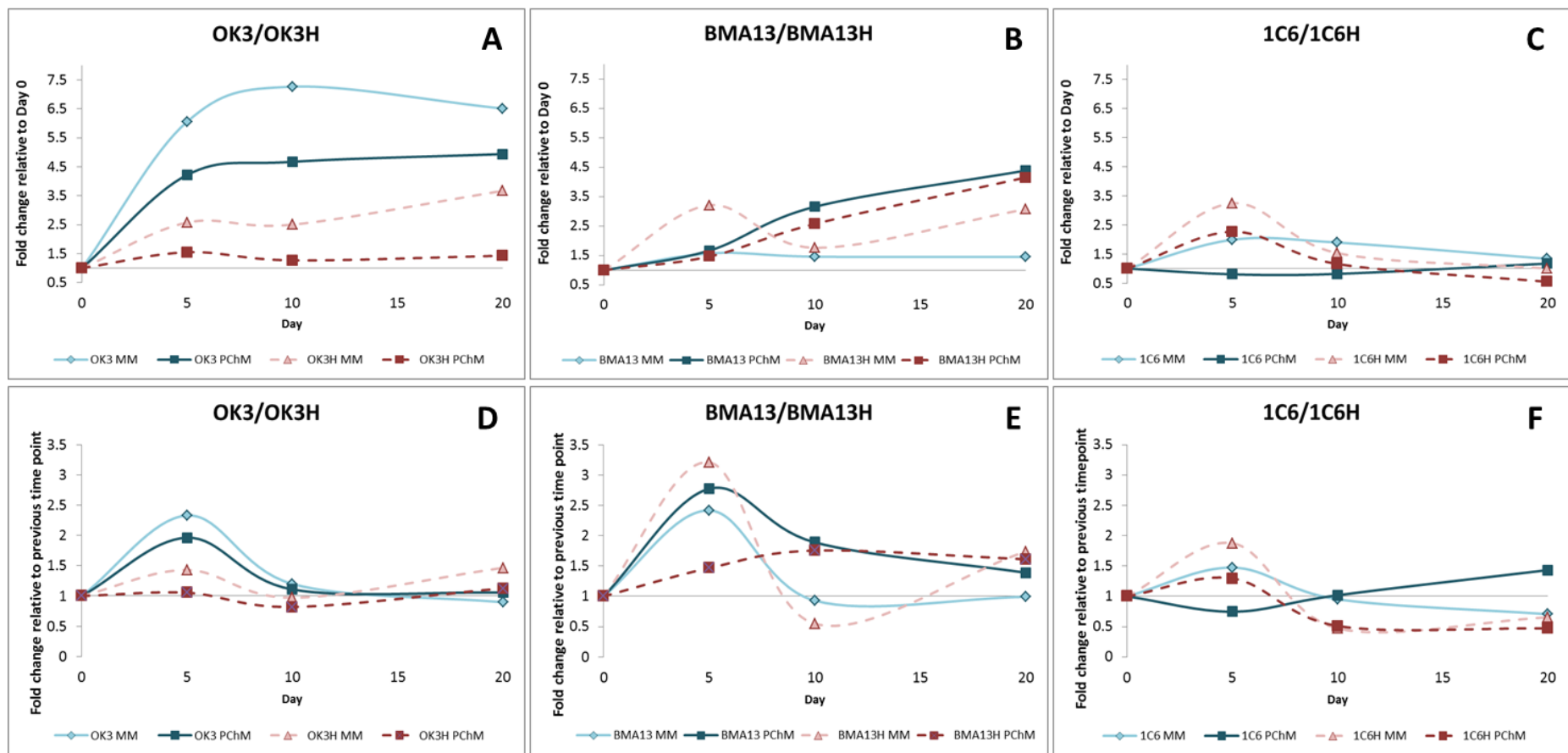


**Figure 5-8. Fold change in DNA content.** For comparison purposes data were expressed as mean fold change relative to the day 0 DNA content of the monolayer (A-C) and relative to the previous time point (D-E). PD level was as follows: OK3 PD6, OK3H PD50, BMA13 PD6, BMA13H PD16, 1C6 PD42, 1C6H PD84.

#### 5.4.5 Monolayer sGAG normalised to DNA

As sGAG is associated with all cells even in the absence of a pro-chondrogenic stimulus normalisation of sGAG to DNA ( $\mu\text{g}/\mu\text{g}$ ) enables a comparison of changes in sGAG due to increased or decreased cell numbers, as a result of cell proliferation or death, to be somewhat separated from increases in sGAG synthesis induced by pro-chondrogenic influences (Figure 5-9).

Normalised sGAG in OK3 showed a 2.8 fold increase ( $p \leq 0.0001$ ) in cultures in PChM ( $3.36 \pm 0.707 \mu\text{g}/\mu\text{g}$ ) compared to MM ( $1.20 \pm 0.304 \mu\text{g}/\mu\text{g}$ ) at day 20, similar to the 2.5 fold difference ( $p \leq 0.0001$ ) seen in absolute sGAG levels. In contrast to this the difference in sGAG in BMA13 cultures in PChM compared to MM in absolute terms equated to a 7.4 fold increase ( $p \leq 0.0001$ ) which decreased to 2.1 fold ( $p \leq 0.0001$ ) ( $2.41 \pm 0.142 \mu\text{g}/\mu\text{g}$  in PChM,  $1.17 \pm 0.222 \mu\text{g}/\mu\text{g}$  in MM) when normalised to DNA as a result of the large increase in DNA content. As a result of minimal changes in DNA in 1C6 the difference at day 20 between MM and PChM cultures equated to a 1.4 fold increase ( $p \leq 0.0001$ ) in both absolute and relative terms ( $8.50 \pm 0.846 \mu\text{g}/\mu\text{g}$  in PChM,  $6.05 \pm 0.253 \mu\text{g}/\mu\text{g}$  in MM).

Normalisation in the transduced cells had the effect of reducing the difference at day 20 in PChM to MM to 0.7 times and 1.8 times in OK3H ( $1.27 \pm 0.107 \mu\text{g}/\mu\text{g}$  in PChM,  $1.80 \pm 0.070 \mu\text{g}/\mu\text{g}$  in MM,  $p \leq 0.0001$ ) and BMA13H ( $0.737 \pm 0.070 \mu\text{g}/\mu\text{g}$  in PChM,  $0.417 \pm 0.176 \mu\text{g}/\mu\text{g}$  in MM) respectively compared to absolute differences of 0.3 times and 3.0 times. The reverse was true in 1C6H where reductions in cell numbers at later time points without a concomitant reduction in sGAG led to an increase in the difference in PChM compared to MM of 3.0 fold ( $12.3 \pm 3.94 \mu\text{g}/\mu\text{g}$  in PChM,  $4.03 \pm 0.457 \mu\text{g}/\mu\text{g}$  in MM,  $p \leq 0.0001$ ) compared to an absolute sGAG difference of 1.7 fold.

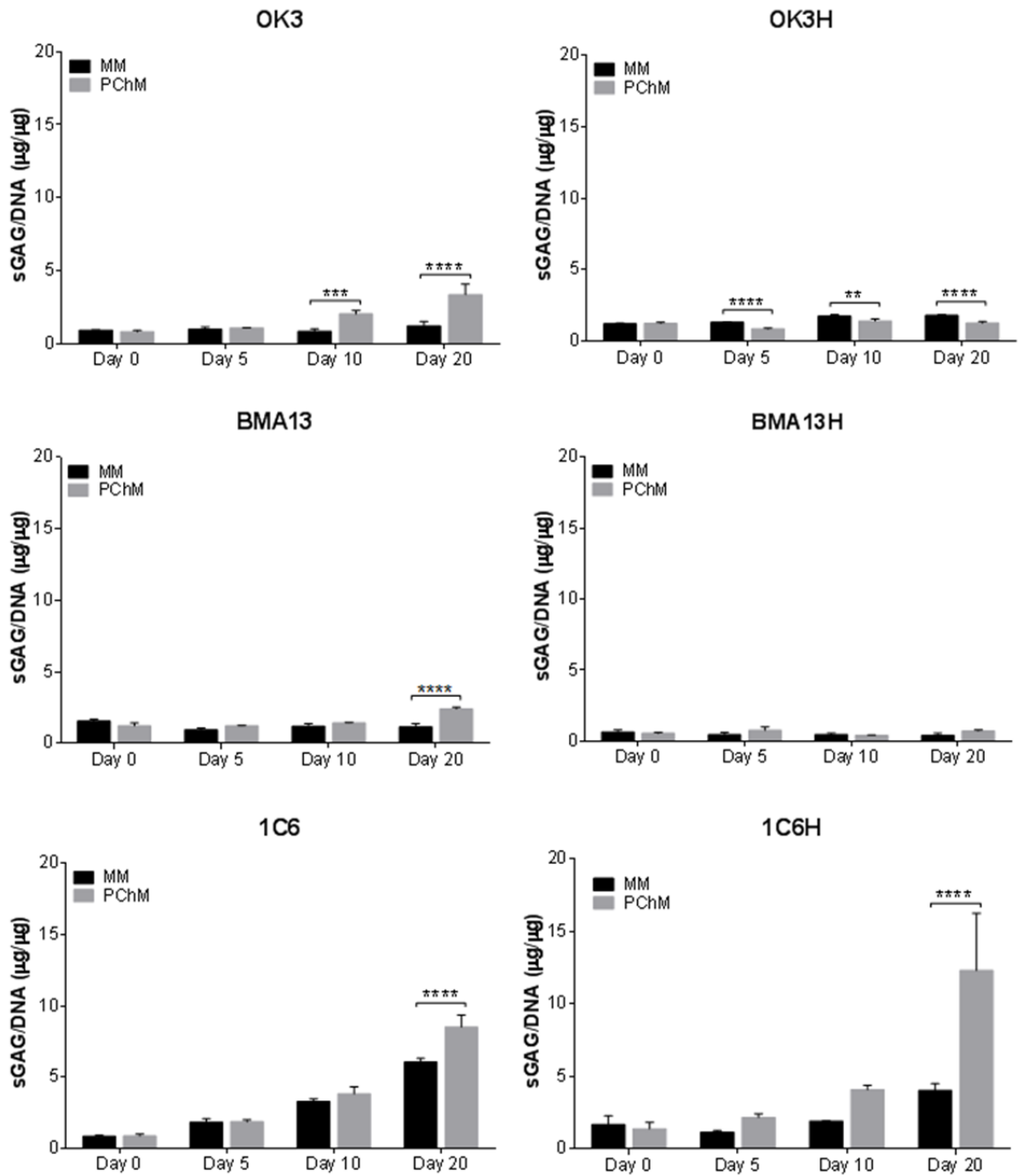


**Figure 5-9. Monolayer associated sGAG normalised to DNA content.** sGAG associated with cell monolayers was normalised to DNA of the same monolayers to give a µg/µg ratio at day 0, 5, 10 and 20 for all cell types after culture in MM or PChM. Data are expressed as mean ± standard deviation, N=3, \*\*p<0.01, \*\*\*p<0.001, \*\*\*\*p<0.0001. PD level was as follows: OK3 PD6, OK3H PD50, BMA13 PD6, BMA13H PD16, 1C6 PD42, 1C6H PD84.

#### 5.4.6 Media sGAG normalised to monolayer DNA

The sGAG content of the spent culture media was normalised to the DNA level of the corresponding monolayer (Figure 5-10). Following normalisation, as with absolute media sGAG levels OK3 and OK3H MM cultures still had the highest sGAG at  $38.085 \pm 0.853 \mu\text{g}/\mu\text{g}$  and  $57.507 \pm 1.879 \mu\text{g}/\mu\text{g}$  respectively followed by 1C6 MM cultures at  $29.513 \pm 6.624 \mu\text{g}/\mu\text{g}$  and BMA13 MM cultures at  $22.941 \pm 3.172 \mu\text{g}/\mu\text{g}$ .

Following normalisation five of the six cell types had significantly reduced sGAG/DNA in the media of PChM cultures compared to the MM cultures. The difference was largest in OK3H where PChM had 0.24 times the sGAG of MM ( $p \leq 0.0001$ ) and similarly OK3 with 0.27 times the sGAG in PChM compared to MM ( $p \leq 0.0001$ ). BMA13, BMA13H and 1C6 had similar differences at 0.37 times ( $p \leq 0.0001$ ), 0.34 times ( $p \leq 0.0001$ ) and 0.36 times ( $p \leq 0.0001$ ) the sGAG in PChM compared to MM respectively. Notably normalisation of the media sGAG brought BMA13 in-line with the results in the other primary cell types of higher sGAG in MM compared to PChM. In contrast, 1C6H was no longer significantly different at any time point although results expressed as normalised levels were more similar to 1C6 than when absolute sGAG levels were considered.

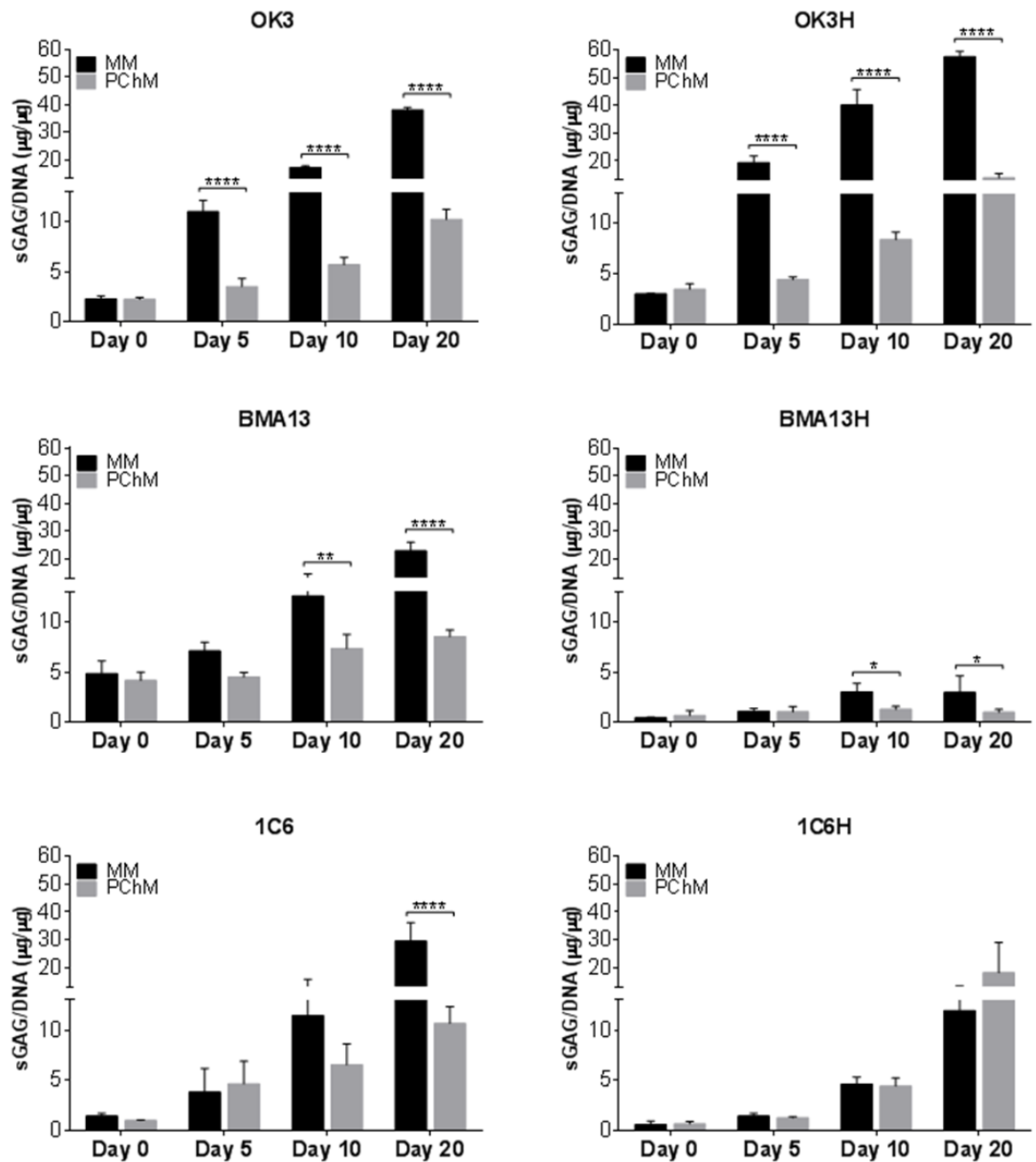


**Figure 5-10. Media sGAG normalised to DNA.** sGAG associated with spent cell culture media was normalised to DNA of the monolayers to give a µg/µg ratio at day 0, 5, 10 and 20 for all cell types after culture in MM or PChM. Data are expressed as mean ± standard deviation, N=3, \*p<0.05, \*\*p<0.01, \*\*\*\*p<0.0001. PD level was as follows: OK3 PD6, OK3H PD50, BMA13 PD6, BMA13H PD16, 1C6 PD42, 1C6H PD84.

### 5.4.7 Total normalised sGAG

Total sGAG from both monolayer and medium fractions was combined and normalised to total monolayer DNA and is shown at day 20 in Figure 5-11 and as a fold change in Figure 5-12. As with absolute total levels, normalised total sGAG was significantly higher for all cell types except 1C6H in MM rather than PChM due to the large media sGAG contribution. In MM normalised sGAG was highest in OK3H at 59.31  $\mu\text{g}/\mu\text{g}$  followed by OK3 (39.29  $\mu\text{g}/\mu\text{g}$ ), 1C6 (35.56  $\mu\text{g}/\mu\text{g}$ ), BMA13H (33.91  $\mu\text{g}/\mu\text{g}$ ), BMA13 (24.11  $\mu\text{g}/\mu\text{g}$ ) and 1C6H (15.97  $\mu\text{g}/\mu\text{g}$ ). These values corresponded to 14.09, 12.32, 3.18, 3.01, 3.76 and 7.10 fold changes from day 0 values respectively.

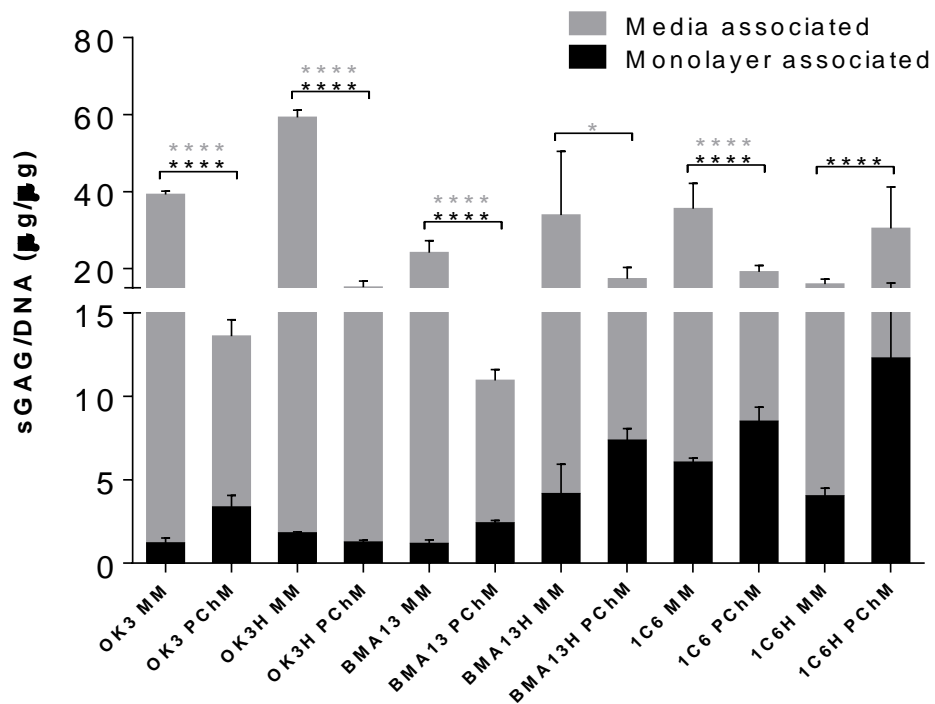


**Figure 5-11. Total normalised sGAG at day 20.** Day 20 summary of total normalised sGAG with both monolayer and media contribution at day 20. Data are expressed as mean  $\pm$  standard deviation, N=3, \* $p < 0.05$ , \*\*\*\* $p < 0.0001$ . Black asterisks indicate significance between monolayer associated sGAG; grey asterisks indicate significance between media associated sGAG. PD level was as follows: OK3 PD6, OK3H PD50, BMA13 PD6, BMA13H PD16, 1C6 PD42, 1C6H PD84.

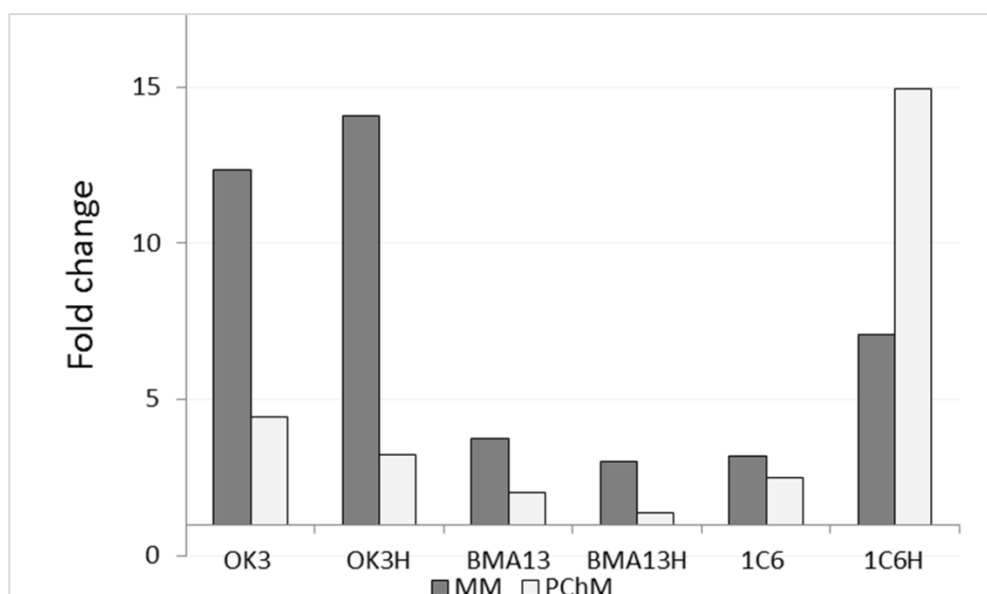


**Figure 5-12. Total normalised mean fold change.** Total sGAG normalised to DNA mean fold change at day 20 relative to day 0. PD level was as follows: OK3 PD6, OK3H PD50, BMA13 PD6, BMA13H PD16, 1C6 PD42, 1C6H PD84.

PChM culture values were highest in 1C6H (30.40  $\mu\text{g}/\mu\text{g}$ ) followed by 1C6 (19.17  $\mu\text{g}/\mu\text{g}$ ), BMA13H (17.36  $\mu\text{g}/\mu\text{g}$ ), OK3H (15.19  $\mu\text{g}/\mu\text{g}$ ), OK3 (13.60  $\mu\text{g}/\mu\text{g}$ ) and BMA13 (10.95  $\mu\text{g}/\mu\text{g}$ ) with corresponding fold changes of 14.92, 2.48, 1.39, 3.23, 4.46 and 2.02 fold respectively. Overall these results suggest that 1C6H may be the cell type most responsive to PChM as this had the greatest fold increase from day 0 however the results should only be interpreted with knowledge of absolute sGAG and DNA changes as much of the increase in 1C6H results from a reduction in DNA not an increase in sGAG synthesis.

#### 5.4.8 Empty vector cell cultures

The available empty vector cells BMA13EV and 1C6EV were also treated as per the *hTERT* transduced and parental cells (Figure 5-13 and Figure 5-14).

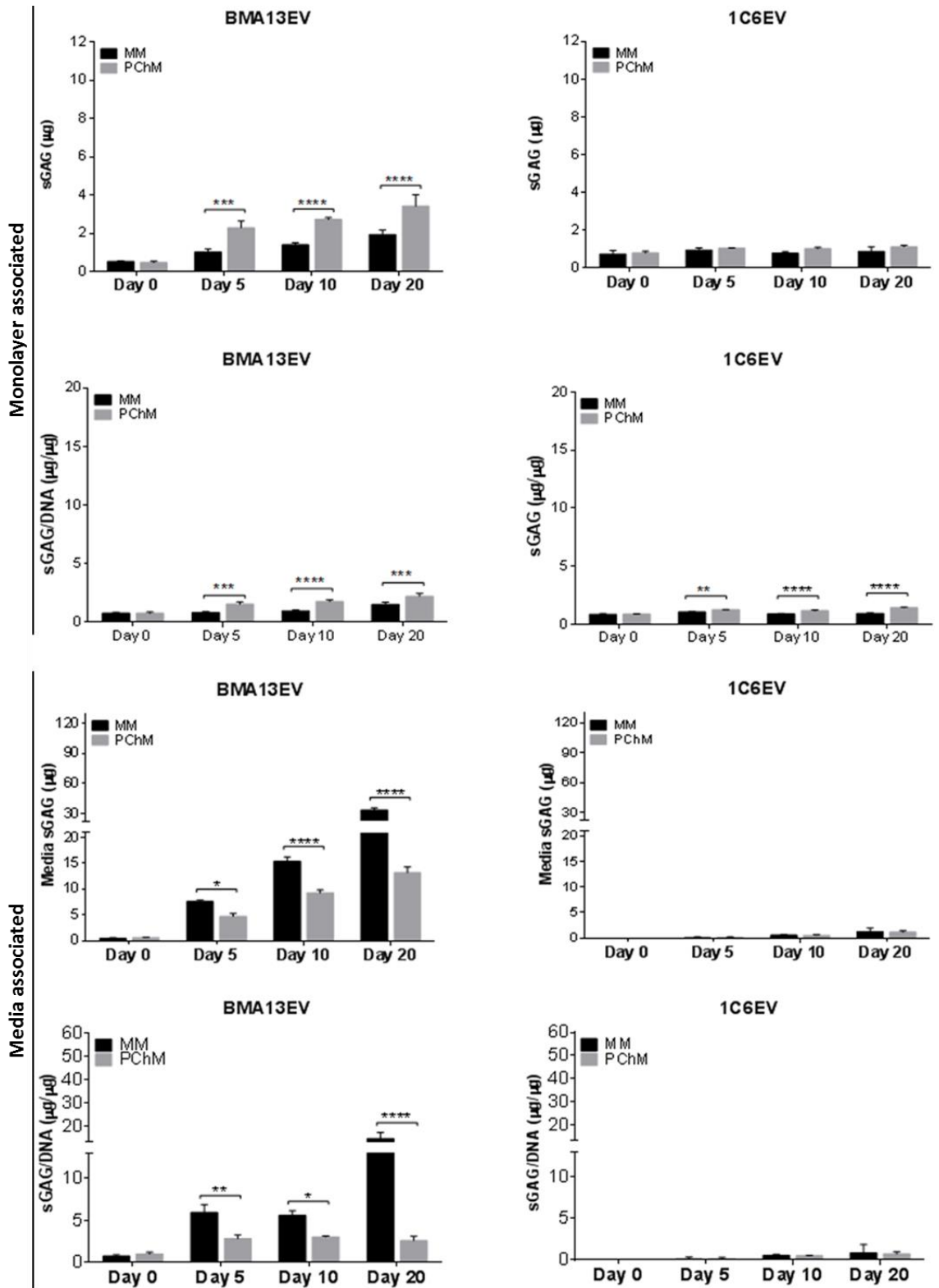


**Figure 5-13. Monolayer and media associated absolute and normalised sGAG from empty vector cells.** sGAG associated with cell monolayers and cumulative media sGAG was quantified using the DMMB assay at day 0, 5, 10 and 20 for all cells after culture in MM or PChM. Normalised data are expressed as a ratio of sGAG/DNA. Data are expressed as mean  $\pm$  standard deviation, N=3, \* $p \leq 0.05$ , \*\* $p \leq 0.01$ , \*\*\* $p \leq 0.001$ , \*\*\*\* $p \leq 0.0001$ . PD level was as follows: OK3 PD6, OK3H PD50, BMA13 PD6, BMA13H PD16, 1C6 PD42, 1C6H PD84.

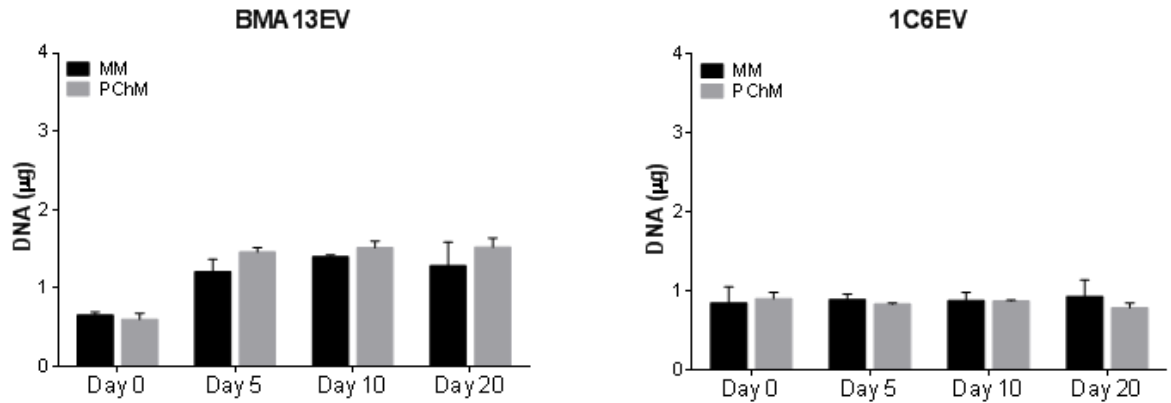


**Figure 5-14. Empty vector monolayer DNA content.** DNA associated with empty vector cell monolayers was quantified using the PicoGreen assay at day 0, 5, 10 and 20 for all cells after culture in MM or PChM. Data are expressed as mean  $\pm$  standard deviation, N=3. PD level was as follows: OK3 PD6, OK3H PD50, BMA13 PD6, BMA13H PD16, 1C6 PD42, 1C6H PD84.

The BMA13EV response was comparable to the primary cell response with regards to the trends in the results; a significantly higher monolayer associated sGAG was seen from day 5 ( $p \leq 0.001$ ) onwards resulting on 1.8 fold higher ( $p \leq 0.0001$ ) sGAG content in PChM than MM by day 20. This was concurrent with a significantly decreased media associated sGAG in PChM, resulting in an overall reduction in total sGAG in PChM compared to MM. In contrast 1C6EV had a much lower response to PChM, although this still followed the same trends, with only a 1.4 fold increase in monolayer associated sGAG with the difference between the sGAG monolayer content in the two media types not reaching significance. There was also no evidence of cell proliferation in 1C6EV with DNA content of the monolayer remaining relatively unchanged from day 0.

## 5.5 Discussion

During *in vitro* culture cells synthesise and secrete ECM molecules including sGAG containing proteoglycans to fill intercellular spaces<sup>369</sup>. In this work primary and transduced chondrocytes (OK3/OK3H), MSCs (BMA13/BMA13H) and hESC derived cells (1C6/1C6H) were seeded in a simple monolayer, 2D environment to quantitate their response to soluble pro-chondrogenic cues in the form of media supplementation with TGF- $\beta$ 3. This would be expected to increase proteoglycan and sGAG synthesis in cells undergoing chondrogenesis. Considering either total (monolayer plus media) sGAG or monolayer associated sGAG, chondrocytes produced higher levels than the other primary cell types, although they also showed a significant response to PChM. In comparison the transduced cells had a greatly reduced response and in the case of OK3H, as with the qualitative assessment, no increase in sGAG was seen in response to pro-chondrogenic signals.

All cell types, in pro-chondrogenic conditions induced by TGF- $\beta$ 3<sup>370</sup> or in standard MM, produced sGAG in measurable quantities associated with both the pellet and in relatively large amounts in the spent culture media. Interestingly total sGAG was generally determined to be higher in cells exposed to MM than in PChM, where much of the sGAG was found in the media rather than in association with the monolayer. Reports of sGAG quantities in media during *in vitro* culture vary ranging from negligible amounts<sup>371</sup> to a large fraction (35-90% depending on the cell culture conditions) of the total sGAG produced<sup>372</sup> this is in line with the range of values found across the cell types here which varied considerably. Media sGAG has been used as a proxy for total sGAG production<sup>373</sup>; however, these results do not support this technique, as we found large cell type dependent differences in the proportion of retained versus secreted sGAG, one is not necessarily indicative of the other. Evidence from other investigations into media sGAG indicates that the losses to the media from the monolayer are probably as a result of the inability of the ECM to retain the proteoglycan and associated sGAG which then diffuse into the media<sup>372</sup>; however, proteoglycan degradation due to catabolic activity cannot be ruled out as a potential cause.

Cells exhibited variable proliferation responses during the experiment in response to the MM and PChM. Chondrocytes in MM had a burst of proliferation in the first five days of culture which then plateaued. In PChM there was also the greatest amount of proliferation in the first five days that was followed by much smaller incremental increases at days five and ten. This suggests that chondrocytes proliferated until confluent and then switched to sGAG synthesis beyond day five. BMA13 exhibited a similar response in MM although maximum DNA levels were much lower than those in OK3 possibly due to the formation of high density chondrogenic condensations. In PChM BMA13 had a continual increase in DNA meaning that a considerable fraction of the sGAG was attributable to cell proliferation. Nevertheless some cells had increased sGAG synthesis as normalised sGAG also increased and these results may be representative of a mixed cell population.

Normalisation of the sGAG to DNA can effectively show whether the sGAG synthesis increases on a per cell basis and is a reliable measure when both are increasing or DNA is stable. However, as exemplified with 1C6H, it should never be considered in isolation without the absolute data. In 1C6 DNA decreased probably due to over-confluence and cell losses, whilst sGAG remained high possibly due to its incorporation in a stable ECM. As a result of this the number of cells actually contributing to the sGAG is underestimated whilst sGAG per cell becomes overestimated. In a situation where both the numerator and the denominator are both affected, potentially in either direction, it is impossible to interpret the resulting ratio.

Transduction with *hTERT* appeared to have had a particularly detrimental effect on monolayer associated sGAG with OK3H in both absolute and normalised terms. This may be reflective of the particular difficulties that seem to be associated with chondrocyte transduction<sup>347,348</sup>. Although the chondrocytes used were from a commercial supplier they were nevertheless from an elderly donor and may have accumulated age-related changes. Furthermore the transduction procedure is lengthy and cells continue to proliferate, and therefore de-differentiate, during this process and may have passed a critical point for successful re-differentiation. The cells are also polyclonal,

polyclonal expansion favours selection of rapidly growing cells over those with more favourable differentiation properties<sup>374</sup>; clonal expansion and colony characterisation and selection may enable the identification of a subpopulation of cells with a greater proliferative capacity; however, the requirement to expand cell numbers from a single cell level would make this impractical. To enable rapid assessment of the multiple cell types described herein experiments were performed in monolayer culture; however, it is accepted that a 3D environment can provide a more pro-chondrogenic influence<sup>375,376</sup>.

## 5.6 Conclusion

To regenerate articular cartilage, transplanted cells must produce large quantities of sGAGs that are retained within the area of damaged tissue. All three primary cell types assessed herein produced and retained significant amounts of sGAG in association with the monolayer in response to a pro-chondrogenic influence. Two (1C6H and BMA13H) of three *hTERT* transduced cell types exhibited similar responses to non-transduced cell types particularly when sGAG was normalised to DNA level. However, in contrast, the *hTERT* transduced chondrocyte line OK3H performed poorly in response to PChM and had no increase in sGAG retained in the monolayer. These preliminary findings indicate that whilst *hTERT* transduction can be useful in prolonging cell proliferation, complex changes in cell phenotype and a loss of differentiated cell function can be induced in a variable and cell specific manner.

To enable rapid assessment of the multiple cell types described herein experiments were performed in monolayer culture; however, it is accepted that a 3D environment can provide a more pro-chondrogenic influence<sup>375,376</sup> and this is explored in Chapter 6.



Keele University

---

## **Chapter 6**

---

### ***Chondrogenesis of cells in pellet culture***

## 6.1 Introduction

It is accepted that when chondrocytes are cultured *in vitro* in monolayer they undergo a process of de-differentiation<sup>87</sup> becoming increasingly less responsive to pro-chondrogenic stimuli with a corresponding reduction in cartilage ECM molecule production. The reintroduction of a 3D culture environment concurrent with pro-chondrogenic growth factor supplementation<sup>366</sup> is reported to be beneficial both to promoting the redifferentiation of expanded, dedifferentiated chondrocytes<sup>376</sup> and to initiating chondrogenesis in MSCs, possibly as a result of mimicking the mesenchymal condensation stage of chondrogenesis during embryonic development<sup>377</sup>. The culture of cells in a 3D environment is more representative of their *in vivo* physiological situation allowing for increased interaction of cells both with each other and with a more complex extracellular environment, with the possibility of improved growth factor retention via sequestration by ECM molecules and the creation of a number of morphogenetic gradients<sup>378</sup>.

3D environments can be created *in vitro* either by the incorporation of cells into biomaterials, most commonly gels, including agarose<sup>379</sup>, alginate<sup>376</sup>, and hyaluronic acid<sup>380,381</sup>, or simply by creating very high density cultures by centrifugation of cells into pellets<sup>382</sup>. Interestingly, despite speculation regarding the importance of recapitulation of mesenchymal condensations and the resulting cell-cell contacts, chondrogenesis in both hydrogel, with no direct cell-cell contact, and pellet cultures is reported to be equivalent<sup>383</sup>.

Nevertheless although mechanisms have yet to be fully elucidated the results are relatively clear for example when cultured in 3D environments, either in an alginate hydrogel or pellets chondrocyte cultures had upregulated gene expression of the key chondrogenic markers *SOX9*, *COL2A1* and *ACAN* along with a reduction in some hypertrophic markers when compared to monolayer cultures<sup>376</sup>. Similarly MSC chondrogenesis has previously been demonstrated to be partial in monolayer, whilst cells in monolayer do respond to pro-chondrogenic influences the response is significantly improved in 3D as evidenced by increased chondrogenic gene

expression<sup>384</sup>. Human adipose derived MSCs in monolayer have upregulated *COL2A1* and *ACAN* in response to PChM, particularly in hypoxia, but the extent of upregulation reported was small at 2 fold and 1.3 fold increased respectively. Relative expression of the transcripts was significantly increased by culturing the cells in 3D hydrogels<sup>368,385</sup>.

The work described in this chapter further tests the hypothesis that *hTERT* transduced cells retain a capacity for chondrogenesis similar to that of the relevant primary cells and that chondrogenesis is enhanced in a 3D environment when compared to a 2D environment.

## **6.2 Aim**

The overall aim of this chapter was to determine whether the additional cues provided by a 3D environment in the form of cell pellets, in addition to the influence of TGF- $\beta$ 3 as described in Chapter 5, impacted on chondrogenesis in the primary and transduced cells under investigation. The assessment of chondrogenesis was via a number of markers of chondrogenesis including pellet size, sGAG production, gene expression analysis and cartilage ECM production.

## **6.3 Methods**

The sequence of experiments for this chapter is summarised in Scheme 4.

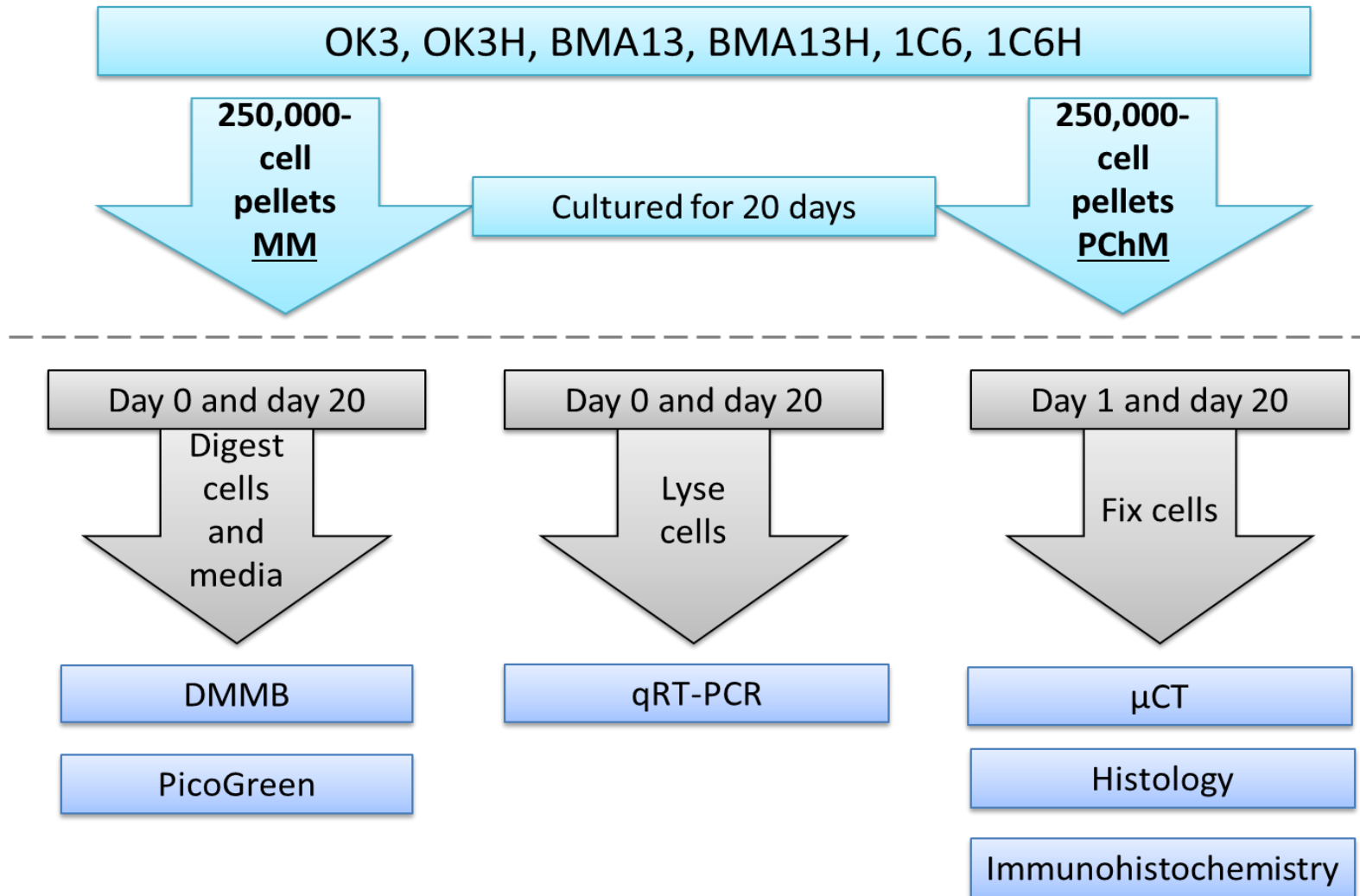
Once a sufficient number of cells had been attained by expanding the cells in their respective MM, in 2% O<sub>2</sub>, pellets of all parental and transduced cells consisting of 2.5x10<sup>5</sup> cells/pellet were created by centrifugation from cell suspensions in both MM or PChM and cultured in 2% O<sub>2</sub>, as described in section 2.16. At day 1 and day 20 of culture pellets were harvested and fixed for imaging and sizing as per section 2.17 and for  $\mu$ CT as described in section 2.18. Pellets were also harvested at day 1 and day 20 for paraffin embedding and sectioning followed by histological staining as per section 2.24 with haematoxylin and eosin, picrosirius red for collagen and toluidine blue for sGAGs. Further sections were used for immunohistochemistry performed as described in section 2.25 for collagen type I, collagen type II, collagen type VI, collagen type X and aggrecan.

At day 0 (after approximately 30 minutes in either MM or PChM whilst cells were re-suspended in the media, centrifuged and the sample media then collected) and day 20 cell pellets and accumulated, collected spent culture media were proteinase K digested overnight as described in section 2.13. The resulting digests were assayed for sGAG using the DMMB assay as per section 2.14, the same pellet digests were also assessed for DNA content using the PicoGreen assay as per section 2.15. Also at day 0 and day 20 pellets were lysed as described in section 2.19.2, RNA extracted as per section 2.20 and qRT-PCR performed as described in section 2.23 for the genes *COL1A2*, *COL2A1*, *COL3A1*, *COL6A3*, *COL10A1*, *ACAN*, *COMP* and *SOX9*. As pellet lysis proved to be difficult and recovered RNA levels low, in particular in MM cultures, triplicate pellets were combined and lysed together in triplicate to allow the analysis to be performed on the same samples for all genes (i.e. a total of 9 pellets were combined in 3 batches to produce 3 samples for each cell type for qRT-PCR).

### **6.3.1 Statistical significance**

Pellet volume (calculated from images and by  $\mu$ CT), pellet density, absolute monolayer sGAG, normalised monolayer sGAG and pellet DNA were compared using two-way repeated measures ANOVA with Bonferroni corrected pairwise comparisons of MM to PChM at each time point and of day 0 to day 20 for MM and PChM to determine statistical significance,  $p \leq 0.05$  was considered significant. Analysis was performed using Graphpad Prism V6.01. Relative gene expression statistical significance was determined using a randomisation algorithm as part of the REST 2009 software,  $p \leq 0.05$  was considered significant.

Unless otherwise stated all values quoted in the results are mean  $\pm$  standard deviation.



Scheme 4. Summary of the methodology adopted in Chapter 6.

## 6.4 Results

### 6.4.1 Pellet formation and size determination

Cell pellets of approximately 250,000 cells were formed by centrifugation at 300 g; following overnight culture in either MM or PChM the mechanically aggregated cells were visibly integrated into masses which could be detached freely from the microcentrifuge tube walls (Figure 6-1).

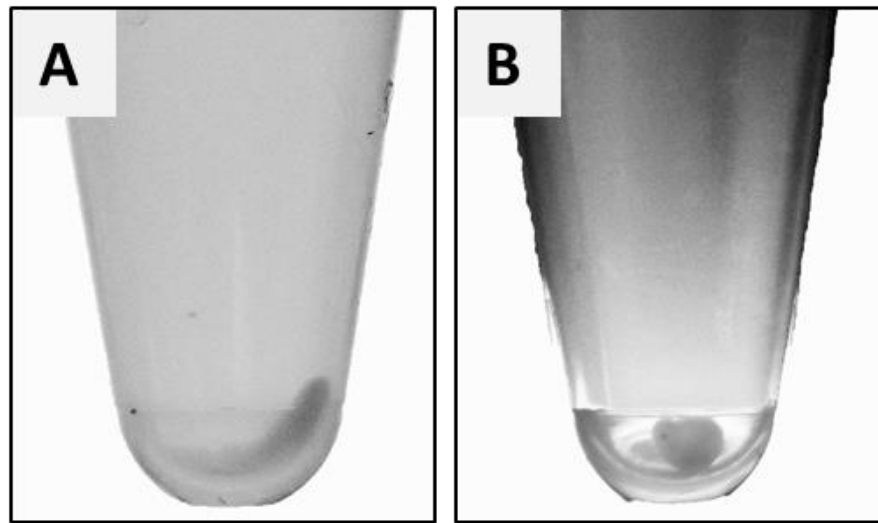


**Figure 6-1. Cell pellet formation.** Centrifugation pelleted cells (A) that formed free floating masses within 24 hours (B).

Pellets were paraformaldehyde fixed and the size (volume) determined and compared at day 1 and day 20 of culture in MM or PChM. Fixed pellets were firstly imaged using light microscopy (Figure 6-2). Images at day 1 showed that pellets appeared to form via a process of aggregation to form a multi-layered sheet, which then folded or rolled from the edges towards the centre resulting in heterogeneous pellets. In general pellets became more spherical and homogeneous by day 20; however, some heterogeneity in light transmission was still sometimes present indicating heterogeneity in tissue depth or density, being particularly apparent with OK3H pellets (Figure 6-2B).

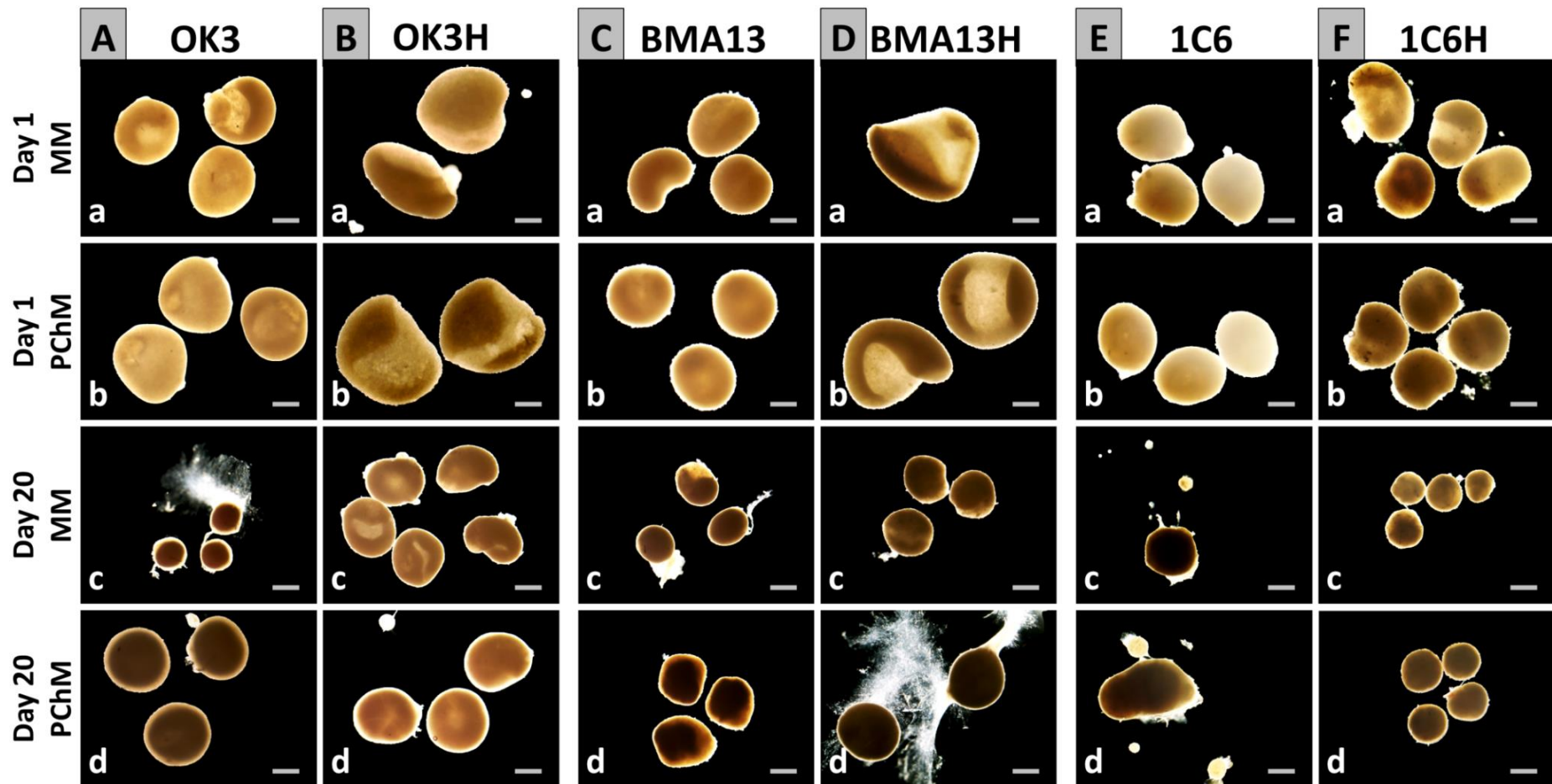


**Figure 6-2. Cell pellet images.** Images were taken post-fixation of whole pellets after 1 day or 20 days of culture in MM or PChM. Scale bar = 500  $\mu$ m. PD level for cells was as follows: OK3 PD6, OK3H PD50, BMA13 PD6, BMA13H PD16, 1C6 PD36, 1C6H PD86.

Pellet size was then determined by the acquisition of pellet diameters on both the long and short axes of the pellets from the images, with these values used to calculate the ellipsoid volumes shown in Figure 6-3. At day 1 pellets were larger in PChM than in MM with this trend becoming statistically significant in OK3 ( $p \leq 0.01$ ) and OK3H ( $p \leq 0.05$ ) pellets. Pellets were always smaller at day 20 than at day 1 with the difference being greater in MM than PChM and by day 20 pellets were always larger in PChM than in MM. The size differences between pellets cultured in MM and PChM at day 20 were greater in all three primary cell types, achieving statistical significance ( $p \leq 0.0001$  for OK3,  $p \leq 0.05$  in BMA13 and  $p \leq 0.01$  in 1C6). Whilst the same trend for larger pellets in PChM compared to MM at D20 was present for transduced cells this did not reach statistically significant levels.

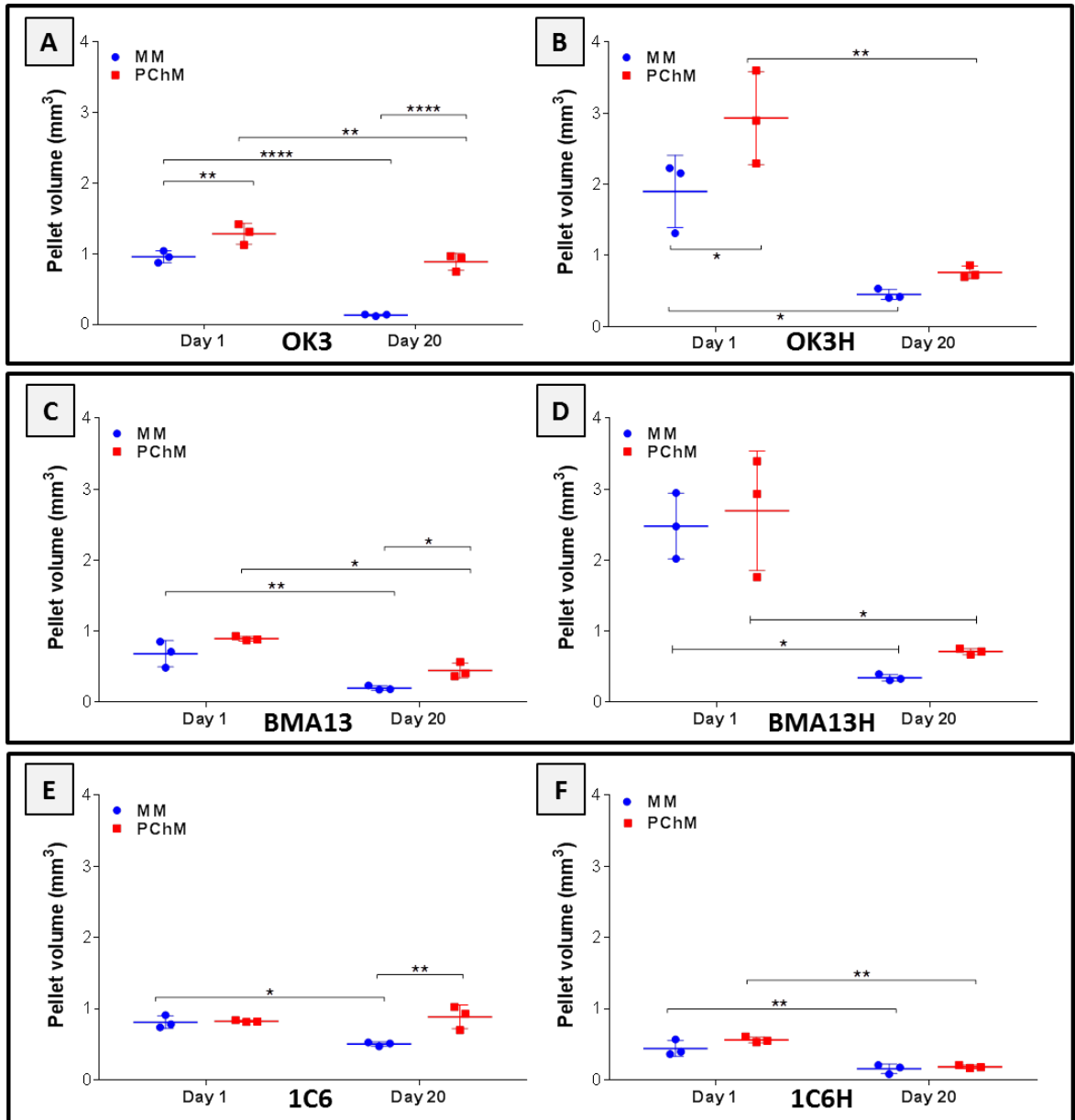


**Figure 6-3. Calculated pellet volume.** Cell pellet volumes for all samples were determined by taking diameter measurements from light micrographs and calculating the corresponding ellipsoid volume. Data are plotted as mean  $\pm$  standard deviation, N=3. \* $p \leq 0.05$ , \*\* $p \leq 0.01$ , \*\*\*\* $p \leq 0.0001$ . PD level for cells was as follows: OK3 PD6, OK3H PD50, BMA13 PD6, BMA13H PD16, 1C6 PD36, 1C6H PD86.

While the determination of day 20 volumes was likely to be reasonably accurate when calculated from measured diameters due to the more spheroidal/ellipsoidal shape of the pellets, day 1 pellets were much more variable in shape, often being relatively flat. This led to an over-estimation of the pellet volume with this being highly dependent on the degree of curvature present. This was particularly the case for OK3H and BMA13H and this is reflected in the much

larger standard deviations in these pellets. As such, a second set of pellets was prepared and subjected to  $\mu$ CT analysis to improve accuracy for size comparisons and to gain more information about pellet morphology and density.

$\mu$ CT images confirmed that pellets form concave disks against the microcentrifuge tube walls that then roll or fold to eventually form a spheroid shape (Figure 6-4). This can also have the effect of forming folds or cavities within pellets. Although these are usually absent by day 20 some of the earlier gross structure was seen to persist, particularly after culture in MM.

To obtain an accurate volume assessment a thresholded volume was obtained; with the threshold set to 50/1000. A lower threshold set to 50 included all material within the pellet in the volume determination whilst still separating the pellet from the background as shown in materials and methods 2.18.2. The upper limit of 1000 is the maximum and ensures that no denser material is excluded from the analysis. The  $\mu$ CT acquired volumes are shown in Figure 6-5.

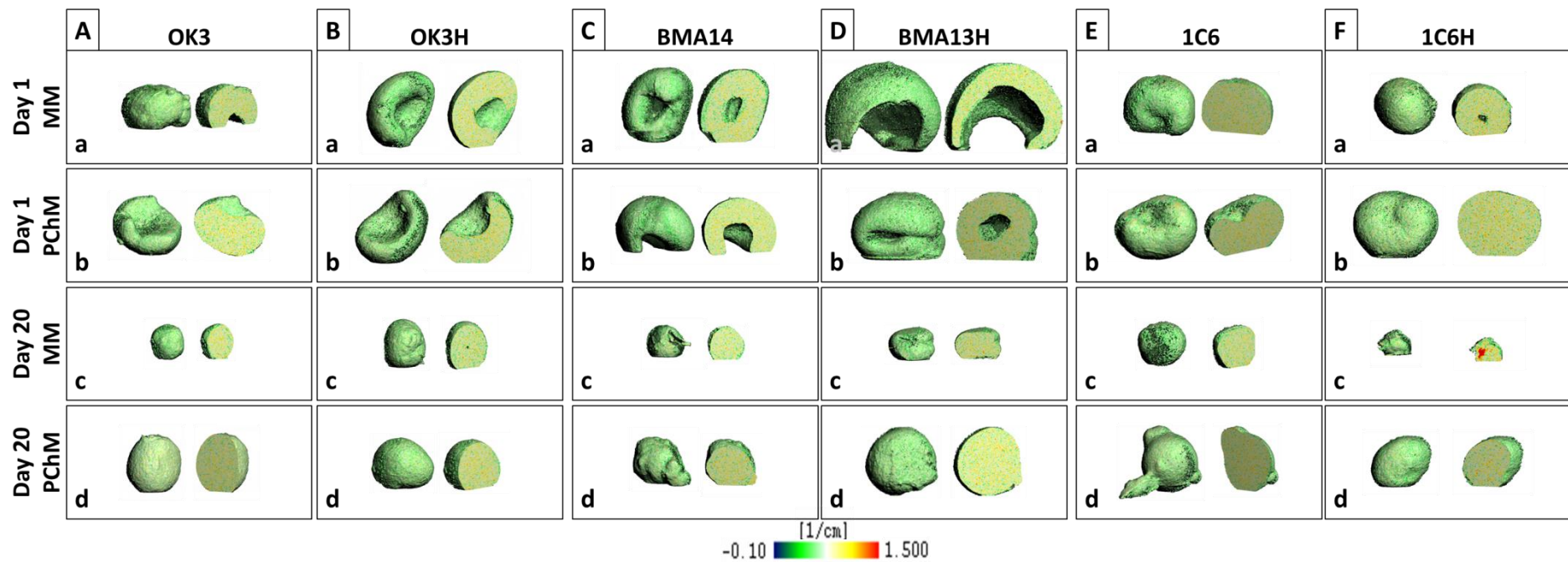


**Figure 6-4.  $\mu$ Ct determined pellet images.**  $\mu$ CT images were taken post-fixation of pellets after 24 hours or 20 days pf culture in MM or PChM.  $\mu$ CT confirmed that pellets are formed by flattened, multi-layered cell sheets folding or rolling to eventually form spheroids. This can result in pellets containing folded structures or cavities that may persist to some extent for the culture duration. PD level for cells was as follows: OK3 PD6, OK3H PD50, BMA13 PD1, BMA13H PD16, 1C6 PD36, 1C6H PD107.

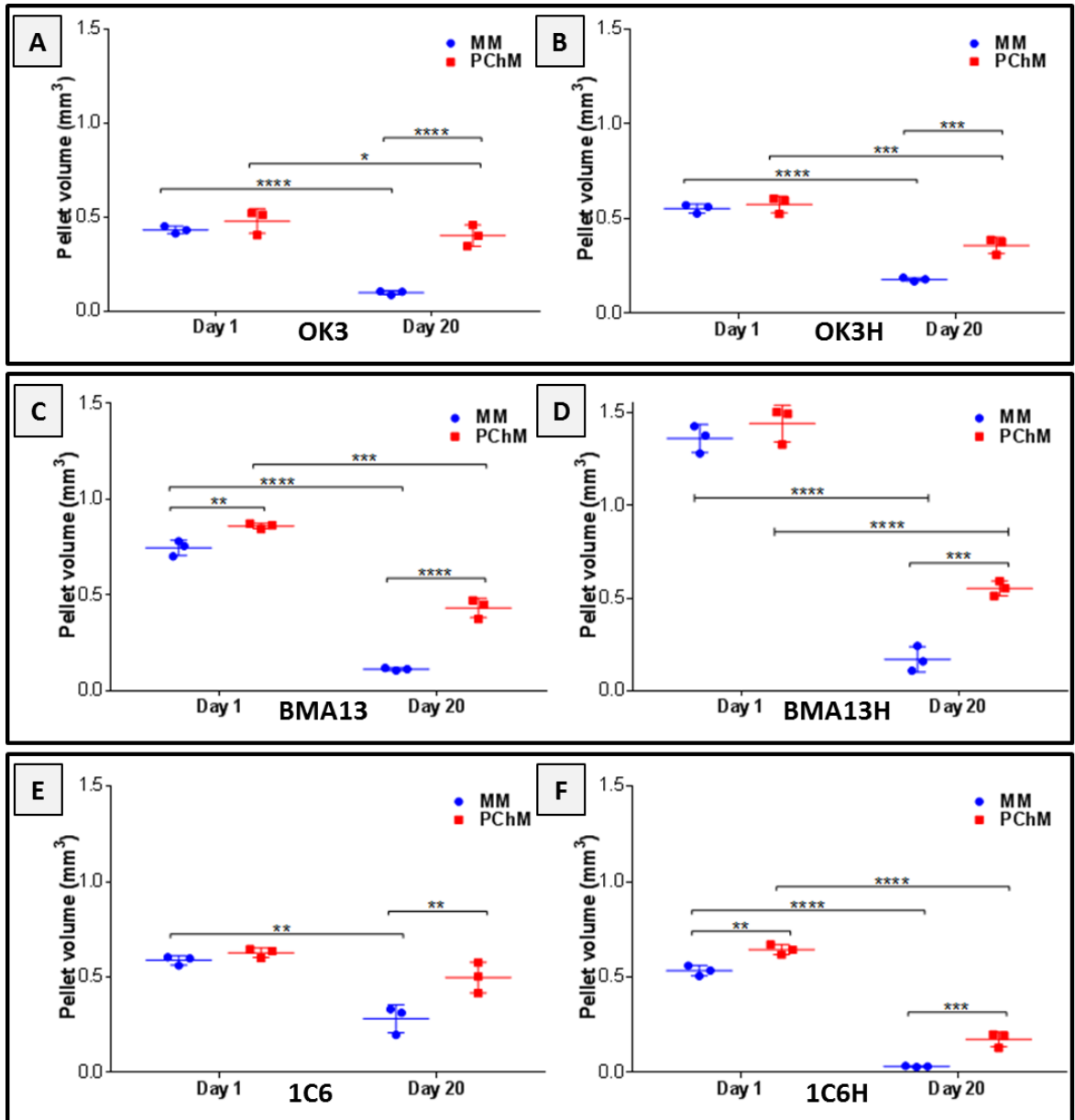


**Figure 6-5.  $\mu$ CT determined pellet volume.** Pellet volumes determined by 50/1000 threshold analysis of pellets at day 1 and day 20 after culture in MM or PChM for OK3 (A), OK3H (B), BMA13 (C), BMA13H (D), 1C6 (E), and 1C6H (E). Data are plotted as mean  $\pm$  standard deviation, N=3. \*p $\leq$ 0.05, \*\*p $\leq$ 0.01, \*\*\*p $\leq$ 0.001, \*\*\*\*p $\leq$ 0.0001. PD level for cells was as follows: OK3 PD6, OK3H PD50, BMA13 PD1, BMA13H PD16, 1C6 PD36, 1C6H PD107.

The improved accuracy gained from using this technique compared to image analysis is apparent in the reduced standard deviation error bar range and by a general increase in the significance p value. As with the previously calculated volumes from imaging, pellets at day 1 were still slightly larger on average after forming in PChM compared to pellet formation in MM (Figure 6-6),

although this was significant only in BMA13 (1.1 fold higher,  $p \leq 0.01$ ) and 1C6H (1.2 fold higher,  $p \leq 0.01$ ) only. By day 20 all pellets cultured in MM were significantly smaller than at day 1 ranging from a 0.061 fold decrease in 1C6H to 0.48 fold decrease in 1C6. Equally, all pellets excepting 1C6 cultured in PChM were significantly smaller at day 20 than day 1 with the difference ranging from 0.27 fold in 1C6H to 0.84 fold in OK3. The larger decreases in MM meant that at day 20 all pellets cultured in the presence of PChM were significantly larger than the corresponding MM pellets (Figure 6-6). The difference was smallest in 1C6 at 1.8 fold larger increasing to 5.3 fold larger in 1C6H.

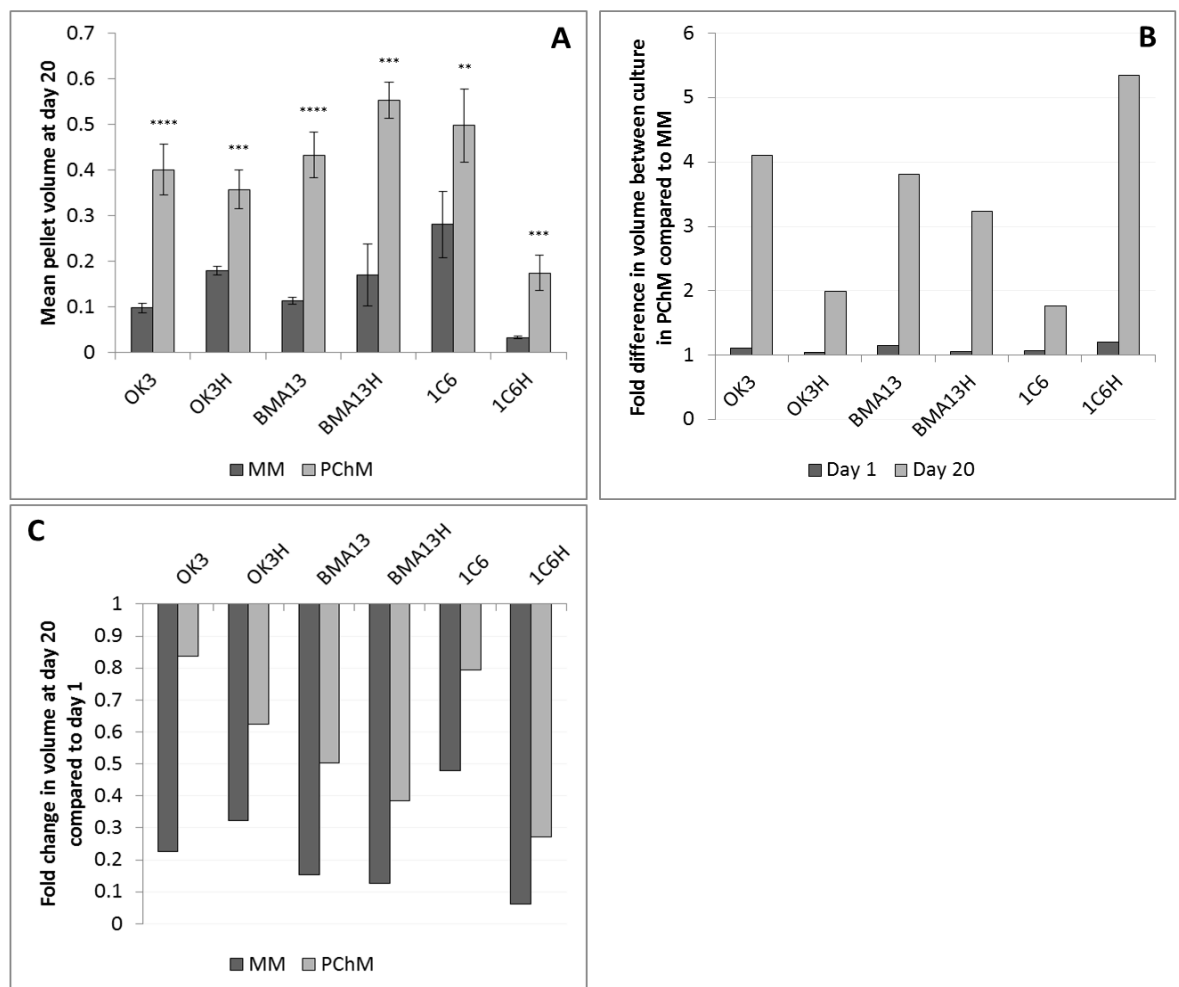


**Figure 6-6. Pellet size at day 20.** Summary pellet volume data for all cell types determined by  $\mu$ CT at day 20 (A) the fold difference in pellets cultured in MM compared to PChM at both day 1 and day 20 (B) and fold change in volume at day 20 compared to day 1 (C). Data in chart A are expressed as mean  $\pm$  standard deviation, \*\* $p \leq 0.01$ , \*\*\* $p \leq 0.001$ , \*\*\*\* $p \leq 0.0001$ , N=3. PD level for cells was as follows: OK3 PD6, OK3H PD50, BMA13 PD1, BMA13H PD16, 1C6 PD36, 1C6H PD107.

#### 6.4.1.1 Pellet density

Relative density was also acquired by  $\mu$ CT and is shown in Figure 6-7, and with day 20 mean densities summarised and the difference expressed as a fold change at day 20 compared to day 1 in Figure 6-8. There were no significant differences across all cell types between culture in MM or PChM at day 1. With the exception of 1C6H cell, pellets were on average denser at day 20 when cultured in PChM than when cultured in MM and were also denser at day 20 than day 1. Differences at day 20 between the culture in MM or PChM were significant with OK3H ( $p \leq 0.001$ ), BMA13 ( $p \leq 0.0001$ ) and 1C6 ( $p \leq 0.05$ ). When cultured in MM pellets most pellets had a reduced density compared to day 1. This is despite the reduced volume of these pellets indicating that pellet contraction is unlikely to be the cause of the reduced pellet volume as this would have been likely to lead to an overall increase in pellet density.

The exception to the trend in pellet density was 1C6H where the mean density in MM was larger than in PChM although this was not significant due to the large standard deviation. This increased overall density was due to dense regions within the pellets, in particular in one pellet, although a second also had some dense spots. Using  $\mu$ CT analysis these dense regions could be visually isolated from the bulk of the pellet by increasing the lower threshold for  $\mu$ CT analysis to 135, a level sufficient to isolate sub-chondral bone completely from the overlying cartilage (Figure 6-9).

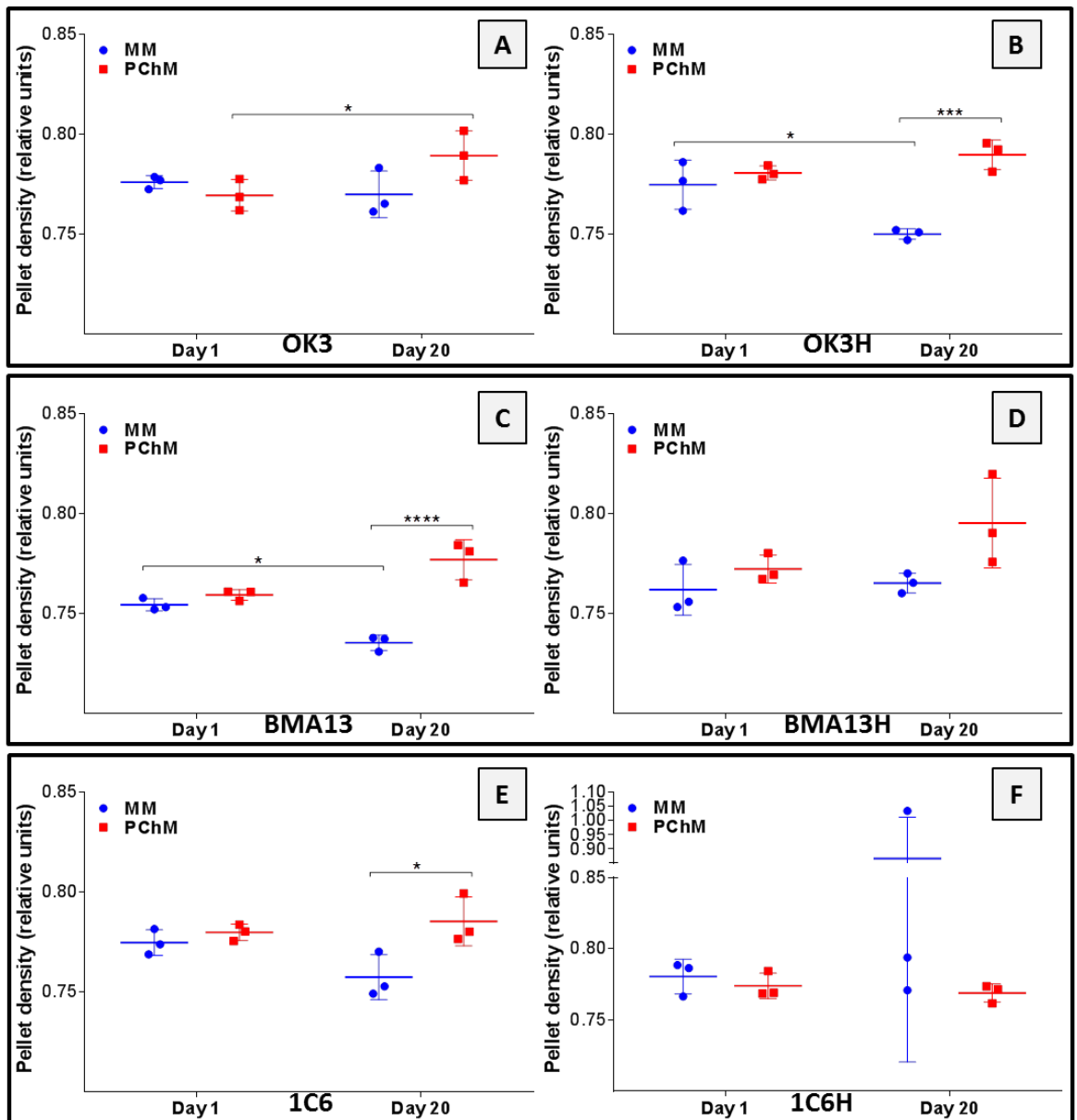


**Figure 6-7.  $\mu$ CT determined density analysis.** Relative pellet density determined by 50/1000 threshold analysis of pellets at day 1 and day 20 after culture in MM or PChM for OK3 (A), OK3H (B), BMA13 (C), BMA13H (D), 1C6 (E), and 1C6H (E). Data are plotted as mean  $\pm$  standard deviation, N=3. \* $p$  $\leq$ 0.05, \*\*\* $p$  $\leq$ 0.001, \*\*\*\* $p$  $\leq$ 0.0001. PD level for cells was as follows: OK3 PD6, OK3H PD50, BMA13 PD1, BMA13H PD16, 1C6 PD36, 1C6H PD107.

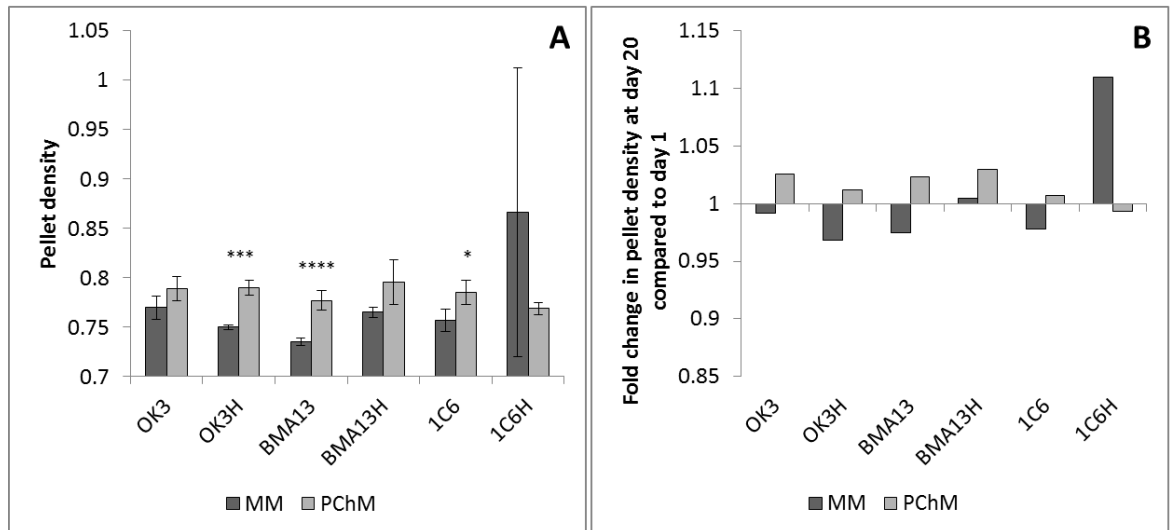


**Figure 6-8. Relative pellet density at day 20.** Summary pellet density data for all cell types determined by  $\mu$ CT at day 20 (A) and the mean day 20 density expressed as a fold change of the day 1 mean pellet density (B). Data in chart A are expressed as mean  $\pm$  standard deviation, N=3, \* $p$ <0.05, \*\*\* $p$ <0.001, \*\*\*\* $p$ <0.0001. PD level for cells was as follows: OK3 PD6, OK3H PD50, BMA13 PD1, BMA13H PD16, 1C6 PD36, 1C6H PD107.

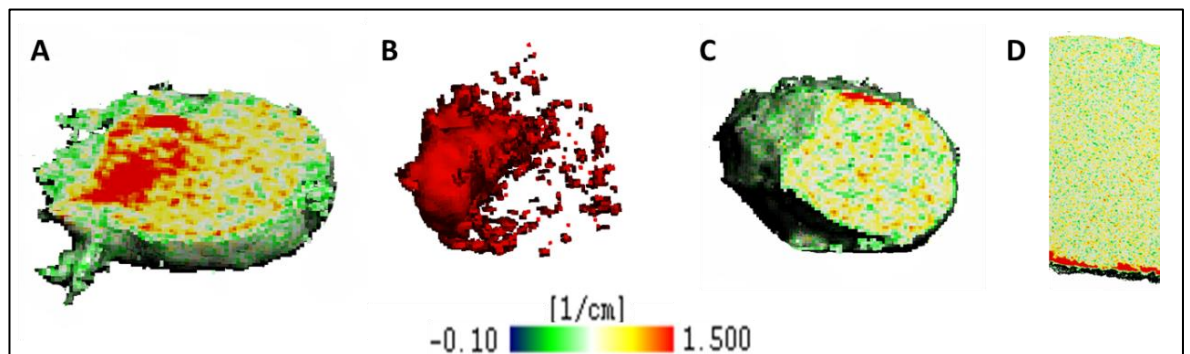


**Figure 6-9. 1C6H  $\mu$ CT density analysis.** 1C6H pellets cultured in MM contained regions that were much denser than any other pellet. These denser regions are shown in red in cross sections (A) and (C) and are visually isolated from the remainder of the pellet in (B) using a higher lower threshold of 135 during the analysis. Denser areas are equivalent in density to the subchondral bone found with full depth osteochondral plugs as shown in (D). PD level for cells was as follows: OK3 PD6, OK3H PD50, BMA13 PD1, BMA13H PD16, 1C6 PD36, 1C6H PD107.

#### 6.4.2 sGAG production in pellets

sGAG production at day 0 and after 20 days culture in MM or PChM was quantified by the spectrophotometric DMMB assay after pellet digestion with proteinase K and is shown in Figure 6-10 and Figure 6-11. All 3 primary cell types had significantly increased sGAG by day 20 when

cultured in PChM compared to day 0, with BMA13 ( $4.906 \pm 1.374 \mu\text{g}$ ,  $p \leq 0.05$ ) > OK3 ( $4.617 \pm 1.202 \mu\text{g}$ ,  $p \leq 0.001$ ) > 1C6 ( $2.886 \pm 0.517 \mu\text{g}$ ,  $p \leq 0.05$ ). In contrast, culture in MM led to a non-significant reduction in sGAG in all three primary cell type pellets where the mean reduction in 1C6 ( $1.265 \pm 0.044 \mu\text{g}$ ) > BMA13 ( $1.221 \pm 0.124 \mu\text{g}$ ) > OK3 ( $0.616 \pm 0.190 \mu\text{g}$ ). This decrease in sGAG in after culture in MM concomitant with an increase in sGAG in PChM resulted in significantly higher amounts of sGAG for all three cell types at day 20 in PChM of 4.00  $\mu\text{g}$  or 7.5 fold in OK3 ( $p \leq 0.0001$ ), 3.69  $\mu\text{g}$  or 4.0 fold in BMA13 ( $p \leq 0.001$ ) and 1.62  $\mu\text{g}$  or 2.3 fold in 1C6 ( $p \leq 0.01$ ).

In contrast to the primary cell pellets the transduced cell pellets had no significant increase in sGAG from day 0 levels by day 20 when cultured in PChM with 1C6H decreasing significantly by 66% from  $1.495 \pm 0.117 \mu\text{g}$  to  $0.515 \pm 0.015 \mu\text{g}$ ,  $p \leq 0.0001$ . As with the culture of primary cell pellets sGAG content still decreased over time in MM, significantly so in OK3H to  $1.385 \pm 0.095 \mu\text{g}$ ,  $p \leq 0.01$  and 1C6 to a very low  $0.118 \pm 0.212 \mu\text{g}$ ,  $p \leq 0.0001$ . Nevertheless, it is important to note that a partial response to pro-chondrogenic stimuli was still apparent in transduced cells indicated by the differential response to MM compared to PChM. As a result of this as at day 20 OK3H and 1C6H pellets still had significantly more sGAG following culture in PChM than in MM by 2.0 fold ( $p \leq 0.0001$ ) and 2.4 fold and ( $p \leq 0.05$ ) respectively. BMA13H also had 1.6 fold more sGAG after culture in PChM compared to MM; however, this was not significant.

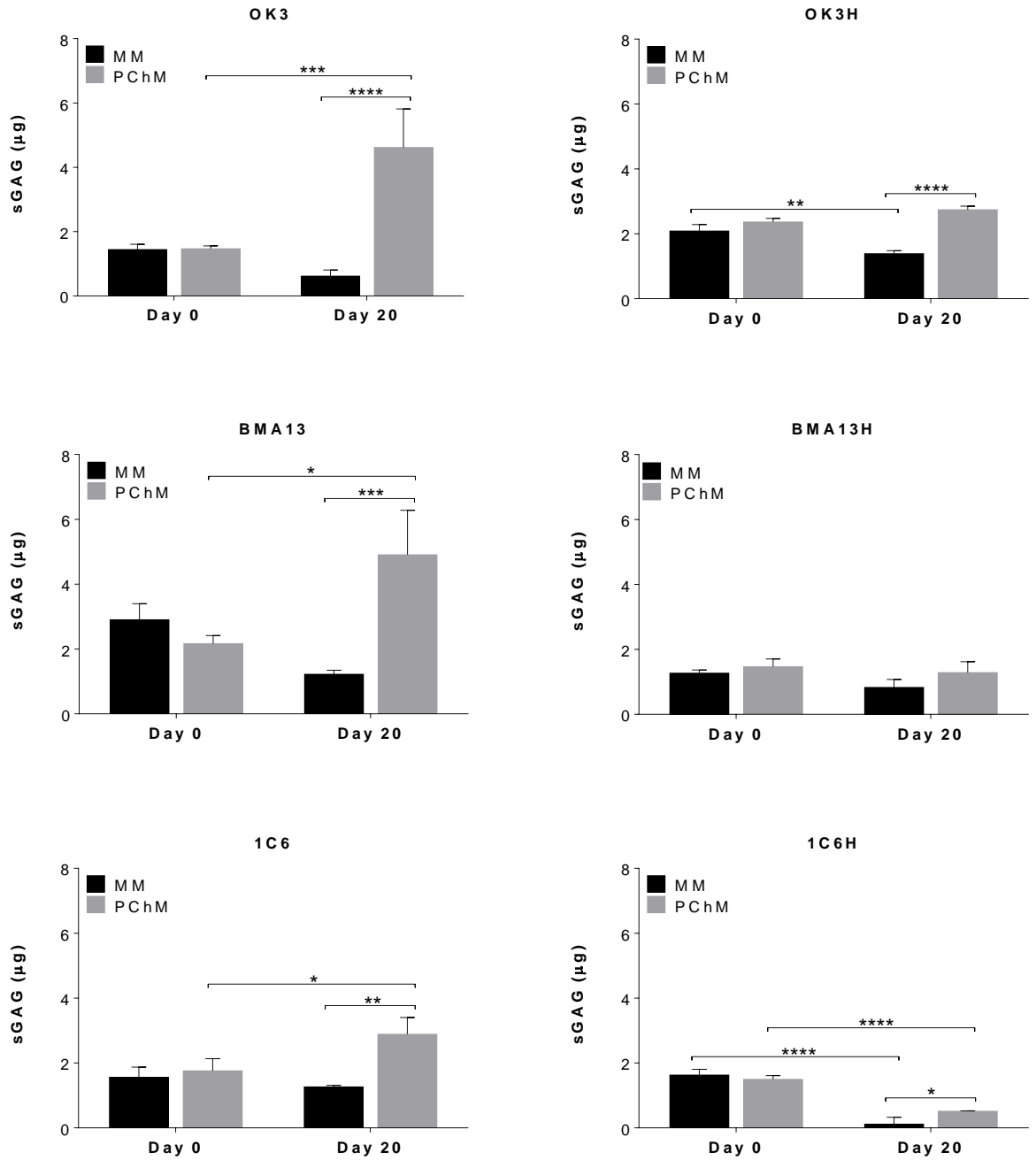


**Figure 6-10. sGAG content of cell pellets.** Total absolute sGAG content in pellets was quantified using the DMMB assay at day 0 in MM or PChM and at day 20 after culture in MM or PChM for all cell pellets. Data are expressed as mean  $\pm$  standard deviation, \* $p \leq 0.05$ ,  $N=3$ , \*\* $p \leq 0.01$ , \*\*\* $p \leq 0.001$ , \*\*\*\* $p \leq 0.0001$ . PD level for cells was as follows: OK3 PD6, OK3H PD50, BMA13 PD6, BMA13H PD16, 1C6 PD36, 1C6H PD86.

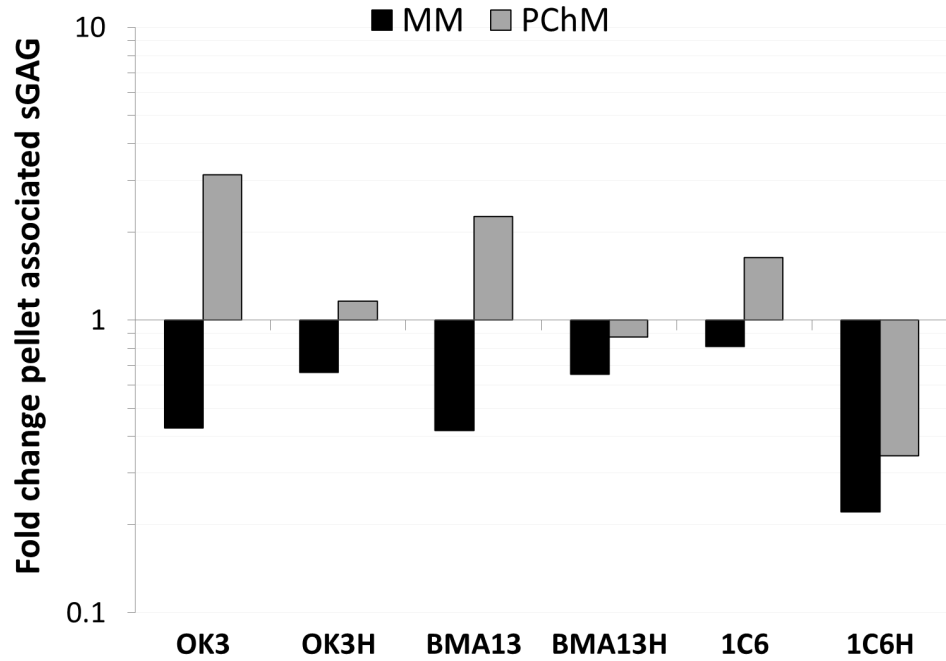


**Figure 6-11. Fold change in pellet associated sGAG.** Absolute sGAG quantities determined by DMMB assay were used to calculate fold change in sGAG content at day 20 relative to day 0 levels. PD level for cells was as follows: OK3 PD6, OK3H PD50, BMA13 PD6, BMA13H PD16, 1C6 PD36, 1C6H PD86.

#### 6.4.3 sGAG content of pellet media

Media levels of sGAG were much lower overall than those from monolayer cultures (Figure 5-4); however, as with monolayer culture they were highest in OK3 and OK3H cell cultures compared to the other cell types (Figure 6-12). As the pellets were measured at day 0 following centrifugation, rather than after overnight culture as for the monolayer cells, day 0 values were essentially 0 and are therefore not shown, this also prevents the calculation of fold-change values. Statistically significant differences between MM and PChM at day 20 were found only for two comparisons: OK3H was higher in MM than PChM,  $17.083 \pm 1.941 \mu\text{g}$  compared to  $5.213 \pm 1.398 \mu\text{g}$ ,  $p \leq 0.001$  and BMA13H was also higher in MM than PChM at  $1.382 \pm 0.196 \mu\text{g}$  compared to  $0.470 \pm 0.163 \mu\text{g}$ ,  $p \leq 0.01$ . These results are also in agreement with the monolayer culture experiments where culture in MM resulted in higher levels of sGAG than in PChM.

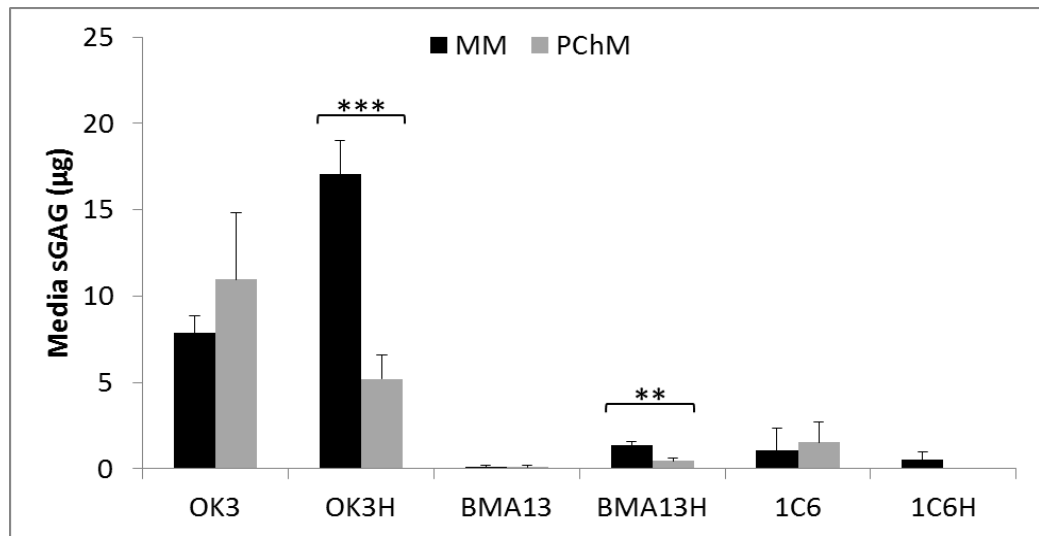


**Figure 6-12. sGAG in spent culture media at day 20.** sGAG content of the spent culture media was determined by DMMB assay. Data are expressed as mean  $\pm$  standard deviation, N=3, \*\*p $\leq$ 0.01, \*\*\*p $\leq$ 0.001. PD level for cells was as follows: OK3 PD6, OK3H PD50, BMA13 PD6, BMA13H PD16, 1C6 PD36, 1C6H PD86.

#### 6.4.4 Total sGAG changes

Total sGAG at day 20 as a result of the contributions from the pellet associated sGAG and the media associated sGAG are shown in Figure 6-13 and with the contribution from each fraction expressed as a percentage of the total amount of sGAG in Figure 6-14A and as total fold change in Figure 6-14B.

Cultures of all cells excepting 1C6H had an overall increase in total sGAG after 20 days in culture in PChM when compared to day 0 starting amounts with OK3 (10.6 fold) > BMA13 (2.3 fold) > 1C6 (2.2 fold). Culture in MM led to overall increases in OK3, OK3H, BMA13H and 1C6 (5.4, 8.9, 1.2 and 1.5 fold respectively) and decreases in BMA13 and 1C6H (0.46, 0.51 fold). In contrast to the monolayer total sGAG results the three primary cell types had larger total fold increases in PChM than MM due to a larger percentage contribution from the pellet associated sGAG compared to media associated sGAG. The media percentage contribution to the total ranged from 8.1% to 92.7% in MM with a mean of  $60.2 \pm 31.7\%$  and 0.0% to 70.4% in PChM with a mean of  $33.3 \pm 30.1\%$ . This compares to monolayer results of a mean of  $88.9 \pm 9.1\%$  in MM and

69.2 ± 14.7% in PChM respectively. As a result of the reduced contribution from the media were in general reduced MM cultures

As with the monolayer results, all three primary cell types had greater fold increases and total sGAG production than their corresponding transduced cell types when cultured in PChM.

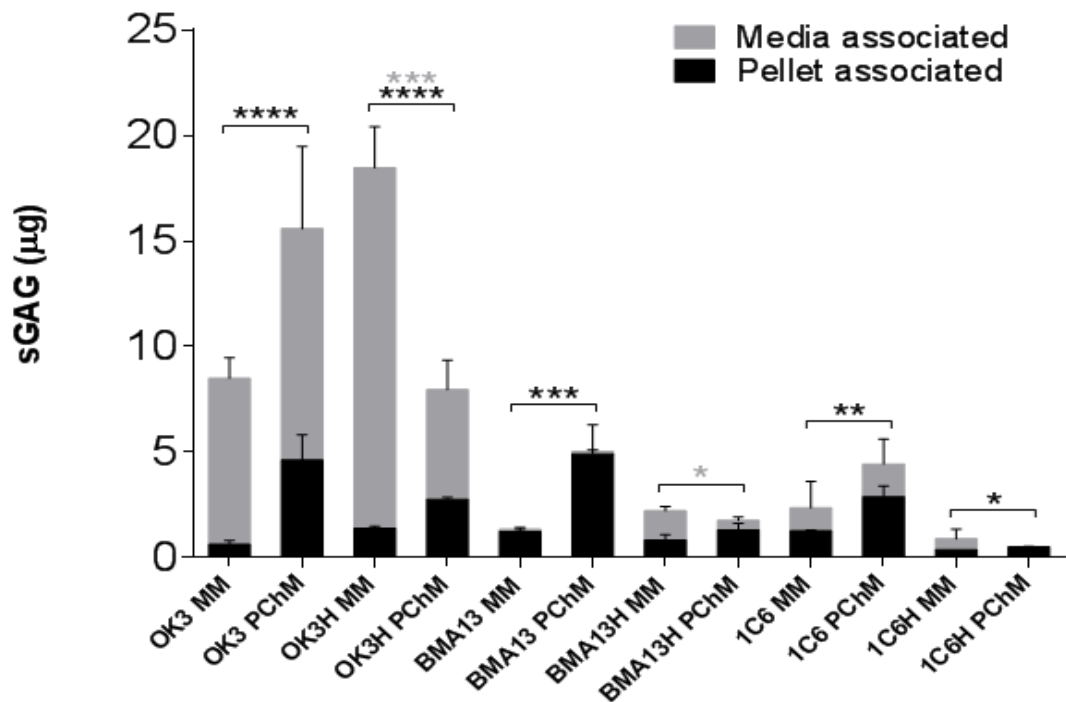


**Figure 6-13. Total sGAG in pellets and spent culture media at day 20.** Absolute sGAG contribution to total sGAG content from the pellet and spent culture media. Data are expressed as mean ± standard deviation, N=3, \*p<0.05, \*\*p<0.01, \*\*\*p<0.001, \*\*\*\*p<0.0001. Black asterisks indicate significance between pellet associated sGAG; grey asterisks indicate significance between media associated sGAG. PD level for cells was as follows: OK3 PD6, OK3H PD50, BMA13 PD6, BMA13H PD16, 1C6 PD36, 1C6H PD86.

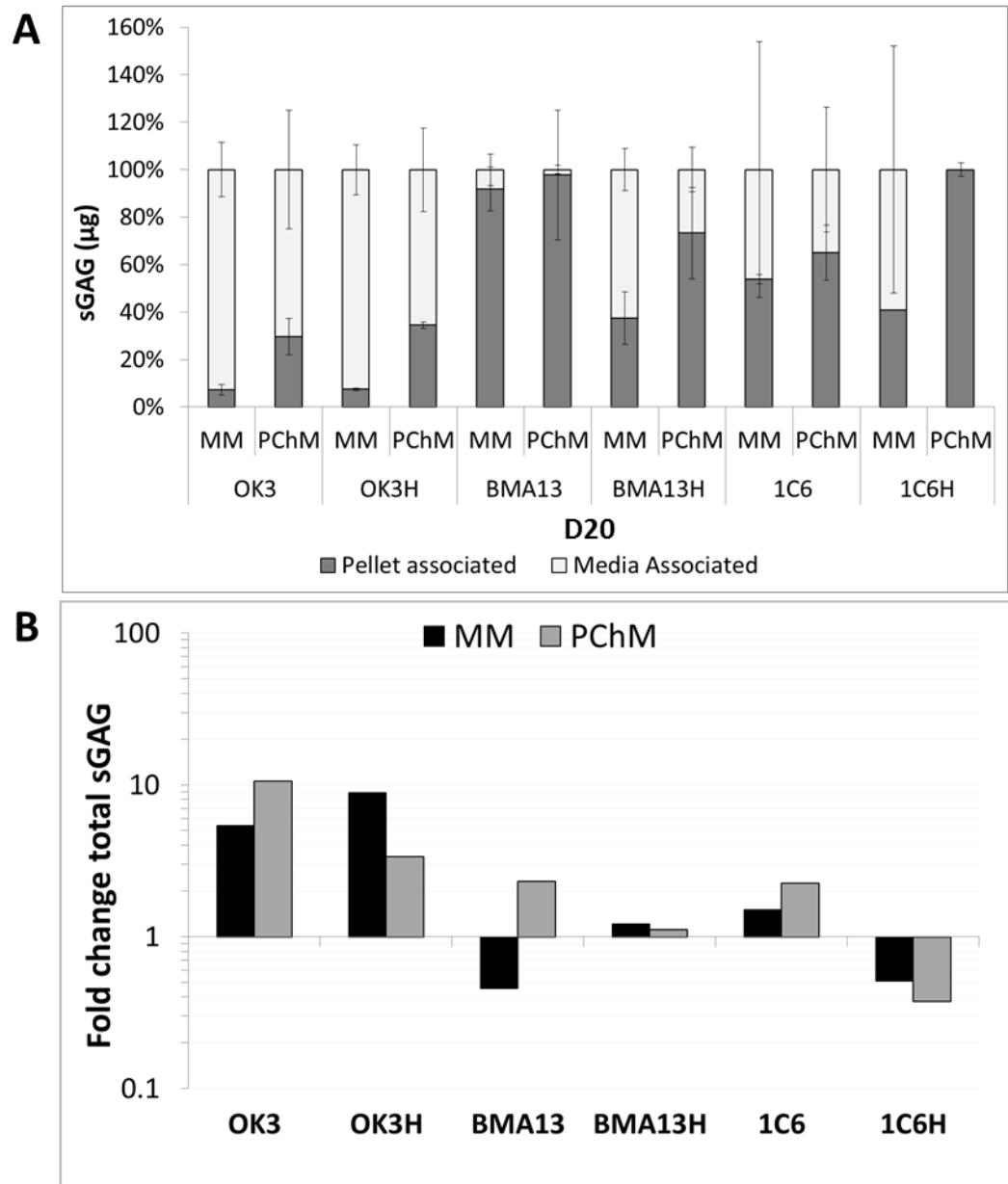


**Figure 6-14. Total sGAG.** (A) Percentage of total sGAG contributed by the pellet and media associated fractions. (B) Total mean fold change at day 20 relative to day 0. PD level for cells was as follows: OK3 PD6, OK3H PD50, BMA13 PD6, BMA13H PD16, 1C6 PD36, 1C6H PD86.

#### 6.4.5 DNA content of cell pellets

DNA content of all pellets at day 0 and day 20 was determined using the PicoGreen DNA assay (Figure 6-15 and Figure 6-16). The DNA content of pellets decreased significantly in all primary cell pellets cultured in MM from day 0 values with pellets containing 24.7% of the starting DNA in OK3 ( $p \leq 0.01$ ), 52.6% ( $p \leq 0.05$ ) in BMA13 and 39.8% ( $p \leq 0.0001$ ) in 1C6. Transduced cells OK3H and

BMA13H retained more DNA over the culture period, ending at 90.7% ( $p \leq 0.01$ ) and 59.1% respectively ( $p \leq 0.01$ ). 1C6H on the other hand had a very low DNA content, ending the experiment at day 20 with only 12.6% ( $p \leq 0.0001$ ) of the starting DNA content.

The DNA content also decreased in two out of the three primary cell types in PChM, although as with the sGAG content, much less so, with primary pellets having 90.4%, 120.4% and 95.9% of the starting DNA amount in OK3, BMA13 and 1C6 respectively with no change being significant. In contrast two of the three transduced cell types had pellets that were significantly reduced compared to day 0 DNA values with BMA13H at 83.2% ( $p \leq 0.05$ ) of the starting DNA and again representing a very large decrease, 1C6H down to just 20.5% ( $p \leq 0.0001$ ) of initial levels.

The different behaviour of cells with respect to final DNA content in the two media types resulted in all pellets in MM having less DNA than pellets in PChM with a significant difference in DNA content by day 20 in four out of six cell types. The magnitude of the difference was greater in primary cells with OK3 having 70.7% ( $p \leq 0.001$ ) more DNA in PChM than MM, OK3H 14.4% ( $p \leq 0.01$ ), BMA13 32.4%, BMA13H 29.2% ( $p \leq 0.001$ ), 1C6 57.9% ( $p \leq 0.0001$ ) and 1C6H 30.8%.

These differences in DNA content were not always only attributable to changes isolated to the primary pellets; pellets, particularly in PChM often had secondary smaller pellets form during the culture period (Figure 6-2Ec and Ed). These are believed to be as a result of cell condensations forming on the walls of the microcentrifuge tubes which may then detach (Figure 6-17). In some cases these small pellets remain separate but imaging indicates that these can also become integrated with the primary pellet as shown in Figure 6-4E d.

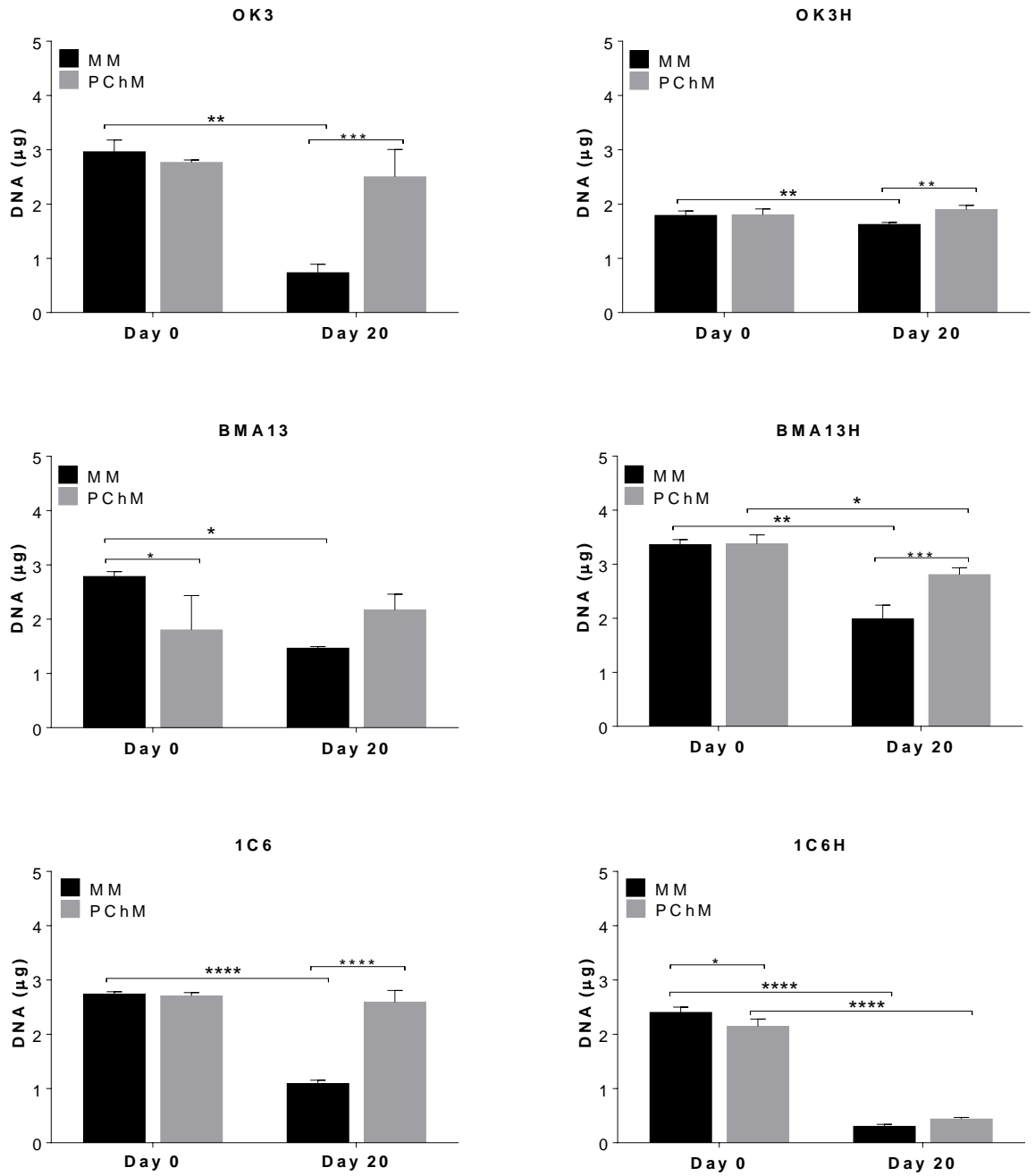


**Figure 6-15. Cell pellet DNA content.** Total DNA content was determined using the PicoGreen assay for all cell pellets following digestion with proteinase K. Data are expressed as mean  $\pm$  standard deviation, N=3, \* $p$  $\leq$ 0.05, \*\* $p$  $\leq$ 0.01, \*\*\* $p$  $\leq$ 0.001, \*\*\*\* $p$  $\leq$ 0.0001. PD level for cells was as follows: OK3 PD6, OK3H PD50, BMA13 PD6, BMA13H PD16, 1C6 PD36, 1C6H PD86.

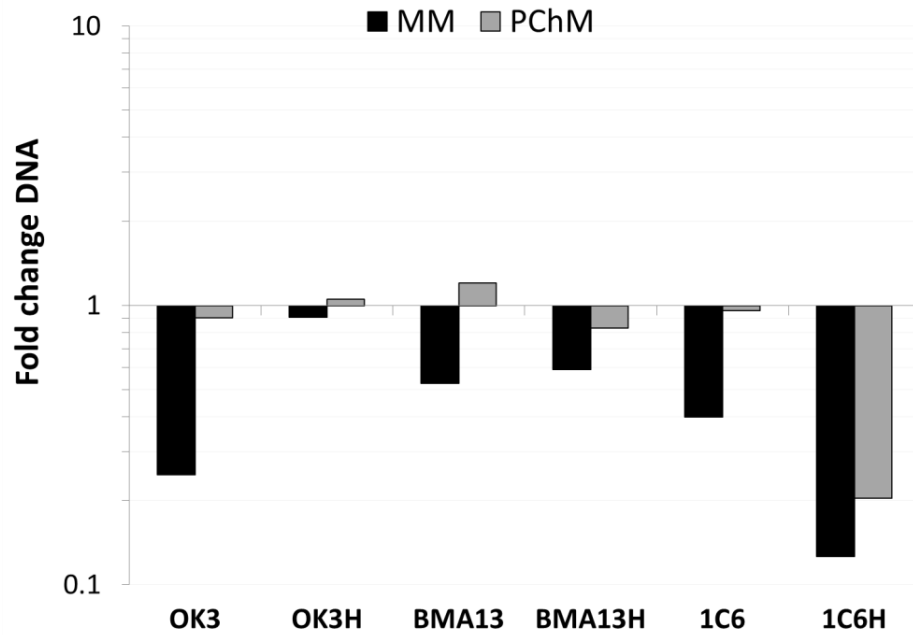


**Figure 6-16. Fold change in pellet DNA content.** Absolute DNA quantities determined by PicoGreen assay were used to calculate fold change in DNA content at day 20 relative to day 0 levels. PD level for cells was as follows: OK3 PD6, OK3H PD50, BMA13 PD6, BMA13H PD16, 1C6 PD36, 1C6H PD86.

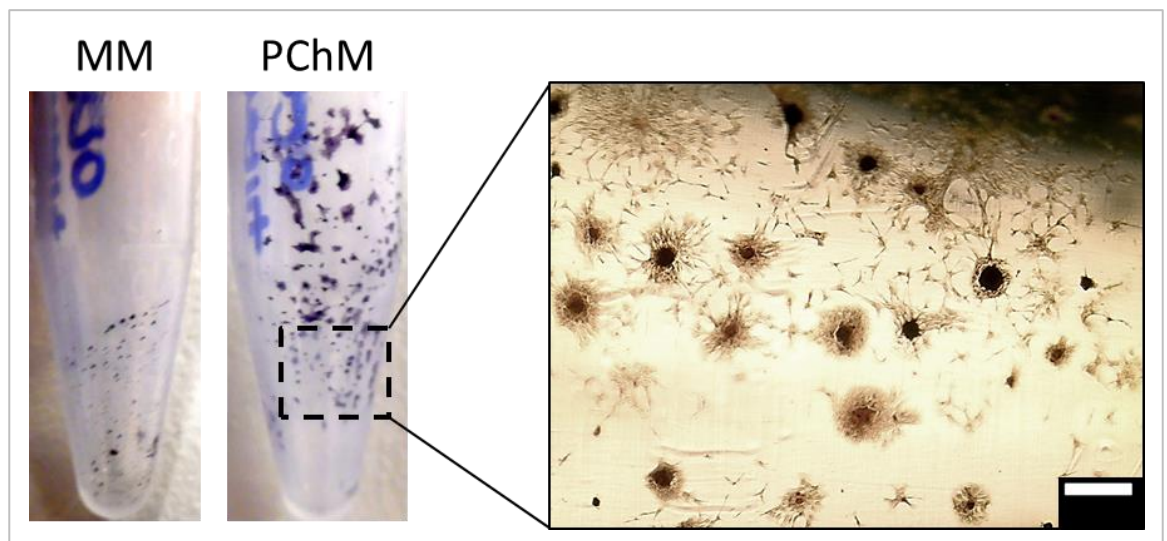


**Figure 6-17. Cellular material on microcentrifuge tubes.** Photographs of 1.5 mL microcentrifuge tubes illustrating the formation of cellular material after 20 day culture in MM or PChM and magnification under brightfield microscopy. Cells are stained with haematoxylin for visualisation. Scale bar=500 µm.

#### 6.4.6 Pellet sGAG normalised to DNA

Normalisation of pellet associated sGAG to DNA had little effect on the trends previously observed across OK3, OK3H, BMA13 and BMA13H for absolute sGAG levels. In PChM BMA13 remained the highest sGAG producer at  $2.23 \pm 0.31 \mu\text{g}/\mu\text{g}$  followed by OK3 at  $1.87 \pm 0.41 \mu\text{g}/\mu\text{g}$  and lastly 1C6 at  $1.13 \pm 0.29 \mu\text{g}/\mu\text{g}$ . OK3H and BMA13H were reduced in comparison at  $1.45 \pm 0.03 \mu\text{g}/\mu\text{g}$  and  $0.46 \pm 0.14 \mu\text{g}/\mu\text{g}$  respectively (Figure 6-18). Again as with absolute level these values were significantly higher than those obtained for pellets cultured in MM with the difference greatest in BMA13 at 2.68 fold higher ( $p \leq 0.001$ ) followed by OK3 at 2.68 fold higher ( $p \leq 0.001$ ), OK3H at 1.69 fold higher ( $p \leq 0.0001$ ) and BMA13H not significantly different (Figure 6-19).

Post-normalisation 1C6 and 1C6H cell pellets cultured in PChM were no longer significantly different to MM pellet cultures (0.97 and 0.97 fold differences respectively), and most strikingly normalised levels in 1C6H were similar to 1C6 levels at  $1.20 \pm 0.15 \mu\text{g}/\mu\text{g}$  and  $1.16 \pm 0.03 \mu\text{g}/\mu\text{g}$  and in MM and  $1.18 \pm 0.08 \mu\text{g}/\mu\text{g}$  and  $1.13 \pm 0.29 \mu\text{g}/\mu\text{g}$  in PChM.

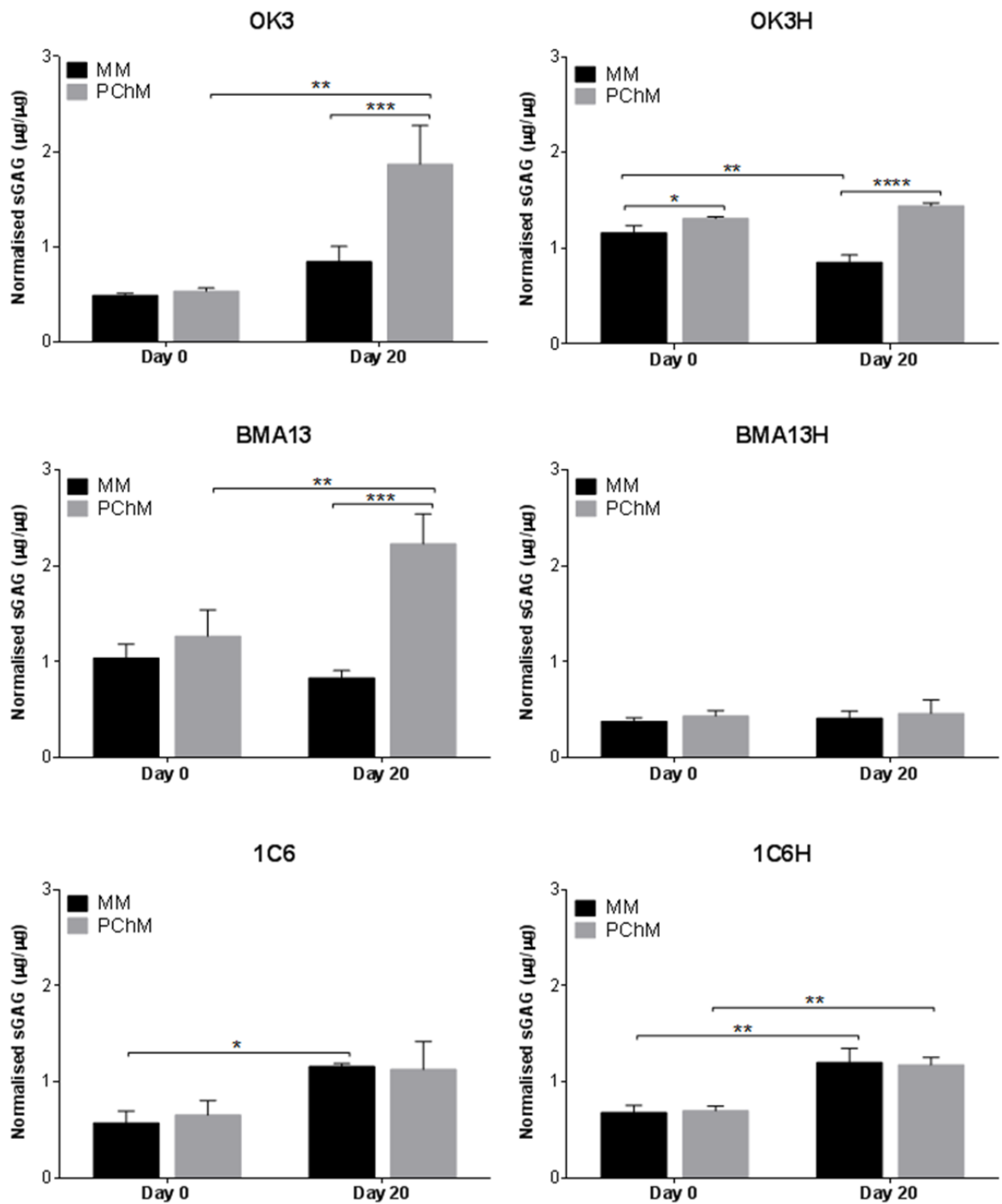


**Figure 6-18. Pellet associated sGAG normalised to DNA content.** sGAG associated with cell pellets was normalised to DNA of the same pellets to give a µg/µg ratio at day 0 and day 20 for all cell types after culture in MM or PChM. Data are expressed as mean ± standard deviation, N=3, \*p<0.05, \*\*p<0.01, \*\*\*p<0.001, \*\*\*\*p<0.0001. PD level for cells was as follows: OK3 PD6, OK3H PD50, BMA13 PD6, BMA13H PD16, 1C6 PD36, 1C6H PD86.

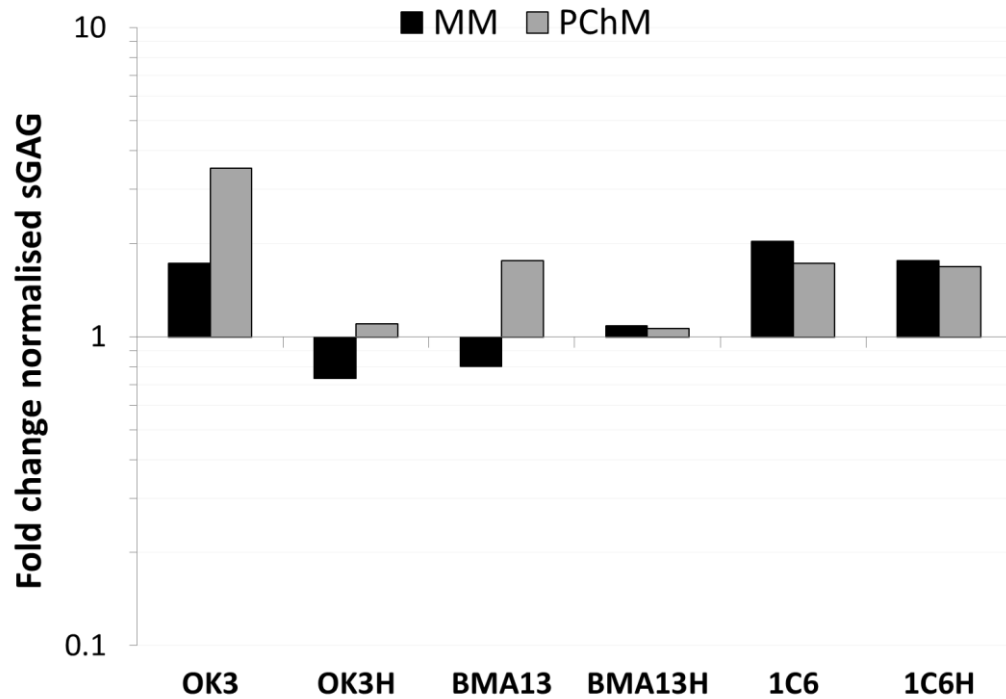


**Figure 6-19. Fold change in normalised pellet associated sGAG.** sGAG was normalised to DNA ( $\mu\text{g}/\mu\text{g}$ ) and expressed as fold change at day 20 relative to day 0. PD level for cells was as follows: OK3 PD6, OK3H PD50, BMA13 PD6, BMA13H PD16, 1C6 PD36, 1C6H PD86.

#### 6.4.7 Media sGAG normalised to pellet DNA

Likewise normalisation of media sGAG generally had little effect on the trends and differences noted with absolute media sGAG levels (Figure 6-20) with the exception of OK3, where results following normalisation were then similar to each other and to previous monolayer results, with significantly more sGAG in MM than PChM cultures for both OK3 and OK3H at 2.5 fold more ( $p \leq 0.04$ ) and 3.6 fold more ( $p \leq 0.001$ ) respectively.

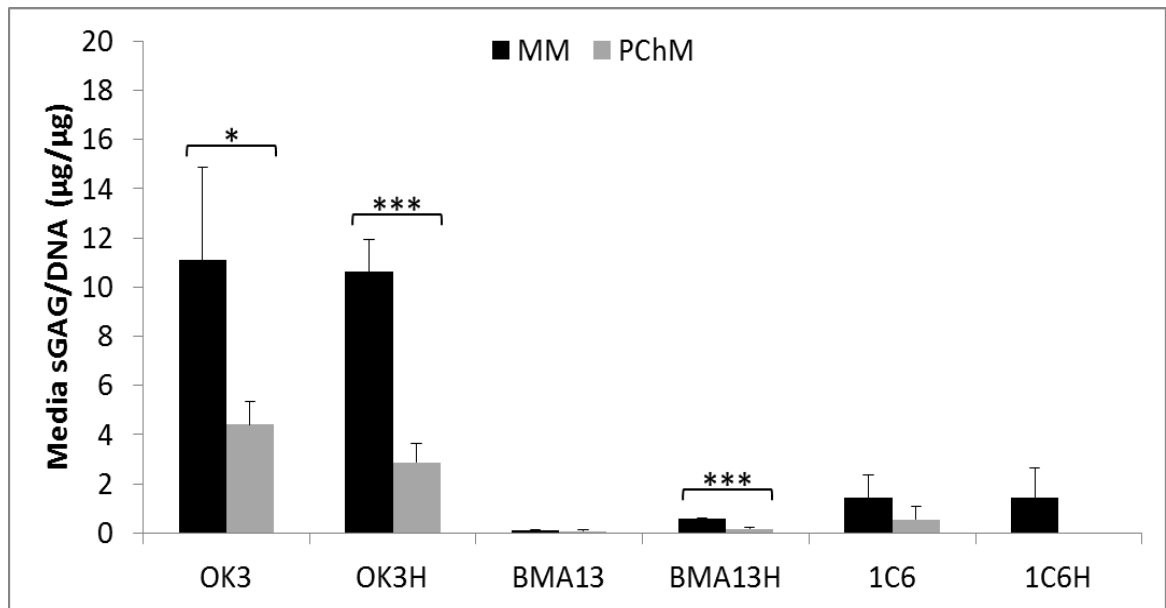


**Figure 6-20. Media sGAG normalised to pellet DNA.** sGAG associated with spent cell culture media was normalised to DNA of the corresponding pellets to give a  $\mu\text{g}/\mu\text{g}$  ratio at day 20 for all cell types after culture in MM or PChM. Data are expressed as mean  $\pm$  standard deviation,  $N=3$ ,  $*p\leq 0.05$ ,  $***p\leq 0.001$ . PD level for cells was as follows: OK3 PD6, OK3H PD50, BMA13 PD6, BMA13H PD16, 1C6 PD36, 1C6H PD86.

#### 6.4.8 Total normalised sGAG

When normalised pellet associated and media associated values are considered together (Figure 6-21) the day 20 data show similar trends to the absolute data. Total normalised values are highest in OK3 and OK3H with greater normalised sGAG in MM (OK3  $11.93 \mu\text{g}/\mu\text{g}$ , OK3H  $11.47 \mu\text{g}/\mu\text{g}$ ) than in PChM (OK3  $6.27 \mu\text{g}/\mu\text{g}$ , OK3H  $4.31 \mu\text{g}/\mu\text{g}$ ). The higher levels total levels in MM are again due to the larger contribution from the media associated fraction, this contribution may also appear higher once normalised as total sGAG throughout the experiment is normalised to the final DNA amount, which in MM decreases significantly from day 0 values. Further temporal investigation would be required to more clearly determine changes throughout the whole experimental time period. Across the other cell types although the media contribution is much lower than for OK3 and OK3H, with the exception of BMA13, MM cultures still have higher total sGAG than PChM cultures with levels in MM of  $2.62 \mu\text{g}/\mu\text{g}$  in 1C6H,  $2.60 \mu\text{g}/\mu\text{g}$  in 1C6,  $0.993 \mu\text{g}/\mu\text{g}$  in BMA13H and  $0.927 \mu\text{g}/\mu\text{g}$  in BMA13. PChM cultures had total normalised sGAG

values of 1.17  $\mu\text{g}/\mu\text{g}$  for 1C6H, 1.67  $\mu\text{g}/\mu\text{g}$  for 1C6, 0.624  $\mu\text{g}/\mu\text{g}$  for BMA13H and 2.32  $\mu\text{g}/\mu\text{g}$  for BMA13 with this almost entirely as a result of the pellet associated fraction.

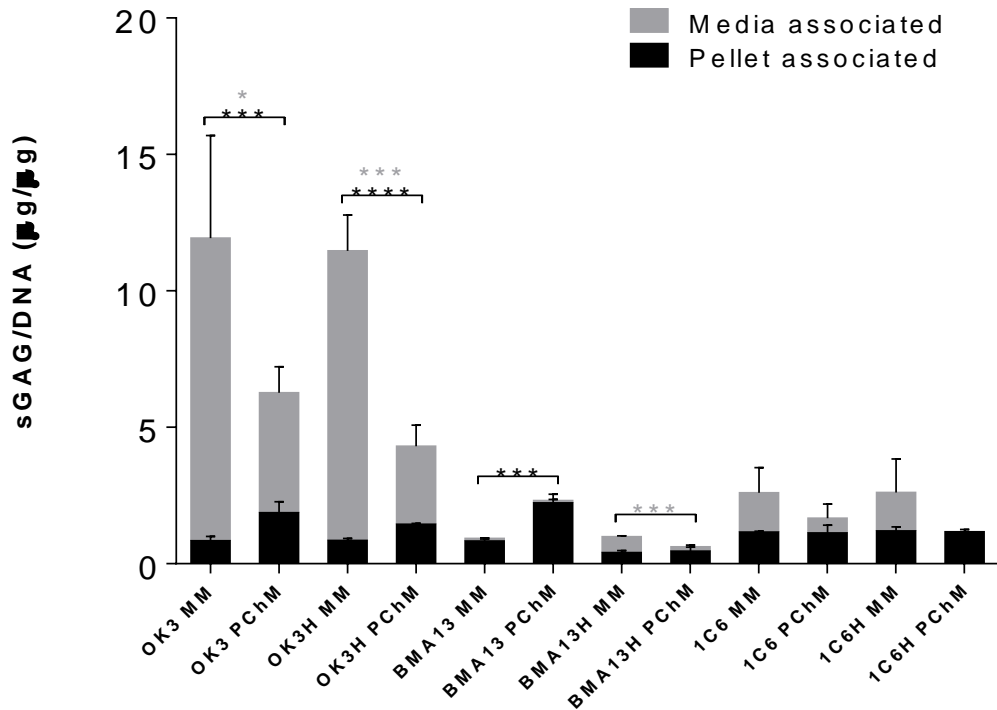


**Figure 6-21. Total normalised sGAG at day 20.** Day 20 summary of total normalised sGAG with both pellet and media contribution at day 20. Data are expressed as mean  $\pm$  standard deviation, N=3, \* $p \leq 0.05$ , \*\*\* $p \leq 0.001$ , \*\*\*\* $p \leq 0.0001$ . Black asterisks indicate significance between pellet associated sGAG; grey asterisks indicate significance between media associated sGAG. PD level for cells was as follows: OK3 PD6, OK3H PD50, BMA13 PD6, BMA13H PD16, 1C6 PD36, 1C6H PD86.

#### 6.4.9 Gene expression

Relative gene expression was determined by qRT-PCR for ECM protein genes *COL1A2*, *COL2A1*, *COL3A1*, *COL6A3*, *COL10A1*, *ACAN*, *COMP* and transcription factor *SOX9*. Following initial analysis it was apparent that basal levels of expression were often somewhat different in the transduced cells in comparison to the parental cells therefore expression was determined both relative to the parental cell type day 0 MM control for all parental and transduced groups, and separately for

transduced cells relative to the transduced day 0 MM sample using REST-2009 software which also provides the error range and the statistical significance determined by a randomisation algorithm<sup>242</sup>.

To determine similarities in gene expression profiles across all of the genes examined hierarchical clustering was performed using Gene Cluster3.0 and visualised with Java TreeView with relative gene expression changes determined for each cell type relative to day 0 MM sample for that cell type. Clustering was first considered within cell type (Figure 6-22), then between transduced and non-transduced within cell-type (Figure 6-23) and finally across all results (Figure 6-24), correlation coefficients for all clusters of both samples and genes are listed in Table 6-1.

Day 0 correlations between groups were poor with only low correlation indicating a degree of variability across samples possibly as a result of rapid gene expression changes induced while pellets were being prepared, when cells were exposed to either MM or PChM for approximately 30 minutes before lysis. Within each cell type the two day 20 results from both MM and PChM clustered most closely with each other and not with either day 0 result indicating similarities in expression patterns induced by pellet formation and culture irrespective of whether this was in MM or PChM. The correlation was strongest (i.e. the expression pattern was most similar) in OK3H (0.967879) followed by OK3 (0.949404), 1C6H (0.939310), 1C6 (0.887813), and BMA13 (0.766945), the exception to this was BMA13H where there were only weak correlations between all groups ( $\leq 0.204302$ ) indicating very dissimilar gene expression after culture in either MM or PChM.

Clustering of pellets from transduced and parental cells together showed that expression after culture in either MM or PChM for OK3/OK3H and 1C6/1C6H remained more likely to be clustered within rather than between cell types at day 20 indicating the differences between the gene expression patterns of the paired cell types were greater than the differences induced within a cell types by culture in MM or PChM despite their shared origin. In contrast BMA13 and BMA13H

day 20 PChM clustered with a correlation of 0.800285, indicating a similar response to a pro-chondrogenic environment; BMA13H day 20 MM was distinctly different with a weak negative correlation with all other clusters (-1.92969). Again, although there were strong paired correlations in gene expression across the groups there were no particular common trends in gene clustering.

Finally all groups were compared simultaneously (excluding day 0 MM for clarity as this is inherently defined as unchanged by the  $2^{-\Delta\Delta CT}$  method and did not cluster strongly with any other group when included), this also provides the strongest information for gene clustering analysis as all changes are included. When all groups were considered together day 0 values were in general poorly correlated with day 20 with the exception of BMA13H and BMA13 day 20 MM cultures indicating distinct differences following pellet formation and culture. OK3H and 1C6H day 20 remained strongly correlated independent of culture in MM or PChM. However, the gene expression changes in the two primary cell types OK3 and 1C6 correlated more highly with each other when cultured in both MM and PChM (0.961132 in MM and 0.955835 in PChM) than with the same cell type in both MM and PChM indicating strong similarities in expression patterns between the two cell types.

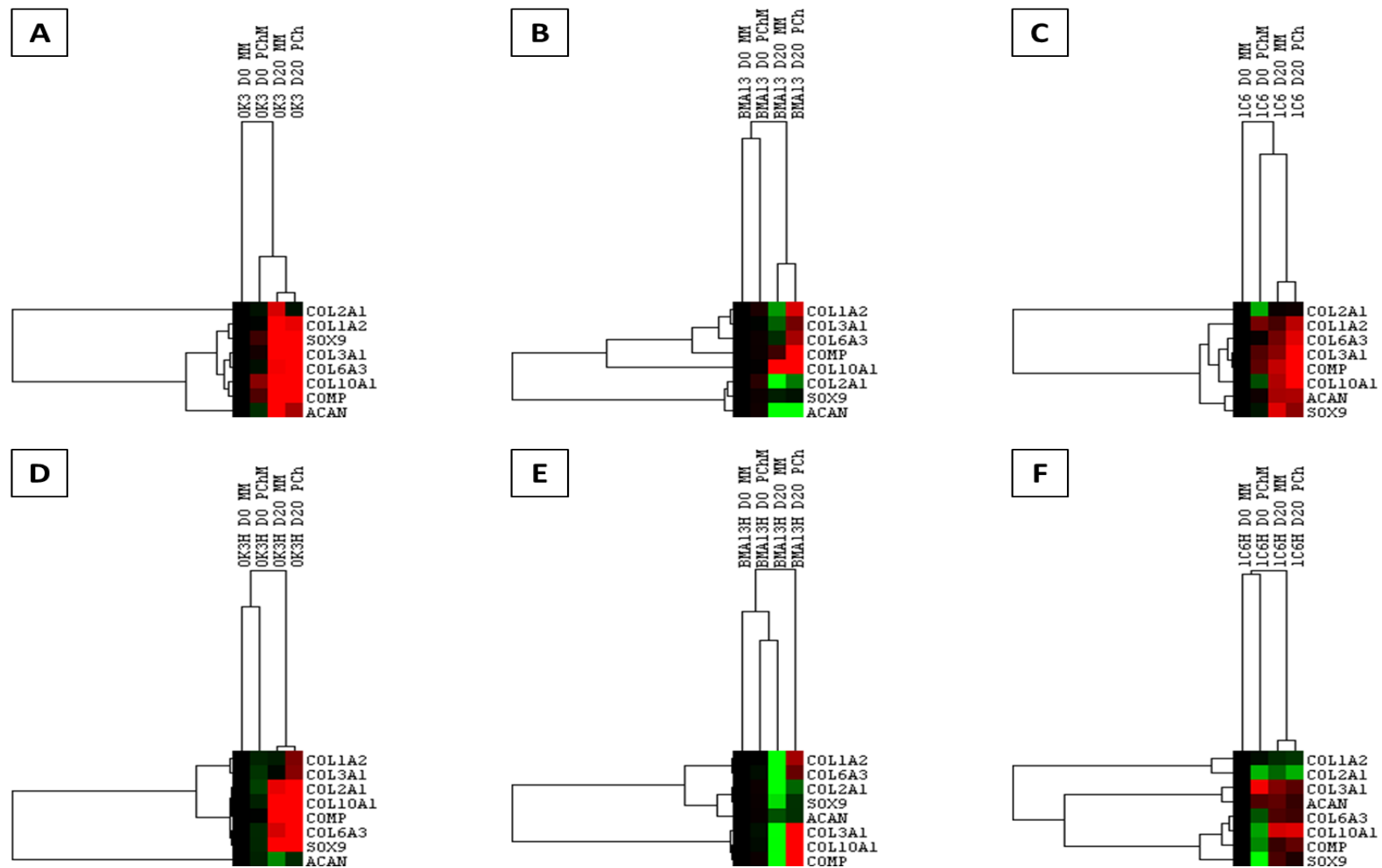


**Figure 6-22. Heatmaps of relative gene expression.** Hierarchical clustering to determine correlations in expression patterns was performed for each cell type across all genes. (A) OK3, (B) BMA13, (C) 1C6, (D) OK3H, (E) BMA13H, (F) 1C6H. Red indicates upregulated genes, green downregulated genes and black no change in expression. All expression changes are determined relative to the day 0 MM condition. The closer the dendrogram cluster pair indicator to the heatmap the stronger the correlation in gene expression. PD level of cells as as follows: OK3 PD6, OK3H PD50, BMA13 PD1, BMA13H PD18, 1C6 PD36, 1C6H PD107.

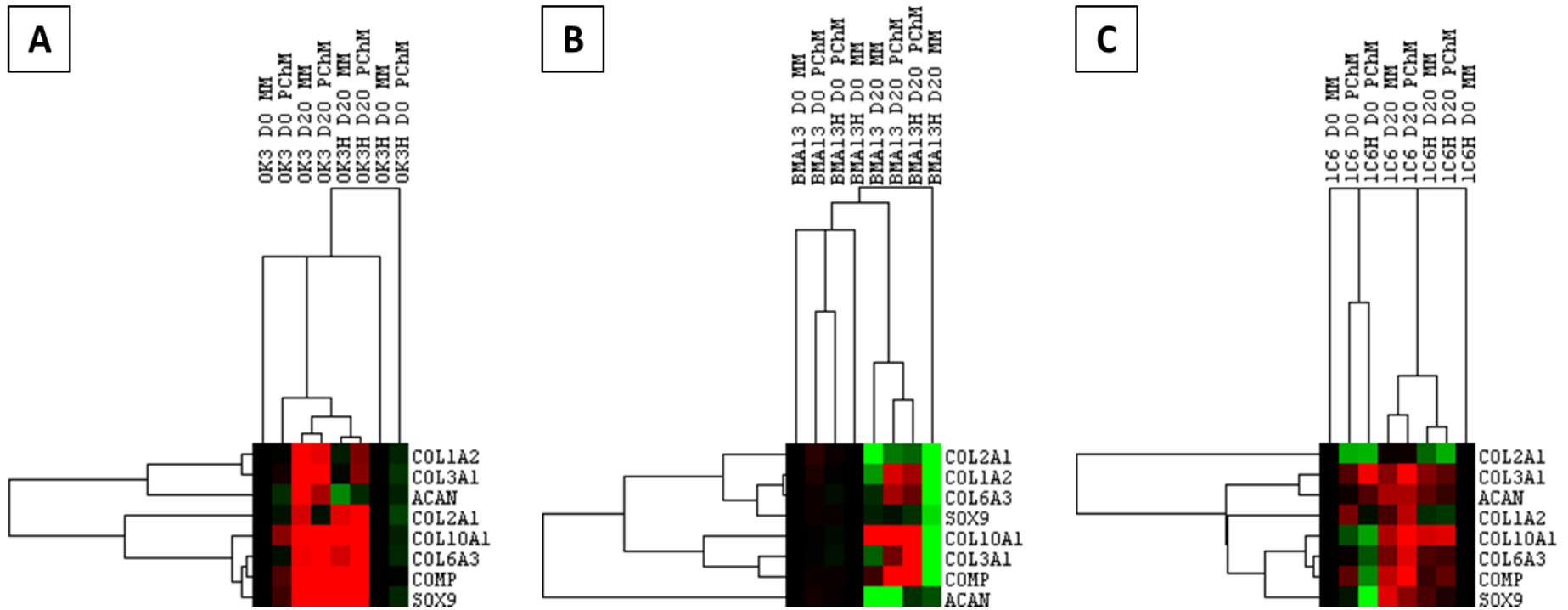


**Figure 6-23. Heatmaps of relative gene expression.** Hierarchical clustering to determine correlations in expression patterns was performed for each parental and transduced cell pair across all genes. (A) OK3/OK3H, (B) BMA13/BMA13H, (C) 1C6/1C6H. Red indicates upregulated genes, green downregulated genes and black no change in expression. All expression changes are determined relative to the day 0 MM condition. PD level of cells as as follows: OK3 PD6, OK3H PD50, BMA13 PD1, BMA13H PD18, 1C6 PD36, 1C6H PD107.

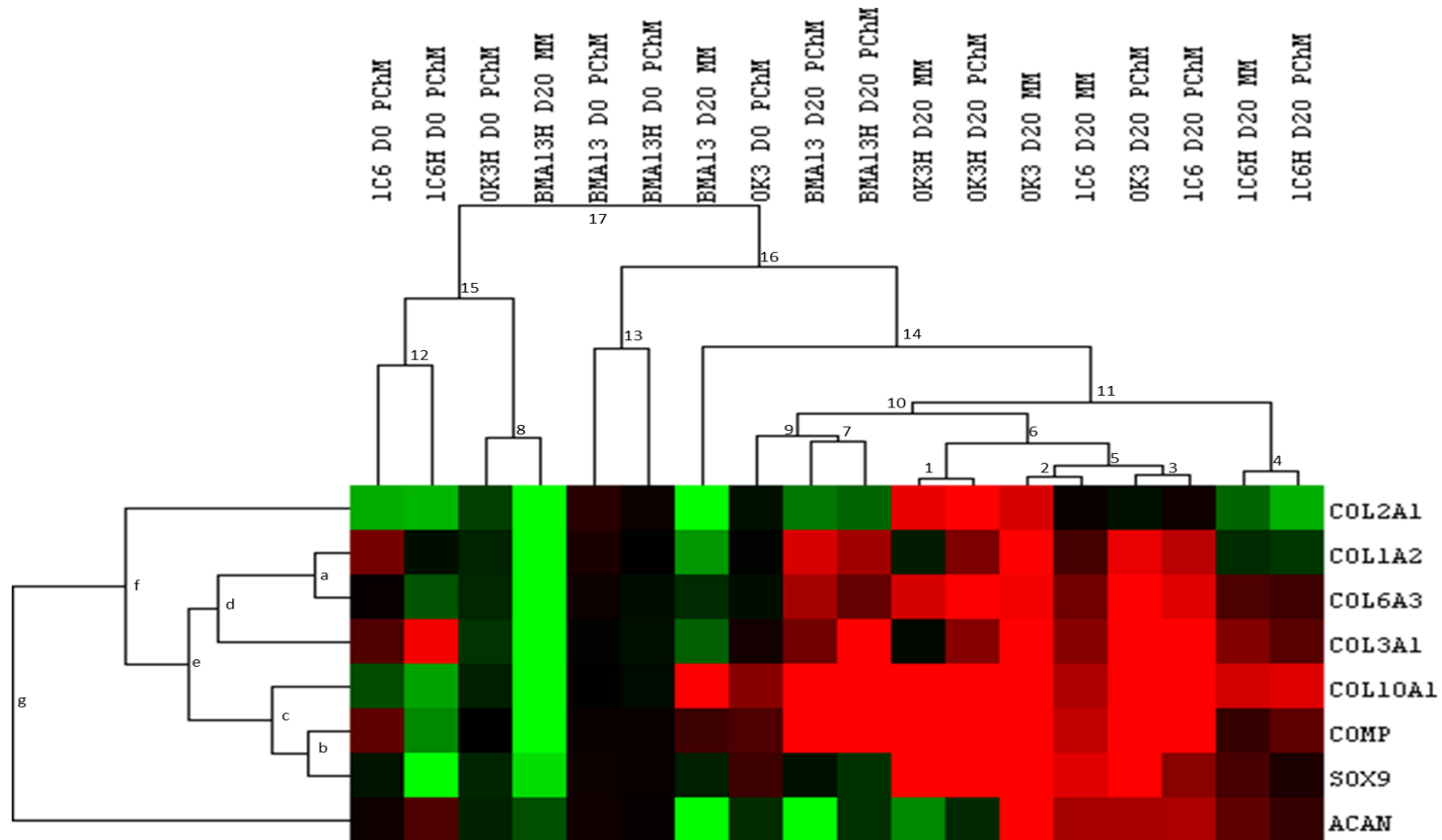


**Figure 6-24. Complete gene expression hierarchical clustering dendrograms and heatmap.** Samples (excluding the day 0 MM) were subjected to hierarchical clustering to find between sample group correlations in expression patterns. Red indicates upregulated genes, green downregulated genes and black no change in expression. All expression changes are determined relative to the day 0 MM condition. Each cluster is assigned a number or letter and the corresponding correlation coefficients are listed in Table 6-1. PD level of cells as as follows: OK3 PD6, OK3H PD50, BMA13 PD1, BMA13H PD18, 1C6 PD36, 1C6H PD107.

**Table 6-1. Dendrogram clustering correlation coefficients.** Each cluster (referred to as a node in the software) has been assigned a letter or a number and the corresponding correlation coefficients reported by Cluster 3.0 are listed. (A) Sample clustering dendrogram information, (B) Gene clustering dendrogram information. Coefficients are listed in decreasing numerical order, i.e. strongest positive correlation first.

<b>A</b>	<b>Cluster</b>	<b>Correlation co-efficient</b>
	1	0.967879
	2	0.961132
	3	0.955835
	4	0.93931
	5	0.913776
	6	0.805275
	7	0.800285
	8	0.781219
	9	0.774547
	10	0.673164
	11	0.624597
	12	0.452949
	13	0.379659
	14	0.368298
	15	0.149904
	16	-0.000690
	17	-0.272853

<b>B</b>	<b>Cluster</b>	<b>Correlation co-efficient</b>
	a	0.915010
	b	0.896799
	c	0.810271
	d	0.680196
	e	0.606606
	f	0.452498
	g	0.175859

A more detailed analysis of the PCR data is presented in the form of the box and whisker plots of up- and down regulation of genes in Figure 6-25 OK3, Figure 6-26 OK3H, Figure 6-27 BMA13, Figure 6-28 BMA13H, Figure 6-29 1C6 and Figure 6-30 1C6H.

When gene expression in the transduced cells day 0 MM expression was relative to the parental day 0 MM media there were differences apparent in the basal expression levels, particularly in OK3H compared to OK3 where 4 genes were expressed at levels > 2 fold higher (*COL1A2*, *COL3A1*, *COL6A3*, *ACAN*) with 2 of these (*COL3A1* and *ACAN*) being deemed significant at  $p \leq 0.05$ . Similarly, 1C6H day 0 MM had upregulation in comparison to OK3 day 0 MM in all 8 genes with significant upregulation in *COL1A2*, *COL2A1*, *COL3A1*, *ACAN*, *COMP* and *SOX9*. As such all determinations of gene expression changes were expressed relative to the specific cell type day 0 MM to establish changes due to intervention not inherent differences post transduction.

At day 20 of the 96 expression changes determined a majority of 60% (67) were upregulations with 76% (51) of these being statistically significant ( $p \leq 0.05$ ), of the remaining 30% (29) downregulations 45% (13) were statistically significant. Significant downregulation was almost exclusively seen in the MSCs BMA13 and BMA13H where for BMA13 MM 6 genes were downregulated, 3 significantly (*COL2A1*, *COL3A1* and *ACAN*), and for BMA13H MM all 8 genes were downregulated, all but *ACAN* significantly so. *ACAN* was also significantly downregulated in BMA13 cultured in PChM. Otherwise only *COL2A1* was significantly downregulated in 1C6H in both MM and PChM.

Of the upregulated expression changes at day 20 all eight genes examined were most upregulated in either the primary chondrocytes OK3 (*COL1A2* 8.9 fold, *COL3A1* 39.5 fold, *COL10A1* 1272 fold, *ACAN* 11.47 fold) or the transduced chondrocytes OK3H (*COL2A1* 49.52 fold, *COL6A3* 12.73 fold, *COMP* 8135 fold, *SOX9* 133.1 fold).

BMA13 and BMA13H cultures showed the greatest variation in gene expression as a result of culture PChM compared to MM. In contrast for OK3/OK3H and 1C6/1C6H several genes were found to be significantly upregulated in either MM or PChM as indicated in

Figure 6-31.

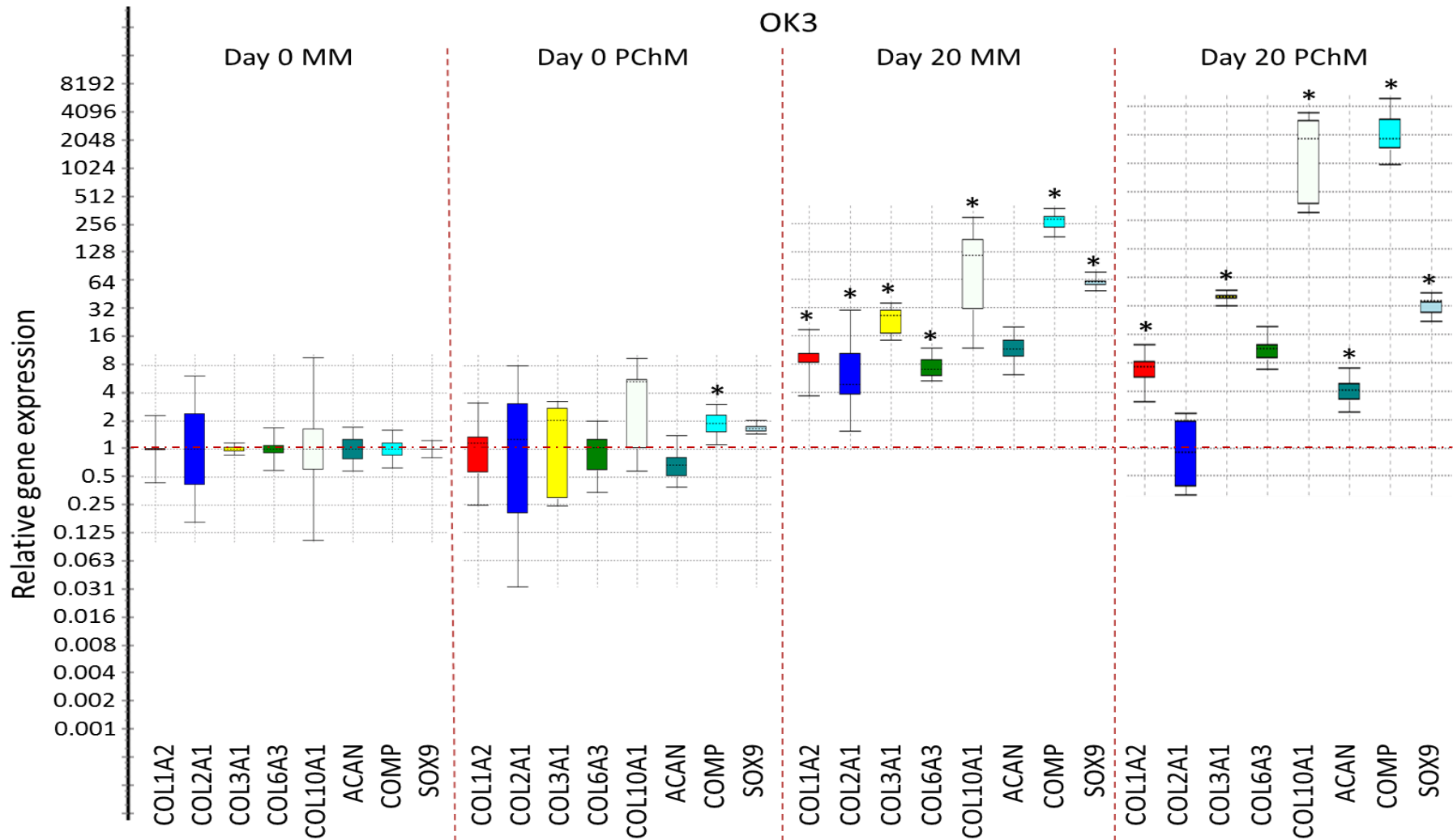


**Figure 6-25. Box and whisker plots of relative gene expression in OK3 cell pellets.** Changes in gene expression were determined using the  $2^{\Delta\Delta CT}$  with expression relative to the day 0 MM sample. The box represents the interquartile range, the whiskers the outer quartiles and the line the median expression. N=3x3 pellets, \*p<0.05. Cells were used at PD6.

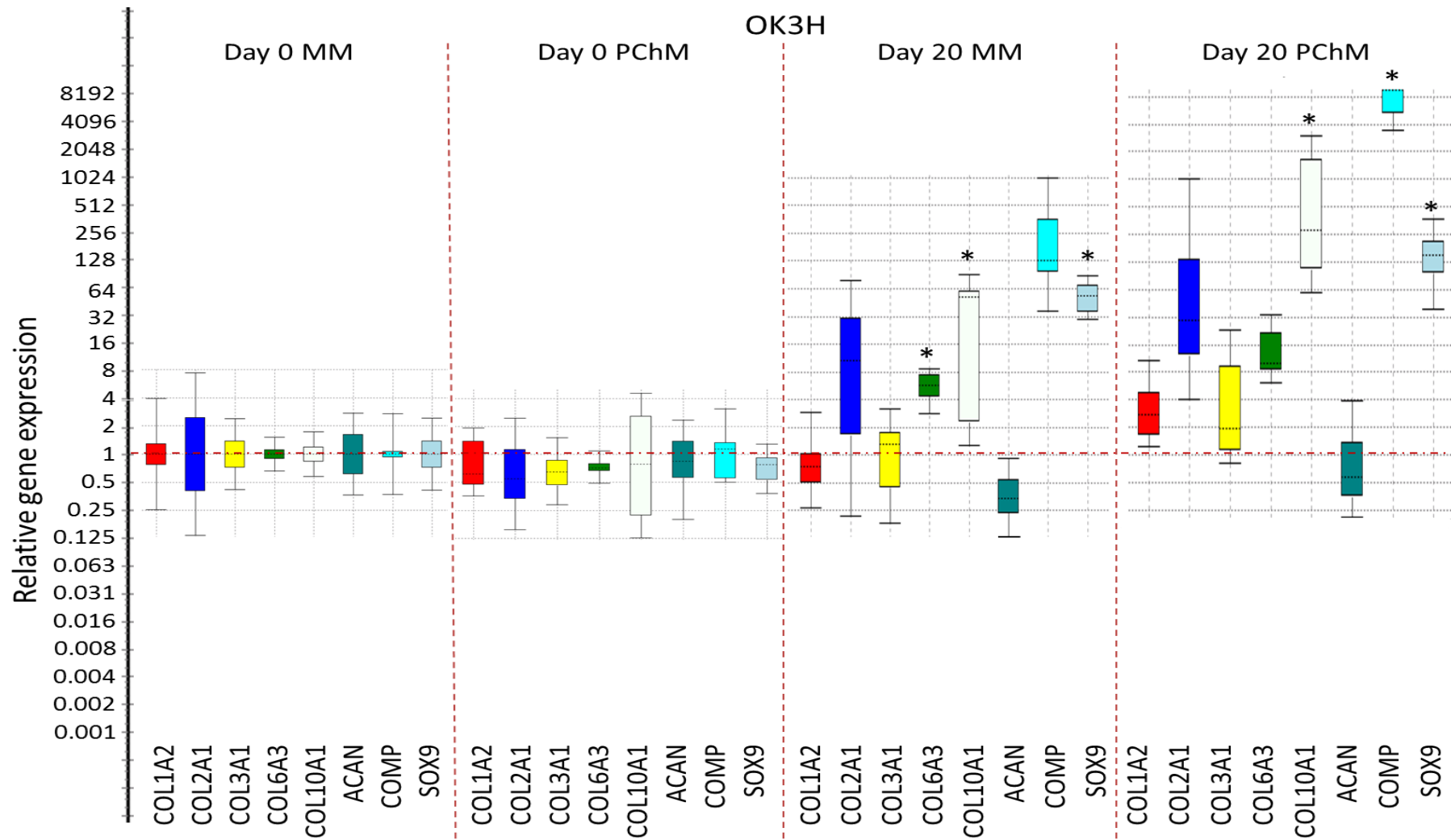


**Figure 6-26. Box and whisker plots of relative gene expression in OK3H cell pellets.** Changes in gene expression were determined using the  $2^{\Delta\Delta CT}$  with expression relative to the day 0 MM sample. The box represents the interquartile range, the whiskers the outer quartiles and the line the median expression. N=3x3 pellets, \*p<0.05. Cells were used at PD50.

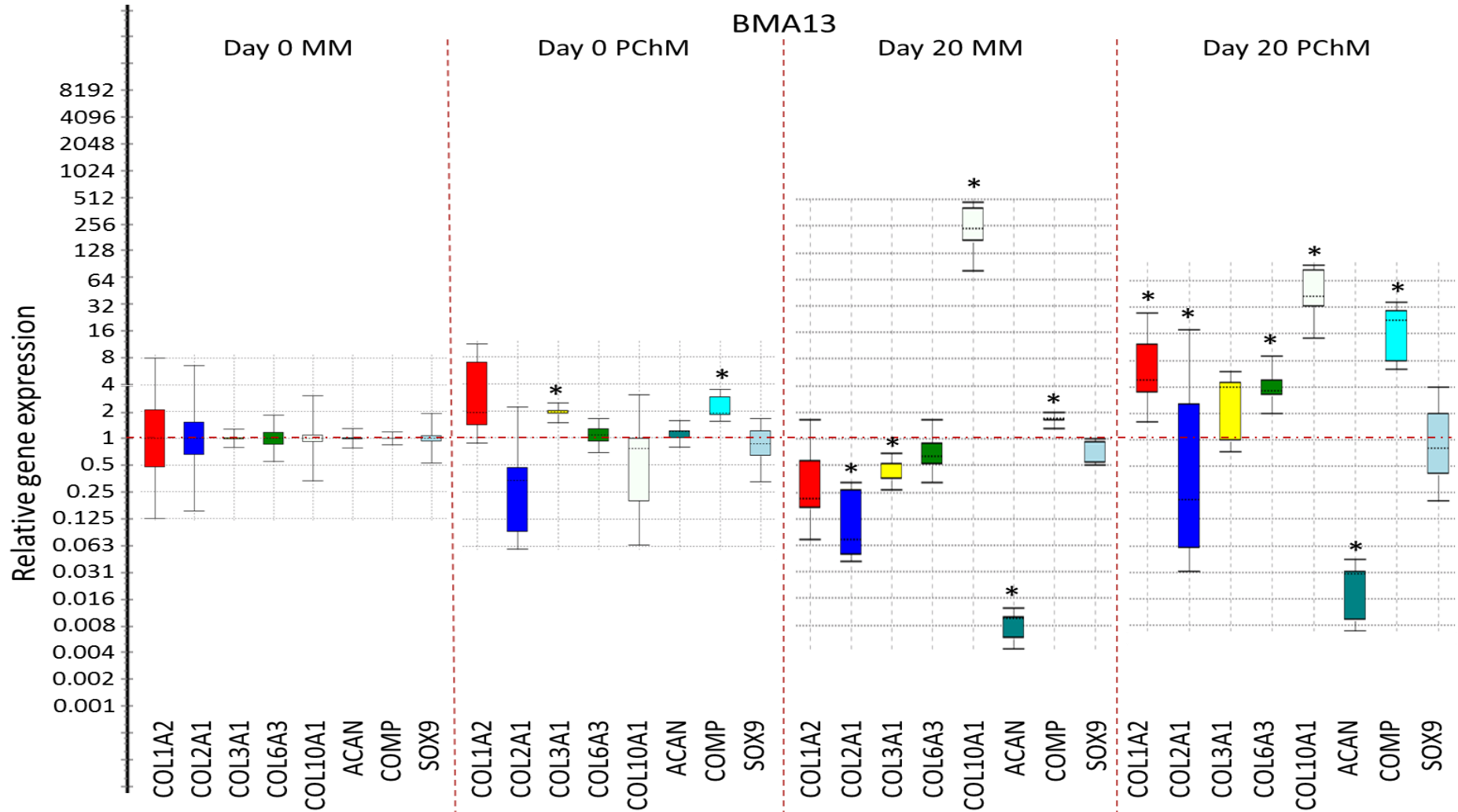


**Figure 6-27. Box and whisker plots of relative gene expression in BMA13 cell pellets.** Changes in gene expression were determined using the  $2^{\Delta\Delta CT}$  with expression relative to the day 0 MM sample. The box represents the interquartile range, the whiskers the outer quartiles and the line the median expression. N=3x3 pellets, \*p<0.05. Cells were used at PD1.

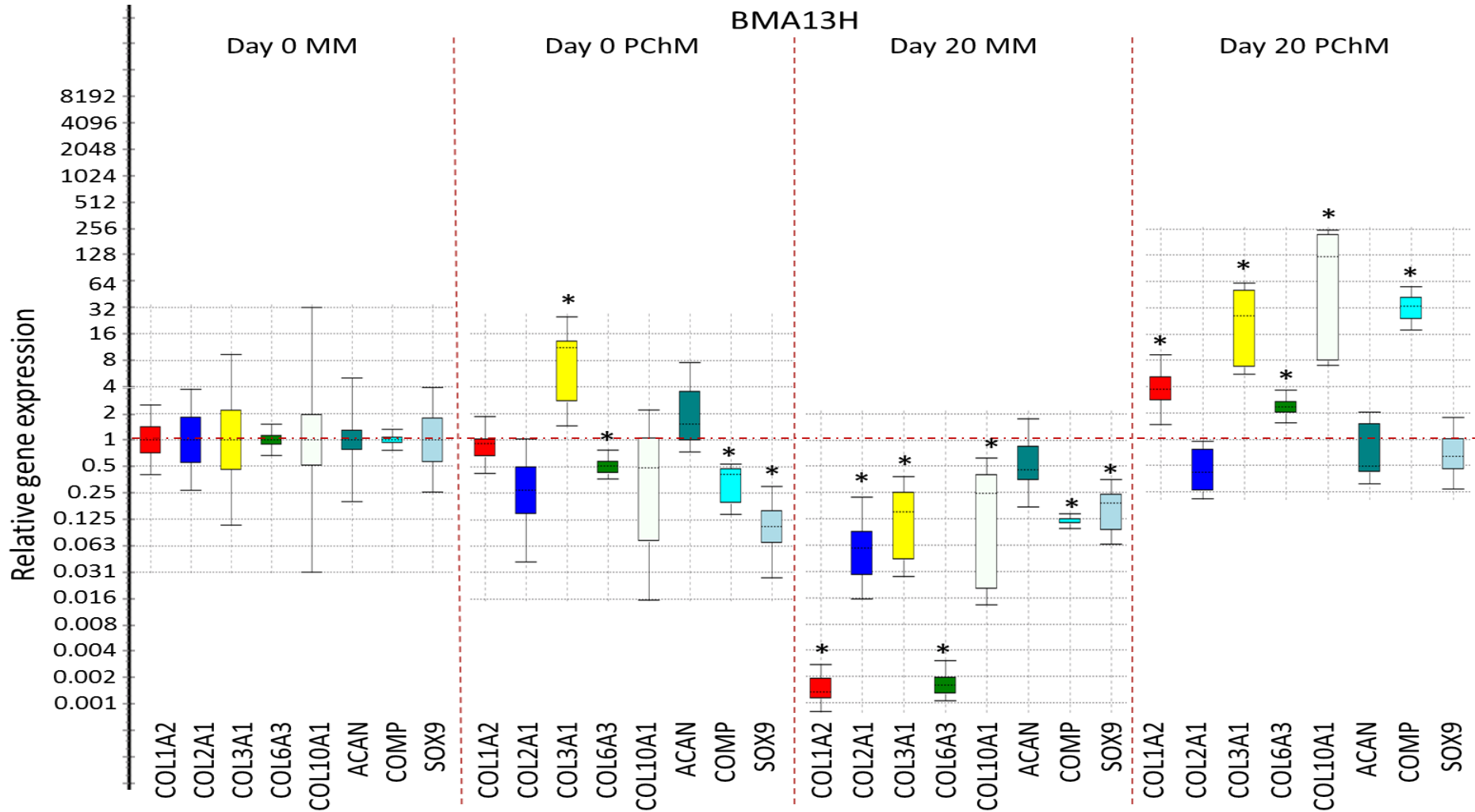


**Figure 6-28. Box and whisker plots of relative gene expression in BMA13H cell pellets.** Changes in gene expression were determined using the  $2^{\Delta\Delta CT}$  with expression relative to the day 0 MM sample. The box represents the interquartile range, the whiskers the outer quartiles and the line the median expression. N=3x3 pellets, \* $p \leq 0.05$ . Cells were used at PD18.

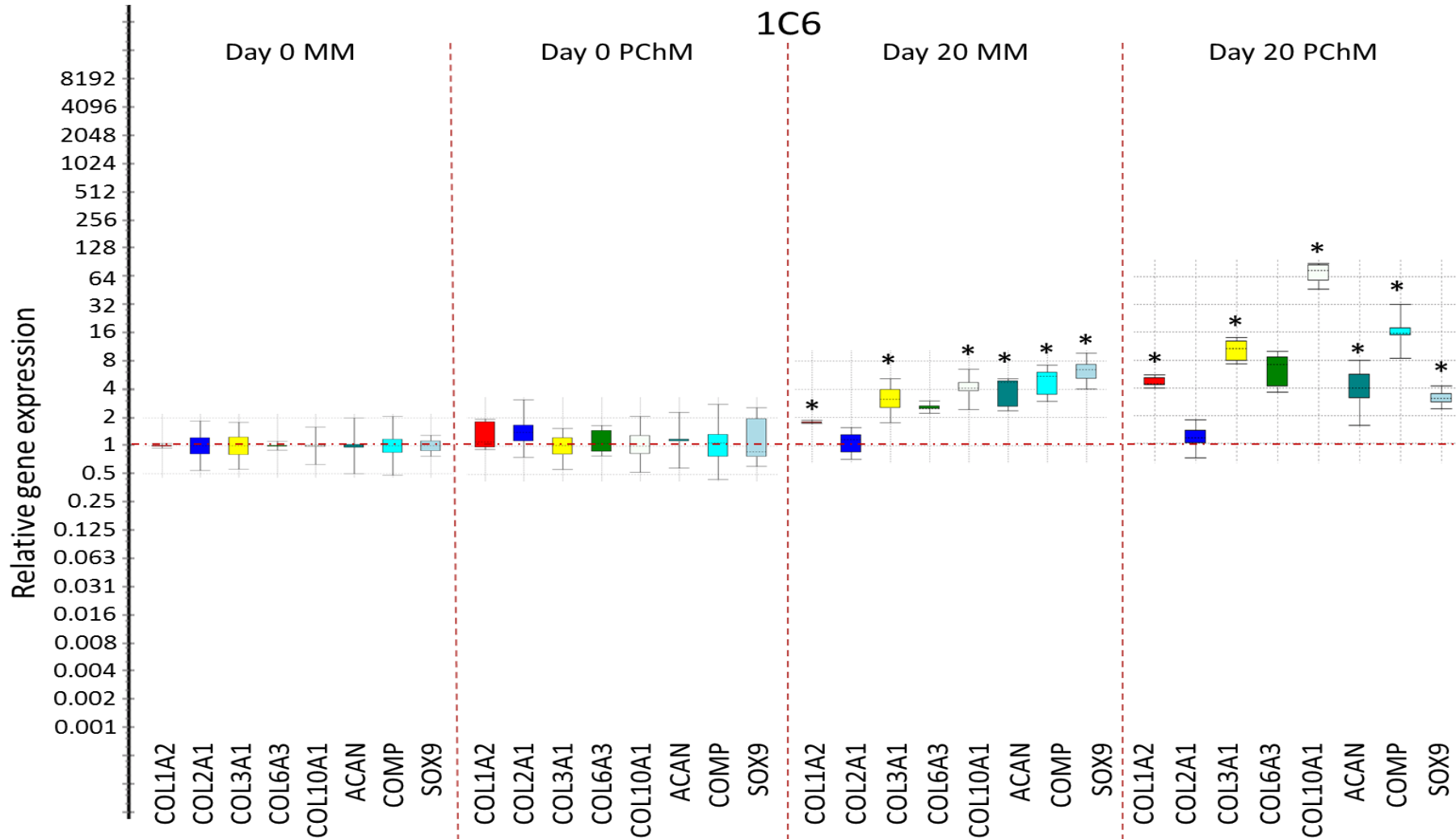


**Figure 6-29. Box and whisker plots of relative gene expression in 1C6 cell pellets.** Changes in gene expression were determined using the  $2^{\Delta\Delta CT}$  with expression relative to the day 0 MM sample. The box represents the interquartile range, the whiskers the outer quartiles and the line the median expression. N=3x3 pellets, \*p<0.05. Cells were used at PD36.

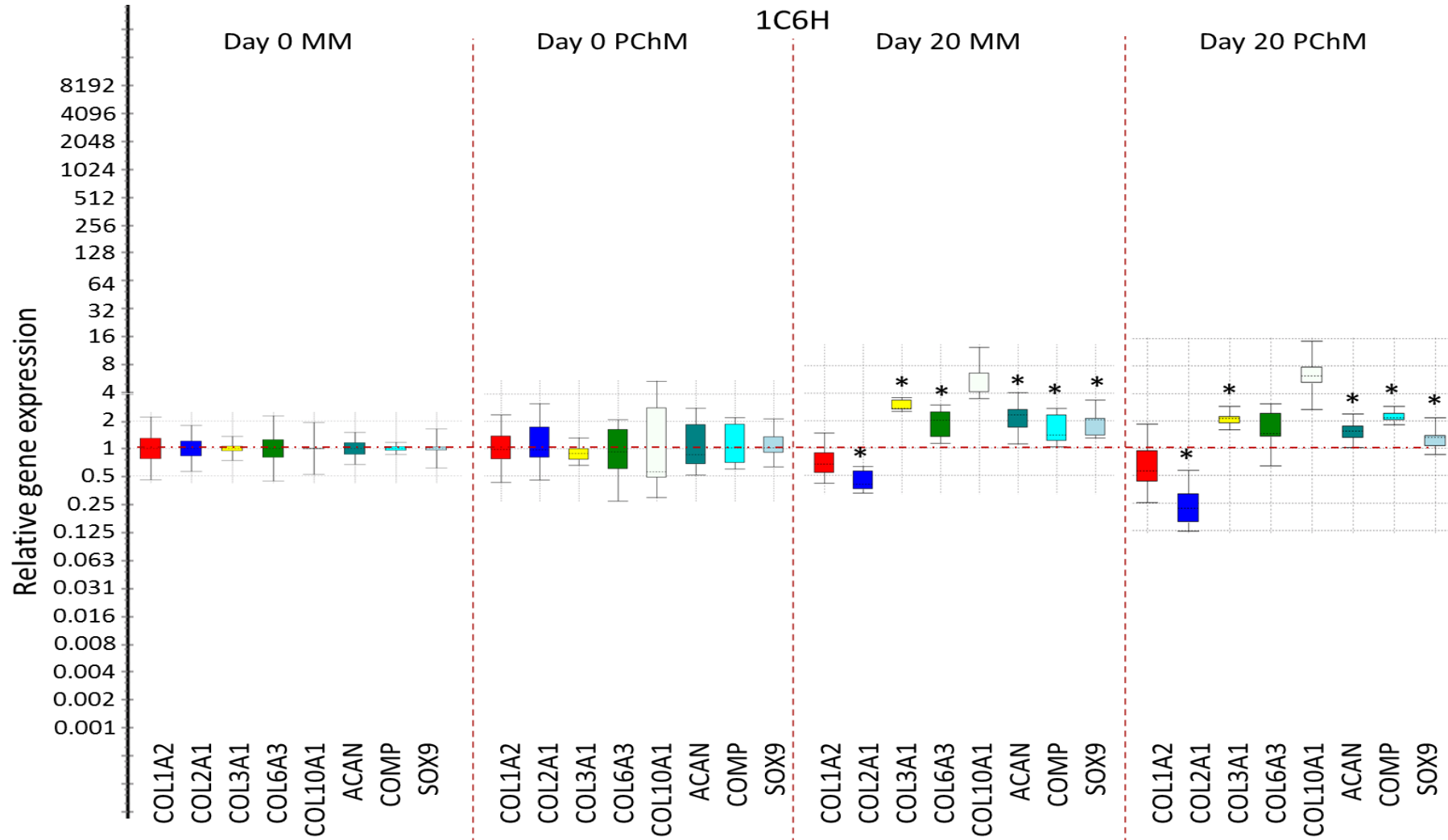


**Figure 6-30. Box and whisker plots of relative gene expression in 1C6H cell pellets.** Changes in gene expression were determined using the  $2^{\Delta\Delta CT}$  with expression relative to the day 0 MM sample. The box represents the interquartile range, the whiskers the outer quartiles and the line the median expression. N=3x3 pellets, \*p<0.05. Cells were used at PD107.

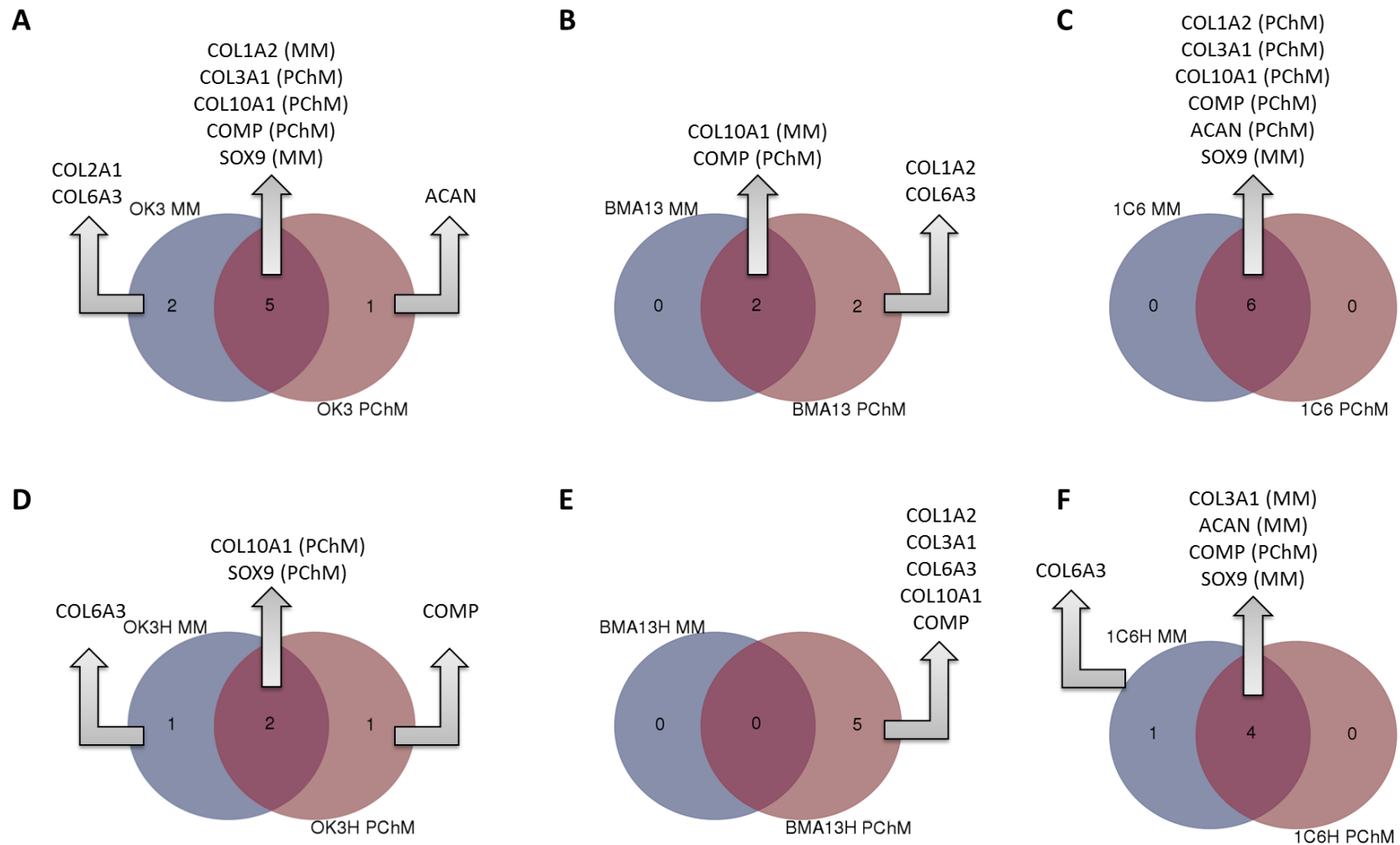


**Figure 6-31. Genes upregulated in both MM and PChM.** Venn diagrams of genes statistically significantly upregulated ( $p \leq 0.05$ ) in OK3 (A), BMA13 (B), 1C6 (C), OK3H (D), BMA13H (E), and 1C6H (F) in MM and PChM, overlap indicates genes upregulated in common in both MM and PChM. All expression changes are determined relative to the day 0 MM condition. The condition in which upregulation had a greater magnitude indicated in parentheses for common genes.

## 6.4.10 Pellet histology

### 6.4.10.1 Haematoxylin and eosin staining

H and E staining was first performed on porcine articular cartilage tissue sections shown in Figure 6-32. The cartilage tissue had variation in the depth of colour obtained from eosin staining depending on the cartilage tissue zone.

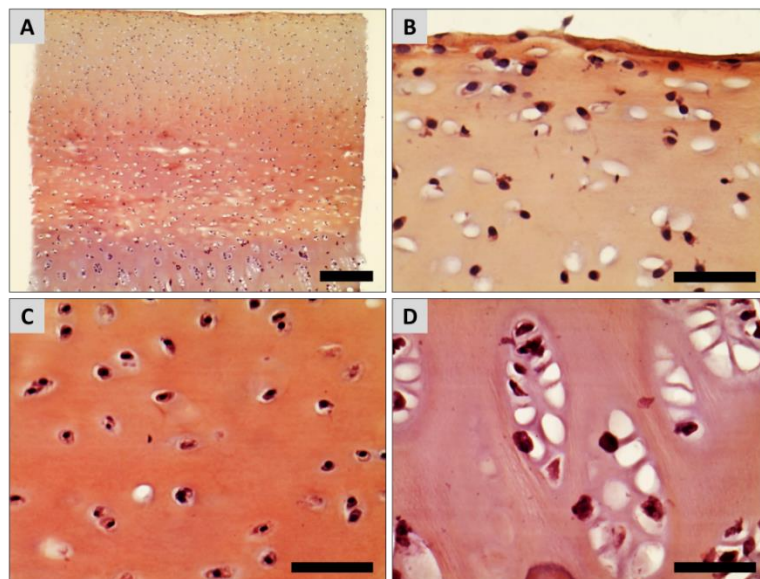


**Figure 6-32. H and E staining of porcine articular cartilage.** Brightfield micrographs of 10  $\mu\text{m}$  sectioned porcine articular cartilage stained with H and E to illustrate normal articular cartilage structure. Full depth cartilage is illustrated in (A), the superficial and upper middle zone in (B), the middle zone in (C) and the deep zone in (D). Scale bar=250  $\mu\text{m}$  (A), 50  $\mu\text{m}$  (B), (C) and (D).

Pellet tissue sections were then stained for all pellets in both MM and PChM at day 1 (allowing approximately 24 hours for pellet formation) and day 20 (Figure 6-33).

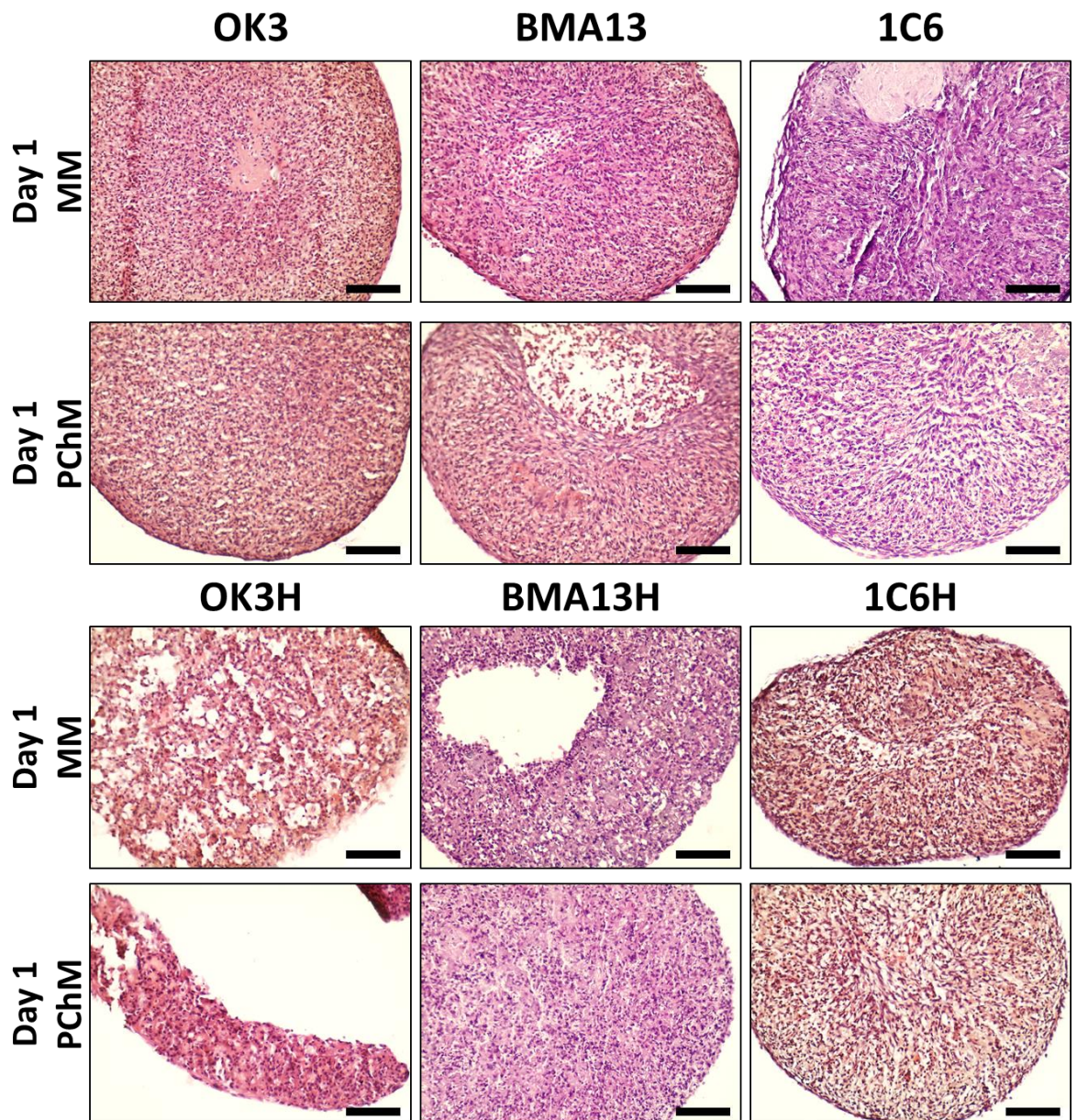


**Figure 6-33. H and E staining of pellets at day 1.** Brightfield micrographs of H and E stained 10  $\mu\text{m}$  sections of pellets after 24 hours cultured in MM or PChM. Scale bar=100  $\mu\text{m}$ . PD level for cells was as follows: OK3 PD6, OK3H PD50, BMA13 PD6, BMA13H PD16, 1C6 PD36, 1C6H PD86.

By day 1, immediately following pellet formation, differences in cell morphology could be seen following H and E staining with the appearance of elongated cells at the periphery of pellets, especially in BMA13, and more rounded cells within the pellet cores (Figure 6-34A). As a result of pellets forming via folding rather than overall contraction of the mass around the centre it was possible for these more elongated cells to be folded into the pellet centre (Figure 6-34B). At this early stage there were no overt differences in the appearance of pellets cultured in MM or PChM.

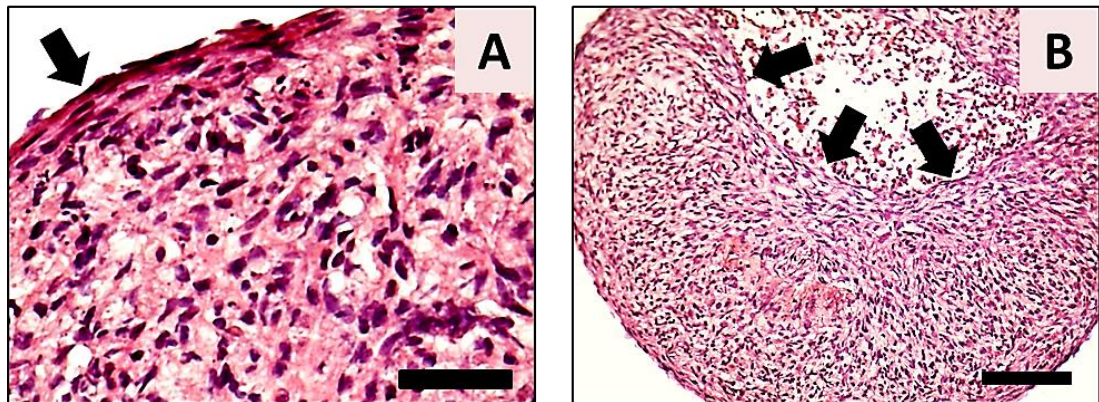


**Figure 6-34. H and E staining.** Brightfield micrographs of elongated cells (arrows) at the periphery of pellets at day 1 (A) Scale bar = 50  $\mu$ m, (B) scale bar = 100  $\mu$ m.

By day 20 H and E staining showed clear differences between pellets cultured in MM compared to PChM that were most apparent in OK3 and BMA13 primary cell pellet cultures (Figure 6-35). OK3 pellets cultured in MM were very small and had minimal staining of a continuous intercellular ECM with the exception of a region around the edge of the pellet. BMA13 also had minimal intercellular staining; additionally the pellets were poorly integrated appearing friable and prone to splitting during sectioning. In contrast, culture of OK3 in PChM led to the production of a more continuous ECM with a reduced cell density particularly towards the centre of the pellet. BMA13 on the other hand had clear regional variation in ECM and cell morphology with a more cartilaginous appearance in a broad peripheral band encompassing around half the visible area with cells sometimes located in lacuna-like structures and at a much reduced cell density. Cells located more centrally were smaller and more numerous with no evidence of lacuna development.

OK3H and BMA13H in MM at day 20 were similar in appearance to day 1; culture in MM was less detrimental to the overall formation of pellets than with the corresponding primary cells.

However, the changes seen in primary cells in PChM were also less apparent in the transduced cells. 1C6H pellets, in contrast to the other transduced cell pellets, were very small with only

minimal intercellular matrix apparent in both MM and in PChM, pellets had a spongy or porous appearance with considerable amounts of discontinuity in the ECM, with the exception of a narrow peripheral band or capsule encompassing the pellet.

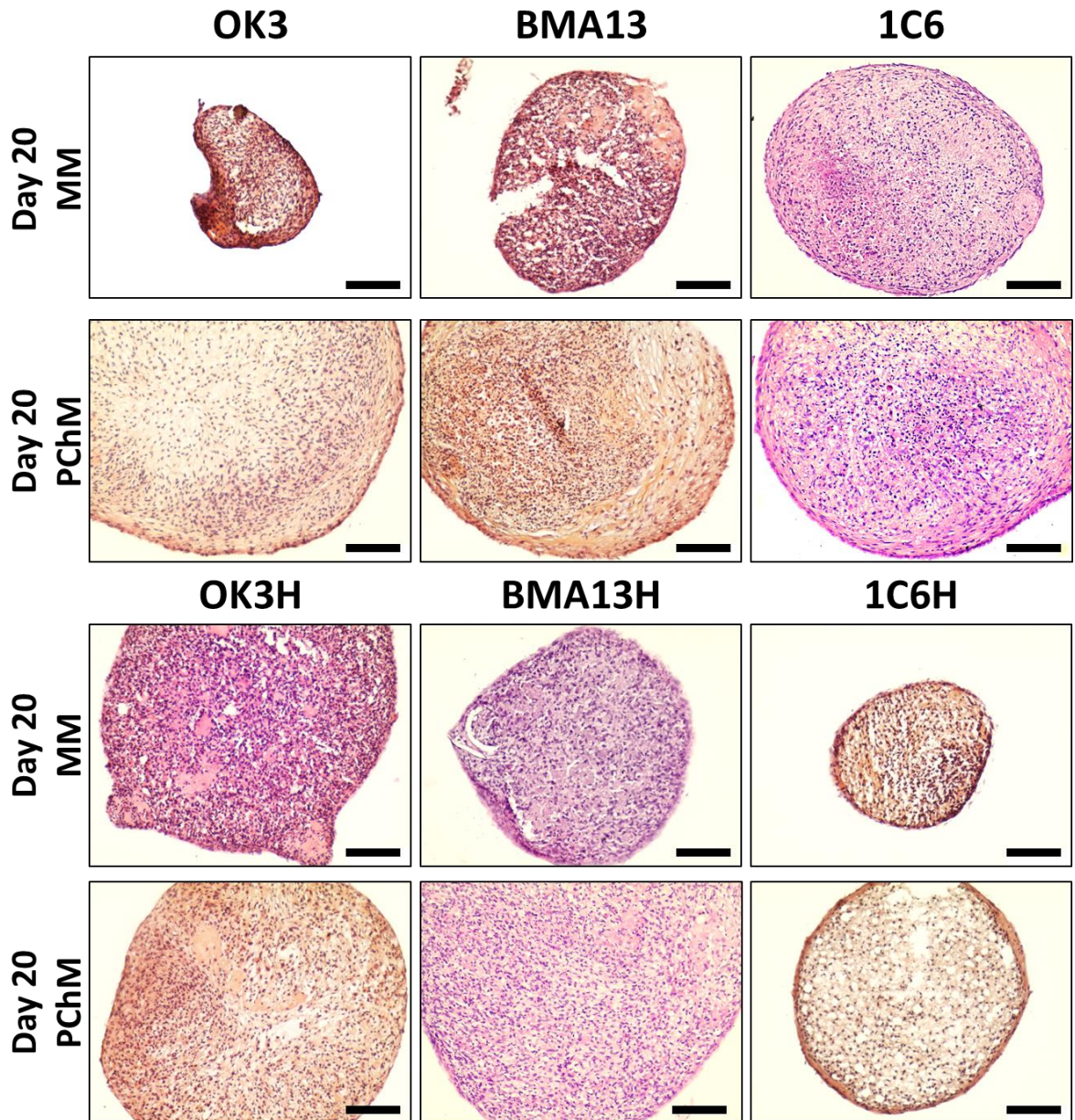


**Figure 6-35. H and E staining of pellets at day 20.** Brightfield micrographs of H and E stained 10  $\mu$ m sections of pellets after 20 days cultured in MM or PChM. Scale bar=100  $\mu$ m. PD level for cells was as follows: OK3 PD6, OK3H PD50, BMA13 PD6, BMA13H PD16, 1C6 PD36, 1C6H PD86.

#### 6.4.10.2 Picrosirius red staining

Picrosirius red staining was first performed on porcine articular cartilage and tendon sections as shown in Figure 6-36. Picrosirius red results in red staining where collagen is present on a yellow background as a result of the picric acid content. Cartilage tissue stained relatively uniformly throughout for collagen with no obvious fibre formation whilst tendon had strong collagen alignment with a wave-like pattern highlighted by staining as expected.

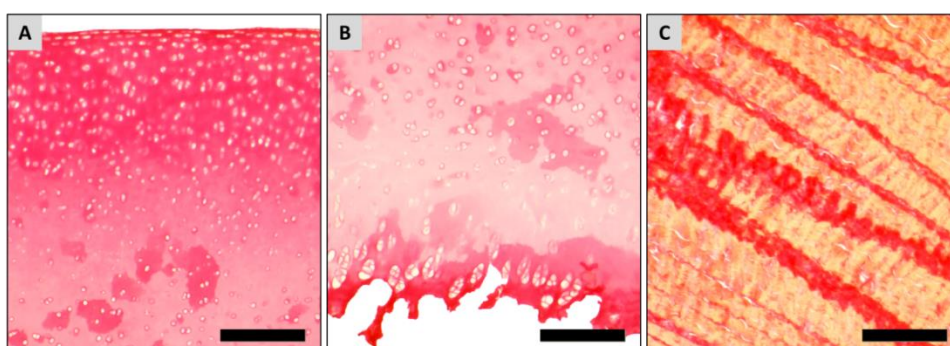


**Figure 6-36. Picrosirius red staining of porcine cartilage and tendon.** Brightfield micrographs of 10  $\mu\text{m}$  tissue sections of porcine cartilage superficial and middle (A) and deep and calcified (B) zones and tendon tissue illustrating the strong collagen alignment. Scale bar=100  $\mu\text{m}$ .

Pellet sections were then stained for all pellets following culture in both MM and PChM at day 1 (Figure 6-37) and at 20 days (Figure 6-38). At day 1, after 24 hours of culture there was some evidence of collagen fibre formation in most of the sections. Although for the most part the fibres remained small imbuing sections with a pinkish hue there were also regions of intensely red positive staining indicating very rapid changes within the cells leading to patchy collagen synthesis by day 1 staining. By day 20 all pellets cultured in MM still stained only weakly for collagen with the exception of 1C6 where staining intensity was of a similar level to that of pellets cultured in PChM. All primary cell pellets cultured in PChM stained strongly for collagen throughout the pellet, tending to be stronger and more fibrous at the periphery. None of the sections had the smooth/uniform appearance found in articular cartilage with all having some degree of fibrous

staining as collagen surrounded the cell lacunae. This was particularly apparent in the BMA13 PChM pellets where staining was highly heterogeneous with strong regional variation in the pellet appearance and contrasted with OK3 where staining was much more uniform but still obviously surrounding lacunae. Transduced cell pellets all stained more weakly for collagen than the corresponding parental cell pellet.

Images of picosirius red stained sections were also acquired under cross polarised light (Figure 6-39). Samples under cross polarised light are only visible if birefringent material is present, i.e. organised collagen fibres; picosirius red staining enhances this and the resulting birefringent fibres are coloured according to their size and degree of organisation. Large highly organised fibres result in orange/red images with increasingly smaller and less organised fibres showing yellow and then green.

Images obtained under polarised light show more clearly the trends in collagen deposition. BMA13 in PChM contains large amounts of large organised fibres encapsulating the pellet with smaller fibres in the centre. 1C6 also has considerable birefringence; however, there were fewer orange/red fibres and an increased number of green fibres indicative of a finer collagen network. OK3 had little evidence of central collagen fibre organisation but did have a relatively narrow band of encapsulation. Transduced pellets clearly contained much less organised collagen fibres than primary pellets with only minimal birefringence apparent.

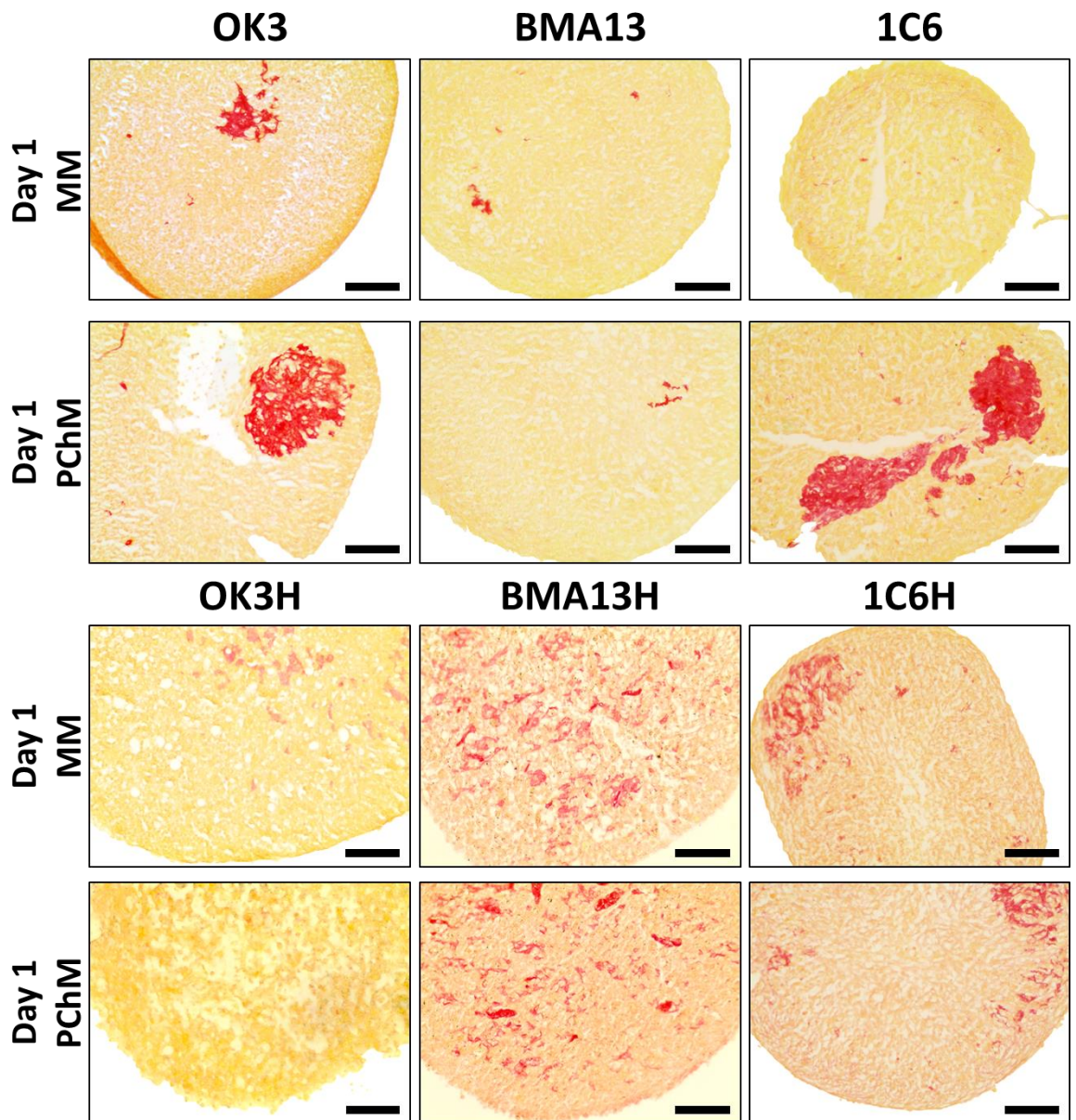


**Figure 6-37. Picosirius red collagen staining at day 1.** Brightfield micrographs of picosirius red stained 10  $\mu\text{m}$  sections of pellets at day 1 after 24 hours culture in MM or PChM. Scale bar=100  $\mu\text{m}$ . PD level for cells was as follows: OK3 PD6, OK3H PD50, BMA13 PD6, BMA13H PD16, 1C6 PD36, 1C6H PD86.

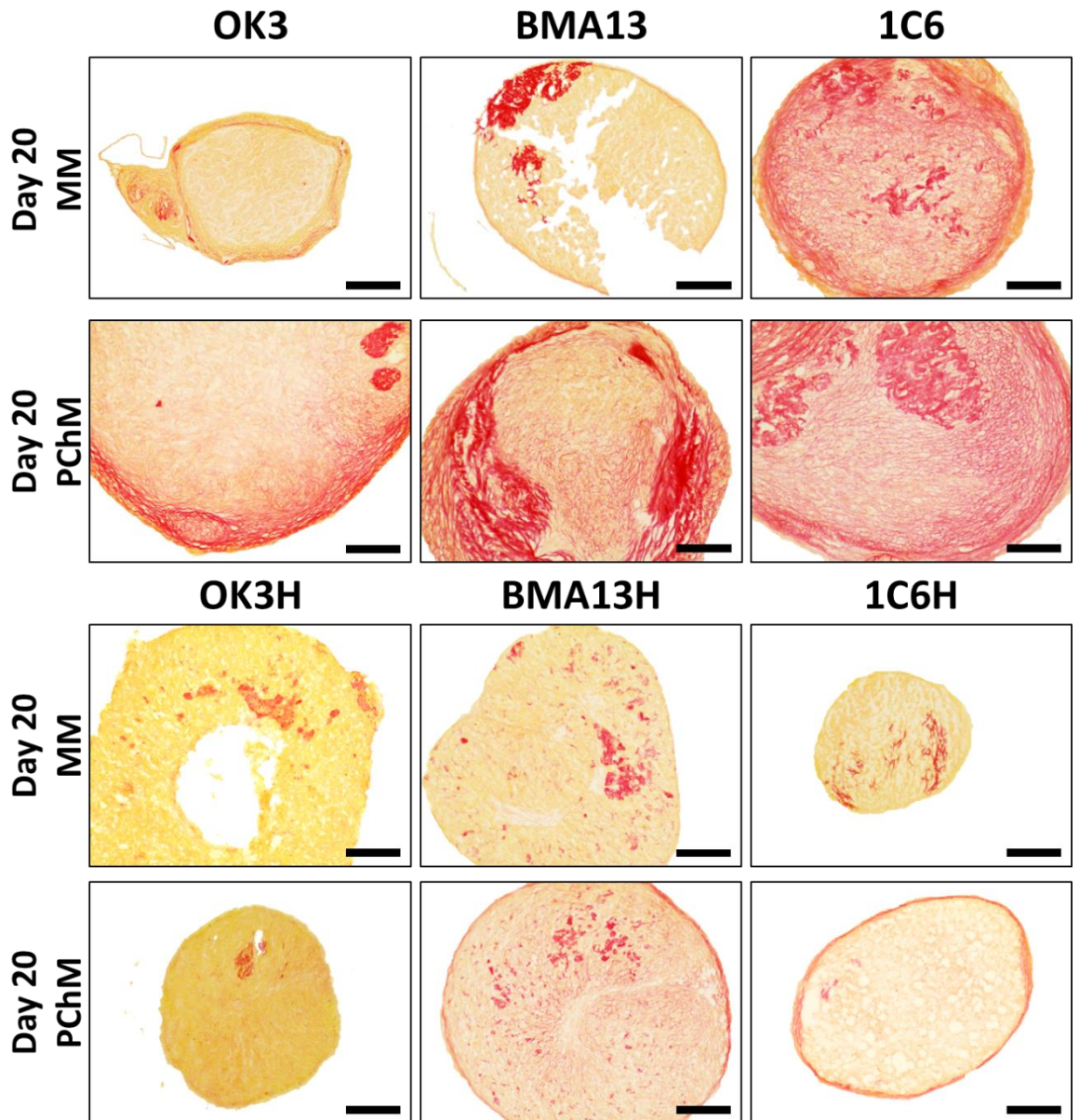


**Figure 6-38. Picosirius red collagen staining at day 20.** Brightfield micrographs of picosirius red stained 10  $\mu\text{m}$  sections of pellets at day 20 cultured in MM or PChM. Scale bar=100  $\mu\text{m}$ . PD level for cells was as follows: OK3 PD6, OK3H PD50, BMA13 PD6, BMA13H PD16, 1C6 PD36, 1C6H PD86.

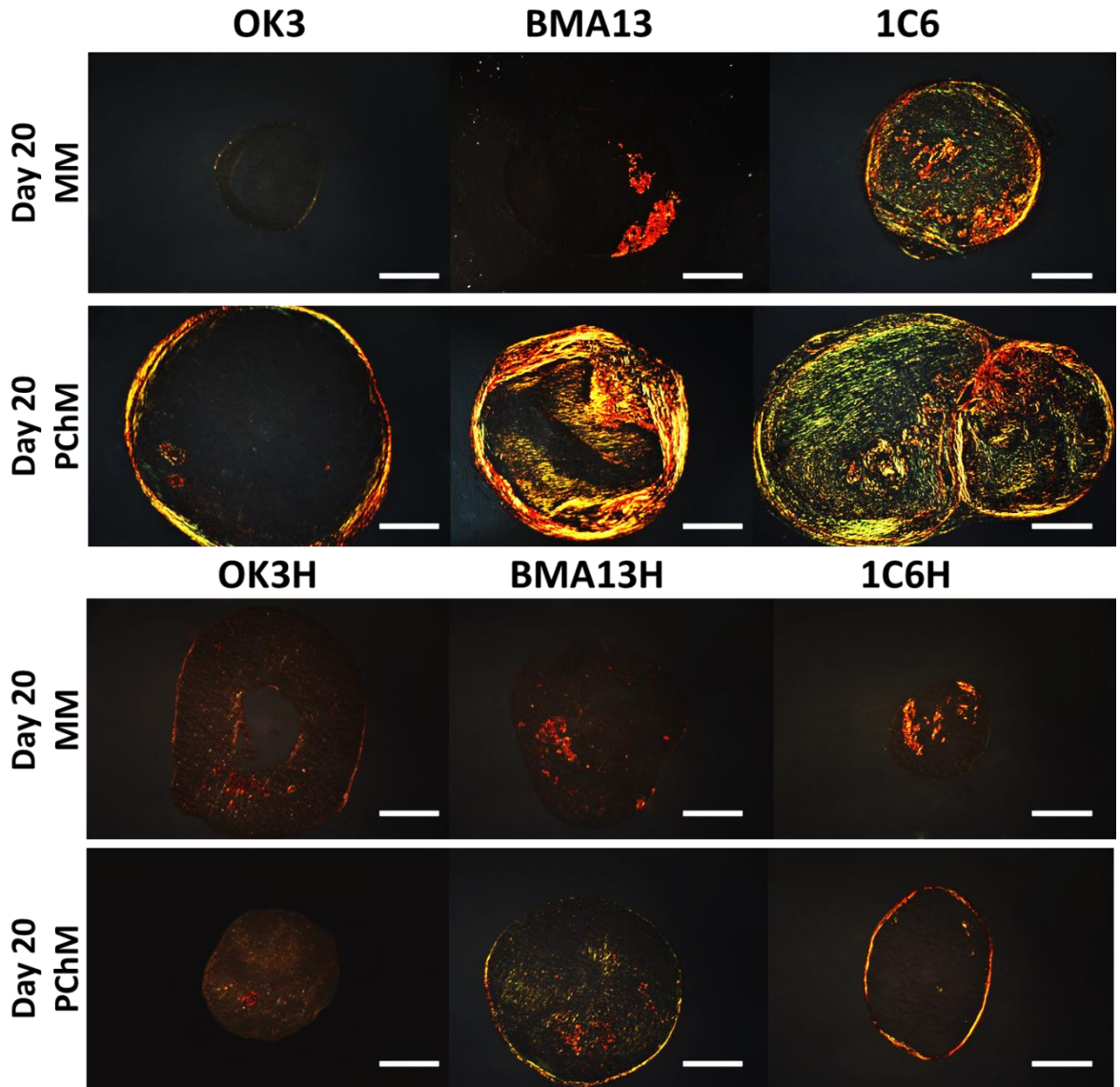


**Figure 6-39. Picrosirius red cross-polarised light collagen staining at day 20.** Cross-polarised light micrographs of picrosirius red stained 10  $\mu\text{m}$  sections of pellets at day 20 cultured in MM or PChM. Scale bar=250  $\mu\text{m}$ . PD level for cells was as follows: OK3 PD6, OK3H PD50, BMA13 PD6, BMA13H PD16, 1C6 PD36, 1C6H PD86.

### 6.4.10.3 Toluidine blue staining

Toluidine blue staining was first performed on porcine articular cartilage and E11 chick femur sections as shown in Figure 6-40. Toluidine blue is a metachromatic stain that results in purple staining where sGAG is present with blue staining of background structures e.g. nuclei. Cartilage stained strongly purple throughout with blue nuclei still visible within lacunae. The metachromatic nature of toluidine blue is best shown in the chick femur where only regional production of sGAG in areas that are undergoing endochondral ossification is apparent.

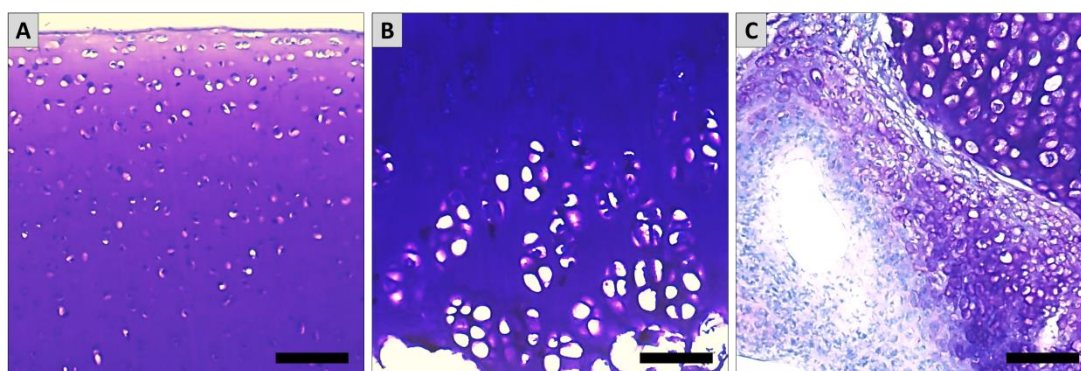


**Figure 6-40. Toluidine blue staining of porcine cartilage and E11 chick femur.** Brightfield micrographs of 10  $\mu\text{m}$  tissue sections of porcine cartilage superficial and middle (A) and deep and calcified (B) zones and E11 chick femur tissue illustrating metachromatic toluidine blue staining. Scale bar=100  $\mu\text{m}$ .

Pellet sections were then stained for all pellets in both MM and PChM at day 1 (Figure 6-41) and after 20 (Figure 6-42) days of culture in MM or PChM.

At day 1 there was no overt metachromatic staining apparent in any cell pellet. After 20 days in MM there was no staining in BMA13 pellets, some staining peripherally in OK3 and faint diffuse staining of 1C6. In contrast pellets cultured in PChM had increased metachromatic staining; this was apparent throughout the pellet ECM in OK3 pellets with some regions with slightly stronger metachromatic staining, more zonally, but more intensely in BMA13 and throughout 1C6 although only relatively weakly. Strongly stained regions in BMA13 coincided with the regions that also stained strongly for collagen with picrosirius red. Staining of transduced cell pellets was again

reduced in comparison to parental cell pellets. These staining results are in agreement with sGAG quantification by DMMB assay.

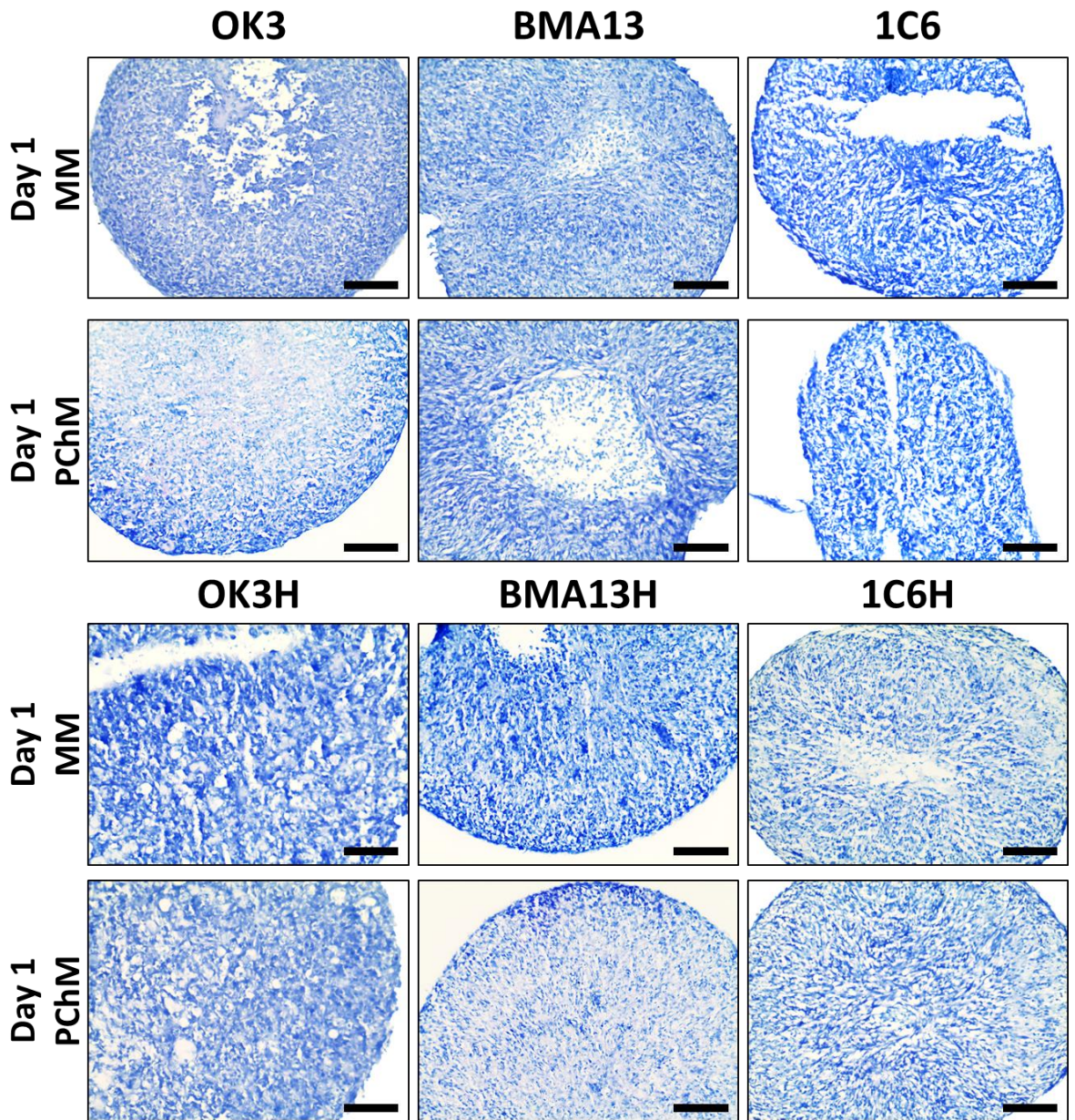


**Figure 6-41. Toluidine blue sGAG staining at day 1.** Brightfield micrographs of toluidine blue stained 10 µm sections of pellets at day 1 cultured in MM or PChM. Scale bar=100 µm. PD level for cells was as follows: OK3 PD6, OK3H PD50, BMA13 PD6, BMA13H PD16, 1C6 PD36, 1C6H PD86.

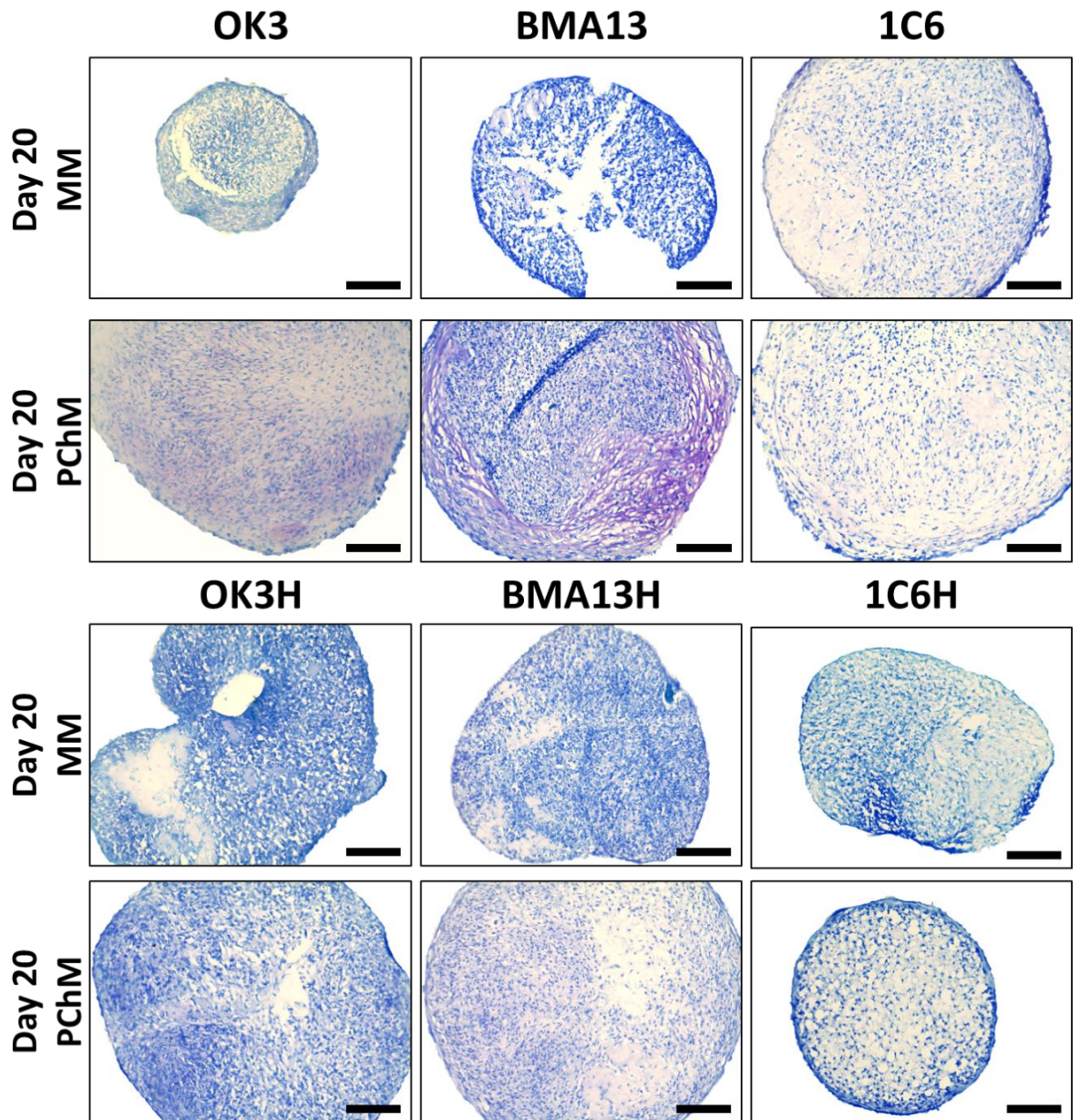


**Figure 6-42. Toluidine blue sGAG staining at day 20.** Brightfield micrographs of toluidine blue stained 10  $\mu$ m sections of pellets at day 20 cultured in MM or PChM. Scale bar=100  $\mu$ m. PD level for cells was as follows: OK3 PD6, OK3H PD50, BMA13 PD6, BMA13H PD16, 1C6 PD36, 1C6H PD86.

## 6.4.11 Pellet immunohistochemistry

### 6.4.11.1 Tissue controls

Antibodies against collagen I, collagen II, collagen VI, collagen X and aggrecan were first tested on positive control tissue samples with immunoperoxidase staining (Figure 6-43). All tissue samples were positive for the tested antibody and no non-specific staining was seen on any of the secondary antibody only negative controls.

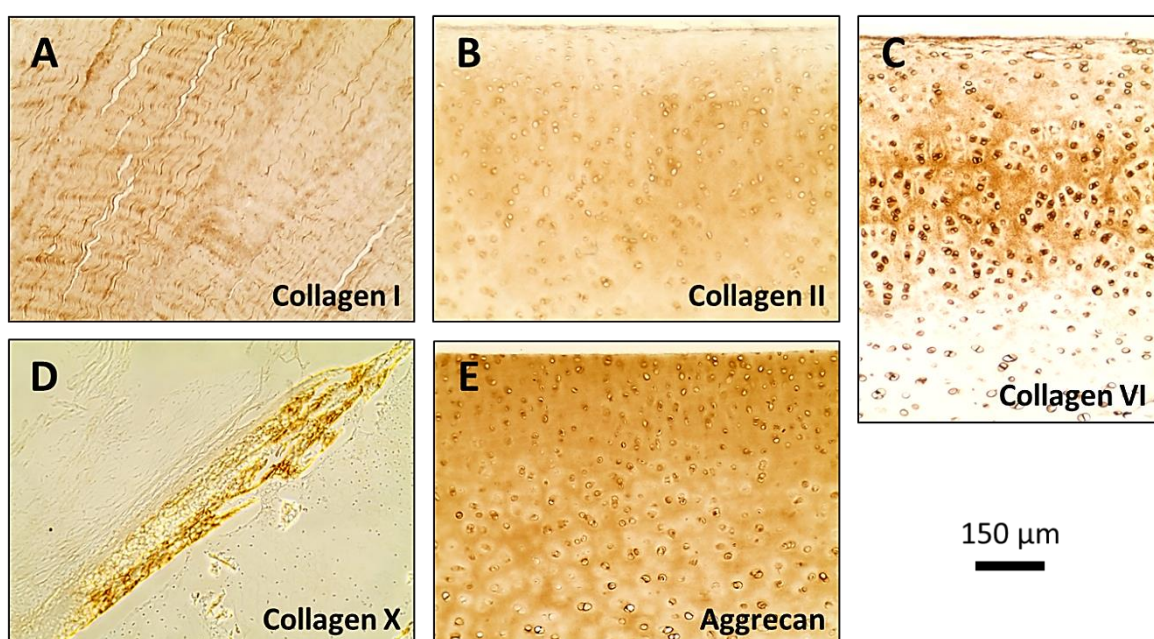


**Figure 6-43. Positive control antibody staining.** Positive controls for immunoperoxidase antibody staining using collagen I staining of porcine tendon (A), collagen II staining of porcine cartilage (B), collagen VI staining of porcine cartilage (C), collagen X staining of E11 chick femur (D) and aggrecan staining of porcine cartilage (E). (A), (B), (C) and (E) are brightfield images; (D) is taken under phase contrast to view unstained regions. Cartilage sections are oriented with the articular surface at the top of the image.

Pellet sections were then stained with all of the above antibodies. For all stains a negative control with the secondary antibody only were performed on the same slide for all samples and a positive tissue control was included. Again, there was no evidence of any non-specific staining when the primary antibody was omitted from the staining protocol.

Type I collagen staining in primary cell pellets (Figure 6-44) appeared to be slightly stronger following culture in MM compared to PChM with slightly stronger staining at the pellet periphery compared to the interior. Both OK3H and 1C6H barely stained for collagen type I; however, it was present with strong staining through BMA13H pellets in both MM and PChM.

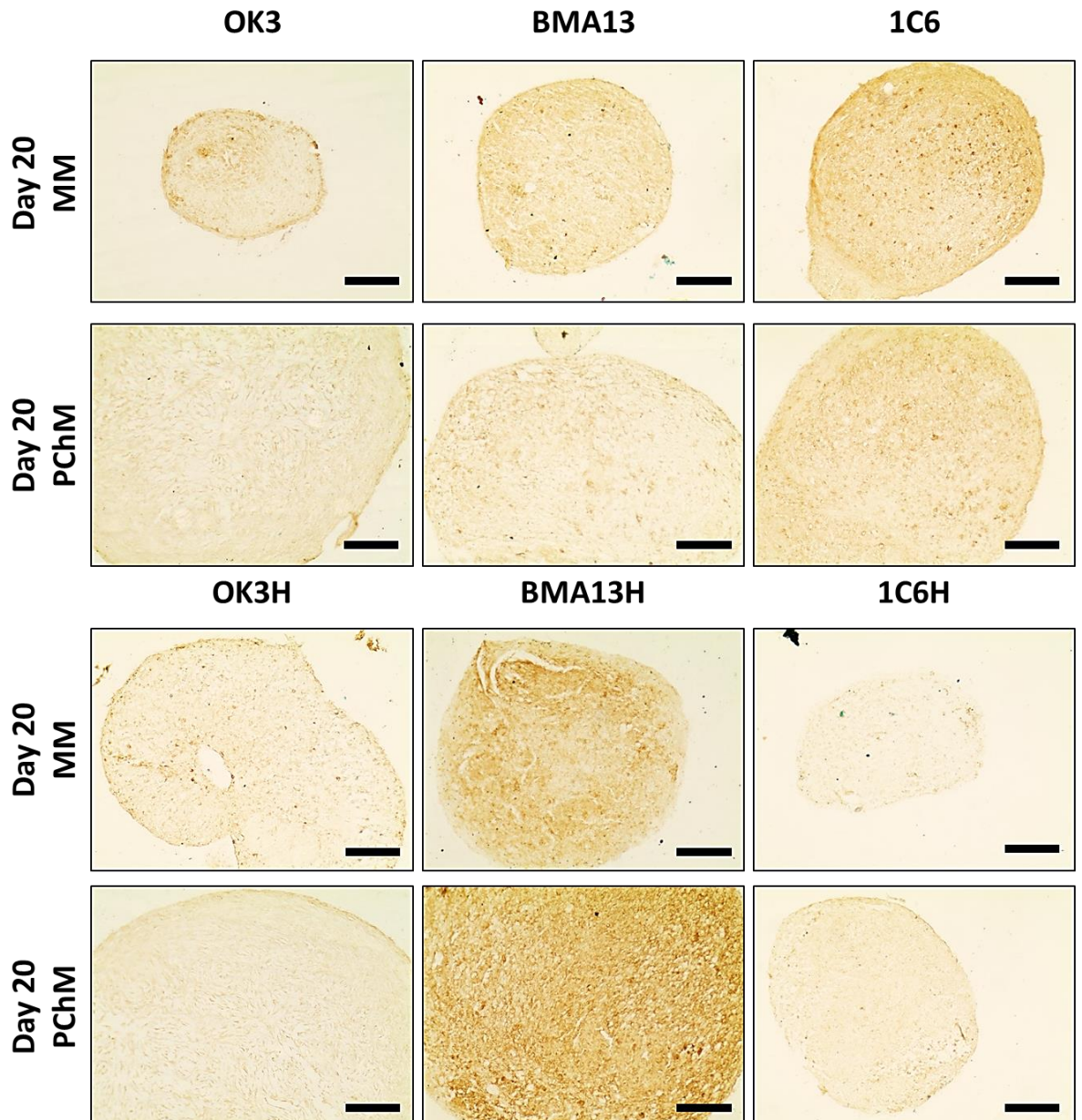


**Figure 6-44. Collagen I day 20 immunoperoxidase staining.** Representative brightfield images of collagen I immunoperoxidase stained sections of all pellets at day 20. Scale bar=100 µm. PD level for cells was as follows: OK3 PD6, OK3H PD50, BMA13 PD6, BMA13H PD16, 1C6 PD36, 1C6H PD86.

All pellets were positive to some extent for type II collagen (Figure 6-45). Interestingly ECM staining for collagen II was most apparent in OK3 MM cultures, these cultures also had significantly upregulated *COL2A1* when assessed using qRT-PCR. In other pellets the staining tended to be more localised to the cells and was more evident as a thin band at the periphery of the pellets.

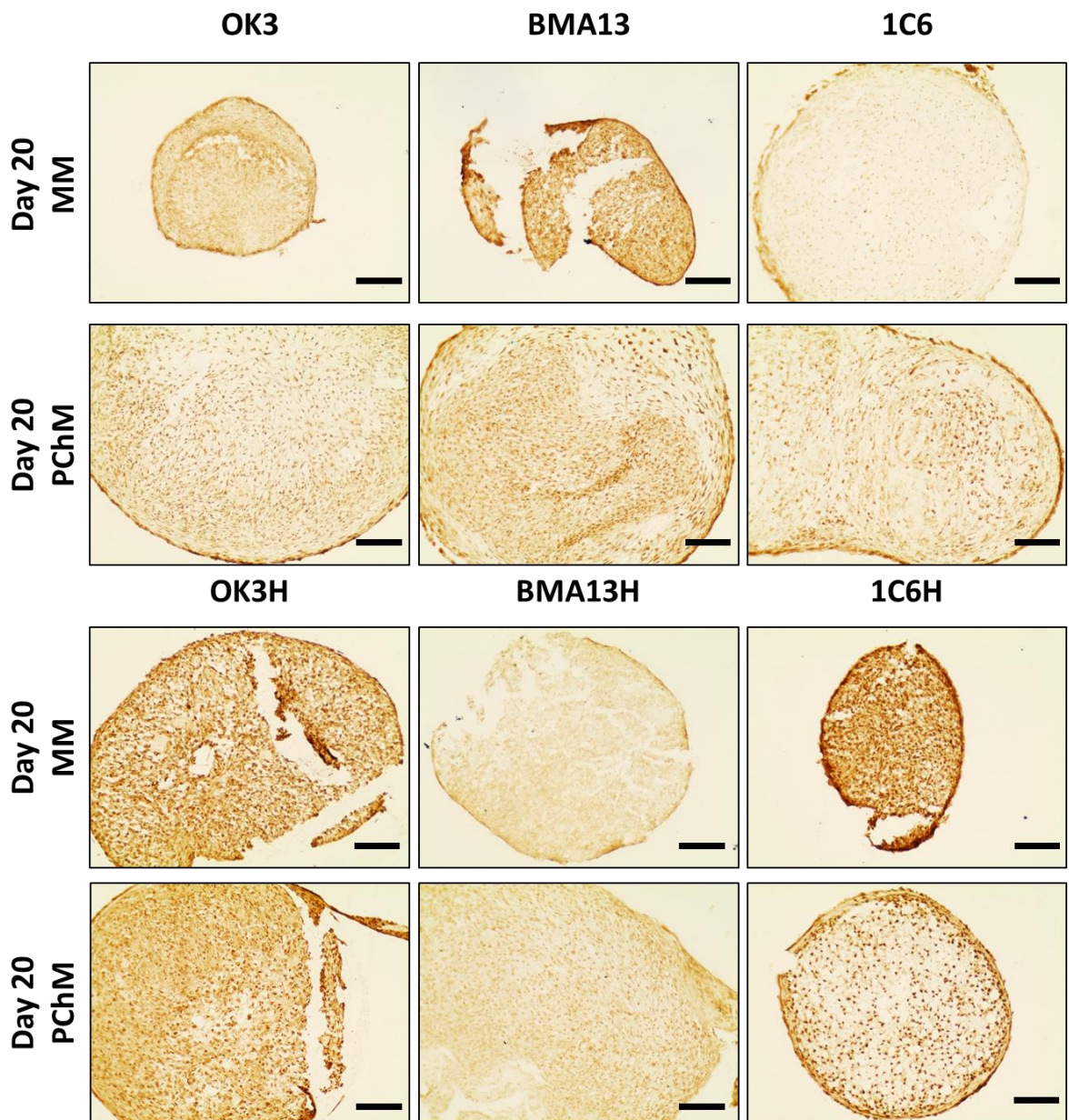


**Figure 6-45. Collagen II day 20 immunoperoxidase staining.** Representative brightfield images of collagen II immunoperoxidase stained sections of all pellets at day 20. Scale bar=100  $\mu$ m. PD level for cells was as follows: OK3 PD6, OK3H PD50, BMA13 PD6, BMA13H PD16, 1C6 PD36, 1C6H PD86.

All primary cell pellets, with the exception of BMA13 in MM, stained strongly for collagen VI throughout the pellet (Figure 6-46). There generally appeared to be more abundant staining in PChM cultures than in MM although OK3 had strong positive staining throughout in MM. Pellets made with transduced cells again stained more weakly than the parental cell pellets particularly in 1C6H cultures. Interestingly some staining patterns were evident, for example in 1C6 MM, that could also be seen with the generalised picrosirius red collagen staining.

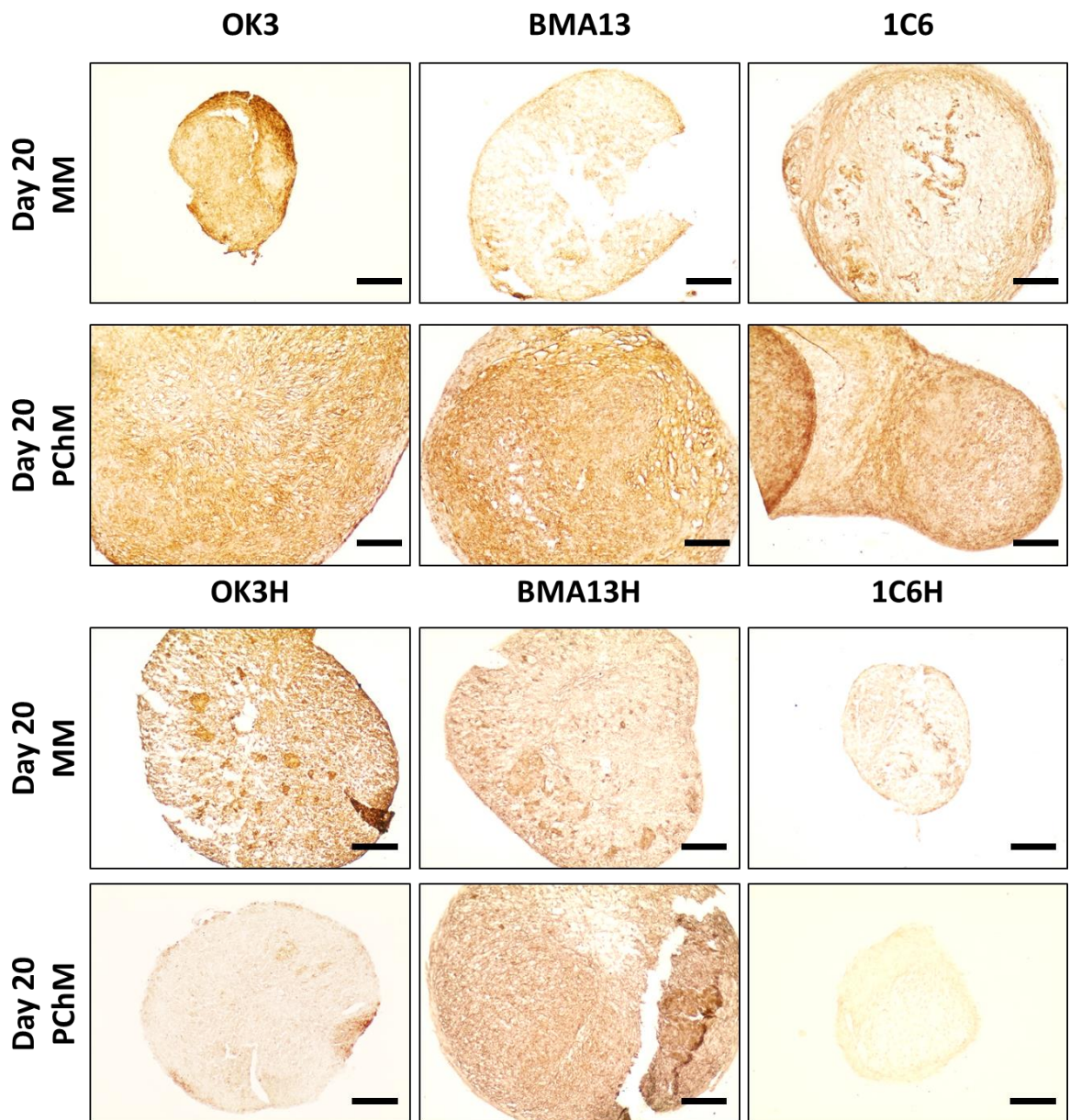


**Figure 6-46. Collagen VI day 20 immunoperoxidase staining.** Representative brightfield images of collagen VI immunoperoxidase stained sections of all pellets at day 20. Scale bar=100  $\mu$ m. PD level for cells was as follows: OK3 PD6, OK3H PD50, BMA13 PD6, BMA13H PD16, 1C6 PD36, 1C6H PD86.

Regional collagen X staining (Figure 6-47) could be seen in primary cell pellets cultured in MM, particularly so in BMA13. In comparison PChM cultures had less collagen X staining that was more localised to cells although again this was most apparent in BMA13 cultures. The transduced cells overall stained less positively for collagen X with little difference between MM and PChM but within this group staining also seemed strongest in the BMA13H MSC group.

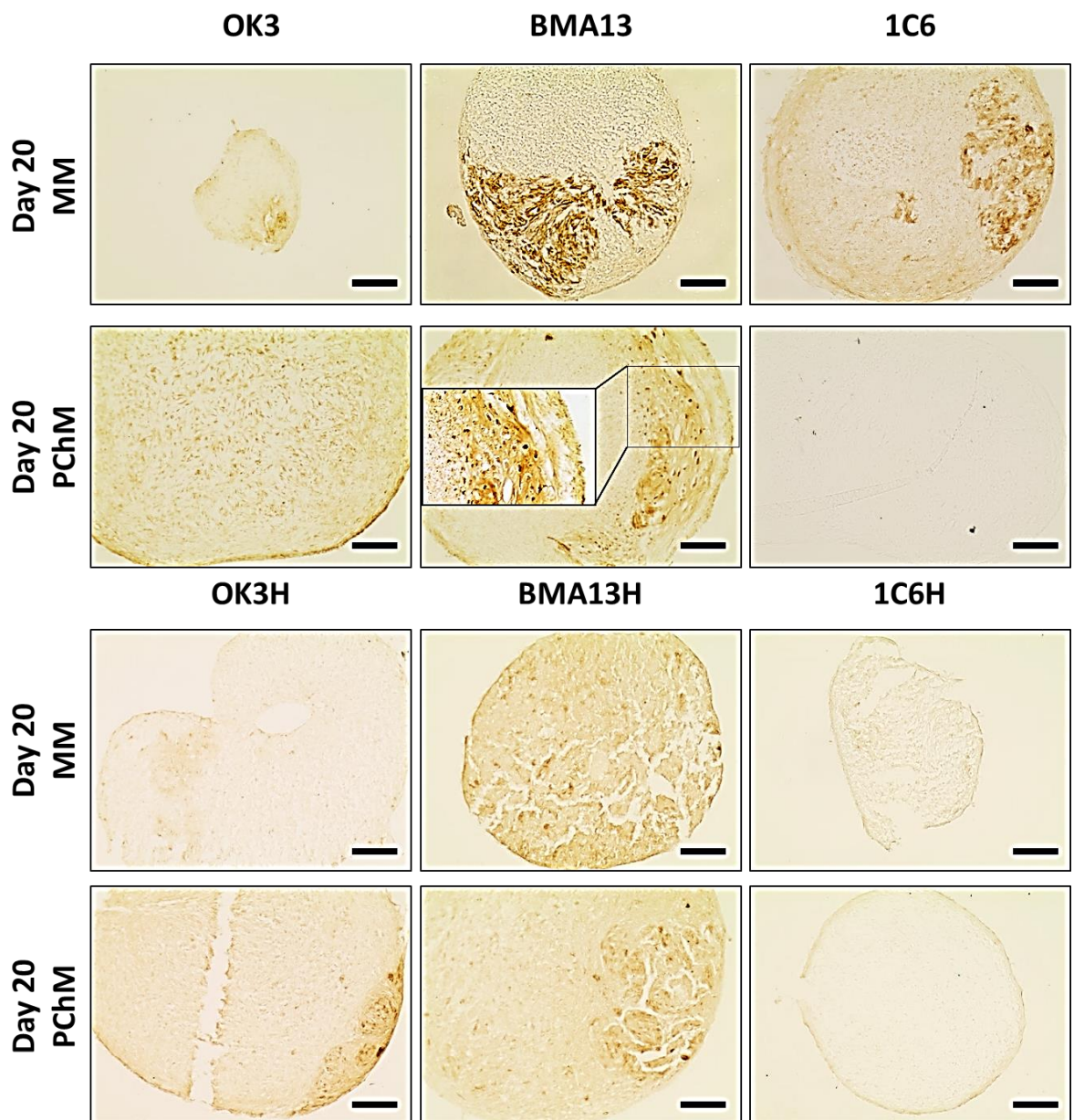


**Figure 6-47. Collagen X day 20 immunoperoxidase staining.** Representative brightfield images of collagen X immunoperoxidase stained sections of all pellets at day 20. Scale bar=100 μm. PD level for cells was as follows: OK3 PD6, OK3H PD50, BMA13 PD6, BMA13H PD16, 1C6 PD36, 1C6H PD86.

In accordance with previous toluidine blue staining and DMMB quantification of sGAG, aggrecan staining (Figure 6-48) was most prominent in OK3 and BMA13 pellets following culture in PChM. As with toluidine blue staining in OK3 was present throughout the pellet and with BMA13 faithfully mirrored the distinct regions where toluidine blue staining was observed. Similarly with OK3 cultured in MM there was a band of positive staining peripherally. Staining was much less apparent and more diffuse in 1C6 pellet cultures. Staining was reduced in comparison in transduced cells, being almost entirely absent in BMA13H cultures

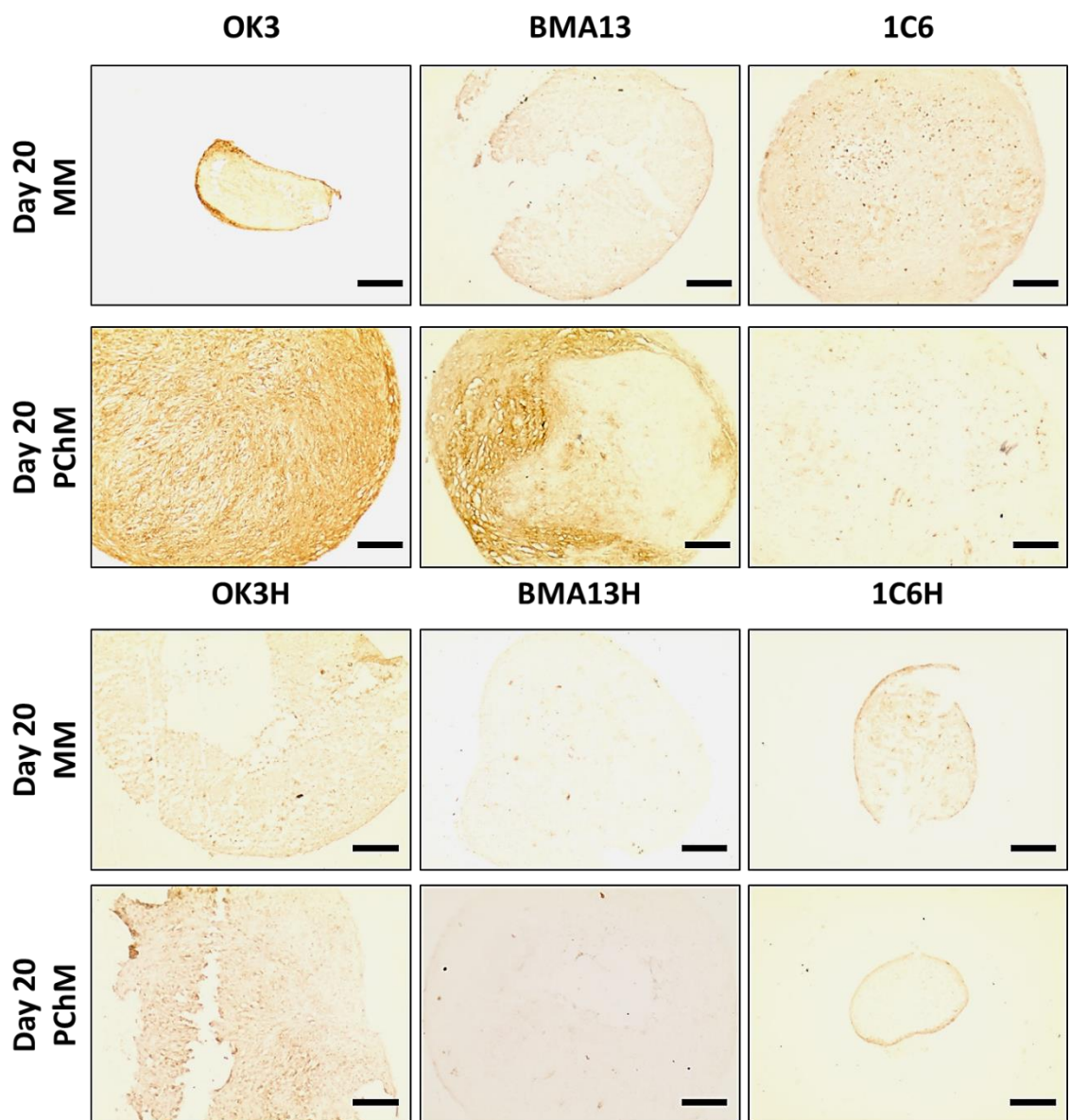


**Figure 6-48. Aggrecan day 20 immunoperoxidase staining.** Representative brightfield images of aggrecan immunoperoxidase stained sections of all pellets at day 20. Scale bar=100  $\mu$ m. PD level for cells was as follows: OK3 PD6, OK3H PD50, BMA13 PD6, BMA13H PD16, 1C6 PD36, 1C6H PD86.

## 6.5 Discussion

The adoption of a 3D culture format has several benefits including the re-creation of an *in vitro* milieu more reminiscent of the *in vivo* situation of cells, particularly as experienced during pre-cartilaginous condensations. It is associated with increased cell-cell contacts, has the potential to create dynamic morphogenetic gradients-including with oxygen and nutrients, a reduced influence from an artificial substrate- usually tissue culture plastic, and the benefit of reducing de-differentiation in chondrocytes *in vitro*, the application for which pellet culture systems were initially used<sup>382</sup>. This work explored the use of a 3D pellet culture system to further extend the assessment of chondrogenesis carried out in Chapter 5 on the three primary cell types and the telomerised cell lines.

The formation of stable pellets with a significant increase in a cartilage-like ECM was identified only in the three primary cell types and there was a strong requirement for pro-chondrogenic conditions. Biochemical analysis of the sGAG content of pellets in PChM found that this was approximately equal in both chondrocytes and MSCs whilst being somewhat lower in hESC derived cells. In contrast to monolayer cultures increases in sGAG were entirely attributable to increased sGAG synthesis not cell proliferation as there were no significant changes in DNA content in PChM. Despite this biochemical equivalence, gene expression analysis showed that MSCs rapidly down-regulated genes associated with chondrogenesis and produced a heterogeneous and fibrous tissue in comparison to chondrocytes where collagen fibres were small and sGAG deposition more widespread. hESC derived 1C6 cells produced an intermediate tissue type with features of both the chondrocytes and MSCs although gene expression similarities to chondrocytes rather than MSCs suggest that they may have the capacity to undergo a more sustained period of chondrogenesis compared to the bone marrow MSCs. Transduced cell chondrogenic responses were all considerably reduced in comparison to primary cells; however, interestingly the 3D environment elicited the greatest chondrogenic response amongst the

transduced cells in OK3H whereas no positive response was previously seen in 2D culture as shown qualitatively in Chapter 4 and quantitatively in Chapter 5.

All of the cells used in this study, whether primary or transduced readily formed cell pellets, the formation of pellets at early stages was observed in both MM and PChM at approximately equal speeds, this is in contrast to results reported by Johnstone *et al* where MSC pellets did not properly aggregate in a standard MM (DMEM 10% (v/v) FBS)<sup>382</sup>; however, that study used rabbit, rather than human bone marrow derived cells. Pellets from all cells were consistently significantly larger at day 20 after culture in PChM rather than MM although overall pellets in both conditions were smaller at day 20 compared to day 1. The cause of the changes in the sizes of the pellets seemingly varied depending upon culture media condition. In MM pellets became much smaller and generally less dense, concomitant with this was a significant decrease in pellet DNA content indicating that the reduction in size was due to a loss of pellet material, or disaggregation, over the course of the experiment. This material may in turn have contributed to the sGAG media associated fraction which was often higher in MM. In the absence of a pro-chondrogenic stimulus standard MM, even inclusive of FBS, was able to support neither long-term pellet stability nor cell proliferation. This was particularly the case for 1C6H cells which experienced dramatic shrinkage and greatly reduced DNA in both MM and PChM. This can be attributed to the *hTERT* transduction and/or subsequent cell expansion as 1C6 cells readily formed pellets in the same MM condition. Interestingly 1C6 pellets in MM were much more stable than those of OK3 and BMA13 this may be a specific feature inherent to these cells; alternatively, it may also be a result of the different MM formulation used for the hESC-derived cells in comparison to the chondrocytes and MSCs. 1C6 and 1C6H were cultured routinely in MM consisting of KO-DMEM rather than DMEM, and media was supplemented with 100 nM dexamethasone as per their previous culture condition following initial isolation. Dexamethasone is included in PChM for all cells and is effective in promoting chondrogenesis in MSCs when paired with TGF- $\beta$ <sup>386</sup>.

In contrast to MM, PChM cultures generally had a relatively static or slightly reduced DNA content concomitant with increased density indicating that pellets continued to contract beyond the day 1 size. Although ongoing cell proliferation is sometimes reported during pellet chondrogenesis<sup>387</sup> it would not be unusual for proliferation to cease<sup>388</sup>, as appeared to be the case in this study. As the media DNA content was not determined further experiments, e.g. bromodeoxyuridine staining, would be needed to confirm a lack of proliferation rather than a balance of cell proliferation and loss.

Changes in pellet sGAG in MM also generally correlated with changes in size, density and DNA content and by day 20 MM cultured pellets all contained significantly less sGAG than PChM pellets with the exception of BMA13H where the difference was not significant. In contrast pellets in PChM, in the case of primary pellets had significantly increased sGAG, and in the case of OK3H and BMA13H maintained day 0 sGAG levels. 1C6H pellets, as with DNA, had significantly less sGAG demonstrating that 1C6H pellet culture is unsupportable in the long term in either MM or PChM. OK3 and BMA13 pellets cultured in PChM in particular also proved to be extremely difficult to disaggregate for RNA analysis even with the application of mechanical force and chemical dissociation, indicating a large increase in the biomechanical properties of the aggregates.

Quantification with DMMB showed that both the OK3 and BMA13 pellets in PChM had similar sGAG levels at the conclusion of the experiment; however, further histological analyses showed distinct differences between the pellets formed. In particular culture of OK3 in PChM resulted in relatively homogeneous deposition of sGAG, aggrecan and collagen with evidence of fibrous tissue mainly restricted to the pellet surface. BMA13 on the other hand was clearly stained very heterogeneously for sGAG, aggrecan and collagen with strong positive staining around the periphery of the pellet and minimal staining in the centre. It should be noted that the peripheral staining of BMA13 was not uniform as was the case with the fibrous encapsulation of the OK3 pellets. Instead the staining appeared as a broad semi-circular band of staining which was then connected with a narrower band. Regional variations in staining of pellets have previously been

attributed to biochemical gradients, of for example nutrients or oxygen that results in a nutrient deficient or hypoxic core. In various circumstances the creation of a hypoxic core has been described as either beneficial<sup>389</sup> due to the positive effects of hypoxia on chondrogenesis or detrimental when a necrotic region has formed<sup>390</sup>.

The pattern of staining seen in this work is reminiscent of the curve of the cell pellet formed by the initial centrifugation step that was very clear when pellets were subjected to  $\mu$ CT analysis. As noted, the cells on the periphery of centrifuged pellets can become elongated in comparison to those in the bulk; these peripheral cells are then folded into the central mass of the pellet as it becomes more spherical. It is possible that these early differences in cell phenotype result in the elongated external cells behaving differently than the central mass cells even after their relocation within the pellet. Changes such as elongation in cells can be induced by the higher tension at the periphery of masses and are mediated by changes in the cell cytoskeleton; these changes can induce significant downstream effects on cell behaviour including influencing cell differentiation. Higher stresses can influence MSCs such that they are directed more towards the osteogenic lineage<sup>391</sup>, a tendency which the cells already appear to have innately. Studies where centrifuged cells are compared to naturally aggregated micromasses generally report more optimal results in the micromasses indicating that the centrifugation technique impacts on the subsequent cell biology even within the same population<sup>392,393</sup>. The overall result of this is that while biochemical cues remain important cells are also receiving potentially competing cues as a result of mechanical forces and spatial patterning. The results herein suggest that MSCs are more sensitive than the chondrocytes to these competing cues, probably due to their multipotent nature. As this was well beyond the scope of this thesis this suggested effect of spatial or mechanical patterning could not be investigated to any great extent. However, a preliminary experiment showed that an increase in BMA13 pellet size resulted in strikingly similar patterns of sGAG staining to at least a similar proportion of the pellet (Supplementary figure 2) indicating the unlikelihood of BMA13 pellet heterogeneity being a simple morphogen gradient mediated effect.

Gene expression data should be interpreted with several caveats in mind. Firstly the expression is representative of only a single time point. In this case day 20 was chosen as chondrogenesis should be well established and markers of hypertrophy, especially relevant to MSCs, should be becoming apparent if they are being expressed. Secondly mRNA levels are not necessarily representative of protein levels due to variations in translation, accumulation and degradation<sup>394,395</sup>. Indeed the protein may not be expressed at all and if it is, its activity regulated by many other factors. Nevertheless expression data can be informative particularly where sample availability is limited.

Overall the gene expression data was quite variable with large error bars; however, this may be due to the mRNA contribution to the total mRNA pool of the cells that adhered to the walls of the microcentrifuge tubes. These cells appeared after some time in culture and represent an adherent population potentially undergoing chondrogenesis at a different rate or not at all. It should also be noted that as is vastly more common, relative expression analysis using the  $2^{-\Delta\Delta CT}$  calculation was performed, if baseline gene expression is already elevated e.g. from hypoxic culture then changes in expression may be less apparent. For future studies the adoption of absolute quantification strategies should be considered particularly when some genes may be present in very low abundance e.g. *COL10A1* which was at the limits of detection in this study in some starting samples. When relative upregulation of these genes is calculated large changes are seen even where the absolute abundance may be low.

The gene expression data for the OK3 chondrocytes and hESC derived 1C6 was in general agreement with the histological staining and hierarchical clustering revealed that the two cell types had similar patterns of expression although changes in expression levels overall were much lower in 1C6. In both of these cell types the genes under consideration were often also upregulated in the MM condition although to a lesser extent most probably indicating that cells are responding to the transfer to 3D culture; however, other results indicate that this is insufficient to produce significant cartilage tissue. Perhaps most significantly *SOX9* expression was

still upregulated in these cell types at day 20 suggesting a capacity for continued chondrogenesis with increased time in culture.

In contrast BMA13 had significant down-regulation of *SOX9* at day 20 and therefore the associated suppression of the endochondral ossification pathway. Most other chondrogenic genes were also down-regulated at this time point, including aggrecan for which strong positive staining was seen histologically. This, along with upregulation of *COL1A2* and *COL10A1* suggests that the BMA13 cells had progressed rapidly through the chondrogenic phase and were becoming hypertrophic in accordance with the progression of endochondral ossification. Pellet culture of MSCs has previously been shown to reduce the expression of hypertrophy markers but does not remove them completely<sup>376</sup>.

The limited ability of all of the cell types described herein to form cartilaginous tissue in the absence of adequate pro-chondrogenic stimuli may be one explanation for the variable outcomes from clinical trials. Following implantation the complex milieu of the *in vivo* environment may not provide adequate or appropriate cues for cells to initiate and sustain chondrogenesis, or may even be 'hostile' due to hypoxia, inflammation, and high mechanical forces; in this eventuality the results described here, particularly for cells in MM, strongly suggest that the cells are unlikely to undergo successful chondrogenesis even where they may have exhibited that capacity in more pro-chondrogenic conditions. Liu *et al*<sup>396</sup> assessed the ability of an extended *in vitro* culture period in pro-chondrogenic conditions to promote the maintenance of a cartilaginous tissue type in MSCs implanted subcutaneously. MSCs are prone to osteogenesis when implanted ectopically<sup>95</sup> and there is no evidence as yet that they spontaneously form any other lineage specific tissue type<sup>397</sup> in the absence of the appropriate pro-differentiation stimulus. This tendency of MSCs towards osteogenesis is also reflected in the *in vivo* results of MSC implantation where fibrous, endochondral and even mineralised tissue can form even after *in vitro* chondrogenic differentiation. The Liu study, like this study, found that hMSCs required a pro-chondrogenic stimulus when in a 3D environment, in their case a scaffold based construct. As with the pellets in

this study, in the absence of PChM constructs shrunk continually over the course of the experiment and formed fibrous tissue. Interestingly they also showed that a much longer *in vitro* pro-chondrogenic differentiation period (12 weeks compared to 4 weeks) led to the formation of an apparently stable cartilaginous tissue following *in vitro* subcutaneous implantation. Perhaps most importantly for potential cartilage regeneration therapies the implanted pre-differentiated tissue continued to become more cartilage-like<sup>396</sup>.

## 6.6 Conclusions

The work in this chapter successfully extended and supported the results described in the previous two chapters. The formation and culture of the cells under investigation into 3D pellets in both standard culture conditions i.e. a sub-optimal chondrogenic environment and in a pro-chondrogenic, TGF- $\beta$ 3 supplemented environment illuminated key differences in chondrogenesis in each cell type. It was clear that stable cell pellets undergoing robust chondrogenesis and ECM synthesis were only formed in the three primary cell types and that they were absolutely reliant upon a pro-chondrogenic environment to do so. In the absence of the appropriate cues cell pellets gradually diminished in size, DNA content and, with some slight exceptions, positive staining for the major chondrogenic ECM proteins assessed. In the clinical context if any of these cells were implanted into a defect that could not provide adequate pro-chondrogenic cues it would likely result in an unsuccessful treatment. Chondrocytes and MSCs were found at 20 days to have biochemically equivalent sGAG contents but significant differences in the spatial distributions of the ECM proteins. This resulted in highly heterogeneous and fibrous tissue formation in the MSC pellets, a highly undesirable outcome for articular cartilage regenerative therapies that would likely result in failure. hESC derived cells appeared to have an intermediate propensity to undergo chondrogenesis with reduced sGAG compared to MSCs and chondrocytes but also producing a somewhat less fibrous tissue than MSCs. Gene expression analysis also highlighted key variations, specifically MSCs in contrast to the other primary cells no longer

expressed *SOX9* and appeared to have progressed to a hypertrophic phenotype. By most of the measures discussed transduced cells were inferior to primary cells and in confirmation of the 2D results they certainly do not represent a suitable replacement for primary cells. However, interestingly there were indications, such as the sustained differential response to MM and PChM and *SOX9* expression and in particular the improvement seen by transferring OK3H from a 2D to a 3D environment, which suggested that the transduction whilst clearly significantly impacting upon the cells' chondrogenic potential had not completely abrogated the chondrogenic response.



Keele University

---

# **Chapter 7**

---

***Summative discussion,  
conclusions, and future  
perspectives***

## 7.1 Summative discussion

Articular cartilage damage and degeneration is a problem for which an ideal solution is yet to be identified. Progress on regenerative medicine alternatives to joint replacement is being made with corresponding improvements to patient outcomes yet the problems that were identified relatively early on in the development of new techniques, primarily around the production of an inappropriate ECM, still persist today. The native articular cartilage is hyaline in nature whilst fibrocartilage is often, at least regionally, found in biopsies of repair tissue. To date two cell types have been the primary component investigated for cell-based therapies, firstly the articular chondrocyte itself and latterly the bone marrow MSC, future therapies are also likely to extend to include pluripotent stem cell derivatives. These cell types all have associated advantages and disadvantages as summarised in Table 7-1. Further consideration is also being given to the cell source where phenotypically similar cells are available from multiple potential sources, particularly with MSCs where cells are being isolated from an increasing diversity of sources. The aims of the work in this thesis were essentially threefold, firstly to establish whether physiological hypoxia levels, determined to have a positive impact on the recovery of bone marrow MSCs, hESCs and chondrogenesis, improved the recovery rate of MSCs from human UCB samples as these are a readily available cell source for allogeneic therapies. The second aim was to investigate the chondrogenic capacity of clinically relevant cells, particularly with respect to their ability to produce a homogeneous, cartilaginous ECM. Finally, to determine whether *hTERT* transduction could extend *in vitro* proliferative capacity and prevent senescence whilst also maintaining cellular chondrogenic capacity.

**Table 7-1. Key advantages and disadvantages associated with cell types with potential cell therapy applications.**

Chondrocytes	<ul style="list-style-type: none"> <li>✓ Cells may already have the desired chondrogenic phenotype.</li> <li>✓ No ethical concerns with the cell source</li> <li>- Limited availability – low cell density in tissue requires larger biopsies which may not be possible.</li> <li>- Acquisition of tissue for cell isolation may cause donor site morbidity in previously healthy regions.</li> <li>- Cells are not suited to <i>in vitro</i> expansion, undergoing de-differentiation.</li> <li>- Although biopsy regions may be macroscopically healthy cells may already be undergoing detrimental phenotypic changes.</li> </ul>
MSCs	<ul style="list-style-type: none"> <li>✓ Available from multiple tissue sources.</li> <li>✓ No ethical concerns surrounding their acquisition</li> <li>- The ideal source of MSCs has yet to be identified.</li> <li>- MSCs appear to follow an intrinsic hypertrophy/endochondral ossification pathway which cannot yet be completely prevented.</li> </ul>
Pluripotent cells and derivatives thereof	<ul style="list-style-type: none"> <li>✓ Can be expanded to potentially unlimited numbers.</li> <li>✓ More naïve cell type – greater differentiation potential.</li> <li>✓ iPSC technology may allow for autologous pluripotent stem cell products.</li> <li>- Ethical concerns surrounding hESCs.</li> <li>- Uncertain epigenetic status of iPSCs.</li> <li>- Potential for teratoma formation if undifferentiated cells persist in a cell therapy product.</li> <li>- More complex differentiation requirements.</li> </ul>

UCB was found not to be a viable source of MSCs, at least on a small laboratory scale, due to lack of reliable recovery. With current techniques yet to identify a unique MSC marker to enable positive selection, UCB should be considered a more suitable source for haematopoietic cells. However, the study did direct further investigation into FBS batch variability with the results having wide-ranging implications regarding the importance and continued use of FBS. FBS has been and continues to be used extensively in cell culture experiments, even being used in many clinical trials if produced in compliance with appropriate good manufacturing practice (GMP) regulations<sup>398</sup>. Although technically already a pooled product as each batch is produced from many foetuses, there nevertheless remains huge batch to batch variability and the nature of this remains largely unknown as FBS is not well characterised<sup>278</sup> (For information Certificates of Analysis for FBS1 and FBS2 are included in Appendix C). Whilst the effects of FBS on cell recovery from biological products have been clearly highlighted in Chapter 3 it is likely that there are also a multitude of other cellular processes that are also being affected in unknown ways and inevitably with down-stream effects.

The effect of oxygen tension on UCB MSC recovery was also compared in Chapter 3. Whilst determination of the effects on recovery from UCB could not be directly assessed due to overall poor performance, the single colony of MSC-like cells that was recovered was found in a more physiologically relevant 2% O<sub>2</sub> environment suggesting that it may prove to be a superior option for future work. Subsequent controlled investigation with bone marrow MNC preparations revealed a strong ameliorating effect of 2% O<sub>2</sub> on the poor recovery of MSCs concomitant with large numbers of monocytes that was found in 21% O<sub>2</sub> when FBS2 was used. Whilst the cause remains unconfirmed as it would require considerable further investigation, there are several possibilities as discussed more fully in Chapter 3.

In order to address the second and third aims three clinically relevant cell types were expanded and then transduced with *hTERT*. Human articular chondrocytes (OK3), MSCs, and as no cells were obtained from UCB these were bone marrow derived (BMA13), and hESC-derived cells (1C6).

Subsequently cell proliferation capacity, phenotype, and chondrogenic differentiation capacity was compared across all primary and transduced cells.

When comparing chondrogenesis across the three primary cell types, chondrocytes remained the most optimal. These cells produced the highest sGAG levels in both 2D and in 3D. Although on this measure BMA13 was similar, chondrocytes appeared to more readily switch from a proliferative to a synthetic phenotype. In 3D culture they had the greatest overall and most persistent upregulation of chondrogenic genes particularly *SOX9* the master regulator of chondrogenesis, and the matrix that the cells produced stained homogeneously for sGAG and for collagen with minimal fibrous tissue apparent. The tissue produced can by these measures be judged to be the most hyaline-like and therefore the most likely to result in the most successful clinical outcome. The results from the other two primary cells were in comparison sub-optimal, BMA13 whilst promising on the basis of sGAG synthesis retained a more proliferative phenotype in 2D culture although significant sGAG was produced. In 3D the cells no longer maintained a proliferative phenotype as DNA content of pellets did not increase, instead they developed many features of hypertrophic cartilage with down-regulation of chondrogenic genes and up-regulation of type X collagen. Pellets also stained very heterogeneously for sGAG and collagen, with thick highly organised collagen fibres throughout much of the pellet indicating fibrocartilage development. It has been suggested that MSCs may experience a lag period prior to the onset of differentiation due to their stem cell state<sup>399</sup> and extended culture has proved beneficial in some cases<sup>386</sup>. Nevertheless, these results would suggest that this is not the case here as MSCs appeared to progress rapidly through a chondrogenic phase where aggrecan was deposited and to hypertrophy associated with down-regulation of the *ACAN* and *SOX9* genes by day twenty. Overall these results are typical for both chondrocytes and MSCs and support much of the available literature<sup>73,83,385,38684,400</sup>. Alternative sources of MSCs, including those resident in the joint compartment, may provide cells more suited to chondrogenesis and there has been a recent

interest in the application of synovial MSCs<sup>70</sup> and cells from the infra-patellar fat pad<sup>401</sup> as alternatives to bone marrow.

Additionally attempts to improve chondrogenesis particularly in MSCs by further refinement of the culture condition are ongoing<sup>400</sup>. A factorial screening experiment of multiple growth factor supplementation on an array of chondrogenic 'wanted' and 'unwanted' genes found no condition in which optimal gene expression for chondrogenesis of MSCs could be achieved, those conditions that up-regulated wanted genes also up-regulated unwanted genes, the study concluded that TGF- $\beta$ 1, 2 or 3 combined with dexamethasone supplementation still provided the overall best outcome<sup>366</sup>. This combination was used in this study and therefore the results can be interpreted with confidence.

1C6 may present a slightly different case and the results were interesting from the perspective of potential future use. The cell response to the PChM appeared to be muted in comparison to that of both the chondrocytes and the MSCs, less sGAG was produced overall and pellets were somewhat fibrous, although much less so than BMA13; however, sustained up-regulation of chondrogenic genes including *SOX9* was seen. These results suggest capacity for chondrogenesis but that the cues may not be sufficient in standard PChM, unsurprising when the complex routines employed for hESC chondrogenic differentiation<sup>156,157</sup> are compared to the simple PChM used in these experiments. In support of the results seen with 1C6, in a recent report the chondrogenic capacity of another H1 derived MSC-like cell type was compared to that of bone marrow MSCs completely independently, with similar results to those here. The response of the H1 derived cells in that case was improved by the addition of BMP7 to cultures<sup>402</sup> and this may be an option in future work.

Following transduction both the chondrocytes OK3H and the 1C6H hESC derived cells gained considerable proliferative capacity, bypassing replicative senescence and appearing to be immortal, MSCs BMA13H on the other hand had only a very modest increase in expansion

capacity. However, the telomerised cells in all cases deviated from the parental cell phenotype with expanded cells displaying changes in immunophenotype and differentiation capacity. 1C6H cells in particular appeared to perform particularly badly in pellet culture whilst the parental cell line exhibited modest chondrogenesis. Nevertheless the telomerised cells, including 1C6H, retained some degree of differential response to PChM compared to MM indicating that some chondrogenic capacity was retained. Surprisingly OK3H which exhibited no response to PChM in monolayer culture had improved chondrogenic capacity in 3D pellets. It is possible that further improvements in driving chondrogenesis could be measured using the OK3H cell response and that OK3H could be sensitive to further improvements.

There are many reports of the successful application of *hTERT* transduction to immortalise cells whilst preserving their phenotype. However, these tend to be spread across multiple cell types and are sometimes contradictory as others report varied degree of success either with respect to immortalisation or preservation of the initial phenotype<sup>202,203,207,328,338,403-412</sup>. Whilst reports of its use for chondrocytes are very limited and have often reported mixed success, there is more data available for MSCs where success is often reported. This is suggestive of a difference in the system applied here, and the possible candidate identified is the oxygen culture environment. The use of a physiologically relevant 2% oxygen level in culture prior to transduction in combination with transduction in ambient oxygen levels may have provided a hyperoxic insult that had long term effects on the resultant transduced cell phenotype<sup>294,413,414</sup>.

All cell populations used in this study were polyclonal; however, variations are known to occur within the cell types used. MSC isolated from bone marrow are well known to be a mixture of cells with varied potency<sup>109,110</sup> and similarly isolated chondrocytes behave differently depending on the tissue zone of origin, for example gene expression of key matrix molecules differs with middle and deep zone chondrocytes producing higher levels than superficial zone chondrocytes in addition to other basal metabolic differences<sup>415</sup>. Whilst polyclonal populations continue to be used heterogeneity in the outcome will likely continue to be a problem. Furthermore, and most

significantly with the transduced cells due to the extent to which they were expanded, there is evidence that slower growing clones that arise during cell culture are eliminated by apoptosis when in direct contact with faster growing cells<sup>416</sup>. This process appears to be analogous to that of 'cell competition' as described originally during *Drosophila* development as the process by which cells can be categorised as 'loser' cells or 'winner' cells within the context of the local environment with the loser cells being slower growing and eventually undergoing apoptosis<sup>417</sup>. This would favour the selection of more rapidly proliferating cells potentially to the detriment of cells with greater differentiation capacity. Unfortunately unless greater amounts of starting tissue become available the concept of monoclonal cultures would be difficult to implement on a routine basis. Furthermore cell expansion to useful numbers from a single starting cell would result in much greater cell aging.

The concept that more proliferative cells are less likely to undergo differentiation has merit. The two processes of proliferation and differentiation are exclusive, with cells developing and exhibiting the features of a differentiated phenotype during interphase<sup>418</sup>. Cells that spend less time in interphase due to more rapid cell cycling are therefore less likely to exhibit the features associated with a differentiated phenotype. The hESC-derived progenitors used here proliferate at a greater rate than the MSC and the chondrocytes and appear to have a less differentiated phenotype. The transduced cells all had a reduced capacity for differentiation in comparison to the primary cells. hTERT in addition to its canonical role has other more direct effects on the cell cycle<sup>202,206</sup>. One possibility to 'rescue' cells that are more proliferative to potentially increase their differentiation capacity is the application of conditional immortalisation, where the factor driving proliferation can be removed in some way, or transient immortalisation. Transient rather than permanent expression of *hTERT* is sufficient to extend cellular lifespan and should be considered<sup>406</sup>. Conditional or transient immortalisation has been successfully used in several cell types including fibroblasts<sup>406</sup>, beta cells<sup>419</sup>, MSCs<sup>405</sup> and chondrocytes<sup>345</sup>. Interestingly overexpression of *hTERT* in the undifferentiated H1 hESC cell line, the parental line of 1C6, has

independently been found to affect the differentiation capacity of the cells with reduced expression of germline differentiation markers and increased expression of the pluripotency marker *OCT4*<sup>202</sup>. If 1C6 does not reflect a fully differentiated cell type and 1C6H even less so it is possible that the results herein represent a very similar response and explain why ectopic expression in 1C6H resulted in very poor differentiation.

## 7.2 Conclusions

Whilst desirable due to relative ease of access and existing infrastructure the use of UCB for MSC isolation cannot be supported, at least on a small scale, by the results herein. Monocyte contamination of MNC preparations, exacerbated as a result of FBS batch variability and influenced by oxygen tension, was identified as a possible confounding factor. However, despite modifications to the protocol to remove all leukocytes with the CD45 antigen, recovery could not be improved. These results indicate either that MSCs are only present in vanishingly small numbers in UCB or that considerable refinement to culture conditions could be required for reliable isolation. The results also strongly support a move away from FBS to defined serum-free conditions.

A direct comparison of chondrogenesis in three cell types: chondrocytes (OK3), MSCs (BMA13) and hESC-derived cells (1C6) favoured the continued use of chondrocytes in articular cartilage therapies. Whilst chondrocytes and MSCs were biochemically comparable, there were significant gene expression changes suggesting that MSCs were becoming hypertrophic. The ECM produced by chondrocytes was also considerably less heterogeneous and fibrous than that produced by MSCs with chondrocytes more hyaline-like and MSCs more fibrocartilage-like. hESC-derived cells were less responsive to the pro-chondrogenic signals and produced an intermediate tissue type; however, prolonged *SOX9* expression suggest that they may have further unexplored capacity for chondrogenesis. Based on current results; however, chondrocytes still represent the gold standard for cell therapies.

The use of *hTERT* transduction was successful in extending the proliferation capacity of OK3 and 1C6 but not BMA13; however, it was unsuccessful in maintaining the phenotype of all cell types by multiple measures in the current differentiation model. Detailed analysis revealed that responses to pro-chondrogenic signals were greatly diminished although not completely nullified in all three cell types therefore they cannot be considered to be a replacement for primary cells in articular cartilage research. Future optimisation of the immortalisation process may produce cell lines with much greater utility.

### **7.3 Future perspectives**

The work described in this thesis has raised a number of considerations for future work as detailed below.

The successful culture of MSCs from UCB as shown is not a trivial matter with a number of critical parameters identified that should be taken into account in future studies of this nature. Studies would clearly benefit from being much larger in order to establish optimised protocols and effectively observe the effects resulting from modifying isolation parameters. As such, future work would greatly benefit from either the use of, or collaboration with, an UCB bank as a donor source or alternatively cord blood collection from the placenta *in utero* by a trained team to maximise the volume of material collected and to minimise the risk of clotting and haemolysis.

Future studies attempting to isolate UCB MSCs and potentially from other sources should consider the option of serum free culture to remove what are clearly severe confounding factors when FBS is used.

The detrimental effects of FBS batch on MSC recovery were clearly reduced by culture in 2% O<sub>2</sub> compared to 21% O<sub>2</sub> when recovering from BMA MNC preparations; this would suggest that culture in 2% O<sub>2</sub> is also likely to be beneficial to recovery from UCB; however, the mechanisms involved are currently unknown and would be of great interest to future work for both MSC and HSC recovery.

The immortalisation of cells, particularly chondrocytes to create a phenotypically stable cell line would clearly be invaluable for cartilage research, as such further investigations towards this should be investigated. One possibility for the lack of success with hTERT immortalisation is the detrimental effect of oxidative stress in the cultures. It would be of interest to repeat the transductions described here in a stable physiological oxygen level to determine whether it could then be a successful approach. *hTERT* transduction in concert with other promoters of chondrogenic differentiation may also be an option.



Keele University

---

# **References**

---

1. Saladin, K. *Anatomy and Physiology: The Unity of Form and Function*. (McGraw-Hill Publishing Co., 2003).
2. Graaff, K. M. V. D., Strete, D. & Creek, C. H. *MP: Van De Graaff Human Anatomy*. (McGraw Hill Higher Education, 2001).
3. Hui, A. Y., McCarty, W. J., Masuda, K., Firestein, G. S. & Sah, R. L. A Systems Biology Approach to Synovial Joint Lubrication in Health, Injury, and Disease. *Wiley Interdiscip. Rev. Syst. Biol. Med.* **4**, 15–37 (2012).
4. Anatomy & Physiology - OpenStax CNX. Available at: [http://cnx.org/contents/14fb4ad7-39a1-4eee-ab6e-3ef2482e3e22@6.27/Anatomy\\_&\\_Physiology](http://cnx.org/contents/14fb4ad7-39a1-4eee-ab6e-3ef2482e3e22@6.27/Anatomy_&_Physiology). (Accessed: 8th June 2015)
5. Sophia Fox, A. J., Bedi, A. & Rodeo, S. A. The Basic Science of Articular Cartilage: Structure, Composition, and Function. *Sports Health Multidiscip. Approach* **1**, 461–468 (November).
6. van Dijk, C. N., Reilingh, M. L., Zengerink, M. & van Bergen, C. J. A. Osteochondral defects in the ankle: why painful? *Knee Surg. Sports Traumatol. Arthrosc.* **18**, 570–580 (2010).
7. Mackie, E. J., Ahmed, Y. A., Tatarczuch, L., Chen, K.-S. & Mirams, M. Endochondral ossification: how cartilage is converted into bone in the developing skeleton. *Int. J. Biochem. Cell Biol.* **40**, 46–62 (2008).
8. Towers, M. & Tickle, C. Growing models of vertebrate limb. *Development* **136**, 179–190 (2009).
9. Lefebvre, V. & Smits, P. Transcriptional control of chondrocyte fate and differentiation. *Birth Defects Res. Part C Embryo Today Rev.* **75**, 200–212 (2005).
10. Archer, C. W., Morrison, H. & Pitsillides, A. A. Cellular aspects of the development of diarthrodial joints and articular cartilage. *J. Anat.* **184**, 447–456 (1994).
11. Spagnoli, A. *et al.* TGF- $\beta$  signaling is essential for joint morphogenesis. *J. Cell Biol.* **177**, 1105–1117 (2007).
12. Hattori, T. *et al.* SOX9 is a major negative regulator of cartilage vascularization, bone marrow formation and endochondral ossification. *Dev. Camb. Engl.* **137**, 901–911 (2010).
13. Demoor, M. *et al.* Cartilage tissue engineering: Molecular control of chondrocyte differentiation for proper cartilage matrix reconstruction. *Biochim. Biophys. Acta BBA - Gen. Subj.* **1840**, 2414–2440 (2014).
14. Gong, Y. *et al.* Heterozygous mutations in the gene encoding noggin affect human joint morphogenesis. *Nat. Genet.* **21**, 302–304 (1999).
15. Wu, X.-B. *et al.* Impaired osteoblastic differentiation, reduced bone formation, and severe osteoporosis in noggin-overexpressing mice. *J. Clin. Invest.* **112**, 924–934 (2003).

16. Archer, C. W., Dowthwaite, G. P. & Francis-West, P. Development of synovial joints. *Birth Defects Res. Part C Embryo Today Rev.* **69**, 144–155 (2003).
17. Edwards, J. C. *et al.* The formation of human synovial joint cavities: a possible role for hyaluronan and CD44 in altered interzone cohesion. *J. Anat.* **185**, 355–367 (1994).
18. Hyde, G., Dover, S., Aszodi, A., Wallis, G. A. & Boot-Handford, R. P. Lineage tracing using matrilin-1 gene expression reveals that articular chondrocytes exist as the joint interzone forms. *Dev. Biol.* **304**, 825–833 (2007).
19. Murphy, J. M., Heinegård, R., McIntosh, A., Sterchi, D. & Barry, F. P. Distribution of cartilage molecules in the developing mouse joint. *Matrix Biol. J. Int. Soc. Matrix Biol.* **18**, 487–497 (1999).
20. Okimura, A. *et al.* Enhancement of cartilage matrix protein synthesis in arthritic cartilage. *Arthritis Rheum.* **40**, 1029–1036 (1997).
21. Pacifici, M., Koyama, E. & Iwamoto, M. Mechanisms of synovial joint and articular cartilage formation: Recent advances, but many lingering mysteries. *Birth Defects Res. Part C Embryo Today Rev.* **75**, 237–248 (2005).
22. Hunziker, E. B., Kapfinger, E. & Geiss, J. The structural architecture of adult mammalian articular cartilage evolves by a synchronized process of tissue resorption and neoformation during postnatal development. *Osteoarthr. Cartil. OARS Osteoarthr. Res. Soc.* **15**, 403–413 (2007).
23. Hayes, A. J., MacPherson, S., Morrison, H., Dowthwaite, G. & Archer, C. W. The development of articular cartilage: evidence for an appositional growth mechanism. *Anat. Embryol. (Berl.)* **203**, 469–479 (2001).
24. Hunziker, E. B., Quinn, T. M. & Häuselmann, H.-J. Quantitative structural organization of normal adult human articular cartilage. *Osteoarthritis Cartilage* **10**, 564–572 (2002).
25. Jadin, K. D. *et al.* Depth-Varying Density and Organization of Chondrocytes in Immature and Mature Bovine Articular Cartilage Assessed by 3D Imaging and Analysis. *J. Histochem. Cytochem.* **53**, 1109–1119 (2005).
26. Verzijl, N. *et al.* Effect of collagen turnover on the accumulation of advanced glycation end products. *J. Biol. Chem.* **275**, 39027–39031 (2000).
27. Mwale, F., Roughley, P. & Antoniou, J. Distinction between the extracellular matrix of the nucleus pulposus and hyaline cartilage: a requisite for tissue engineering of intervertebral disc. *Eur. Cell. Mater.* **8**, 58–63; discussion 63–64 (2004).
28. Bhosale, A. M. & Richardson, J. B. Articular cartilage: structure, injuries and review of management. *Br. Med. Bull.* **87**, 77–95 (2008).

29. Eyre, D. Collagen of articular cartilage. *Arthritis Res.* **4**, 30–35 (2002).
30. Wang, Q. G., El Haj, A. J. & Kuiper, N. J. Glycosaminoglycans in the pericellular matrix of chondrons and chondrocytes. *J Anat* **213**, 266–273 (2008).
31. Exposito, J.-Y., Valcourt, U., Cluzel, C. & Lethias, C. The Fibrillar Collagen Family. *Int. J. Mol. Sci.* **11**, 407–426 (2010).
32. Kadler, K. E., Hill, A. & Canty-Laird, E. G. Collagen fibrillogenesis: fibronectin, integrins, and minor collagens as organizers and nucleators. *Curr. Opin. Cell Biol.* **20**, 495–501 (2008).
33. Jansen, I. D. C., Hollander, A. P., Buttle, D. J. & Everts, V. Type II and VI collagen in nasal and articular cartilage and the effect of IL-1 $\alpha$  on the distribution of these collagens. *J. Mol. Histol.* **41**, 9–17 (2010).
34. Holmes, D. F. & Kadler, K. E. The 10+4 microfibril structure of thin cartilage fibrils. *Proc. Natl. Acad. Sci. U. S. A.* **103**, 17249–17254 (2006).
35. Buckwalter, J. A. & Mankin, H. J. Articular cartilage: tissue design and chondrocyte-matrix interactions. *Instr. Course Lect.* **47**, 477–486 (1998).
36. Von Der Mark, K. *et al.* Type x collagen synthesis in human osteoarthritic cartilage. indication of chondrocyte hypertrophy, Type x collagen synthesis in human osteoarthritic cartilage. indication of chondrocyte hypertrophy. *Arthritis Rheum. Arthritis Rheum.* **35, 35**, 806, 806–811, 811 (1992).
37. Kolettas, E., Buluwela, L., Bayliss, M. T. & Muir, H. I. Expression of cartilage-specific molecules is retained on long-term culture of human articular chondrocytes. *J. Cell Sci.* **108 ( Pt 5)**, 1991–1999 (1995).
38. Ross, M. H. & Pawlina, W. *Histology: A Text and Atlas - With Correlated Cell and Molecular Biology.* (Lippincott Williams and Wilkins, 2006).
39. Wu, J.-J., Weis, M. A., Kim, L. S. & Eyre, D. R. Type III collagen, a fibril network modifier in articular cartilage. *J. Biol. Chem.* **285**, 18537–18544 (2010).
40. Maroudas, A., Bayliss, M. T., Uchitel-Kaushansky, N., Schneiderman, R. & Gilav, E. Aggrecan turnover in human articular cartilage: use of aspartic acid racemization as a marker of molecular age. *Arch. Biochem. Biophys.* **350**, 61–71 (1998).
41. Ng, L. *et al.* Individual cartilage aggrecan macromolecules and their constituent glycosaminoglycans visualized via atomic force microscopy. *J. Struct. Biol.* **143**, 242–257 (2003).
42. Hardingham, T. E. & Fosang, A. J. Proteoglycans: many forms and many functions. *FASEB J. Off. Publ. Fed. Am. Soc. Exp. Biol.* **6**, 861–870 (1992).

43. Snow, H. E., Riccio, L. M., Mjaatvedt, C. H., Hoffman, S. & Capehart, A. A. Versican expression during skeletal/joint morphogenesis and patterning of muscle and nerve in the embryonic mouse limb. *Anat. Rec. A. Discov. Mol. Cell. Evol. Biol.* **282**, 95–105 (2005).
44. Shepard, J. B., Krug, H. A., LaFoon, B. A., Hoffman, S. & Capehart, A. A. Versican expression during synovial joint morphogenesis. *Int. J. Biol. Sci.* **3**, 380–384 (2007).
45. Patil, A. S., Sable, R. B. & Kothari, R. M. An update on transforming growth factor- $\beta$  (TGF- $\beta$ ): Sources, types, functions and clinical applicability for cartilage/bone healing. *J. Cell. Physiol.* **226**, 3094–3103 (2011).
46. Bayliss, M. T., Osborne, D., Woodhouse, S. & Davidson, C. Sulfation of chondroitin sulfate in human articular cartilage. The effect of age, topographical position, and zone of cartilage on tissue composition. *J. Biol. Chem.* **274**, 15892–15900 (1999).
47. Sharma, A., Wood, L. D., Richardson, J. B., Roberts, S. & Kuiper, N. J. Glycosaminoglycan profiles of repair tissue formed following autologous chondrocyte implantation differ from control cartilage. *Arthritis Res. Ther.* **9**, R79 (2007).
48. Plaas, A. H. K., West, L. A., Wong-Palms, S. & Nelson, F. R. T. Glycosaminoglycan Sulfation in Human Osteoarthritis. Disease-Related Alterations at the Non-Reducing Termini of Chondroitin and Dermatan Sulfate. *J. Biol. Chem.* **273**, 12642–12649 (1998).
49. Roughley, P. J. The structure and function of cartilage proteoglycans. *Eur. Cell. Mater.* **12**, 92–101 (2006).
50. Holmes, M. W., Bayliss, M. T. & Muir, H. Hyaluronic acid in human articular cartilage. Age-related changes in content and size. *Biochem. J.* **250**, 435–441 (1988).
51. Loeser, R. F. *et al.* Reduction in the chondrocyte response to insulin-like growth factor 1 in aging and osteoarthritis: studies in a non-human primate model of naturally occurring disease. *Arthritis Rheum.* **43**, 2110–2120 (2000).
52. Grogan, S. P. & D’Lima, D. D. Joint aging and chondrocyte cell death. *Int. J. Clin. Rheumatol.* **5**, 199–214 (2010).
53. Hunter, W. Of the structure and disease of articulating cartilages. 1743. *Clin. Orthop.* 3–6 (1995).
54. Namba, R. S., Meuli, M., Sullivan, K. M., Le, A. X. & Adzick, N. S. Spontaneous repair of superficial defects in articular cartilage in a fetal lamb model. *J. Bone Joint Surg. Am.* **80**, 4–10 (1998).
55. Prevalence and Most Common Causes of Disability Among Adults --- United States, 2005. Available at: <http://www.cdc.gov/mmwr/preview/mmwrhtml/mm5816a2.htm>. (Accessed: 19th February 2016)

56. Choices, N. H. S. Arthritis - NHS Choices. (2016). Available at:  
<http://www.nhs.uk/Conditions/Arthritis/Pages/Introduction.aspx>. (Accessed: 19th February 2016)
57. Lawrence, R. C. *et al.* Estimates of the prevalence of arthritis and other rheumatic conditions in the United States. Part II. *Arthritis Rheum.* **58**, 26–35 (2008).
58. Murphy, L. *et al.* Lifetime risk of symptomatic knee osteoarthritis. *Arthritis Rheum.* **59**, 1207–1213 (2008).
59. Felson, D. T. *et al.* Osteoarthritis: New Insights. Part 1: The Disease and Its Risk Factors. *Ann. Intern. Med.* **133**, 635–646 (2000).
60. Loeser, R. F. Age-related changes in the musculoskeletal system and the development of osteoarthritis. *Clin. Geriatr. Med.* **26**, 371–386 (2010).
61. Mazor, M. *et al.* Mesenchymal stem-cell potential in cartilage repair: an update. *J. Cell. Mol. Med.* **18**, 2340–2350 (2014).
62. Dreier, R. Hypertrophic differentiation of chondrocytes in osteoarthritis: the developmental aspect of degenerative joint disorders. *Arthritis Res. Ther.* **12**, 216 (2010).
63. Peterson, L., Minas, T., Brittberg, M. & Lindahl, A. Treatment of Osteochondritis Dissecans of the Knee with Autologous Chondrocyte Transplantation Results at Two to Ten Years. *J. Bone Jt. Surg. Am.* **85**, 17–24 (2003).
64. CG59 Osteoarthritis: NICE guideline. Available at:  
<http://www.nice.org.uk/guidance/CG59/NICEGuidance>. (Accessed: 23rd March 2012)
65. Wieland, H. A., Michaelis, M., Kirschbaum, B. J. & Rudolphi, K. A. Osteoarthritis — an untreatable disease? *Nat. Rev. Drug Discov.* **4**, 331–344 (2005).
66. Find data - Health & Social Care Information Centre. Available at:  
<http://www.hscic.gov.uk/searchcatalogue?productid=13264&q=title%3a%22Hospital+Episode+Statistics%2c+Admitted+patient+care+-+England%22&sort=Relevance&size=10&page=1#top>. (Accessed: 4th January 2015)
67. Langer, R. & Vacanti, J. P. Tissue engineering. *Science* **260**, 920–926 (1993).
68. Pridie, K. H. A method of resurfacing osteoarthritic knee joints. *J Bone Jt. Surg Br* **41**, 618–619 (1959).
69. Insall, J. N. Intra-articular surgery for degenerative arthritis of the knee. A report of the work of the late K. H. Pridie. *J. Bone Joint Surg. Br.* **49**, 211–228 (1967).
70. Caldwell, K. L. & Wang, J. Cell-based articular cartilage repair: the link between development and regeneration. *Osteoarthr. Cartil. OARS Osteoarthr. Res. Soc.* **23**, 351–362 (2015).

71. Muller, S., Breederveld, R. S. & Tuinebreijer, W. E. Results of osteochondral autologous transplantation in the knee. *Open Orthop. J.* **4**, 111–114 (2010).
72. Karataglis, D. & Learmonth, D. J. A. Management of big osteochondral defects of the knee using osteochondral allografts with the MEGA-OATS technique. *The Knee* **12**, 389–393 (2005).
73. Brittberg, M. *et al.* Treatment of deep cartilage defects in the knee with autologous chondrocyte transplantation. *N. Engl. J. Med.* **331**, 889–895 (1994).
74. Moriya, T. *et al.* Evaluation of reparative cartilage after autologous chondrocyte implantation for osteochondritis dissecans: histology, biochemistry, and MR imaging. *J. Orthop. Sci. Off. J. Jpn. Orthop. Assoc.* **12**, 265–273 (2007).
75. Perera, J., Gikas, P. & Bentley, G. The present state of treatments for articular cartilage defects in the knee. *Ann. R. Coll. Surg. Engl.* **94**, 381–387 (2012).
76. Haddo, O. *et al.* The use of chondroguide membrane in autologous chondrocyte implantation. *The Knee* **11**, 51–55 (2004).
77. Jakobsen, R. B., Engebretsen, L. & Slauterbeck, J. R. An analysis of the quality of cartilage repair studies. *J. Bone Joint Surg. Am.* **87**, 2232–2239 (2005).
78. Fickert, S. *et al.* One-Year Clinical and Radiological Results of a Prospective, Investigator-Initiated Trial Examining a Novel, Purely Autologous 3-Dimensional Autologous Chondrocyte Transplantation Product in the Knee. *Cartilage* **3**, 27–42 (2012).
79. Marlovits, S., Zeller, P., Singer, P., Resinger, C. & Vécsei, V. Cartilage repair: Generations of autologous chondrocyte transplantation. *Eur. J. Radiol.* **57**, 24–31 (2006).
80. Nehrer, S. & Brix, M. Long-Term Outcomes of Chondrocyte-Based Cartilage Repair. *Oper. Tech. Orthop.* **24**, 48–53 (2014).
81. Behrens, P. *et al.* [New therapy procedure for localized cartilage defects. Encouraging results with autologous chondrocyte implantation]. *MMW Fortschr. Med.* **141**, 49–51 (1999).
82. Dunkin, B. S. & Lattermann, C. New and Emerging Techniques in Cartilage Repair: Matrix-Induced Autologous Chondrocyte Implantation. *Oper. Tech. Sports Med.* **21**, 100–107 (2013).
83. Gobbi, A., Chaurasia, S., Karnatzikos, G. & Nakamura, N. Matrix-Induced Autologous Chondrocyte Implantation versus Multipotent Stem Cells for the Treatment of Large Patellofemoral Chondral Lesions A Nonrandomized Prospective Trial. *Cartilage* **6**, 82–97 (2015).
84. Filardo, G. *et al.* Matrix-Assisted Autologous Chondrocyte Transplantation for Cartilage Regeneration in Osteoarthritic Knees Results and Failures at Midterm Follow-up. *Am. J. Sports Med.* **41**, 95–100 (2013).

85. Barbero, A. *et al.* Age related changes in human articular chondrocyte yield, proliferation and post-expansion chondrogenic capacity. *Osteoarthritis Cartilage* **12**, 476–484 (2004).
86. Murphy, C. L. & Polak, J. M. Control of human articular chondrocyte differentiation by reduced oxygen tension. *J. Cell. Physiol.* **199**, 451–459 (2004).
87. Holtzer, H., Abbott, J., Lash, J. & Holtzer, S. The Loss of Phenotypic Traits by Differentiated Cells In Vitro, I. Dedifferentiation of Cartilage Cells. *Proc. Natl. Acad. Sci. U. S. A.* **46**, 1533–1542 (1960).
88. Hegert, C. *et al.* Differentiation plasticity of chondrocytes derived from mouse embryonic stem cells. *J. Cell Sci.* **115**, 4617–4628 (2002).
89. Nandoe Tewarie, R. S., Hurtado, A., Bartels, R. H., Grotenhuis, A. & Oudega, M. Stem cell-based therapies for spinal cord injury. *J. Spinal Cord Med.* **32**, 105–114 (2009).
90. Mitalipov, S. & Wolf, D. Totipotency, Pluripotency and Nuclear Reprogramming. *Adv. Biochem. Eng. Biotechnol.* **114**, 185–199 (2009).
91. Caplan, A. I. & Dennis, J. E. Mesenchymal stem cells as trophic mediators. *J. Cell. Biochem.* **98**, 1076–1084 (2006).
92. Banfi, A. *et al.* Replicative Aging and Gene Expression in Long-Term Cultures of Human Bone Marrow Stromal Cells. *Tissue Eng.* **8**, 901–910 (2002).
93. Pittenger, M. F. *et al.* Multilineage Potential of Adult Human Mesenchymal Stem Cells. *Science* **284**, 143–147 (1999).
94. Parekkadan, B. & Milwid, J. M. Mesenchymal Stem Cells as Therapeutics. *Annu. Rev. Biomed. Eng.* **12**, 87–117 (2010).
95. Friedenstein, A. J., Piatetzky-Shapiro, I. I. & Petrakova, K. V. Osteogenesis in transplants of bone marrow cells. *J. Embryol. Exp. Morphol.* **16**, 381–390 (1966).
96. Trivanović, D. *et al.* Mesenchymal stem cells isolated from peripheral blood and umbilical cord Wharton's jelly. *Srp. Arh. Celok. Lek.* **141**, 178–186 (2013).
97. Seale, P., Asakura, A. & Rudnicki, M. A. The potential of muscle stem cells. *Dev. Cell* **1**, 333–342 (2001).
98. Vaculik, C. *et al.* Human dermis harbors distinct mesenchymal stromal cell subsets. *J. Invest. Dermatol.* **132**, 563–574 (2012).
99. Struys, T. *et al.* Ultrastructural and immunocytochemical analysis of multilineage differentiated human dental pulp- and umbilical cord-derived mesenchymal stem cells. *Cells Tissues Organs* **193**, 366–378 (2011).
100. de Mara, C. S. *et al.* Periosteum as a source of mesenchymal stem cells: the effects of TGF- $\beta$ 3 on chondrogenesis. *Clinics* **66**, 487–492 (2011).

101. Arai, F., Ohneda, O., Miyamoto, T., Zhang, X. Q. & Suda, T. Mesenchymal stem cells in perichondrium express activated leukocyte cell adhesion molecule and participate in bone marrow formation. *J. Exp. Med.* **195**, 1549–1563 (2002).
102. Romanov, Y. A., Darevskaya, A. N., Merzlikina, N. V. & Buravkova, L. B. Mesenchymal Stem Cells from Human Bone Marrow and Adipose Tissue: Isolation, Characterization, and Differentiation Potentialities. *Bull. Exp. Biol. Med.* **140**, 138–143 (2005).
103. Bieback, K., Kern, S., Klüter, H. & Eichler, H. Critical parameters for the isolation of mesenchymal stem cells from umbilical cord blood. *Stem Cells Dayt. Ohio* **22**, 625–634 (2004).
104. McELREAVEY, K. D., Irvine, A. I., Ennis, K. T. & McLEAN, W. H. I. Isolation, culture and characterisation of fibroblast-like cells derived from the Wharton's jelly portion of human umbilical cord. *Biochem. Soc. Trans.* **19**, 29S–29S (1991).
105. Arufe, M. C. *et al.* Analysis of the chondrogenic potential and secretome of mesenchymal stem cells derived from human umbilical cord stroma. *Stem Cells Dev.* **20**, 1199–1212 (2011).
106. Park, S.-B., Seo, M.-S., Kang, J.-G., Chae, J.-S. & Kang, K.-S. Isolation and characterization of equine amniotic fluid-derived multipotent stem cells. *Cytotherapy* **13**, 341–349 (2011).
107. Barlow, S. *et al.* Comparison of human placenta- and bone marrow-derived multipotent mesenchymal stem cells. *Stem Cells Dev.* **17**, 1095–1107 (2008).
108. Arufe, M. C., De la Fuente, A., Fuentes, I., de Toro, F. J. & Blanco, F. J. Chondrogenic potential of subpopulations of cells expressing mesenchymal stem cell markers derived from human synovial membranes. *J. Cell. Biochem.* **111**, 834–845 (2010).
109. Dominici, M., Paolucci, P., Conte, P. & Horwitz, E. M. Heterogeneity of multipotent mesenchymal stromal cells: from stromal cells to stem cells and vice versa. *Transplantation* **87**, S36–42 (2009).
110. Russell, K. C. *et al.* In vitro high-capacity assay to quantify the clonal heterogeneity in trilineage potential of mesenchymal stem cells reveals a complex hierarchy of lineage commitment. *Stem Cells Dayt. Ohio* **28**, 788–798 (2010).
111. Heng, B. C., Cao, T. & Lee, E. H. Directing stem cell differentiation into the chondrogenic lineage in vitro. *Stem Cells Dayt. Ohio* **22**, 1152–1167 (2004).
112. Catacchio, I. *et al.* Evidence for Bone Marrow Adult Stem Cell Plasticity: Properties, Molecular Mechanisms, Negative Aspects, and Clinical Applications of Hematopoietic and Mesenchymal Stem Cells Transdifferentiation, Evidence for Bone Marrow Adult Stem Cell Plasticity: Properties, Molecular Mechanisms, Negative Aspects, and Clinical Applications of

- Hematopoietic and Mesenchymal Stem Cells Transdifferentiation. *Stem Cells Int. Stem Cells Int.* **2013, 2013**, e589139 (2013).
113. Barry, F. P. & Murphy, J. M. Mesenchymal stem cells: clinical applications and biological characterization. *Int. J. Biochem. Cell Biol.* **36**, 568–584 (2004).
  114. Ikebe, C. & Suzuki, K. Mesenchymal Stem Cells for Regenerative Therapy: Optimization of Cell Preparation Protocols. *BioMed Res. Int.* **2014**, (2014).
  115. Dominici, M. *et al.* Minimal criteria for defining multipotent mesenchymal stromal cells. The International Society for Cellular Therapy position statement. *Cytotherapy* **8**, 315–317 (2006).
  116. James, S. *et al.* Multiparameter Analysis of Human Bone Marrow Stromal Cells Identifies Distinct Immunomodulatory and Differentiation-Competent Subtypes. *Stem Cell Rep.* **4**, 1004–1015 (2015).
  117. Schütt, C. CD14. *Int. J. Biochem. Cell Biol.* **31**, 545–549 (1999).
  118. Sato, S., Hasegawa, M., Fujimoto, M., Tedder, T. F. & Takehara, K. Quantitative Genetic Variation in CD19 Expression Correlates with Autoimmunity. *J. Immunol.* **165**, 6635–6643 (2000).
  119. Sidney, L. E., Branch, M. J., Dunphy, S. E., Dua, H. S. & Hopkinson, A. Concise Review: Evidence for CD34 as a Common Marker for Diverse Progenitors. *STEM CELLS* **32**, 1380–1389 (2014).
  120. Atlin, J. G. & Sloan, E. K. The role of CD45 and CD45-associated molecules in T cell activation. *Immunol. Cell Biol.* **75**, 430 (1997).
  121. Griffin, J. D. *et al.* Differential expression of HLA-DR antigens in subsets of human CFU-GM. *Blood* **66**, 788–795 (1985).
  122. Boxall, S. A., Jones, E., Boxall, S. A. & Jones, E. Markers for Characterization of Bone Marrow Multipotential Stromal Cells, Markers for Characterization of Bone Marrow Multipotential Stromal Cells. *Stem Cells Int. Stem Cells Int.* **2012, 2012**, e975871 (2012).
  123. Chung, M. T. *et al.* CD90 (Thy-1)-positive selection enhances osteogenic capacity of human adipose-derived stromal cells. *Tissue Eng. Part A* **19**, 989–997 (2013).
  124. Barry, F. P., Boynton, R. E., Haynesworth, S., Murphy, J. M. & Zaia, J. The Monoclonal Antibody SH-2, Raised against Human Mesenchymal Stem Cells, Recognizes an Epitope on Endoglin (CD105). *Biochem. Biophys. Res. Commun.* **265**, 134–139 (1999).
  125. Reppel, L. *et al.* Hypoxic Culture Conditions for Mesenchymal Stromal/Stem Cells from Wharton's Jelly: A Critical Parameter to Consider in a Therapeutic Context. *Curr. Stem Cell Res. Ther.* **9**, 306–318 (2014).

126. Niehage, C. *et al.* The Cell Surface Proteome of Human Mesenchymal Stromal Cells. *PLoS ONE* **6**, (2011).
127. Majumdar, M. K., Banks, V., Peluso, D. P. & Morris, E. A. Isolation, characterization, and chondrogenic potential of human bone marrow-derived multipotential stromal cells. *J. Cell. Physiol.* **185**, 98–106 (2000).
128. YOO, J. U. *et al.* The Chondrogenic Potential of Human Bone-Marrow-Derived Mesenchymal Progenitor Cells\*. *J. Bone Jt. Surg. Am.* **80**, 1745–57 (1998).
129. Jose, S., Hughbanks, M. L., Binder, B. Y. K., Ingavle, G. C. & Leach, J. K. Enhanced trophic factor secretion by mesenchymal stem/stromal cells with Glycine-Histidine-Lysine (GHK)-modified alginate hydrogels. *Acta Biomater.* **10**, 1955–1964 (2014).
130. English, K. & Mahon, B. P. Allogeneic mesenchymal stem cells: agents of immune modulation. *J. Cell. Biochem.* **112**, 1963–1968 (2011).
131. Caplan, A. I. Adult mesenchymal stem cells for tissue engineering versus regenerative medicine. *J. Cell. Physiol.* **213**, 341–347 (2007).
132. Krampera, M. *et al.* Immunological characterization of multipotent mesenchymal stromal cells--The International Society for Cellular Therapy (ISCT) working proposal. *Cytotherapy* **15**, 1054–1061 (2013).
133. Arzi, B. *et al.* Cartilage immunoprivilege depends on donor source and lesion location. *Acta Biomater.* **23**, 72–81 (2015).
134. Carrade, D. D. *et al.* Clinicopathologic findings following intra-articular injection of autologous and allogeneic placentally derived equine mesenchymal stem cells in horses. *Cytotherapy* **13**, 419–430 (2011).
135. Stenderup, K., Justesen, J., Clausen, C. & Kassem, M. Aging is associated with decreased maximal life span and accelerated senescence of bone marrow stromal cells. *Bone* **33**, 919–926 (2003).
136. Zimmermann, S. *et al.* Lack of telomerase activity in human mesenchymal stem cells. *Leuk. Off. J. Leuk. Soc. Am. Leuk. Res. Fund UK* **17**, 1146–1149 (2003).
137. Alsalameh, S., Amin, R., Gemba, T. & Lotz, M. Identification of mesenchymal progenitor cells in normal and osteoarthritic human articular cartilage. *Arthritis Rheum.* **50**, 1522–1532 (2004).
138. Pretzel, D. *et al.* Relative percentage and zonal distribution of mesenchymal progenitor cells in human osteoarthritic and normal cartilage. *Arthritis Res. Ther.* **13**, R64 (2011).

139. Births and Fertility - ONS. Available at:  
<http://www.ons.gov.uk/ons/taxonomy/index.html?nscl=Births+and+Fertility#tab-data-tables>. (Accessed: 16th August 2015)
140. Erices, A., Conget, P. & Minguell, J. J. Mesenchymal progenitor cells in human umbilical cord blood. *Br. J. Haematol.* **109**, 235–242 (2000).
141. Kern, S., Eichler, H., Stoeve, J., Klüter, H. & Bieback, K. Comparative Analysis of Mesenchymal Stem Cells from Bone Marrow, Umbilical Cord Blood, or Adipose Tissue. *STEM CELLS* **24**, 1294–1301 (2006).
142. Wagner, W. *et al.* Comparative characteristics of mesenchymal stem cells from human bone marrow, adipose tissue, and umbilical cord blood. *Exp. Hematol.* **33**, 1402–1416 (2005).
143. Kögler, G. *et al.* A new human somatic stem cell from placental cord blood with intrinsic pluripotent differentiation potential. *J. Exp. Med.* **200**, 123–135 (2004).
144. Zhang, X. *et al.* Isolation and characterization of mesenchymal stem cells from human umbilical cord blood: Reevaluation of critical factors for successful isolation and high ability to proliferate and differentiate to chondrocytes as compared to mesenchymal stem cells from bone marrow and adipose tissue. *J. Cell. Biochem.* **112**, 1206–1218 (2011).
145. Hass, R., Kasper, C., Böhm, S. & Jacobs, R. Different populations and sources of human mesenchymal stem cells (MSC): A comparison of adult and neonatal tissue-derived MSC. *Cell Commun. Signal. CCS* **9**, 12 (2011).
146. Forraz, N., Pettengell, R. & McGuckin, C. P. Characterization of a Lineage-Negative Stem-Progenitor Cell Population Optimized for Ex Vivo Expansion and Enriched for LTC-IC. *STEM CELLS* **22**, 100–108 (2004).
147. Lee, Y.-H. Is cord blood worth saving for public or private banking? *Blood Res.* **50**, 3–4 (2015).
148. Bassiouny, M. r., El-Chennawi, F., Mansour, A. k., Yahia, S. & Darwish, A. Optimal method for collection of umbilical cord blood: an Egyptian trial for a public cord blood bank. *Transfusion (Paris)* **55**, 1263–1268 (2015).
149. Evans, M. J. & Kaufman, M. H. Establishment in culture of pluripotential cells from mouse embryos. *Nature* **292**, 154–6 (1981).
150. Martin, G. R. Isolation of a pluripotent cell line from early mouse embryos cultured in medium conditioned by teratocarcinoma stem cells. *Proc. Natl. Acad. Sci. U. S. A.* **78**, 7634–8 (1981).
151. Thomson, J. A. *et al.* Isolation of a primate embryonic stem cell line. *Proc. Natl. Acad. Sci. U. S. A.* **92**, 7844–7848 (1995).

152. Thomson, J. A. *et al.* Pluripotent cell lines derived from common marmoset (*Callithrix jacchus*) blastocysts. *Biol. Reprod.* **55**, 254–259 (1996).
153. Thomson, J. A. *et al.* Embryonic stem cell lines derived from human blastocysts. *Science* **282**, 1145–7 (1998).
154. Thomson, J. A. *et al.* Embryonic Stem Cell Lines Derived from Human Blastocysts. *Science* **282**, 1145–1147 (1998).
155. Yodmuang, S., Marolt, D., Marcos-Campos, I., Gadjanski, I. & Vunjak-Novakovic, G. Synergistic Effects of Hypoxia and Morphogenetic Factors on Early Chondrogenic Commitment of Human Embryonic Stem Cells in Embryoid Body Culture. *Stem Cell Rev.* **11**, 228–241 (2015).
156. Cheng, A., Hardingham, T. E. & Kimber, S. J. Generating cartilage repair from pluripotent stem cells. *Tissue Eng. Part B Rev.* **20**, 257–266 (2014).
157. Oldershaw, R. A. *et al.* Directed differentiation of human embryonic stem cells toward chondrocytes. *Nat. Biotechnol.* **28**, 1187–1194 (2010).
158. Craft, A. M. *et al.* Generation of articular chondrocytes from human pluripotent stem cells. *Nat. Biotechnol.* **33**, 638–645 (2015).
159. Cheng, A. *et al.* Cartilage Repair Using Human Embryonic Stem Cell-Derived Chondroprogenitors. *Stem Cells Transl. Med.* **3**, 1287–1294 (2014).
160. Hwang, N. S., Varghese, S., Zhang, Z. & Elisseeff, J. Chondrogenic differentiation of human embryonic stem cell-derived cells in arginine-glycine-aspartate-modified hydrogels. *Tissue Eng.* **12**, 2695–2706 (2006).
161. Toh, W. S., Lee, E. H. & Cao, T. Potential of human embryonic stem cells in cartilage tissue engineering and regenerative medicine. *Stem Cell Rev.* **7**, 544–559 (2011).
162. Safety Study of GRNOPC1 in Spinal Cord Injury - Full Text View - ClinicalTrials.gov. Available at: <http://clinicaltrials.gov/ct2/show/NCT01217008?term=geron&rank=10>. (Accessed: 9th April 2012)
163. Frantz, S. Embryonic stem cell pioneer Geron exits field, cuts losses. *Nat. Biotechnol.* **30**, 12–13 (2012).
164. Safety and Tolerability of Sub-retinal Transplantation of hESC Derived RPE (MA09-hRPE) Cells in Patients With Advanced Dry Age Related Macular Degeneration - Full Text View - ClinicalTrials.gov. Available at: <http://clinicaltrials.gov/ct2/show/NCT01344993?term=embryonic+stem+cell&rank=6>. (Accessed: 9th April 2012)

165. Sub-retinal Transplantation of hESC Derived RPE(MA09-hRPE)Cells in Patients With Stargardt’s Macular Dystrophy - Full Text View - ClinicalTrials.gov. Available at: <http://clinicaltrials.gov/ct2/show/NCT01345006?term=embryonic+stem+cell&rank=5>. (Accessed: 9th April 2012)
166. Takahashi, K. & Yamanaka, S. Induction of pluripotent stem cells from mouse embryonic and adult fibroblast cultures by defined factors. *Cell* **126**, 663–676 (2006).
167. Takahashi, K. *et al.* Induction of pluripotent stem cells from adult human fibroblasts by defined factors. *Cell* **131**, 861–72 (2007).
168. Yu, J. *et al.* Induced Pluripotent Stem Cell Lines Derived from Human Somatic Cells. *Science* **318**, 1917–1920 (2007).
169. Nakagawa, M. *et al.* Generation of induced pluripotent stem cells without Myc from mouse and human fibroblasts. *Nat. Biotechnol.* **26**, 101–106 (2008).
170. Kang, R. *et al.* Mesenchymal stem cells derived from human induced pluripotent stem cells retain adequate osteogenicity and chondrogenicity but less adipogenicity. *Stem Cell Res. Ther.* **6**, (2015).
171. Guzzo, R. M., Gibson, J., Xu, R.-H., Lee, F. Y. & Drissi, H. Efficient differentiation of human iPSC-derived mesenchymal stem cells to chondroprogenitor cells. *J. Cell. Biochem.* **114**, 480–490 (2013).
172. Wei, Y. *et al.* Chondrogenic differentiation of induced pluripotent stem cells from osteoarthritic chondrocytes in alginate matrix. *Eur. Cell. Mater.* **23**, 1–12 (2012).
173. Ishiuchi, T. *et al.* Early embryonic-like cells are induced by downregulating replication-dependent chromatin assembly. *Nat. Struct. Mol. Biol.* **advance online publication**, (2015).
174. Witkowski, J. A. Dr. Carrel’s immortal cells. *Med. Hist.* **24**, 129–142 (1980).
175. Hayflick, L. & Moorhead, P. S. The serial cultivation of human diploid cell strains. *Exp. Cell Res.* **25**, 585–621 (1961).
176. Hayflick, L. The Limited In Vitro Lifetime of Human Diploid Cell Strains. *Exp. Cell Res.* **37**, 614–636 (1965).
177. Harley, C. B., Futcher, A. B. & Greider, C. W. Telomeres shorten during ageing of human fibroblasts. *Nature* **345**, 458–460 (1990).
178. Allsopp, R. C. *et al.* Telomere length predicts replicative capacity of human fibroblasts. *Proc. Natl. Acad. Sci.* **89**, 10114–10118 (1992).
179. Allsopp, R. C. *et al.* Telomere Shortening Is Associated with Cell Division in Vitro and in Vivo. *Exp. Cell Res.* **220**, 194–200 (1995).
180. Aubert, G. & Lansdorp, P. M. Telomeres and aging. *Physiol. Rev.* **88**, 557–579 (2008).

181. Watson, J. D. & Crick, F. H. Molecular structure of nucleic acids; a structure for deoxyribose nucleic acid. *Nature* **171**, 737–738 (1953).
182. Bessman, M. J., Lehman, I. R., Simms, E. S. & Kornberg, A. Enzymatic synthesis of deoxyribonucleic acid. II. General properties of the reaction. *J. Biol. Chem.* **233**, 171–177 (1958).
183. Olovnikov, A. M. A theory of marginotomy. The incomplete copying of template margin in enzymic synthesis of polynucleotides and biological significance of the phenomenon. *J. Theor. Biol.* **41**, 181–190 (1973).
184. Swiggers, S. J. J. *et al.* Telomerase activity level, but not hTERT mRNA and hTR level, regulates telomere length in telomerase-reconstituted primary fibroblasts. *Exp. Cell Res.* **297**, 434–443 (2004).
185. Shay, J. W. & Wright, W. E. Senescence and immortalization: role of telomeres and telomerase. *Carcinogenesis* **26**, 867–874 (2005).
186. Doksani, Y., Wu, J. Y., de Lange, T. & Zhuang, X. Super-Resolution Fluorescence Imaging of Telomeres Reveals TRF2-Dependent T-loop Formation. *Cell* **155**, 345–356 (2013).
187. Ben-Porath, I. & Weinberg, R. A. When cells get stressed: an integrative view of cellular senescence. *J. Clin. Invest.* **113**, 8–13 (2004).
188. Rodier, F. & Campisi, J. Four faces of cellular senescence. *J. Cell Biol.* **192**, 547–556 (2011).
189. Cristofalo, V. J., Lorenzini, A., Allen, R. G., Torres, C. & Tresini, M. Replicative senescence: a critical review. *Mech. Ageing Dev.* **125**, 827–848 (2004).
190. Dimri, G. P. *et al.* A biomarker that identifies senescent human cells in culture and in aging skin in vivo. *Proc. Natl. Acad. Sci. U. S. A.* **92**, 9363–9367 (1995).
191. Dai, S.-M. *et al.* Catabolic stress induces features of chondrocyte senescence through overexpression of caveolin 1: possible involvement of caveolin 1-induced down-regulation of articular chondrocytes in the pathogenesis of osteoarthritis. *Arthritis Rheum.* **54**, 818–831 (2006).
192. Martin, J. A. & Buckwalter, J. A. Human chondrocyte senescence and osteoarthritis. *Biorheology* **39**, 145–152 (2002).
193. Itahana, K., Campisi, J. & Dimri, G. P. Mechanisms of cellular senescence in human and mouse cells. *Biogerontology* **5**, 1–10 (2004).
194. Ribault, D., Habib, M., Abdel-Majid, K., Barbara, A. & Mitrovic, D. Age-related decrease in the responsiveness of rat articular chondrocytes to EGF is associated with diminished number and affinity for the ligand of cell surface binding sites. *Mech. Ageing Dev.* **100**, 25–40 (1998).

195. Jesus, B. B. de & Blasco, M. A. Assessing Cell and Organ Senescence Biomarkers. *Circ. Res.* **111**, 97–109 (2012).
196. Philipot, D. *et al.* p16INK4a and its regulator miR-24 link senescence and chondrocyte terminal differentiation-associated matrix remodeling in osteoarthritis. *Arthritis Res. Ther.* **16**, R58 (2014).
197. Tchkonina, T., Zhu, Y., van Deursen, J., Campisi, J. & Kirkland, J. L. Cellular senescence and the senescent secretory phenotype: therapeutic opportunities. *J. Clin. Invest.* **123**, 966–972 (2013).
198. Coppé, J.-P. *et al.* A human-like senescence-associated secretory phenotype is conserved in mouse cells dependent on physiological oxygen. *PLoS One* **5**, e9188 (2010).
199. Martin, J. A. & Buckwalter, J. A. The role of chondrocyte senescence in the pathogenesis of osteoarthritis and in limiting cartilage repair. *J. Bone Joint Surg. Am.* **85-A Suppl 2**, 106–110 (2003).
200. Forsyth, N. R., Wright, W. E. & Shay, J. W. Telomerase and differentiation in multicellular organisms: turn it off, turn it on, and turn it off again. *Differ. Res. Biol. Divers.* **69**, 188–197 (2002).
201. Harrington, L. *et al.* A mammalian telomerase-associated protein. *Science* **275**, 973–977 (1997).
202. Yang, C. *et al.* A key role for telomerase reverse transcriptase unit in modulating human embryonic stem cell proliferation, cell cycle dynamics, and in vitro differentiation. *Stem Cells Dayt. Ohio* **26**, 850–863 (2008).
203. MacKenzie, K. L., Franco, S., May, C., Sadelain, M. & Moore, M. A. Mass cultured human fibroblasts overexpressing hTERT encounter a growth crisis following an extended period of proliferation. *Exp. Cell Res.* **259**, 336–350 (2000).
204. Zhou, J., Ding, D., Wang, M. & Cong, Y.-S. Telomerase reverse transcriptase in the regulation of gene expression. *BMB Rep.* **47**, 8–14 (2014).
205. Lee, J. *et al.* TERT promotes cellular and organismal survival independently of telomerase activity. *Oncogene* **27**, 3754–3760 (2008).
206. Jaiswal, R. K., Kumar, P. & Yadava, P. K. Telomerase and its extracurricular activities. *Cell. Mol. Biol. Lett.* **18**, 538–554 (2013).
207. Chapman, E. J. *et al.* Expression of hTERT immortalises normal human urothelial cells without inactivation of the p16/Rb pathway. *Oncogene* **25**, 5037–5045 (2006).
208. Böcker, W. *et al.* Introducing a single-cell-derived human mesenchymal stem cell line expressing hTERT after lentiviral gene transfer. *J. Cell. Mol. Med.* **12**, 1347–1359 (2008).

209. Vaziri, H. & Benchimol, S. Reconstitution of telomerase activity in normal human cells leads to elongation of telomeres and extended replicative life span. *Curr. Biol. CB* **8**, 279–282 (1998).
210. Kay, A., Richardson, J. & Forsyth, N. R. Physiological normoxia and chondrogenic potential of chondrocytes. *Front. Biosci. Elite Ed.* **3**, 1365–1374 (2011).
211. Kay, A. Characterisation of Clinically Relevant Cell Types in an Optimised Hypoxic Environment for Isolation, Expansion and Chondrogenic differentiation. (Keele University, 2010).
212. Harrison, J. S., Rameshwar, P., Chang, V. & Bandari, P. Oxygen saturation in the bone marrow of healthy volunteers. *Blood* **99**, 394 (2002).
213. Lavrentieva, A., Majore, I., Kasper, C. & Hass, R. Effects of hypoxic culture conditions on umbilical cord-derived human mesenchymal stem cells. *Cell Commun. Signal. CCS* **8**, 18 (2010).
214. Abdollahi, H. *et al.* The role of hypoxia in stem cell differentiation and therapeutics. *J. Surg. Res.* **165**, 112–117 (2011).
215. Silver, I. A. Measurement of pH and ionic composition of pericellular sites. *Philos. Trans. R. Soc. Lond. B. Biol. Sci.* **271**, 261–272 (1975).
216. Bruick, R. K. Oxygen Sensing in the Hypoxic Response Pathway: Regulation of the Hypoxia-Inducible Transcription Factor. *Genes Dev.* **17**, 2614–2623 (2003).
217. Dunwoodie, S. L. The Role of Hypoxia in Development of the Mammalian Embryo. *Dev. Cell* **17**, 755–773 (2009).
218. Grayson, W. L., Zhao, F., Bunnell, B. & Ma, T. Hypoxia enhances proliferation and tissue formation of human mesenchymal stem cells. *Biochem. Biophys. Res. Commun.* **358**, 948–953 (2007).
219. Adesida, A. B. *et al.* Human meniscus cells express hypoxia inducible factor-1alpha and increased SOX9 in response to low oxygen tension in cell aggregate culture. *Arthritis Res. Ther.* **9**, R69 (2007).
220. Ezashi, T., Das, P. & Roberts, R. M. Low O<sub>2</sub> tensions and the prevention of differentiation of hES cells. *Proc. Natl. Acad. Sci. U. S. A.* **102**, (2005).
221. Forsyth, N. R. *et al.* Physiologic oxygen enhances human embryonic stem cell clonal recovery and reduces chromosomal abnormalities. *Cloning Stem Cells* **8**, 16–23 (2006).
222. Forsyth, N. R., Evans, A. P., Shay, J. W. & Wright, W. E. Developmental differences in the immortalization of lung fibroblasts by telomerase. *Aging Cell* **2**, 235–43 (2003).

223. Grayson, W. L., Zhao, F., Izadpanah, R., Bunnell, B. & Ma, T. Effects of hypoxia on human mesenchymal stem cell expansion and plasticity in 3D constructs. *J. Cell. Physiol.* **207**, 331–339 (2006).
224. Nekanti, U., Dastidar, S., Venugopal, P., Totey, S. & Ta, M. Increased Proliferation and Analysis of Differential Gene Expression in Human Wharton’s Jelly-derived Mesenchymal Stromal Cells under Hypoxia. *Int. J. Biol. Sci.* **6**, 499–512 (2010).
225. Can, A. & Balci, D. Isolation, culture, and characterization of human umbilical cord stroma-derived mesenchymal stem cells. *Methods Mol. Biol. Clifton NJ* **698**, 51–62 (2011).
226. Foldager, C. B. *et al.* Combined 3D and hypoxic culture improves cartilage-specific gene expression in human chondrocytes. *Acta Orthop.* **82**, 234–240 (2011).
227. Lafont, J. E., Talma, S., Hopfgarten, C. & Murphy, C. L. Hypoxia promotes the differentiated human articular chondrocyte phenotype through SOX9-dependent and -independent pathways. *J. Biol. Chem.* **283**, 4778–4786 (2008).
228. Portron, S. *et al.* Oxygen tension-mediated regulation of chondrogenic differentiation: application to stem cells based osteochondral repair. *Bone Abstr.* (2013). doi:10.1530/boneabs.1.PP254
229. Forsyth, N. R. [1] *et al.* Transcriptome alterations due to physiological normoxic (2% O<sub>2</sub>) culture of human embryonic stem cells. *Regen. Med.* **3**, 817–833 (2008).
230. Kay, A. G. *et al.* BMP2 repression and optimized culture conditions promote human bone marrow-derived mesenchymal stem cell isolation. *Regen. Med.* **10**, 109–125 (2015).
231. Ongena, K., Das, C., Smith, J. L., Gil, S. & Johnston, G. Determining Cell Number During Cell Culture using the Scepter Cell Counter. *J. Vis. Exp. JoVE* (2010). doi:10.3791/2204
232. D’Ippolito, G. *et al.* Marrow-isolated adult multilineage inducible (MIAMI) cells, a unique population of postnatal young and old human cells with extensive expansion and differentiation potential. *J. Cell Sci.* **117**, 2971–2981 (2004).
233. Mastrogiacomo, M., Cancedda, R. & Quarto, R. Effect of different growth factors on the chondrogenic potential of human bone marrow stromal cells. *Osteoarthr. Cartil. OARS Osteoarthr. Res. Soc.* **9 Suppl A**, S36–40 (2001).
234. Forsyth, N. R. & McWhir, J. Human embryonic stem cell telomere length impacts directly on clonal progenitor isolation frequency. *Rejuvenation Res.* **11**, 5–17 (2008).
235. Evans, M. J., Bacharach, E. & Goff, S. P. RNA sequences in the Moloney murine leukemia virus genome bound by the Gag precursor protein in the yeast three-hybrid system. *J. Virol.* **78**, 7677–7684 (2004).

236. Burn, S. F. Detection of  $\beta$ -galactosidase activity: X-gal staining. *Methods Mol. Biol. Clifton NJ* **886**, 241–250 (2012).
237. Schindelin, J. *et al.* Fiji: an open-source platform for biological-image analysis. *Nat. Methods* **9**, 676–682 (2012).
238. Egyházi, S. *et al.* Proteinase K added to the extraction procedure markedly increases RNA yield from primary breast tumors for use in microarray studies. *Clin. Chem.* **50**, 975–976 (2004).
239. Untergasser, A. *et al.* Primer3--new capabilities and interfaces. *Nucleic Acids Res.* **40**, e115 (2012).
240. Koressaar, T. & Remm, M. Enhancements and modifications of primer design program Primer3. *Bioinforma. Oxf. Engl.* **23**, 1289–1291 (2007).
241. Livak, K. J. & Schmittgen, T. D. Analysis of relative gene expression data using real-time quantitative PCR and the 2<sup>(-Delta Delta C(T))</sup> Method. *Methods San Diego Calif* **25**, 402–408 (2001).
242. Pfaffl, M. W., Horgan, G. W. & Dempfle, L. Relative expression software tool (REST) for group-wise comparison and statistical analysis of relative expression results in real-time PCR. *Nucleic Acids Res.* **30**, e36 (2002).
243. de Hoon, M. J. L., Imoto, S., Nolan, J. & Miyano, S. Open source clustering software. *Bioinforma. Oxf. Engl.* **20**, 1453–1454 (2004).
244. Saldanha, A. J. Java Treeview—extensible visualization of microarray data. *Bioinformatics* **20**, 3246–3248 (2004).
245. Maddox, P. H. & Jenkins, D. 3-Aminopropyltriethoxysilane (APES): a new advance in section adhesion. *J. Clin. Pathol.* **40**, 1256–1257 (1987).
246. Schmitz, N., Laverty, S., Kraus, V. B. & Aigner, T. Basic methods in histopathology of joint tissues. *Osteoarthritis Cartilage* **18**, Supplement 3, S113–S116 (2010).
247. in (eds. Ceuninck, F. D., Sabatini, M. & Pastoureau, P.) (Humana Press, 2004).
248. Gluckman, E. *et al.* Transplantation of umbilical cord blood in Fanconi's anemia. *Nouv. Rev. Fr. Hématologie* **32**, 423–425 (1990).
249. Robinson, S. N. *et al.* Mesenchymal stem cells in ex vivo cord blood expansion. *Best Pract. Res. Clin. Haematol.* **24**, 83–92 (2011).
250. Basford, C., Forraz, N., Habibollah, S., Hanger, K. & McGuckin, C. The Cord Blood Separation League Table: a Comparison of the Major Clinical Grade Harvesting Techniques for Cord Blood Stem Cells. *Int. J. Stem Cells* **3**, 32 (2010).

251. Barker, J. N. *et al.* Availability of cord blood extends allogeneic hematopoietic stem cell transplant access to racial and ethnic minorities. *Biol. Blood Marrow Transplant. J. Am. Soc. Blood Marrow Transplant.* **16**, 1541–1548 (2010).
252. Behzad-Behbahani, A. *et al.* Risk of Viral Transmission Via Bone Marrow Progenitor Cells Versus Umbilical Cord Blood Hematopoietic Stem Cells in Bone Marrow Transplantation. *Transplant. Proc.* **37**, 3211–3212 (2005).
253. Secunda, R. *et al.* Isolation, expansion and characterisation of mesenchymal stem cells from human bone marrow, adipose tissue, umbilical cord blood and matrix: a comparative study. *Cytotechnology* 1–15 (2014). doi:10.1007/s10616-014-9718-z
254. Jin, H. J. *et al.* Comparative Analysis of Human Mesenchymal Stem Cells from Bone Marrow, Adipose Tissue, and Umbilical Cord Blood as Sources of Cell Therapy. *Int. J. Mol. Sci.* **14**, 17986–18001 (2013).
255. Munoz, J. *et al.* Concise Review: Umbilical Cord Blood Transplantation: Past, Present, and Future. *Stem Cells Transl. Med.* **3**, 1435–1443 (2014).
256. WHO | Optimal timing of cord clamping for the prevention of iron deficiency anaemia in infants. WHO Available at: [http://www.who.int/elena/titles/full\\_recommendations/cord\\_clamping/en/](http://www.who.int/elena/titles/full_recommendations/cord_clamping/en/). (Accessed: 27th September 2015)
257. McDonald, S. J., Middleton, P., Dowswell, T. & Morris, P. S. in *Cochrane Database of Systematic Reviews* (John Wiley & Sons, Ltd, 2013).
258. Linderkamp, O., Nelle, M., Kraus, M. & Zilow, E. P. The effect of early and late cord-clamping on blood viscosity and other hemorheological parameters in full-term neonates. *Acta Pædiatrica* **81**, 745–750 (1992).
259. Katsares, V. *et al.* Reference Ranges for Umbilical Cord Blood Hematological Values. *Lab Med.* **40**, 437–439 (2009).
260. Jones, J. *et al.* Obstetric predictors of placental/umbilical cord blood volume for transplantation. *Am. J. Obstet. Gynecol.* **188**, 503–509 (2003).
261. Yang, J., Zhang, L., Yu, C., Yang, X.-F. & Wang, H. Monocyte and macrophage differentiation: circulation inflammatory monocyte as biomarker for inflammatory diseases. *Biomark. Res.* **2**, 1 (2014).
262. Graziani-Bowering, G. M., Graham, J. M. & Fillion, L. G. A quick, easy and inexpensive method for the isolation of human peripheral blood monocytes. *J. Immunol. Methods* **207**, 157–168 (1997).

263. Massey, H. M. & Flanagan, A. M. Human osteoclasts derive from CD14-positive monocytes. *Br. J. Haematol.* **106**, 167–170 (1999).
264. Italiani, P. & Boraschi, D. From Monocytes to M1/M2 Macrophages: Phenotypical vs. Functional Differentiation. *Front. Immunol.* **5**, (2014).
265. El-Sahrigy, S. A., Mohamed, N. A., Talkhan, H. A. & Rahman, A. M. A. Comparison between magnetic activated cell sorted monocytes and monocyte adherence techniques for in vitro generation of immature dendritic cells: an Egyptian trial. *Cent.-Eur. J. Immunol.* **40**, 18–24 (2015).
266. Alfonso, Z. Z. C., Forneck, E. D., Allebrandt, W. F. & Nardi, N. B. Establishment of an adherent cell layer from human umbilical cord blood. *Genet. Mol. Biol.* **23**, 519–522 (2000).
267. Horton, M. A. The  $\alpha\beta 3$  integrin 'vitronectin receptor'. *Int. J. Biochem. Cell Biol.* **29**, 721–725 (1997).
268. Immune interferon induces the receptor for monomeric IgG1 on human monocytic and myeloid cells. *J. Exp. Med.* **158**, 1092–1113 (1983).
269. Kruger, M., Van de Winkel, J. G., De Wit, T. P., Coorevits, L. & Ceuppens, J. L. Granulocyte-macrophage colony-stimulating factor down-regulates CD14 expression on monocytes. *Immunology* **89**, 89–95 (1996).
270. Perdikogianni, C., Dimitriou, H., Stiakaki, E., Martimianaki, G. & Kalmanti, M. Could cord blood be a source of mesenchymal stromal cells for clinical use? *Cytotherapy* **10**, 452–459 (2008).
271. Alvarez-Viejo, M. *et al.* LNGFR (CD271) as Marker to Identify Mesenchymal Stem Cells from Different Human Sources: Umbilical Cord Blood, Wharton's Jelly and Bone Marrow. *J. Bone Marrow Res.* **1**, (2013).
272. Zeddou, M. *et al.* The umbilical cord matrix is a better source of mesenchymal stem cells (MSC) than the umbilical cord blood. *Cell Biol. Int.* **34**, 693–701 (2010).
273. Lee, O. K. *et al.* Isolation of multipotent mesenchymal stem cells from umbilical cord blood. *Blood* **103**, 1669–1675 (2004).
274. Calabrese, G. *et al.* Potential Effect of CD271 on Human Mesenchymal Stromal Cell Proliferation and Differentiation. *Int. J. Mol. Sci.* **16**, 15609–15624 (2015).
275. Gutiérrez-Rodríguez, M., Reyes-Maldonado, E. & Mayani, H. Characterization of the adherent cells developed in Dexter-type long-term cultures from human umbilical cord blood. *Stem Cells Dayt. Ohio* **18**, 46–52 (2000).

276. Majumdar, M. K., Thiede, M. A., Mosca, J. D., Moorman, M. & Gerson, S. L. Phenotypic and functional comparison of cultures of marrow-derived mesenchymal stem cells (MSCs) and stromal cells. *J. Cell. Physiol.* **176**, 57–66 (1998).
277. BIE, Y., XU, Q. & ZHANG, Z. Isolation of dendritic cells from umbilical cord blood using magnetic activated cell sorting or adherence. *Oncol. Lett.* **10**, 67–70 (2015).
278. Honn, K. V., Singley, J. A. & Chavin, W. Fetal Bovine Serum: A Multivariate Standard. *Exp. Biol. Med.* **149**, 344–347 (1975).
279. Zheng, X. *et al.* Proteomic analysis for the assessment of different lots of fetal bovine serum as a raw material for cell culture. Part IV. Application of proteomics to the manufacture of biological drugs. *Biotechnol. Prog.* **22**, 1294–1300 (2006).
280. Capiod, J.-C. *et al.* Characterization and comparison of bone marrow and peripheral blood mononuclear cells used for cellular therapy in critical leg ischaemia: towards a new cellular product. *Vox Sang.* **96**, 256–265 (2009).
281. Pimentel-Coelho, P. M., Rosado-de-Castro, P. H., Barbosa da Fonseca, L. M. & Mendez-Otero, R. Umbilical cord blood mononuclear cell transplantation for neonatal hypoxic-ischemic encephalopathy. *Pediatr. Res.* **71**, 464–473 (2012).
282. Strehl, C. *et al.* Hypoxia: how does the monocyte-macrophage system respond to changes in oxygen availability? *J. Leukoc. Biol.* **95**, 233–241 (2014).
283. Delirez, N., Shojaeefar, E., Parvin, P. & Asadi, B. Comparison The Effects of Two Monocyte Isolation Methods, Plastic Adherence and Magnetic Activated Cell Sorting Methods, on Phagocytic Activity of Generated Dendritic Cells. *Cell J. Yakhteh* **15**, 218–223 (2013).
284. Perera, L. P. & Waldmann, T. A. Activation of human monocytes induces differential resistance to apoptosis with rapid down regulation of caspase-8/FLICE. *Proc. Natl. Acad. Sci.* **95**, 14308–14313 (1998).
285. Rey-Giraud, F., Hafner, M. & Ries, C. H. In Vitro Generation of Monocyte-Derived Macrophages under Serum-Free Conditions Improves Their Tumor Promoting Functions. *PLoS ONE* **7**, e42656 (2012).
286. Gamble, J. R., Elliott, M. J., Jaipargas, E., Lopez, A. F. & Vadas, M. A. Regulation of human monocyte adherence by granulocyte-macrophage colony-stimulating factor. *Proc. Natl. Acad. Sci. U. S. A.* **86**, 7169–7173 (1989).
287. Elliott, M. J., Gamble, J. R., Park, L. S., Vadas, M. A. & Lopez, A. F. Inhibition of human monocyte adhesion by interleukin-4. *Blood* **77**, 2739–2745 (1991).

288. Wahl, S. M., Allen, J. B., Weeks, B. S., Wong, H. L. & Klotman, P. E. Transforming growth factor beta enhances integrin expression and type IV collagenase secretion in human monocytes. *Proc. Natl. Acad. Sci. U. S. A.* **90**, 4577–4581 (1993).
289. Schuh, E. M. *et al.* Identification of variables that optimize isolation and culture of multipotent mesenchymal stem cells from equine umbilical-cord blood. *Am. J. Vet. Res.* **70**, 1526–1535 (2009).
290. Melief, S. M., Geutskens, S. B., Fibbe, W. E. & Roelofs, H. Multipotent stromal cells skew monocytes towards an anti-inflammatory interleukin-10-producing phenotype by production of interleukin-6. *Haematologica* **98**, 888–895 (2013).
291. Tarasova, N. K. *et al.* Proteomics Reveals a Role for Attachment in Monocyte Differentiation into Efficient Proinflammatory Macrophages. *J. Proteome Res.* (2015). doi:10.1021/acs.jproteome.5b00659
292. Sekiya, I. *et al.* Expansion of Human Adult Stem Cells from Bone Marrow Stroma: Conditions that Maximize the Yields of Early Progenitors and Evaluate Their Quality. *STEM CELLS* **20**, 530–541 (2002).
293. Balint, R., Richardson, S. M. & Cartmell, S. H. Low-density subculture: a technical note on the importance of avoiding cell-to-cell contact during mesenchymal stromal cell expansion. *J. Tissue Eng. Regen. Med.* n/a–n/a (2015). doi:10.1002/term.2051
294. Halliwell, B. Oxidative stress in cell culture: an under-appreciated problem? *FEBS Lett.* **540**, 3–6 (2003).
295. Duarte, T. L. & Lunec, J. Review: When is an antioxidant not an antioxidant? A review of novel actions and reactions of vitamin C. *Free Radic. Res.* **39**, 671–86 (2005).
296. Sauer, H., Rahimi, G., Hescheler, J. & Wartenberg, M. Role of reactive oxygen species and phosphatidylinositol 3-kinase in cardiomyocyte differentiation of embryonic stem cells. *FEBS Lett.* **476**, 218–23 (2000).
297. Oxygen supply and oxygen-dependent gene expression in differentiating embryonic stem cells. (1996). Available at: <http://www.pnas.org/content/93/7/2867.abstract>. (Accessed: 9th July 2008)
298. Yen, E. H. K., Sodek, J. & Melcher, A. H. The effect of oxygen partial pressure on protein synthesis and collagen hydroxylation by mature periodontal tissues maintained in organ cultures. *Biochem. J.* **178**, (1979).
299. Ohnishi, S., Yasuda, T., Kitamura, S. & Nagaya, N. Effect of Hypoxia on Gene Expression of Bone Marrow-derived Mesenchymal Stem Cells and Mononuclear Cells. *Stem Cells* 2006–0347 (2007). doi:10.1634/stemcells.2006-0347

300. Bonello, S. *et al.* Reactive Oxygen Species Activate the HIF-1{alpha} Promoter Via a Functional NF{kappa}B Site. *Arter. Thromb Vasc Biol* **27**, 755–761 (2007).
301. Wenger, R. H., Stiehl, D. P. & Camenisch, G. Integration of Oxygen Signaling at the Consensus HRE. *Sci STKE* **2005**, re12 (2005).
302. Kietzmann, T. & Grlach, A. Reactive oxygen species in the control of hypoxia-inducible factor-mediated gene expression. *Semin. Cell Dev. Biol.* **16**, 474–486 (2005).
303. Okazaki, K. & Maltepe, E. Oxygen, epigenetics and stem cell fate. *Regen. Med.* **1**, 71–83 (2006).
304. Lin, Q., Alarcon, R. M. & Yun, Z. Oxygen and Cell Fate Decisions. *Gene Regul. Andj Syst. Biol.* **2**, 43–51 (2008).
305. Kumar, D., Gupta, S., Yang, Y. & Forsyth, N. R.  $\alpha$ V  $\beta$ 5 and CD44 are oxygen-regulated human embryonic stem cell attachment factors. *BioMed Res. Int.* **2013**, 729281 (2013).
306. van der Valk, J. *et al.* Optimization of chemically defined cell culture media – Replacing fetal bovine serum in mammalian in vitro methods. *Toxicol. In Vitro* **24**, 1053–1063 (2010).
307. Pereira, T. *et al.* MSCs Conditioned Media and Umbilical Cord Blood Plasma Metabolomics and Composition. *PLoS ONE* **9**, e113769 (2014).
308. Wang, X. *et al.* Mechanism of simvastatin on induction of heat shock protein in osteoblasts. *Arch. Biochem. Biophys.* **415**, 6–13 (2003).
309. Zhuang, Y. *et al.* Comparison of biological properties of umbilical cord-derived mesenchymal stem cells from early and late passages: Immunomodulatory ability is enhanced in aged cells. *Mol. Med. Rep.* (2014). doi:10.3892/mmr.2014.2755
310. Goldring, M. B. Chondrogenesis, chondrocyte differentiation, and articular cartilage metabolism in health and osteoarthritis. *Ther. Adv. Musculoskelet. Dis.* **4**, 269–285 (2012).
311. Meyer, U. in *Fundamentals of Tissue Engineering and Regenerative Medicine* (eds. Meyer, U., Handschel, J., Wiesmann, H. P. & Meyer, T.) 5–12 (Springer Berlin Heidelberg, 2009).
312. Peterson, L., Vasiliadis, H. S., Brittberg, M. & Lindahl, A. Autologous chondrocyte implantation: a long-term follow-up. *Am. J. Sports Med.* **38**, 1117–1124 (2010).
313. Peterson, L. *et al.* Two- to 9-year outcome after autologous chondrocyte transplantation of the knee. *Clin. Orthop.* 212–34 (2000). doi:10818982
314. Diaz-Romero, J. *et al.* Immunophenotypic analysis of human articular chondrocytes: changes in surface markers associated with cell expansion in monolayer culture. *J. Cell. Physiol.* **202**, 731–742 (2005).
315. Martin, J. A. & Buckwalter, J. A. Telomere Erosion and Senescence in Human Articular Cartilage Chondrocytes. *J. Gerontol. A. Biol. Sci. Med. Sci.* **56**, B172–B179 (2001).

316. Friedenstein, A. J., Chailakhyan, R. K., Latsinik, N. V., Panasyuk, A. F. & Keiliss-Borok, I. V. Stromal cells responsible for transferring the microenvironment of the hemopoietic tissues. Cloning in vitro and retransplantation in vivo. *Transplantation* **17**, 331–340 (1974).
317. Stewart, M. C. & Stewart, A. A. Mesenchymal Stem Cells: Characteristics, Sources, and Mechanisms of Action. *Vet. Clin. North Am. Equine Pract.* **27**, 243–261 (2011).
318. Musina, R. A., Bekchanova, E. S., Belyavskii, A. V., Grinenko, T. S. & Sukhikh, G. T. Umbilical cord blood mesenchymal stem cells. *Bull. Exp. Biol. Med.* **143**, 127–131 (2007).
319. Siddappa, R., Licht, R., van Blitterswijk, C. & de Boer, J. Donor variation and loss of multipotency during in vitro expansion of human mesenchymal stem cells for bone tissue engineering. *J. Orthop. Res.* **25**, 1029–1041 (2007).
320. Stolzing, A., Jones, E., McGonagle, D. & Scutt, A. Age-related changes in human bone marrow-derived mesenchymal stem cells: Consequences for cell therapies. *Mech. Ageing Dev.* **129**, 163–173 (2008).
321. von Zglinicki, T., Saretzki, G., Ladhoff, J., d’Adda di Fagagna, F. & Jackson, S. P. Human cell senescence as a DNA damage response. *Mech. Ageing Dev.* **126**, 111–117 (2005).
322. Fumagalli, M. *et al.* Telomeric DNA damage is irreparable and causes persistent DNA-damage-response activation. *Nat. Cell Biol.* **14**, 355–365 (2012).
323. Hewitt, G. *et al.* Telomeres are favoured targets of a persistent DNA damage response in ageing and stress-induced senescence. *Nat. Commun.* **3**, 708 (2012).
324. Suram, A. *et al.* Oncogene-induced telomere dysfunction enforces cellular senescence in human cancer precursor lesions. *EMBO J.* **31**, 2839–2851 (2012).
325. Kolquist, K. A. *et al.* Expression of TERT in early premalignant lesions and a subset of cells in normal tissues. *Nat. Genet.* **19**, 182–186 (1998).
326. Ducrest, A.-L., Szutorisz, H., Lingner, J. & Nabholz, M. Regulation of the human telomerase reverse transcriptase gene. *Oncogene* **21**, 541–552 (2002).
327. Shay, J. W. & Wright, W. E. Use of Telomerase to Create Bioengineered Tissues. *Ann. N. Y. Acad. Sci.* **1057**, 479–491 (2005).
328. Bodnar, A. G. *et al.* Extension of Life-Span by Introduction of Telomerase into Normal Human Cells. *Science* **279**, 349–352 (1998).
329. Antal, M., Boros, É., Solymosy, F. & Kiss, T. Analysis of the structure of human telomerase RNA in vivo. *Nucleic Acids Res.* **30**, 912–920 (2002).
330. Counter, C. M. *et al.* Telomerase activity is restored in human cells by ectopic expression of hTERT (hEST2), the catalytic subunit of telomerase. *Oncogene* **16**, 1217–1222 (1998).

331. Tew, S. R., Murdoch, A. D., Rauchenberg, R. P. & Hardingham, T. E. Cellular methods in cartilage research: Primary human chondrocytes in culture and chondrogenesis in human bone marrow stem cells. *Methods* **45**, 2–9 (2008).
332. Tew, S. R. *et al.* Retroviral transduction with SOX9 enhances re-expression of the chondrocyte phenotype in passaged osteoarthritic human articular chondrocytes. *Osteoarthr. Cartil. OARS Osteoarthr. Res. Soc.* **13**, 80–89 (2005).
333. Parsch, D., Fellenberg, J., Brümmendorf, T. H., Eschlbeck, A.-M. & Richter, W. Telomere length and telomerase activity during expansion and differentiation of human mesenchymal stem cells and chondrocytes. *J. Mol. Med. Berl. Ger.* **82**, 49–55 (2004).
334. Parsch, D., Brümmendorf, T. H., Richter, W. & Fellenberg, J. Replicative aging of human articular chondrocytes during ex vivo expansion. *Arthritis Rheum.* **46**, 2911–2916 (2002).
335. Zimmermann, S. *et al.* Lack of telomerase activity in human mesenchymal stem cells. *Leukemia* **17**, 1146–1149 (2003).
336. Graakjaer, J., Christensen, R., Kolvraa, S. & Serakinci, N. Mesenchymal stem cells with high telomerase expression do not actively restore their chromosome arm specific telomere length pattern after exposure to ionizing radiation. *BMC Mol. Biol.* **8**, 49 (2007).
337. Serakinci, N., Graakjaer, J. & Kolvraa, S. Telomere stability and telomerase in mesenchymal stem cells. *Biochimie* **90**, 33–40 (2008).
338. Simonsen, J. L. *et al.* Telomerase expression extends the proliferative life-span and maintains the osteogenic potential of human bone marrow stromal cells. *Nat. Biotechnol.* **20**, 592–596 (2002).
339. Piera-Velazquez, S., Jimenez, S. A. & Stokes, D. Increased life span of human osteoarthritic chondrocytes by exogenous expression of telomerase. *Arthritis Rheum.* **46**, 683–693 (2002).
340. Evans, C. H. & Georgescu, H. I. Observations on the senescence of cells derived from articular cartilage. *Mech. Ageing Dev.* **22**, 179–191 (1983).
341. Estrada, J. C. *et al.* Human mesenchymal stem cell-replicative senescence and oxidative stress are closely linked to aneuploidy. *Cell Death Dis.* **4**, e691 (2013).
342. Mihara, K. *et al.* Development and functional characterization of human bone marrow mesenchymal cells immortalized by enforced expression of telomerase. *Br. J. Haematol.* **120**, 846–849 (2003).
343. Kuilman, T., Michaloglou, C., Mooi, W. J. & Peeper, D. S. The essence of senescence. *Genes Dev.* **24**, 2463–2479 (2010).
344. Goldring, M. B. Immortalization of human articular chondrocytes for generation of stable, differentiated cell lines. *Methods Mol. Med.* **100**, 23–36 (2004).

345. Kokenyesi, R., Tan, L., Robbins, J. R. & Goldring, M. B. Proteoglycan production by immortalized human chondrocyte cell lines cultured under conditions that promote expression of the differentiated phenotype. *Arch. Biochem. Biophys.* **383**, 79–90 (2000).
346. Goldring, M. B. Culture of immortalized chondrocytes and their use as models of chondrocyte function. *Methods Mol. Med.* **100**, 37–52 (2004).
347. Martin, J. A., Mitchell, C. J., Klingelhutz, A. J. & Buckwalter, J. A. Effects of Telomerase and Viral Oncogene Expression on the In Vitro Growth of Human Chondrocytes. *J. Gerontol. A. Biol. Sci. Med. Sci.* **57**, B48–B53 (2002).
348. Martin, J. A., Klingelhutz, A. J., Moussavi-Harami, F. & Buckwalter, J. A. Effects of oxidative damage and telomerase activity on human articular cartilage chondrocyte senescence. *J. Gerontol. A. Biol. Sci. Med. Sci.* **59**, 324–337 (2004).
349. Choi, M. & Lee, C. Immortalization of Primary Keratinocytes and Its Application to Skin Research. *Biomol. Ther.* **23**, 391–399 (2015).
350. Lee, B. Y. *et al.* Senescence-associated beta-galactosidase is lysosomal beta-galactosidase. *Aging Cell* **5**, 187–195 (2006).
351. Severino, J., Allen, R. G., Balin, S., Balin, A. & Cristofalo, V. J. Is beta-galactosidase staining a marker of senescence in vitro and in vivo? *Exp. Cell Res.* **257**, 162–171 (2000).
352. Untergasser, G. *et al.* TGF-beta cytokines increase senescence-associated beta-galactosidase activity in human prostate basal cells by supporting differentiation processes, but not cellular senescence. *Exp. Gerontol.* **38**, 1179–1188 (2003).
353. Zhu, C.-H. *et al.* Cellular senescence in human myoblasts is overcome by human telomerase reverse transcriptase and cyclin-dependent kinase 4: consequences in aging muscle and therapeutic strategies for muscular dystrophies. *Aging Cell* **6**, 515–523 (2007).
354. Le Blanc, K., Tammik, C., Rosendahl, K., Zetterberg, E. & Ringdén, O. HLA expression and immunologic properties of differentiated and undifferentiated mesenchymal stem cells. *Exp. Hematol.* **31**, 890–896 (2003).
355. Tarte, K. *et al.* Clinical-grade production of human mesenchymal stromal cells: occurrence of aneuploidy without transformation. *Blood* **115**, 1549–1553 (2010).
356. Bocelli-Tyndall, C. *et al.* Fibroblast growth factor 2 and platelet-derived growth factor, but not platelet lysate, induce proliferation-dependent, functional class II major histocompatibility complex antigen in human mesenchymal stem cells. *Arthritis Rheum.* **62**, 3815–3825 (2010).

357. Benz, K., Stippich, C., Freudigmann, C., Mollenhauer, J. A. & Aicher, W. K. Maintenance of 'stem cell' features of cartilage cell sub-populations during in vitro propagation. *J. Transl. Med.* **11**, 27 (2013).
358. Ichinose, S. *et al.* Morphological differences during in vitro chondrogenesis of bone marrow-, synovium-MSCs, and chondrocytes. *Lab. Investig. J. Tech. Methods Pathol.* **90**, 210–221 (2010).
359. Williams, R. *et al.* Identification and Clonal Characterisation of a Progenitor Cell Sub-Population in Normal Human Articular Cartilage. *PLoS ONE* **5**, (2010).
360. Wagner, W. *et al.* Replicative Senescence of Mesenchymal Stem Cells: A Continuous and Organized Process. *PLoS ONE* **3**, e2213 (2008).
361. Home - ClinicalTrials.gov. Available at: <https://clinicaltrials.gov/ct2/home>. (Accessed: 10th August 2015)
362. The use of autologous chondrocyte implantation for the treatment of cartilage defects in the knee joints | Guidance and guidelines | NICE. Available at: <http://www.nice.org.uk/guidance/ta89>. (Accessed: 28th September 2015)
363. Sutton, P. M. & Holloway, E. S. The young osteoarthritic knee: dilemmas in management. *BMC Med.* **11**, 14 (2013).
364. Wang, W., Rigueur, D. & Lyons, K. M. TGF $\beta$  signaling in cartilage development and maintenance. *Birth Defects Res. Part C Embryo Today Rev.* **102**, 37–51 (2014).
365. Clarke, L. E. *et al.* Growth differentiation factor 6 and transforming growth factor-beta differentially mediate mesenchymal stem cell differentiation, composition, and micromechanical properties of nucleus pulposus constructs. *Arthritis Res. Ther.* **16**, R67 (2014).
366. Jakobsen, R. B., Østrup, E., Zhang, X., Mikkelsen, T. S. & Brinchmann, J. E. Analysis of the Effects of Five Factors Relevant to In Vitro Chondrogenesis of Human Mesenchymal Stem Cells Using Factorial Design and High Throughput mRNA-Profilng. *PLoS ONE* **9**, (2014).
367. Lin, Y. *et al.* Molecular and cellular characterization during chondrogenic differentiation of adipose tissue-derived stromal cells in vitro and cartilage formation in vivo. *J. Cell. Mol. Med.* **9**, 929–939 (2005).
368. Portron, S. *et al.* Effects of In Vitro Low Oxygen Tension Preconditioning of Adipose Stromal Cells on Their In Vivo Chondrogenic Potential: Application in Cartilage Tissue Repair. *PLoS ONE* **8**, e62368 (2013).
369. Dessau, W., Vertel, B. M., von der Mark, H. & von der Mark, K. Extracellular matrix formation by chondrocytes in monolayer culture. *J. Cell Biol.* **90**, 78–83 (1981).

370. Hunziker, E. B., Driesang, I. M. & Morris, E. A. Chondrogenesis in cartilage repair is induced by members of the transforming growth factor-beta superfamily. *Clin. Orthop.* S171–181 (2001).
371. Abbott, R. D., Purmessur, D., Monsey, R. D. & Iatridis, J. C. Regenerative Potential of TGFβ3 + Dex and Notochordal Cell Conditioned Media on Degenerated Human Intervertebral Disc Cells. *J. Orthop. Res.* **30**, 482–488 (2012).
372. Shahin, K. & Doran, P. M. Strategies for enhancing the accumulation and retention of extracellular matrix in tissue-engineered cartilage cultured in bioreactors. *PLoS One* **6**, e23119 (2011).
373. Kuh, S. U. *et al.* A comparison of three cell types as potential candidates for intervertebral disc therapy: Annulus fibrosus cells, chondrocytes, and bone marrow derived cells. *Joint Bone Spine* **76**, 70–74 (2009).
374. Okamoto, T. *et al.* Clonal heterogeneity in differentiation potential of immortalized human mesenchymal stem cells. *Biochem. Biophys. Res. Commun.* **295**, 354–361 (2002).
375. Babur, B. K. *et al.* The Interplay between Chondrocyte Redifferentiation Pellet Size and Oxygen Concentration. *PLoS ONE* **8**, e58865 (2013).
376. Caron, M. M. J. *et al.* Redifferentiation of dedifferentiated human articular chondrocytes: comparison of 2D and 3D cultures. *Osteoarthritis Cartilage* **20**, 1170–1178 (2012).
377. Puetzer, J. L., Petite, J. N. & Lobo, E. G. Comparative Review of Growth Factors for Induction of Three-Dimensional In Vitro Chondrogenesis in Human Mesenchymal Stem Cells Isolated from Bone Marrow and Adipose Tissue. *Tissue Eng. Part B Rev.* **16**, 435–444 (2010).
378. Sart, S., Tsai, A.-C., Li, Y. & Ma, T. Three-Dimensional Aggregates of Mesenchymal Stem Cells: Cellular Mechanisms, Biological Properties, and Applications. *Tissue Eng. Part B Rev.* **20**, 365–380 (2013).
379. Benya, P. D. & Shaffer, J. D. Dedifferentiated chondrocytes reexpress the differentiated collagen phenotype when cultured in agarose gels. *Cell* **30**, 215–224 (1982).
380. Chung, C. & Burdick, J. A. Influence of 3D Hyaluronic Acid Microenvironments on Mesenchymal Stem Cell Chondrogenesis. *Tissue Eng. Part A* **15**, 243–254 (2009).
381. Nettles, D. L., Vail, T. P., Morgan, M. T., Grinstaff, M. W. & Setton, L. A. Photocrosslinkable hyaluronan as a scaffold for articular cartilage repair. *Ann. Biomed. Eng.* **32**, 391–397 (2004).
382. Johnstone, B., Hering, T. M., Caplan, A. I., Goldberg, V. M. & Yoo, J. U. In Vitro Chondrogenesis of Bone Marrow-Derived Mesenchymal Progenitor Cells. *Exp. Cell Res.* **238**, 265–272 (1998).

383. Schrobback, K., Klein, T. J. & Woodfield, T. B. F. The Importance of Connexin Hemichannels During Chondroprogenitor Cell Differentiation in Hydrogel Versus Microtissue Culture Models. *Tissue Eng. Part A* **21**, 1785–1794 (2015).
384. Li, H. *et al.* Comparative analysis with collagen type II distinguishes cartilage oligomeric matrix protein as a primary TGF $\beta$ -responsive gene. *Osteoarthr. Cartil. OARS Osteoarthr. Res. Soc.* **19**, 1246–1253 (2011).
385. Winter, A. *et al.* Cartilage-like gene expression in differentiated human stem cell spheroids: a comparison of bone marrow-derived and adipose tissue-derived stromal cells. *Arthritis Rheum.* **48**, 418–429 (2003).
386. Giovannini, S. *et al.* Micromass co-culture of human articular chondrocytes and human bone marrow mesenchymal stem cells to investigate stable neocartilage tissue formation in vitro. *Eur. Cell. Mater.* **20**, 245–259 (2010).
387. Shu, K., Thatte, H. & Spector, M. Chondrogenic differentiation of adult mesenchymal stem cells and embryonic stem cells. in *Bioengineering Conference, 2009 IEEE 35th Annual Northeast* 1–2 (2009). doi:10.1109/NEBC.2009.4967739
388. Kitagawa, F., Takei, S., Imaizumi, T. & Tabata, Y. Chondrogenic differentiation of immortalized human mesenchymal stem cells on zirconia microwell substrata. *Tissue Eng. Part C Methods* **19**, 438–448 (2013).
389. Sart, S., Tsai, A.-C., Li, Y. & Ma, T. Three-Dimensional Aggregates of Mesenchymal Stem Cells: Cellular Mechanisms, Biological Properties, and Applications. *Tissue Eng. Part B Rev.* **20**, 365–380 (2013).
390. Li, S., Oreffo, R. o. c., Sengers, B. g. & Tare, R. s. The effect of oxygen tension on human articular chondrocyte matrix synthesis: Integration of experimental and computational approaches. *Biotechnol. Bioeng.* **111**, 1876–1885 (2014).
391. Ruiz, S. A. & Chen, C. S. Emergence of patterned stem cell differentiation within multicellular structures. *Stem Cells Dayt. Ohio* **26**, 2921–2927 (2008).
392. Zhang, L. *et al.* Chondrogenic differentiation of human mesenchymal stem cells: a comparison between micromass and pellet culture systems. *Biotechnol. Lett.* **32**, 1339–1346 (2010).
393. Murdoch, A. D. *et al.* Chondrogenic Differentiation of Human Bone Marrow Stem Cells in Transwell Cultures: Generation of Scaffold-Free Cartilage. *STEM CELLS* **25**, 2786–2796 (2007).
394. Kim, K., Zakharkin, S. O. & Allison, D. B. Expectations, validity, and reality in gene expression profiling expectations. *J. Clin. Epidemiol.* **63**, 950–959 (2010).

395. Cheadle, C. *et al.* Stability regulation of mRNA and the control of gene expression. *Ann. N. Y. Acad. Sci.* **1058**, 196–204 (2005).
396. Liu, K. *et al.* The dependence of in vivo stable ectopic chondrogenesis by human mesenchymal stem cells on chondrogenic differentiation in vitro. *Biomaterials* **29**, 2183–2192 (2008).
397. Elahi, K. C. *et al.* Human Mesenchymal Stromal Cells from Different Sources Diverge in Their Expression of Cell Surface Proteins and Display Distinct Differentiation Patterns. *Stem Cells Int.*
398. Lalu, M. M. *et al.* Safety of Cell Therapy with Mesenchymal Stromal Cells (SafeCell): A Systematic Review and Meta-Analysis of Clinical Trials. *PLoS ONE* **7**, e47559 (2012).
399. Farrell, M. J. *et al.* Functional properties of bone marrow-derived MSC-based engineered cartilage are unstable with very long-term in vitro culture. *J. Biomech.* **47**, 2173–2182 (2014).
400. Boeuf, S. & Richter, W. Chondrogenesis of mesenchymal stem cells: role of tissue source and inducing factors. *Stem Cell Res. Ther.* **1**, 31 (2010).
401. Almeida, H. V. *et al.* Controlled release of transforming growth factor- $\beta$ 3 from cartilage-extra-cellular-matrix-derived scaffolds to promote chondrogenesis of human-joint-tissue-derived stem cells. *Acta Biomater.* **10**, 4400–4409 (2014).
402. Brown, P. T., Squire, M. W. & Li, W.-J. Characterization and evaluation of mesenchymal stem cells derived from human embryonic stem cells and bone marrow. *Cell Tissue Res.* **358**, 149–164 (2014).
403. Gentry, T. & Smith, C. Retroviral vector-mediated gene transfer into umbilical cord blood CD34<sup>br</sup>CD38<sup>-</sup>CD33<sup>-</sup> cells. *Exp. Hematol.* **27**, 1244–1254 (1999).
404. Liu, T. M. *et al.* Molecular Basis of immortalization of Human Mesenchymal Stem Cells by Combination of p53 Knockdown and Human Telomerase Reverse Transcriptase Overexpression. *Stem Cells Dev.* **22**, 268–278 (2013).
405. Piper, S. L. *et al.* Inducible immortality in hTERT-human mesenchymal stem cells. *J. Orthop. Res.* **30**, 1879–1885 (2012).
406. Steinert, S., Shay, J. W. & Wright, W. E. Transient expression of human telomerase extends the life span of normal human fibroblasts. *Biochem. Biophys. Res. Commun.* **273**, 1095–1098 (2000).
407. Tang, H. *et al.* Dual expression of hTERT and VEGF prolongs life span and enhances angiogenic ability of aged BMSCs. *Biochem. Biophys. Res. Commun.* **440**, 502–508 (2013).

408. Wolbank, S. *et al.* Telomerase Immortalized Human Amnion- and Adipose-Derived Mesenchymal Stem Cells: Maintenance of Differentiation and Immunomodulatory Characteristics. *Tissue Eng. Part A* **15**, 1843–1854 (2009).
409. Majumdar, M. K. *et al.* Immortalized mouse articular cartilage cell lines retain chondrocyte phenotype and respond to both anabolic factor BMP-2 and pro-inflammatory factor IL-1. *J. Cell. Physiol.* **215**, 68–76 (2008).
410. Robbins, J. R. *et al.* Immortalized human adult articular chondrocytes maintain cartilage-specific phenotype and responses to interleukin-1beta. *Arthritis Rheum.* **43**, 2189–2201 (2000).
411. Dong, F. *et al.* The isolation and characterization of a telomerase immortalized goat trophoblast cell line. *Placenta* **34**, 1243–1250 (2013).
412. Lee, K. M., Choi, K. H. & Ouellette, M. M. Use of exogenous hTERT to immortalize primary human cells. *Cytotechnology* **45**, 33–38 (2004).
413. Halliwell, B. Cell culture, oxidative stress, and antioxidants: Avoiding pitfalls. *Biomed. J.* **0**, 0 (2014).
414. Brandl, A., Meyer, M., Bechmann, V., Nerlich, M. & Angele, P. Oxidative stress induces senescence in human mesenchymal stem cells. *Exp. Cell Res.* **317**, 1541–1547 (2011).
415. Eleswarapu, S. V., Leipzig, N. D. & Athanasiou, K. A. Gene expression of single articular chondrocytes. *Cell Tissue Res.* **327**, 43–54 (2007).
416. Penzo-Méndez, A. I., Chen, Y.-J., Li, J., Witze, E. S. & Stanger, B. Z. Spontaneous Cell Competition in Immortalized Mammalian Cell Lines. *PLoS ONE* **10**, e0132437 (2015).
417. Levayer, R. & Moreno, E. Mechanisms of cell competition: Themes and variations. *J. Cell Biol.* **200**, 689–698 (2013).
418. Strehl, R., Schumacher, K., de Vries, U. & Minuth, W. W. Proliferating cells versus differentiated cells in tissue engineering. *Tissue Eng.* **8**, 37–42 (2002).
419. Scharfmann, R. *et al.* Development of a conditionally immortalized human pancreatic  $\beta$  cell line. *J. Clin. Invest.* **124**, 2087–2098 (2014).



Keele University

---

# **Appendices**

---

## 9.1 Appendix A – Ethical approval documents, Keele Independent Peer Review



RESEARCH AND ENTERPRISE SERVICES

24 April 2012

Dr Nick Forsyth  
Senior Lecturer in Stem Cell Biology  
Guy Hilton Research Centre  
Thornburrow Drive  
Stoke on Trent, ST4 7QB

Dear Nick

### **Recovery and characterisation of mesenchymal stem cells from umbilical cord blood**

As you know the above project was initially awarded a grade 2 but following receipt of your response to the issues raised the project has now received final approval from the Independent Peer Review Committee and proceed for submission to an NHS REC for ethical approval. Please find attached the peer review comments for the above project.

### **Management approval**

You should arrange for all relevant NHS care organisations to be notified that the research will be taking place, and provide a copy of the REC application, the protocol and this letter.

All researchers and research collaborators who will be participating in the research must obtain management approval from the relevant care organisation before commencing any research procedures. Where a substantive contract is not held with the care organisation, it may be necessary for an honorary contract to be issued before approval for the research can be given.

### **Clinical trial of a medicinal product**

Please remember that, if your project is a clinical trial of a medicinal product, MHRA approval is required. You must submit a request for a clinical trial authorisation under the Medicines for Human Use (Clinical Trials) Regulations 2004. Further details can be found at <http://www.mhra.gov.uk/home/groups/l-unit1/documents/websiteresources/con2022633.pdf>

If you have any queries, please do not hesitate to contact Nicola Leighton on 01782 733306.

Yours sincerely

A handwritten signature in black ink, appearing to read "PMS O'Brien", with a horizontal line extending to the right.

Professor PMS O'Brien  
Chair – Independent Peer Review Committee

Enc

CC Dr D Clement, R&D Office, UHNS

Research and Enterprise Services, Keele University, Staffordshire, ST5 5BG, UK  
Telephone: + 44 (0)1782 734466 Fax: + 44 (0)1782 733740

## 9.2 Appendix A – Ethical approval documents, REC committee review



# Health Research Authority

**NRES Committee North East - Newcastle & North Tyneside 1**

TEDCO Business Centre  
Room 002  
Rolling Mill Road  
Jarrow  
NE32 3DT

Telephone: 0191 428 3387  
Facsimile: 0191 428 3432

05 February 2013

Dr Nicholas R Forsyth  
Senior Lecturer  
Keele University  
Guy Hilton Research Centre  
Thornburrow Drive  
Stoke on Trent  
ST4 7QB

Dear Dr Forsyth

**Study title:** Recovery and characterisation of mesenchymal stem cells from umbilical cord blood  
**REC reference:** 13/NE/0045  
**IRAS project ID:** 110583

The Proportionate Review Sub-committee of the NRES Committee North East - Newcastle & North Tyneside 1 reviewed the above application on 05 February 2013.

We plan to publish your research summary wording for the above study on the NRES website, together with your contact details, unless you expressly withhold permission to do so. Publication will be no earlier than three months from the date of this favourable opinion letter. Should you wish to provide a substitute contact point, require further information, or wish to withhold permission to publish, please contact the Assistant Co-ordinator Miss Sarah Grimshaw, [nrescommittee.northeast-newcastleandnorthtyneside1@nhs.net](mailto:nrescommittee.northeast-newcastleandnorthtyneside1@nhs.net).

### Ethical opinion

The Committee wondered whether viable stored material should be linked anonymised in case their use lead to a widely used cell line and many years of research and manipulation that may produce findings of clinical benefit to the donor.

Members noted that Part B Section 4 Question 12 of the IRAS form ("Who is the holder of the samples?") had not been answered.

*You responded that the research team would no longer be using only surplus tissue or existing stored samples not identifiable to the researcher, which removed this question from the IRAS form.*

The REC felt that given the information in the "Further Information" box at question A35 of the IRAS form, it would be more appropriate to state that "it is not predictable for the research team to monitor capacity and continued capacity will be assumed".

*You confirmed that this change had been made.*

Furthermore, Members noted that the response to A51 should be amended to check 'other' and state the results would form part of a PhD thesis.

*You confirmed that this change had been made.*

In addition to this, the Participant Information Sheet should therefore include the mention of a PhD being undertaken as part of the study.

Members felt that the Participant Information Sheet should include information about your intentions to disseminate study findings.

Members felt that a brief explanation of cord blood and stem cells would be useful in the Participant Information Sheet.

The REC noted the possibility that collected material could be used in future studies, but felt that the Participant Information Sheet was ambiguous on the storage of materials (Page 2, Bullet 4). Members advised you that it should indicate a specific time limit for the possible storage of donated material that cannot be used in future studies before destruction plus an indication of how long viable material will be stored and used for future studies, subject to ethical approval.

Furthermore, it was noted that if future use of material is viable then these studies may involve animal and/or commercial organisations, which the Sub-Committee believes donors should be told about in the Participant Information Sheet and given the opportunity to decline use of their material for such studies in the Consent Form.

The Committee requested that you include information about the use of samples in future study such as whether it would involve animals or commercial partners. It was also requested that this was added as an opt in/out point on the Consent Form.

The Committee noted that the Consent Form needed to include the modified version of the standard statement about regulatory authority access to research records.

*You made the amendments and submitted Version 2.0 of the Participant Information Sheet and Consent Form.*

Members felt that the Participant Information Sheet and Consent Form should be more explicit about animal and commercially related studies to exclude use of the donated material for such research, or give donors three options concerning use of their material in future studies, animal studies and use in commercial research.

*You made the amendments and submitted Version 3.0 of the Participant Information Sheet and Consent Form.*

On behalf of the Committee, the sub-committee gave a favourable ethical opinion of the above research on the basis described in the application form, protocol and supporting documentation, subject to the conditions specified below.

#### **Ethical review of research sites**

The favourable opinion applies to all NHS sites taking part in the study, subject to management permission being obtained from the NHS/HSC R&D office prior to the start of the study (see "Conditions of the favourable opinion" below).

#### **Conditions of the favourable opinion**

The favourable opinion is subject to the following conditions being met prior to the start of the study.

Management permission or approval must be obtained from each host organisation prior to the start of the study at the site concerned.

*Management permission (“R&D approval”) should be sought from all NHS organisations involved in the study in accordance with NHS research governance arrangements.*

*Guidance on applying for NHS permission for research is available in the Integrated Research Application System or at <http://www.rdforum.nhs.uk>.*

*Where a NHS organisation’s role in the study is limited to identifying and referring potential participants to research sites (“participant identification centre”), guidance should be sought from the R&D office on the information it requires to give permission for this activity.*

*For non-NHS sites, site management permission should be obtained in accordance with the procedures of the relevant host organisation.*

*Sponsors are not required to notify the Committee of approvals from host organisations.*

**It is the responsibility of the sponsor to ensure that all the conditions are complied with before the start of the study or its initiation at a particular site (as applicable).**

### **Approved documents**

The documents reviewed and approved were:

<i>Document</i>	<i>Version</i>	<i>Date</i>
Covering Letter	Dr Nicholas R Forsyth	25 January 2013
Evidence of insurance or indemnity	Lockton Policy Number SA13328793	26 July 2012
Investigator CV	Nicholas Robert Forsyth	23 January 2013
Investigator CV	Tina Dale	23 January 2013
Other: Response to Request for Further Information	Revised IRAS Form	
Participant Consent Form	3.0	31 January 2013
Participant Information Sheet	3.0	31 January 2013
Protocol	1.0	25 January 2013
REC application	IRAS Version 3.4, 110583/404559/1/165	25 January 2013
Referees or other scientific critique report	Professor PMS O'Brien	24 April 2012

### **Membership of the Proportionate Review Sub-Committee**

The members of the Sub-Committee who took part in the review are listed on the attached sheet.

### **Statement of compliance**

The Committee is constituted in accordance with the Governance Arrangements for Research Ethics Committees and complies fully with the Standard Operating Procedures for Research Ethics Committees in the UK.

### **After ethical review**

#### Reporting requirements

The attached document “After ethical review – guidance for researchers” gives detailed guidance on reporting requirements for studies with a favourable opinion, including:

- Notifying substantial amendments
- Adding new sites and investigators
- Notification of serious breaches of the protocol
- Progress and safety reports
- Notifying the end of the study

The NRES website also provides guidance on these topics, which is updated in the light of changes in reporting requirements or procedures.

#### Feedback

You are invited to give your view of the service that you have received from the National Research Ethics Service and the application procedure. If you wish to make your views known please use the feedback form available on the website.

information is available at National Research Ethics Service website > After Review

<b>13/NE/0045</b>	<b>Please quote this number on all correspondence</b>
-------------------	---

We are pleased to welcome researchers and R & D staff at our NRES committee members' training days – see details at <http://www.hra.nhs.uk/hra-training/>

With the Committee's best wishes for the success of this project.

Yours sincerely



pp

**Mr Chris Turnock**  
**Chair**

Email: nrescommittee.northeast-newcastleandnorthtyneside1@nhs.net

*Enclosures: List of names and professions of members who took part in the review*

*"After ethical review – guidance for researchers" SL-AR2*

*Copy to:*

*Nicola Leighton, Keele University*

*Dr Darren Clement, University Hospital of North Staffordshire*

### **NRES Committee North East - Newcastle & North Tyneside 1**

#### **Attendance at PRS Sub-Committee of the REC meeting on 05 February 2013**

#### **Committee Members:**

<i>Name</i>	<i>Profession</i>	<i>Present</i>	<i>Notes</i>
Mr Chris Turnock	Learning & Teaching Advisor	Yes	
Dr Simon Woods	Senior lecturer	Yes	
Professor Matt Wright	Reader	Yes	

### 9.3 Appendix A – Ethical approval documents, NHS R&D department approval

University Hospital of North Staffordshire   
NHS Trust

#### RESEARCH AND DEVELOPMENT DEPARTMENT

Academic Research Unit  
Courtyard Annexe – C Block  
Newcastle Road  
Stoke-on-Trent  
ST4 6QG  
Telephone: 01782 675387  
Fax: 01782 675399

Email: [Darren.Clement@uhns.nhs.uk](mailto:Darren.Clement@uhns.nhs.uk)  
[research.governance@uhns.nhs.uk](mailto:research.governance@uhns.nhs.uk)

Ref: DC/sg

07 August 2013

Ms Fidelma O'Mahony  
Consultant in Obstetrics and Gynaecology  
Obstetrics and Gynaecology Department  
University Hospital of North Staffordshire NHS Trust  
City General Site  
Newcastle Road  
Stoke-on-Trent  
ST4 6QG

Dear Ms O'Mahony

**Re: Recovery and characterisation of mesenchymal stem cells from umbilical cord blood**

**Chief Investigator: Dr Nicholas Forsyth**

**Sponsor: Keele University**

**Co-Sponsor: University Hospital of North Staffordshire NHS Trust**

I can confirm that the above project has been given NHS Permission for Research by the Research & Development Department for the University Hospital of North Staffordshire NHS Trust and the details entered on to the R&D database.

I note that this research project has been approved by NRES Committee North East – Newcastle & North Tyneside 1 REC reference 13/NE/0045.

NHS permission for the above research has been granted on the basis described in the application form, protocol and supporting documentation. The documents reviewed were:

Document	Version Number	Date
Protocol	1	25 January 2013
Patient Information Sheet	3.0	31 January 2013
Consent	3.0	31 January 2013
Contract/Agreement	N/A	07 August 2013

REDA ID: 5275 UKCRN ID: N/A CSP ID: N/A REC REF: 13/NE/0045

The research sponsor or the Chief Investigator, or the local Principal Investigator at a research site, may take appropriate urgent safety measures in order to protect research participants against any immediate hazard to their health or safety. The R&D office should be notified that such measures have been taken. The notification should also include the reasons why the measures were taken and the plan for further action. The R&D office should be notified within the same time frame of notifying the REC and any other regulatory bodies.

Approval by the R&D Dept therefore assumes that you have read, understand and agree to comply with the:

- ❖ Research Governance Framework ([www.doh.gov.uk/research](http://www.doh.gov.uk/research))
- ❖ Data Protection Act
- ❖ Health and Safety Act
- ❖ ICH Guidelines on good clinical practice
- ❖ All applicable Trust policies & procedures

In line with these requirements may I draw your attention to the need for you to provide the following documentation/notifications to the R&D Department throughout the course of the study and that all amendments (including changes to the local research team) need to be submitted to R&D in accordance with guidance in IRAS:-

- ❖ Annual Progress Report Form (sent to you by this department)
- ❖ End of Study Declaration Form (available on IRAS website)
- ❖ Changes to study start and end dates
- ❖ Changes in study personnel

Please note that the NHS organisation is required to monitor research to ensure compliance with the Research Governance Framework and other legal and regulatory requirements. This will be achieved by random audit by our department.

I would like to take this opportunity to wish you well with your research. If you need any further advice or guidance please do not hesitate to contact us.

Yours sincerely



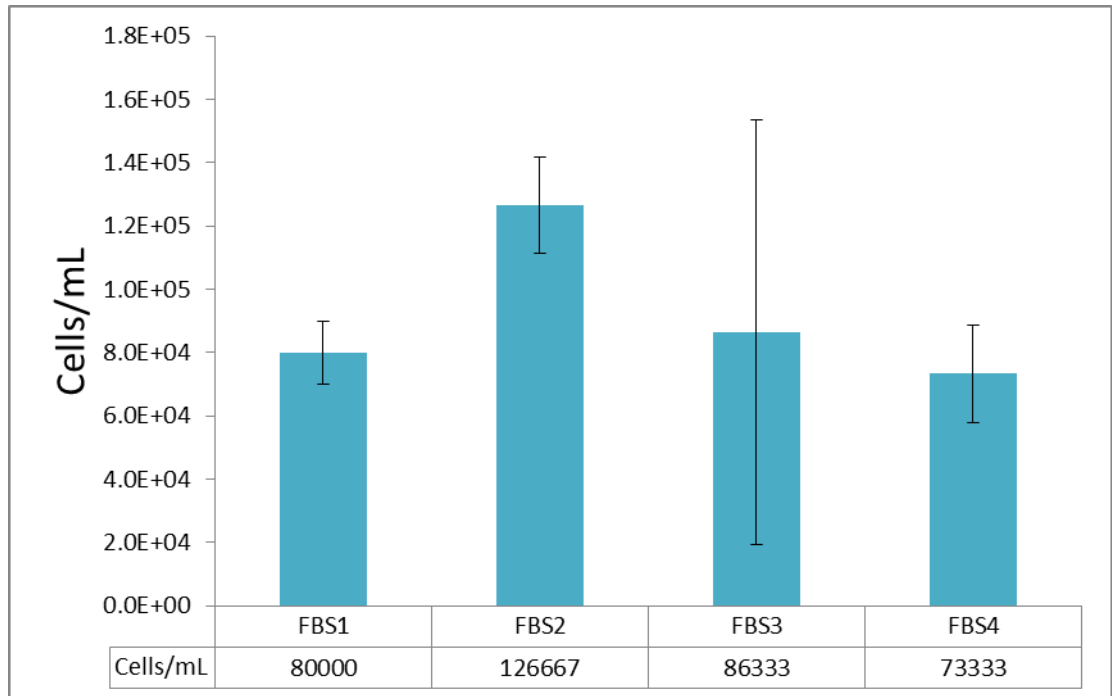
Dr Darren Clement  
R&D Manager – University Hospital of North Staffordshire NHS Trust

Cc Dr Nicholas Forsyth – CI, Keele University  
Tina Dale – Student, Keele University  
Nicola Leighton – Sponsor representative, Keele University  
Dr Darren Clement – Sponsor representative, UHNS  
Professor Shaughn O'Brien – Clinical Director Obstetrics & Gynaecology, UHNS  
Beryl Alcock, Clinical Trials Lead Nurse  
Helen Grocott, Information Governance Manager

REDA ID: 5275 UKCRN ID: N/A CSP ID: N/A REC REF: 13/NE/0045

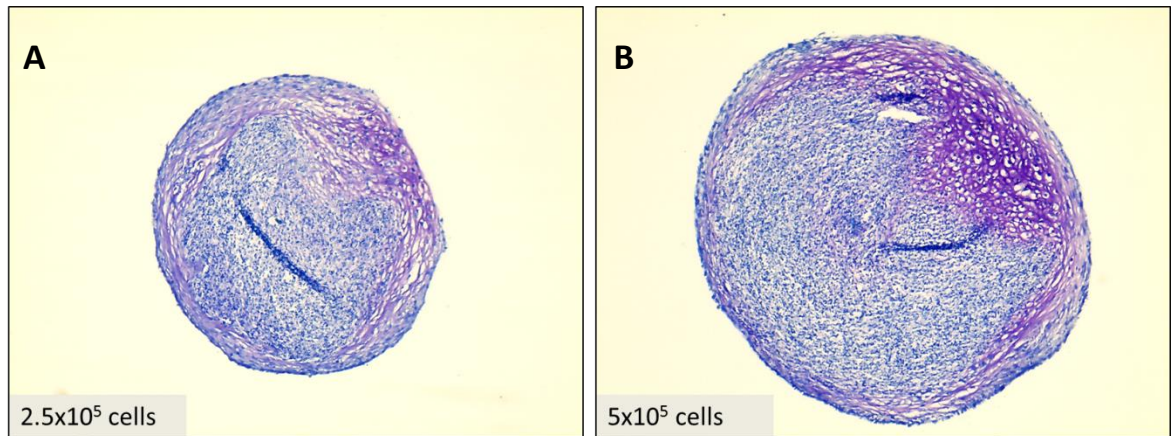
## 9.4 Appendix B – Supplementary figures

### 9.4.1 FBS batch testing results



**Supplementary figure 1. FBS batch test results.** Cell proliferation results from batch testing of three new FBS batches (FBS2-5) compared to original batch FBS1. MSCs were seeded to 6 well plates and cultured in MM supplemented with 10% (v/v) of one of each of the FBS batches and cultured until the best performing batch was approaching confluence at which point cells were trypsinised and counted with a Neubauer Haemocytometer. FBS1 and FBS2 refer to the same FBS1 and FBS2 as previous chapters. N=3, mean  $\pm$  standard deviation.

#### 9.4.2 The influence of BMA13 pellet size on sGAG deposition



#### Supplementary figure 2. Spatial patterning of chondrogenesis independent of cell pellet size.

Cell pellets formed from  $2.5 \times 10^5$  (A) and  $5 \times 10^5$  (B) BMA13 cells after 20 days culture in PChM. The pattern of sGAG production is strikingly similar independent of pellet size suggesting that it is not simply a result of nutrient diffusion dynamics.

## 9.5 Appendix C - Certificates of Analysis for FBS batches

### 9.5.1 FBS1 (Lonza)

Lonza Verviers SPRL  
Parc Industriel  
de Petit-Rechain  
B-4800 Verviers, Belgium  
Tel +32 87 32 16 11  
Fax +32 87 35 19 67  
VAT No: BE463 156 786  
RPM: Verviers – Bruxelles

# Lonza

Printed on, 04-Oct-2015 13:36

Page 1 / 1

### CERTIFICATE OF ANALYSIS

**Product Code:** DE14-801F  
**Product:** FBS - Brazilian Origin  
500ml

**Lot Number:** 1SB020  
**Manufacture Date:** 24-Aug-2011  
**Expiration Date:** 24-Aug-2017

TEST (Method)	SPECIFICATIONS		Results
	Min.	Max.	
Sterility (EP and USP)	Not Detected	Not Detected	Not detected
Mycoplasma detection E.P. (PCR)	Not Detected	Not Detected	Not detected
pH @ 20-25°C (EP)	6.8	8.3	7.1
Osmolality (mOsm/kg)	280	365	298
Hemoglobine, mg/100ml	***	< /= 30	14.6
Total Protein, g/100ml	3	6	4.0
IgG Concentration, mg/ml	***	< /= 0.5	0.068
Endotoxin	***	< /= 50	2.350 EU/ml
Cell Growth assay	Pass	Pass	Pass
Virus Testing by Cell Culture			
BVD	Not Detected	Not Detected	Not detected
IBR	Not Detected	Not Detected	Not detected
PI-3	Not Detected	Not Detected	Not detected

The country of origin of the raw material used to manufacture the above referenced product is Brazil. Brazil is free of Bovine Spongiform Encephalopathy in accordance with the Organization of International Epizooties (OIE). A geographical BSE risk assessment report (GBR) by the European Food Safety Authority has been issued in June 2005 and designated Brazil as a GBR level II risk (unlikely but can not be excluded that domestic cattle are infected with the BSE agent).

## 9.5.2 FBS2 (Biosera)



### CERTIFICATE OF ANALYSIS Fetal Bovine Serum (South America), Gamma Irradi

Batch N° :	11484	Storage :	-20°C
Catalog N° :	FB-1001G/500	Filtration :	Triple 0.1 µm filtered
Validation Date :	05 / 11 / 2013	Origin :	BRAZIL
Expiry date :	05 / 11 / 2018		

QUALITY PROFILE				
Tests	Methods	Units	Specifications	Results
Appearance			Turbid straw to amber liquid	Turbid straw to amber liquid
Bacteria and Fungi			Not detected	Not detected
Mycoplasma	Culture		Not detected	Not detected
pH				7.30
Osmolality	Freezing point . EU Ph. 2.2.35	mOsm/kg		305
Endotoxin	Chromokinetic test . Method D of EU Ph. 2.6.14	EU/ml		1.736
Haemoglobin		mg/100ml		15.35
Total protein	Biuret colorimetry	g/l		36.5
BVD virus	Cell culture observation and ELISA test		Not detected	Not detected
IBR virus	Cell culture observation and ELISA test		Not detected	Not detected
PI3 virus	Cell culture observation and ELISA test		Not detected	Not detected

CHEMICAL PARAMETERS				
Tests	Methods	Units	Specifications	Results
ALAT (SGPT)	UV kinetic at 37°C	IU/l		6
Alkaline Phosphatase	Colorimetry kinetic at 37°C	IU/l		401
ASAT (SGOT)	UV kinetic at 37°C	IU/l		42
Bilirubin	DPD / caffeine colorimetry	mg/100ml		0.28
Calcium	Arsénazo colorimetry	mg/100ml		14.2
Gamma GT	Colorimetry kinetic at 37°C	IU/l		8
Cholesterol	Cholesterolase Trinder colorimetry	mg/100ml		30
Creatinine	Colorimetry Kinetic (Jaffé)	mg/100ml		3.3
Chloride	Indirect potentiometry	mmol/l		100
Glucose	Hexokinase UV	mg/100ml		58
Iron	TPTZ colorimetry	µg/100ml		181
Lactate Dehydrogenase	UV kinetic at 37°C	IU/l		758
Phosphorus	Phosphomolybdate colorimetry	mg/100ml		9.50
Potassium	Indirect potentiometry	mmol/l		11.4
Sodium	Indirect potentiometry	mmol/l		135
Triglycerides	Glycerokinase Trinder colorimetry	mg/100ml		56
Urea	Urease UV	mg/100ml		31
Uric Acid	Uricase trinder colorimetry	mg/100ml		1.6

**CERTIFICATE OF ANALYSIS**  
**Fetal Bovine Serum (South America), Gamma Irradi**

Batch N° :	.11484	Storage :	-20°C
Catalog N° :	FB-1001G/500	Filtration :	Triple 0.1 µm filtered
Validation Date :	05 / 11 / 2013	Origin :	BRAZIL
Expiry date :	05 / 11 / 2018		

PROTEIN ELECTROPHORESIS				
Tests	Methods	Units	Specifications	Results
Albumin	Immunoturbidimetry	g/l		16.0
Alpha Globulins	Immunoturbidimetry	g/l		15.8
Beta Globulins	Immunoturbidimetry	g/l		2.5
Gamma Globulins	Immunoturbidimetry	g/l		2.3

ELISA TEST				
Tests	Methods	Units	Specifications	Results
IgG		mg/l		179.3

BIOLOGICAL PERFORMANCE				
Tests	Methods	Units	Specifications	Results
L929 cell growth : 3rd day		%		97
L929 cell growth : 6th day		%		80
SP2/O-Ag14 cell growth : 3rd day		%		67
SP2/O-Ag14 cell growth : 6th day		%		71
HELA cell growth : 3rd day		%		102
HELA cell growth : 6th day		%		93
MRC-5 cell growth : 3rd day		%		107
MRC-5 cell growth : 6th day		%		75
Plating efficiency - cells implanted			500	500
Plating efficiency - number of colonies				447
Plating efficiency - PE absolute		%		89
Plating efficiency - PE relative		%		94
Cloning efficiency - cells implanted per well			1	1
Cloning efficiency - number of clones				32
Cloning efficiency - CE absolute		%		33
Cloning efficiency - CE relative		%		39

Calleau Laura  
 Quality Service



Date : 24/12/2013